

DEFLECTIONS IN THIN CYLINDRICAL SHELLS

with particular reference to the buckling deformations of  
shells loaded in axial compression.

by

COLIN GEORGE POSTER

M.E. M.I.E.Aust.

Submitted in fulfilment of the requirements  
for the degree of

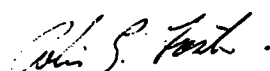
DOCTOR OF PHILOSOPHY

in the  
Faculty of Engineering  
UNIVERSITY OF TASMANIA

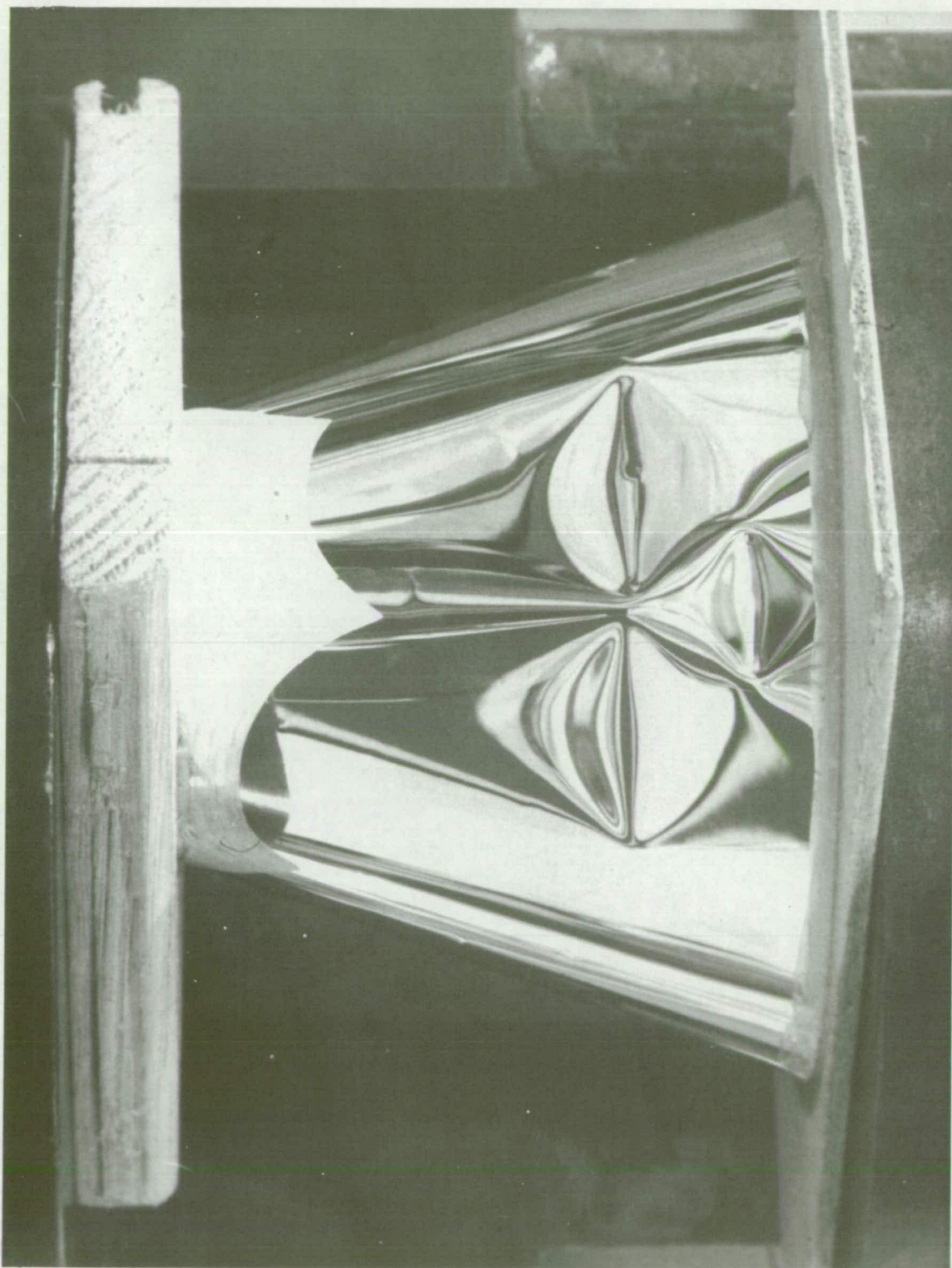
AUSTRALIA.

September 1979

I hereby declare that, except as stated herein, this thesis does not contain any material which has been accepted for the award of any other degree or diploma in any University, and that to the best of my knowledge and belief, this thesis does not contain a copy or paraphrase of material previously written or published by any other person, except when due reference is made in the text of this thesis.

A handwritten signature in cursive script, reading "Colin G. Foster".

Colin G. Foster.



CONTENTS.PAGE.

Preface.

Additional publications.

Acknowledgements.

Chapter 1.	Introduction-buckling in thin walled cylinders.	1.
Chapter 2.	A new theory for the buckling of thin cylinders in axial compression.	34.
Chapter 3.	An examination of the conventional solution method for the axial buckling problem.	81.
Chapter 4.	Finite difference solution of the partial differential equations.	107.
Chapter 5.	Extensions to the space frame model for the collapse of cylinders loaded in axial compression.	126.
Chapter 6.	An experimental technique for measuring radial deformations.	168.
Chapter 7.	Experimental evidence to support the space frame theory.	192.
Chapter 8.	Conclusions.	230.
References.		236.



Appendix A.	Results of combined load buckling tests.	242.
Appendix B.	Results of finite difference solution of partial differential equations.	280.
Appendix C.	Program listing for buckling analysis of cylinder as a space frame and typical output.	316.
Appendix D.	Program listing and typical output of programs used in the finite difference solution of the deflections in a cylindrical shell with a geometrical defect.	320.
Appendix E.	Program listing and typical output of programs used in calculating the fold shape based on the bi-harmonic equation.	344.
Appendix F.	Program listing and typical output of programs used in calculating the fold shape allowing for membrane stresses.	354.

## PREFACE

The primary objective of the work presented in this thesis has been to obtain an understanding of the buckling mechanism in thin cylindrical shells when loaded in axial compression. It was hoped that this understanding could then be applied in developing a quantitative model to describe the behaviour. This could in turn lead to more satisfactory design conditions by linking the collapse load of a cylinder with defect size. The investigation grew out of an enquiry from industry concerning the buckling behaviour of the central column support for process thickeners. These columns were relatively thick walled shells subjected to combined axial compression, torsion and external pressure. These particular structures would yield before the

deformations would be large enough for buckling to be a consideration. However, the nature of the buckling process must be understood to determine when it is important.

In Chapter One the general nature of the known experimental buckling behaviour is described. The discussion is not limited to axial compression but includes torsion and hoop compression as well as combinations of all three. Experimental results are included that show the interaction between these modes and indicate possible weaknesses in existing design data.

Chapter Two is probably the most important chapter of the thesis and forms the basis on which the remainder is built. In this chapter a new theory is presented to describe the buckling behaviour of cylinders. For this theory the cylinder (both in the pre-buckled and post-buckled state) is replaced by an equivalent space frame with the members tracing the folds in the Yoshimura pattern. The buckling problem is then reduced to a buckling analysis of the substituted space frame. The results from this analysis agree remarkably well with published information on post-buckling behaviour.

In Chapter Three an examination of the Donnell equations is made. These equations were meant to describe the buckling and post-buckling behaviour of cylinders. It is shown that perhaps Donnell's membrane equations may be

inadequate. It appears that second derivatives of out of plane displacements (curvatures) may need to be included as additional terms.

A finite difference solution of the partial differential equations is conducted in Chapter Four. This analysis has shown that inclusion of the curvature terms could account for a 15% change in calculated values even in the pre-buckling range for which the calculation was stable.

Some refinements to the space frame theory are considered in Chapter Five. It is shown that considering the member as initially curved leads to more confusion than any possible advantage it could have. However, the analysis allowing for the curved member is included since it is probably the most obvious condition where improvement would be expected. It is hoped that others will profit by the experience and not follow the same reasoning. It is also shown that the aspect ratio of the lobes in the buckled cylinder varies with the radius to thickness ratio. When this variation is taken into account the agreement is not unreasonable between predicted buckling loads and published experimental results for cylinders.

Chapter Six describes a new experimental technique that was developed specifically to measure the radial deformations and imperfections of cylinders. It is based on the Ligtenberg-moiré method.

In Chapter Seven the experimental method is used to determine the size of some defects in experimental cylinders which appear to control the collapse. Allowing for these defects in the theory as developed in chapter five there is remarkable agreement between predicted and measured buckling loads.

## ADDITIONAL PUBLICATIONS

The following papers have been published covering work described in this thesis.

1. Measurement of radial deformations in thin-walled cylinders. Experimental Mechanics. Vol.18, no.11, Nov.1978. (Chapter 6)
2. Some observations on the Yoshimura buckle pattern for thin-walled cylinders. J.of Applied Mechanics. Vol.46 , no.2, June 1979. (Chapter 2)
3. Estimation of the collapse loads of thin-walled cylinders in axial compression. J.of Applied Mechanics. Vol.46 , no.2, June 1979. (Chapter 2)

The following papers have been written and are at present being reviewed.

1. Interaction of buckling loads in thin walled cylinders. Submitted to Experimental Mechanics. (Chapter 1)
2. A note on curvature and twist measurements using the Ligtienberg-moire' method. Submitted to Strain. (Chapter 5)
3. The effect of shell wall flexibility on the collapse of thin walled cylinders loaded in axial compression. Submitted to J.of Applied Mechanics. (Chapter 5)
4. The effect of geometrical defects in buckling of thin walled cylinders in axial compression. Submitted to J.of Applied Mechanics. (Chapter 7)

## ACKNOWLEDGEMENTS

No piece of worthwhile research could be concluded without the assistance of many people. To all those that have helped in any way the author would like to express his gratitude. Special acknowledgement is recorded for the following.

Professor A.R.Oliver and Dr.R.F.Rish. -- The supervisors for the project.

Mr.Basil Stiberc and the other workshop staff who made all of the apparatus used in the experimental investigations.

and

Mr. Peter Jordan for preparing most of the line diagrams.



# CHAPTER 1

---

---

## INTRODUCTION

---

---

## CHAPTER 1

### INTRODUCTION -- BUCKLING IN THIN WALLED CYLINDERS

The work that is described in this thesis originated in an enquiry from industry about the design of cylindrical shells particularly with regard to buckling. The particular cylinder involved was relatively thick walled and would yield before the deformations had grown sufficiently for buckling to be a problem. However, when investigating the buckling situation the work described in this thesis evolved.

A classical buckling load can be obtained for thin walled cylinders loaded in axial compression as explained in Timoshenko and Gere-(ref.1--pages 457-458).

This classical analysis assumes axisymmetric failure in a ripple pattern <sup>or rectangular wave pattern</sup> and is expressed as:-

$$\sigma_{a_c} = \frac{E.T}{R\{3(1-\nu^2)\}^{\frac{1}{2}}} \text{-----1.1}$$

It is well known that the "ripple" pattern illustrated in figure 1.1 occurs only in relatively thick walled shells where yielding has first occurred. If the cylinder collapses elastically then the buckle pattern is a series of diamonds as shown in figure 1.2. Even more important is the fact that the nominal stress at collapse is considerably below that value given by equation 1.1. This discrepancy has led to a great deal of research both experimentally and theoretically. The experimental work is largely summarised in a paper by Harris et.al.(ref.2). That paper statistically analyses the available experimental data to establish 90% confidence limits for design purposes. On the theoretical side, a major contribution was made by Von Karman and Tsien in 1941 (ref.3), based on equations published by Donnell in 1934(ref.4). They considered the post buckling behaviour of the cylinder and allowed for large deflections by taking second order geometry terms into account. In their work the graph shown in figure 1.3 was derived, here reproduced from Flügge (ref.5). Many researchers refined the calculations of Von Karman and Tsien and with the advent of digital computers the solution technique could be extended. Yoshimura (ref.6) showed the diamond pattern obtained in buckling to be a folded, developable surface and eventually Hoff, Madsen and Mayers (ref.7) concluded that the whole Donnell-Von Karman and

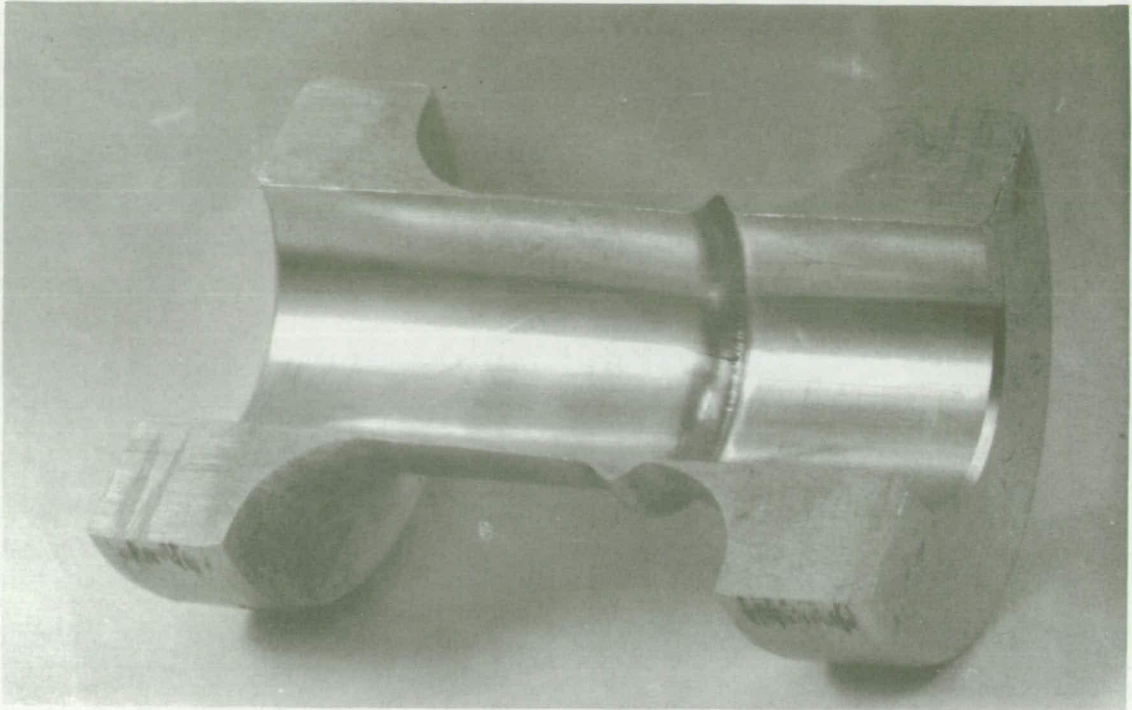


FIGURE 1.1

INELASTIC AXIAL RIPPLE BUCKLING

No. 2011 ALUMINIUM CYLINDER  $R=12.7\text{mm}$ .  $T=0.5\text{mm}$ .

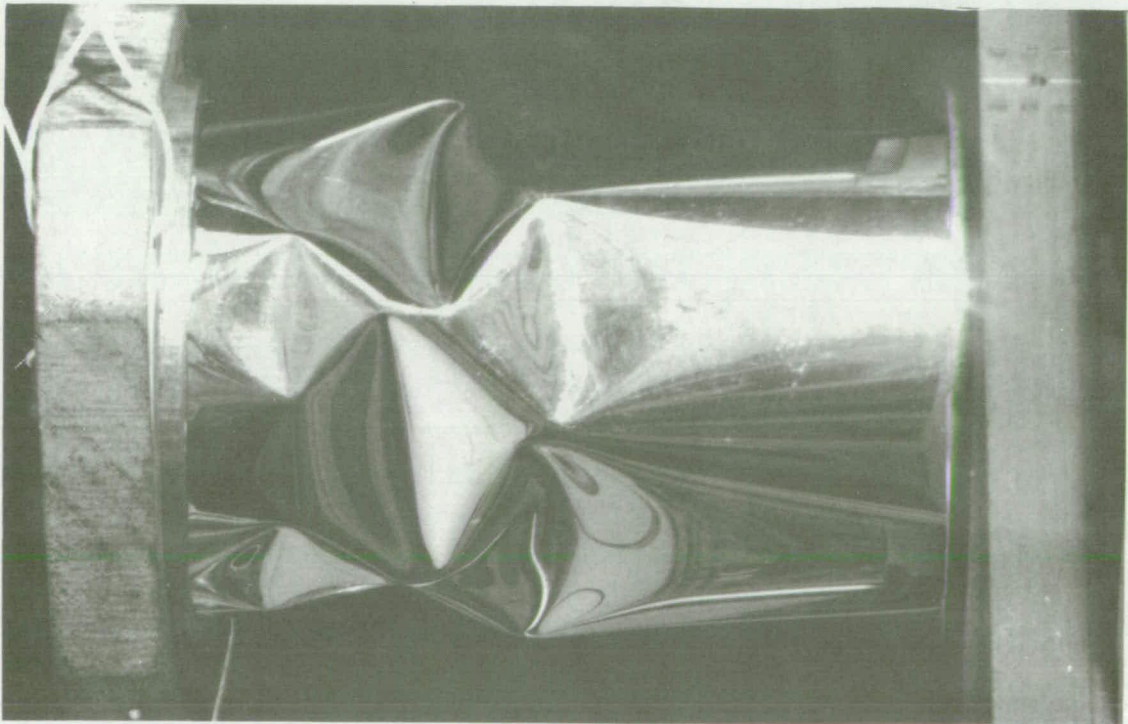


FIGURE 1.2

ELASTIC DIAMOND PATTERN — AXIAL COMPRESSION

MELANEX CYLINDER  $R=44.5\text{mm}$ .  $T=0.1\text{mm}$ .

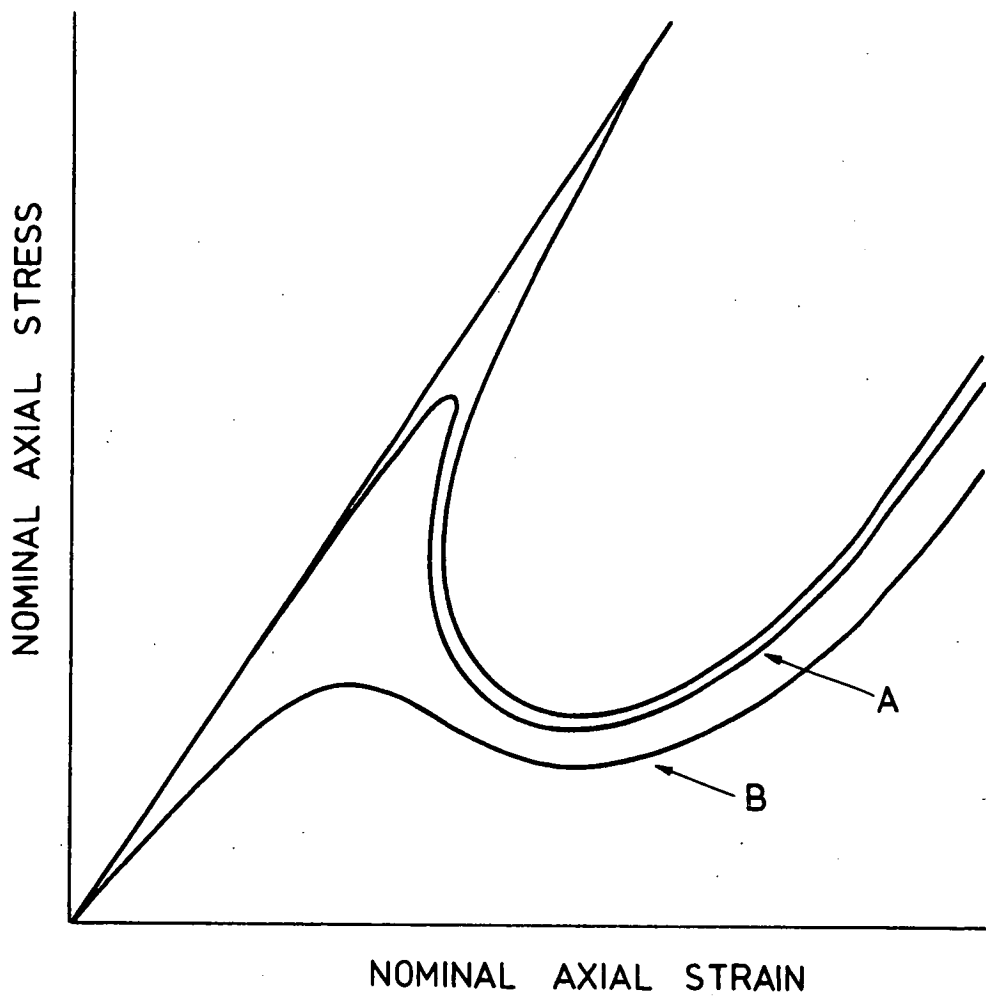


FIGURE 1.3  
THEORETICAL BEHAVIOUR OF AXIALLY  
COMPRESSED CYLINDER

Tsien approach was inappropriate. Using an infinite series solution they came to some rather startling conclusions which are reproduced here, as follows.

"In the limit as  $M$  (the number of terms in the series expansion) tends to infinity, the exact Yoshimura pattern is approached on the basis of an extrapolation of the results obtained with the aid of a digital computer. In this limiting case  $N$  (the number of circumferential lobes) approaches infinity, the amplitude of the displacements tends to zero, the Von Karman-Donnell equations are rigorously valid, the  $T/R$  ratio approaches zero, and the value of the average axial stress capable of maintaining equilibrium in the postbuckling state is zero."

Clearly a solution which leads to conclusions of this nature can not possibly describe the real situation. Anyone who has ever folded a sheet of paper into a Yoshimura pattern is well aware that the structure so formed has considerable strength. The theory developed in the next chapter is an attempt to overcome the difficulties mentioned above. It does appear to supply a reasonable explanation of the buckling behaviour of thin walled cylinders in axial compression.

Before proceeding with that discussion some explanation of the general buckling behaviour of thin walled cylinders is necessary. Von Karman and Tsien in producing

the graph shown in figure 1.3 proposed that an imperfect cylinder would follow the path shown by either curve A or curve B. Curve A represents a cylinder with a small defect while curve B represents a cylinder with rather large defects. In both cases the collapse load is considerably reduced from the theoretical value (the classical load). Thus defects in shape have a considerable influence on the collapse load of axially compressed thin walled cylinders.

Buckling due to bending is very similar in nature to axial compression so that the same type of argument would apply. For failure due to torsion the reduction in critical stress (due to imperfections) from the classical value is not as severe but is still substantial. Collapse from external pressure loading is even less susceptible to imperfections. Figures 1.4 and 1.5 show the type of buckle pattern obtained in torsion loading and from external pressure.

For the reader interested in further reading on the stability of shells two excellent review articles are available (refs. 8 and 9).

In the buckling process, the diamond pattern is often seen to grow out of some imperfection. One or two diamonds may appear together and then others form adjacent to these. Sometimes the first wrinkle may occur at the end support and move towards the centre of the shell. Often, it is possible to move the buckle pattern around



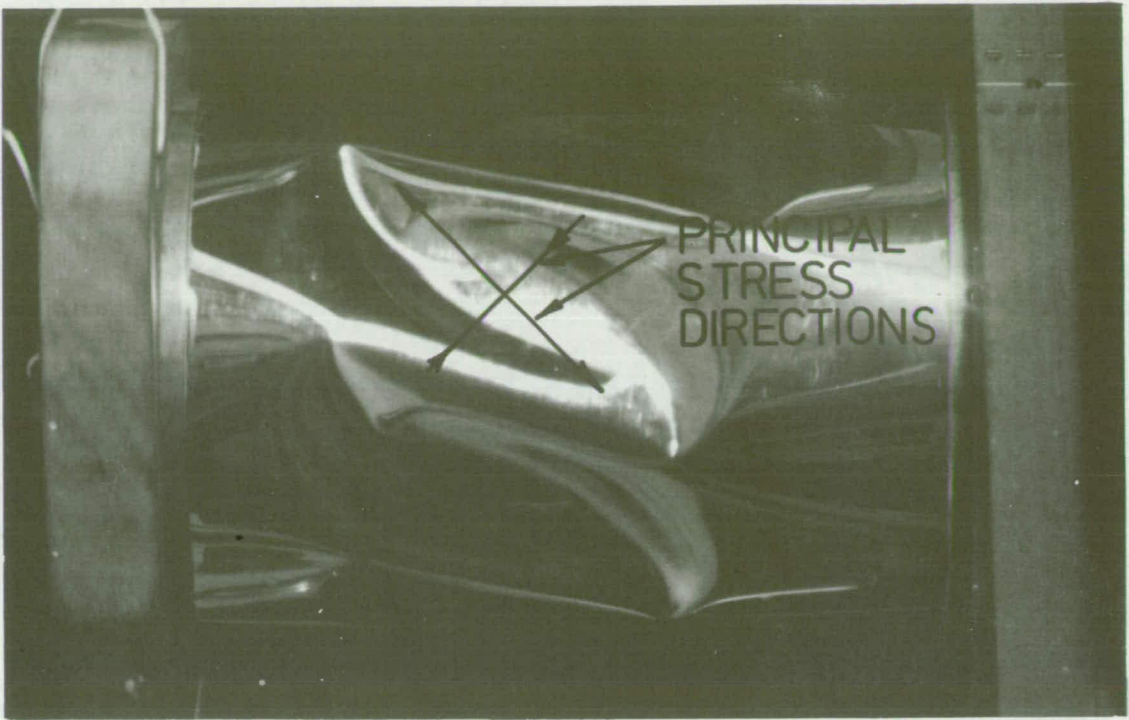


FIGURE 1.4  
MELANEX CYLINDER—IN TORSION

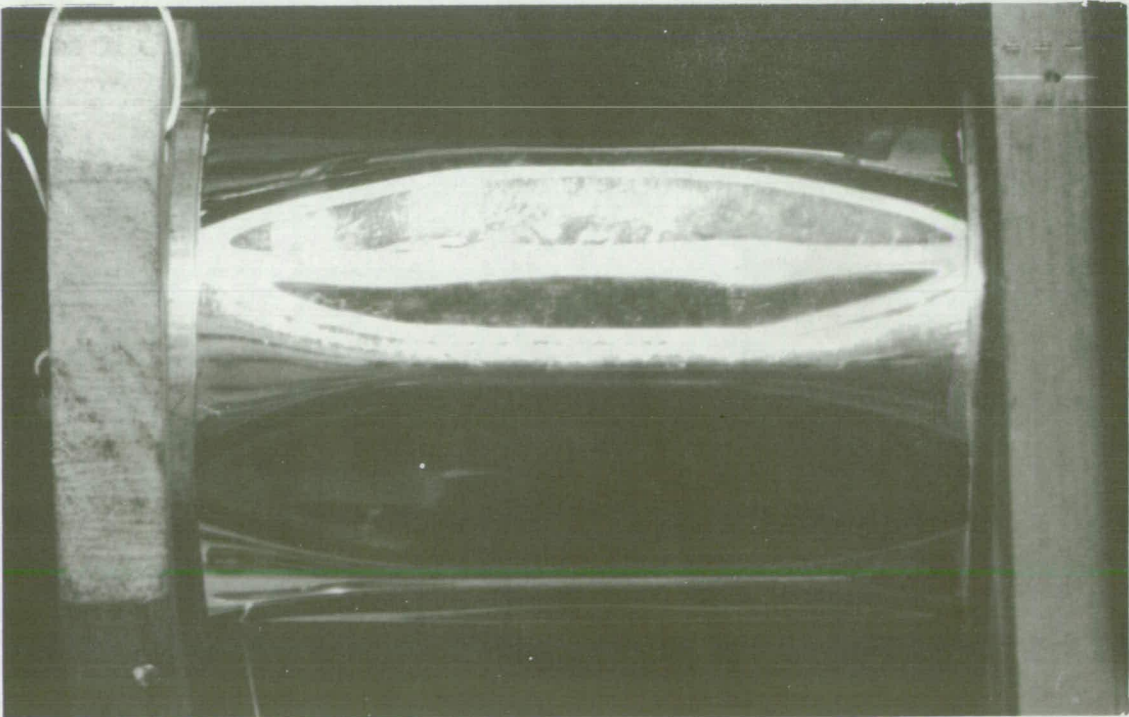


FIGURE 1.5  
MELANEX CYLINDER—EXTERNAL PRESSURE

on the shell. Figure 1.6 shows the growth of the buckle pattern with increasing axial strain on a conical shell made of 0.1mm. thick melanex. The shell was 76mm. long, 45mm. dia. at the small end and 106mm. dia. at the large end. The behaviour of conical shells is very similar to cylindrical shells in axial compression. In figure 1.6A an imperfection can be seen that serves as a nucleation point for the diamond pattern. In subsequent photographs the diamond pattern is seen to spread from this point and intensify as the axial displacement is increased.

Even though the large discrepancy is known to exist between theory and practice, cylindrical shells are used as structures, particularly in the aerospace industry. Thus design formulae must be available. One source of these formulae is Roark(ref. 10) but these formulae need to be treated with caution because of the age of the reference. Another, more modern source is Baker, Kovalevsky and Rish (ref. 11) which is based on the NASA "Shell Analysis Manual"(ref. 12). A summary of these design formulae is given in table 1.1. This last reference is essentially for use in the aerospace industries where shell structures would normally be more perfectly made than the fabricated one from which this investigation started. Thus the size of the imperfections here may make the design formulae useless. To test this hypothesis a melanex cylinder was made and tested. The manufacture of the cylinder was deliberately crude so that imperfections would be large. The cylinder was

TABLE 1.1

DESIGN FORMULAE FOR CALCULATION OF CRITICAL STRESSES

Mode	Source	Formula	Comments
Axial Compression	Roark	$\sigma_{cr} = \frac{E \cdot T}{\sqrt{3(1-\nu^2)} R}$	Classical formula- "actual" value 0.4 to 0.6 of calculated value.
	Baker Kovalevsky &Rish	$\sigma_{cr} = \frac{\gamma \cdot E \cdot T}{R \sqrt{3(1-\nu^2)}}$	$\gamma$ read from graph. allows for imperfections.
Axial Compression Internally Pressurised	Baker Kovalevsky &Rish.	$\sigma_{cr} = \left( \frac{\gamma}{\sqrt{3(1-\nu^2)}} + \Delta C_c \right) \frac{E \cdot T}{R}$	$\gamma$ as above. $\Delta C_c$ read from graph.
Torsion	Roark	$\tau_{cr} = \frac{E}{1-\nu^2} \left( \frac{T}{L} \right)^2 (4.6 + \sqrt{1.8 + 0.59 H^2}) H \sqrt{1-\nu} \frac{L}{R}$	"Actual" value 0.6 to 0.75 of calculated value.
	Baker Kovalevsky &Rish.	$\tau_{cr} = C_s \frac{E \cdot T}{R \cdot Z^{\frac{1}{4}}}$ $Z = \frac{L^2}{RT} \sqrt{1-\nu^2}$	$C_s$ read from graph.
Torsion Internally Pressurised	Baker Kovalevsky &Rish	$\tau_{cr} = C_s \frac{E \cdot T}{R \cdot Z^{\frac{1}{4}}} + \Delta C_s \frac{E \cdot T}{R}$	$\Delta C_s$ read from graph.
External Pressure	Roark	$\sigma_{cr} = 0.807 \frac{ET}{L} \left( \frac{1}{(1-\nu^2)^3} \cdot \frac{T^2}{R^2} \right)^{\frac{1}{4}}$	
	Baker Kovalevsky &Rish.	$\sigma_{cr} = \frac{K_p \cdot T^2 \cdot E}{12(1-\nu^2)} \left( \frac{T}{L} \right)^2$	$K_p$ read from graph.



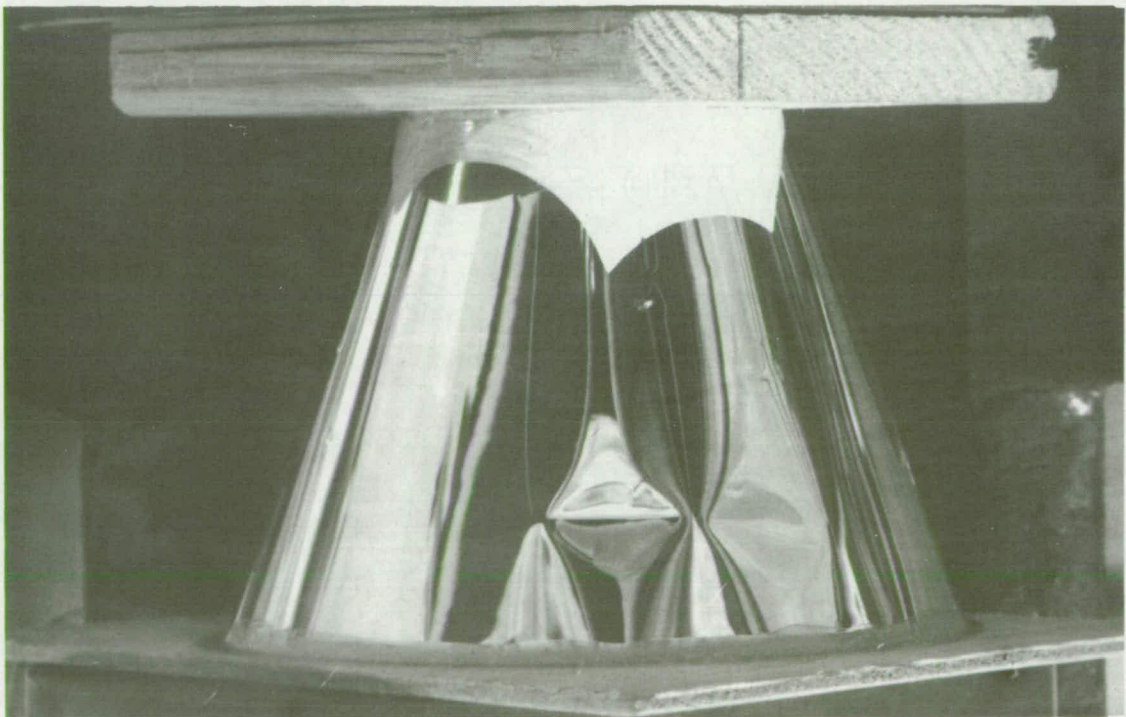
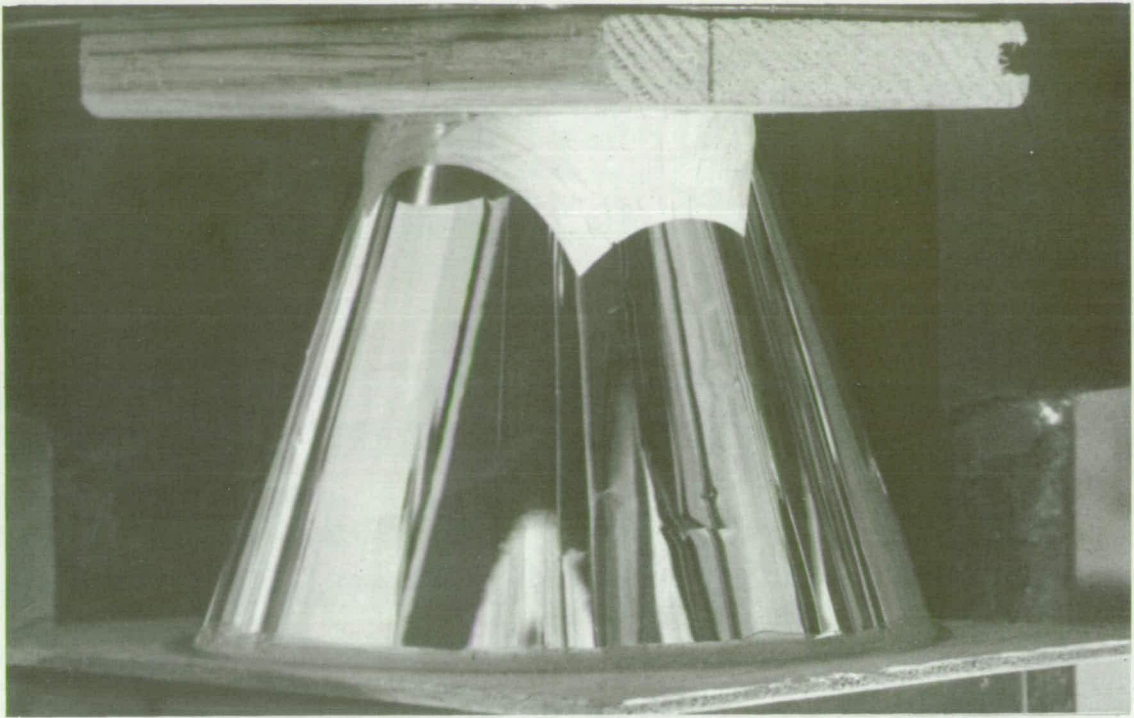


FIGURE 1-6

CONICAL SHELL IN AXIAL COMPRESSION

A. UNDEFORMED SHELL

B. SMALL AXIAL DISPLACEMENT



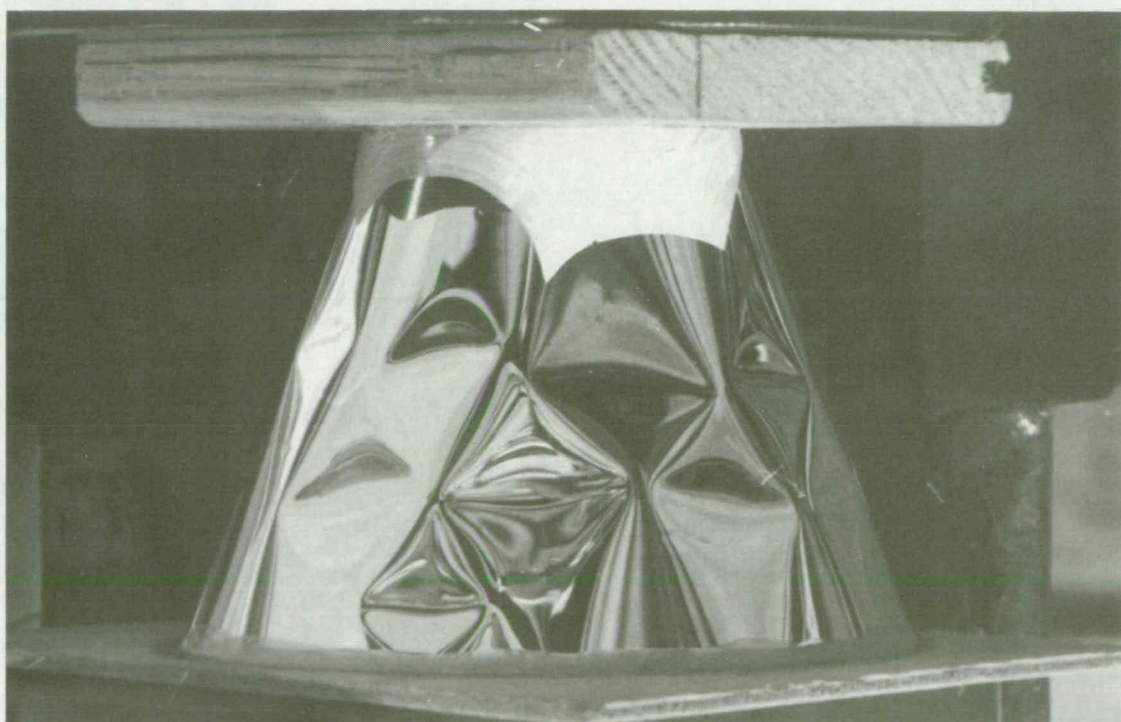
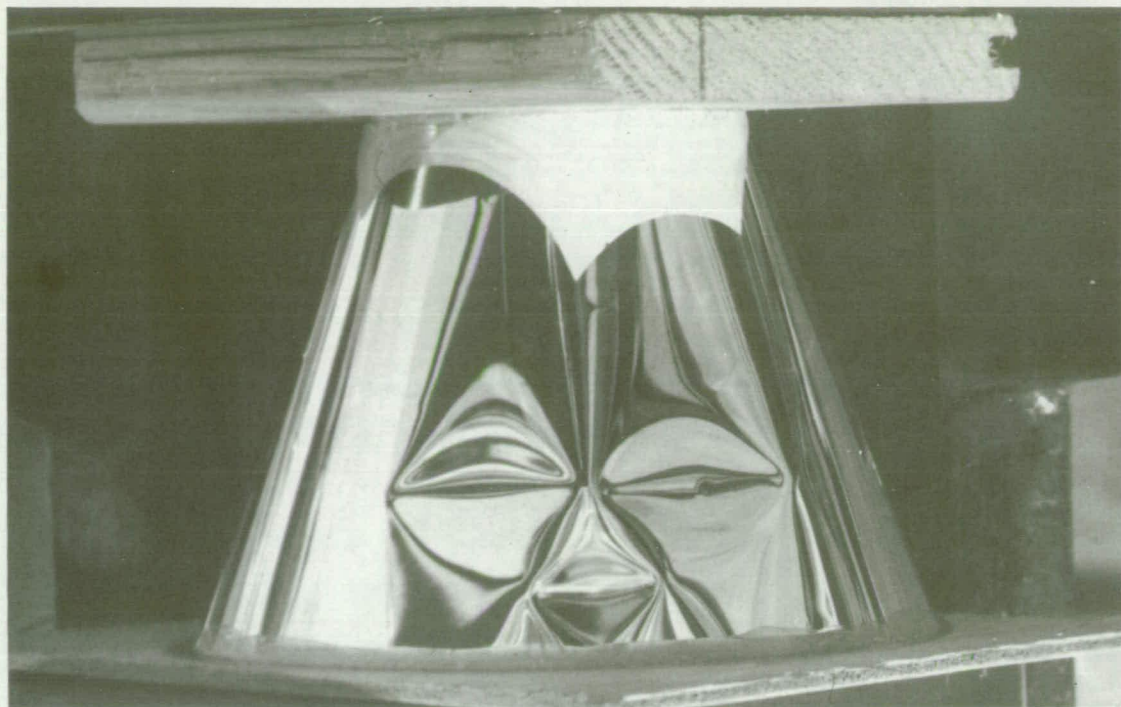


FIGURE 1.6 C and D  
INCREASING AXIAL DEFORMATION



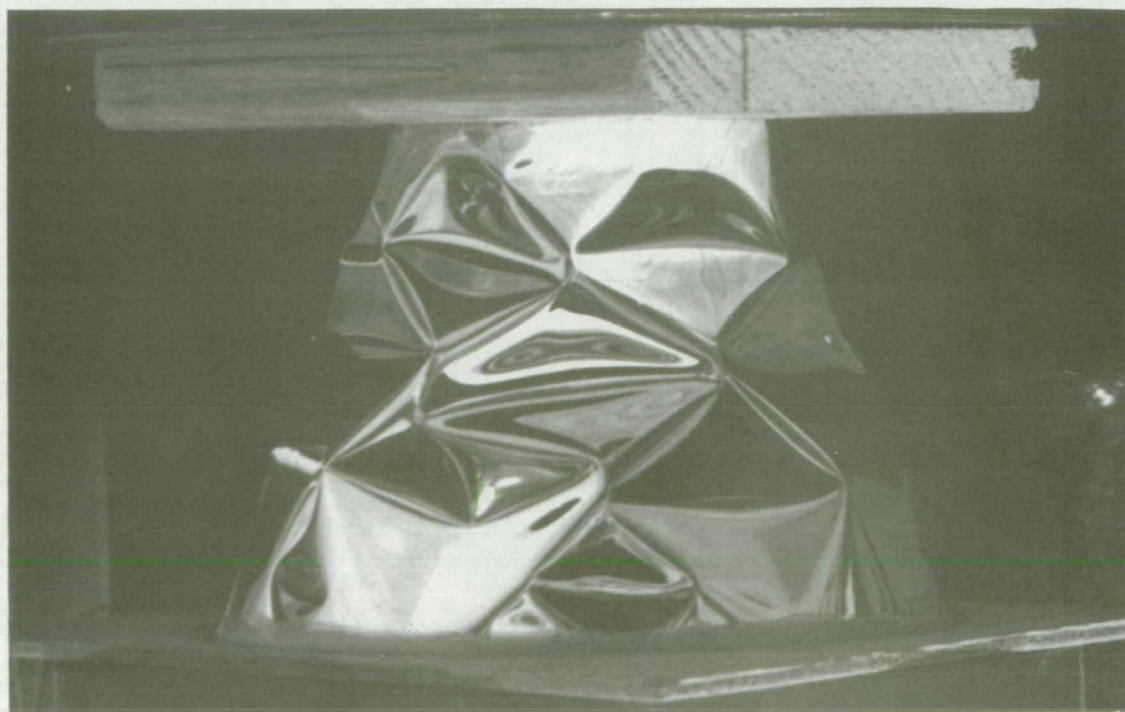
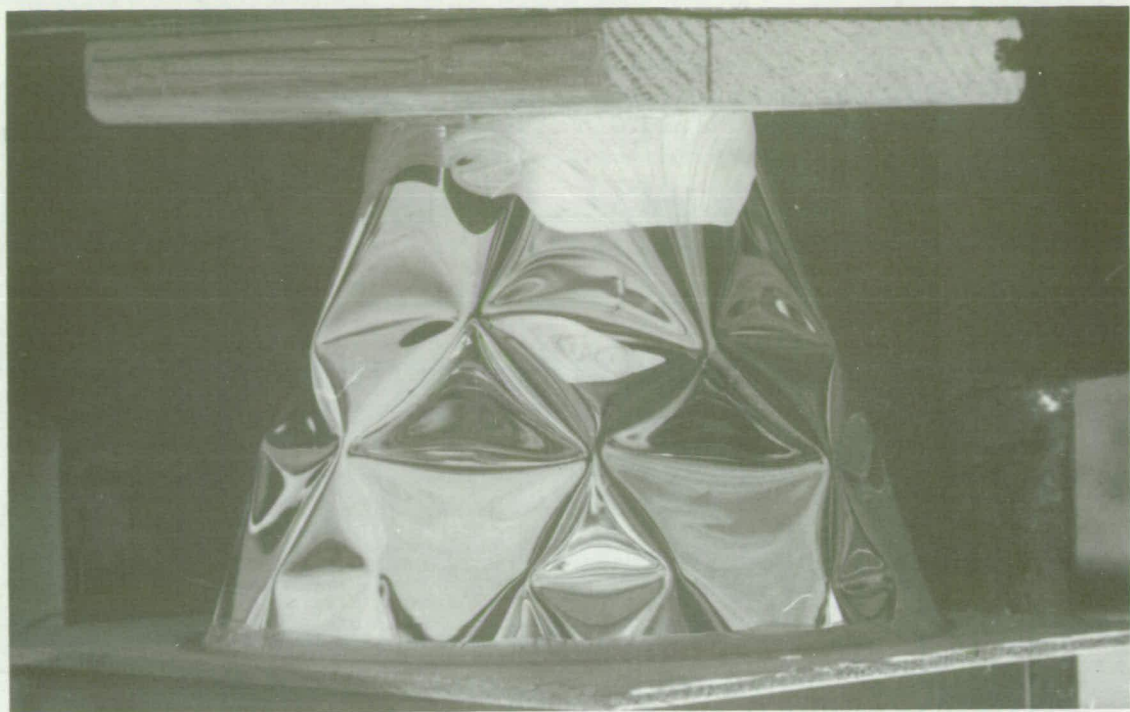


FIGURE 1-6 E and F  
LARGE AXIAL DEFORMATION

127mm. long, 89mm. dia. and had a wall thickness of 0.1mm. A longitudinal seam was made by butting the two ends of the melanex together and lapping the joint with cellulose adhesive tape. The ends of the cylinder were bonded to brass reinforcing rings with contact cement. This cylinder collapsed elastically so that repeated tests were possible on the one cylinder. A simple loading rig was made (figure 1.7) such that the cylinder could be tested with combinations of axial load, torsion and internal vacuum since the magnitude of the external pressure needed to collapse the cylinder was very small. The apparatus could also be internally pressurised to test the stiffening effect that internal pressure has on the stability of the cylinder in axial compression and torsion. Because of the nature of the apparatus the weight of the crosshead was always present as an axial load. Thus for torsion loading and hoop compression the measured values would be slightly lower than the actual critical loads.

The measured nominal stresses at collapse are given in table 1.2 and compared with the values obtained from an application of the design formulae. In applying the design formulae values of Young's modulus and Poisson's ratio were required. Because of the nature of the test material a great deal of difficulty was experienced in measuring these quantities. Young's modulus was eventually measured at 5.6GPa. but this value could not be guaranteed to better than about 5%. Poisson's ratio measurements were hopeless so that a value of 0.35 was guessed. This value has only a small effect on the calculations so that large errors in its value can be accommodated with small



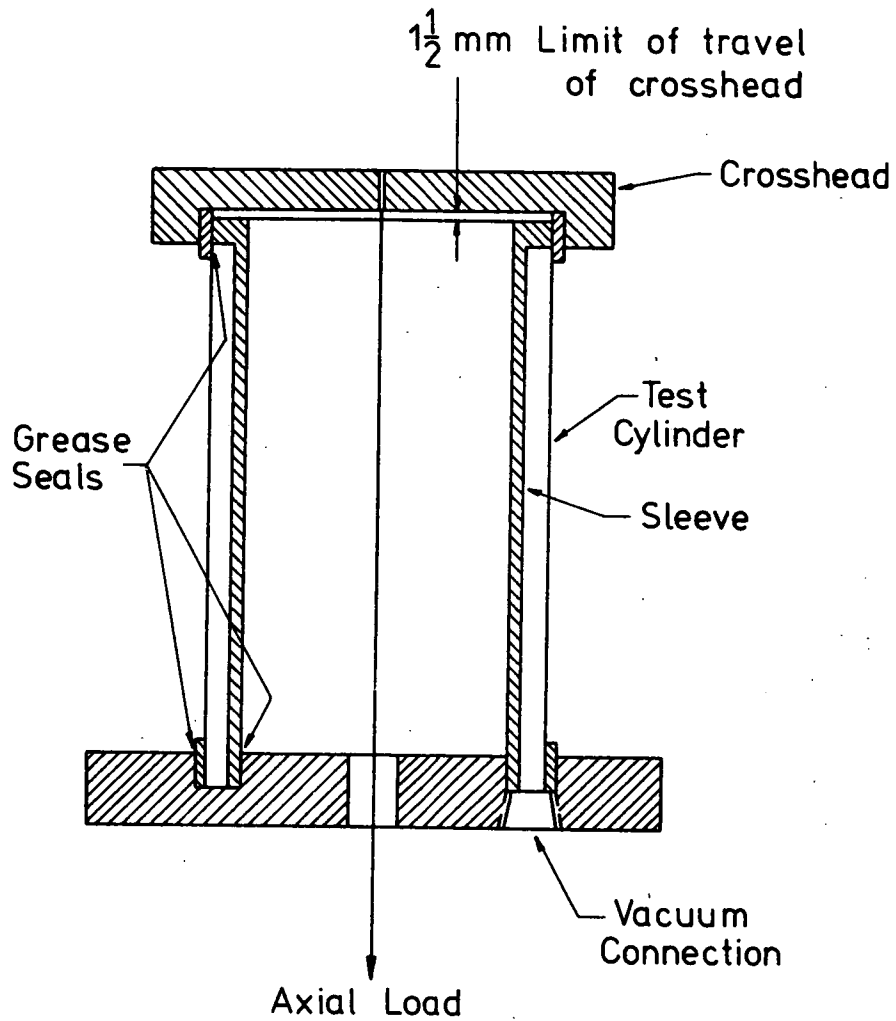
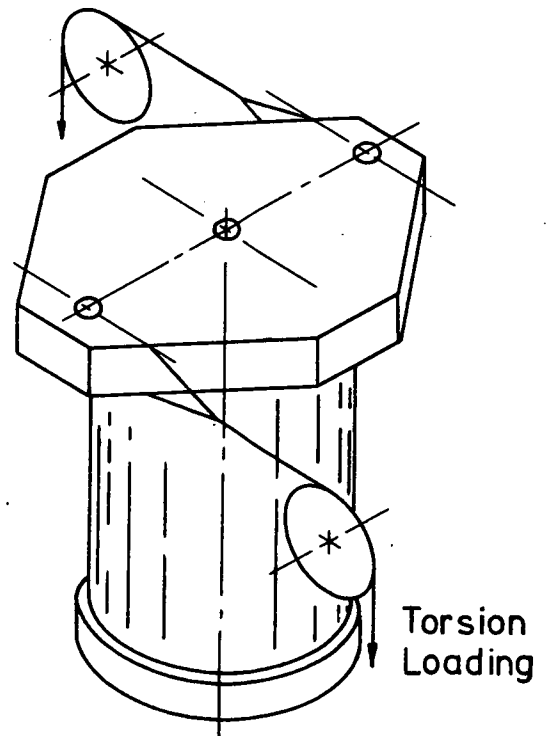


FIGURE 1·7  
LOADING JIG FOR TESTING  
BUCKLING OF CYLINDERS  
IN COMBINED LOADING



variation in the calculated value of buckling stress. The<sup>16.</sup> value of 0.35 was assumed on the basis that both perspex and araldite have values around this figure.

A glance at table 1.2 will show that, as anticipated, the design formulae for axial compression gave values that are too large for this particular cylinder. Thus it could be assumed that the imperfections in shape are much larger in this relatively crudely made cylinder than the design formulae allow. In the case of torsion loading the design formulae could be considered as just adequate. Imperfections do not have as large an effect in torsion as with axial compression which could account for this improvement. With hoop compression, the design formulae appear quite safe. In this case imperfections have the least effect on stability. By internally pressurising, the stiffening of the cylinder for both axial compression and torsion greatly exceeded the design figures. The photograph shown in figure 1.2 is this cylinder under axial compression. The diamond pattern is well established with the axis of the diamond at right angles to the more negative principal stress direction. In torsion loading a similar faceted pattern was obtained (figure 1.4) with the axis of the pattern again at right angles to the more negative principal stress direction. With internal vacuum (or external pressure) the more negative principal stress had rotated a further  $45^{\circ}$  and the axis of the buckle pattern was parallel to the axis of the cylinder (figure 1.5).

Figure 1.8 illustrates the buckling modes for various combinations of loading and in each of these photographs the principal stress directions are marked to illustrate the orientation of the buckle pattern. A summary of the measured nominal stresses at collapse for this cylinder in all the test conditions is given in table 1.3. These values are plotted in figures 1.9 and 1.10 to illustrate the interaction between the various buckling modes. In figure 1.9 the interaction between torsion and axial compression is illustrated while in figure 1.10, torsion is used as the parameter of the graph of the interaction between axial compression and hoop compression, i.e. figure 1.9 appears as the Y axis in figure 1.10.

Baker, Kovalevsky and Rish (ref. 11) give a general relation between buckling <sup>loads</sup> ~~modes~~ as,

$$A^x + B^y + C^z = 1 \text{ ----- } 1.2$$

Where A,B and C are the ratios of the nominal stress at collapse in the combined case for a particular mode, to the nominal stress at collapse if the cylinder was to buckle in that mode only. They then go on to establish values for the indices in two combinations,

$$\frac{\sigma_a}{\sigma_{a_c}} + \left(\frac{\tau}{\tau_c}\right)^2 = 1 \text{ ----- } 1.3$$

and  $\frac{\sigma_a}{\sigma_{a_c}} + \frac{\sigma_h}{\sigma_{h_c}} = 1 \text{ ----- } 1.4$

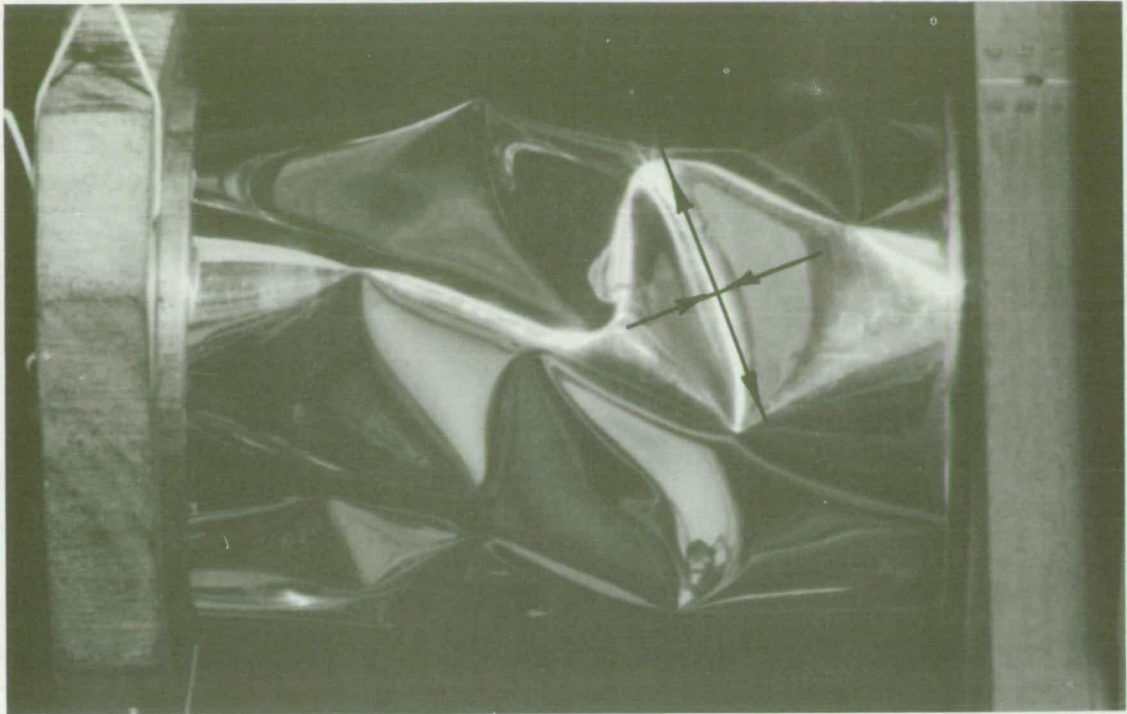
TABLE 1.2

## DETAILS OF CYLINDERS TESTED IN COMBINED LOADING

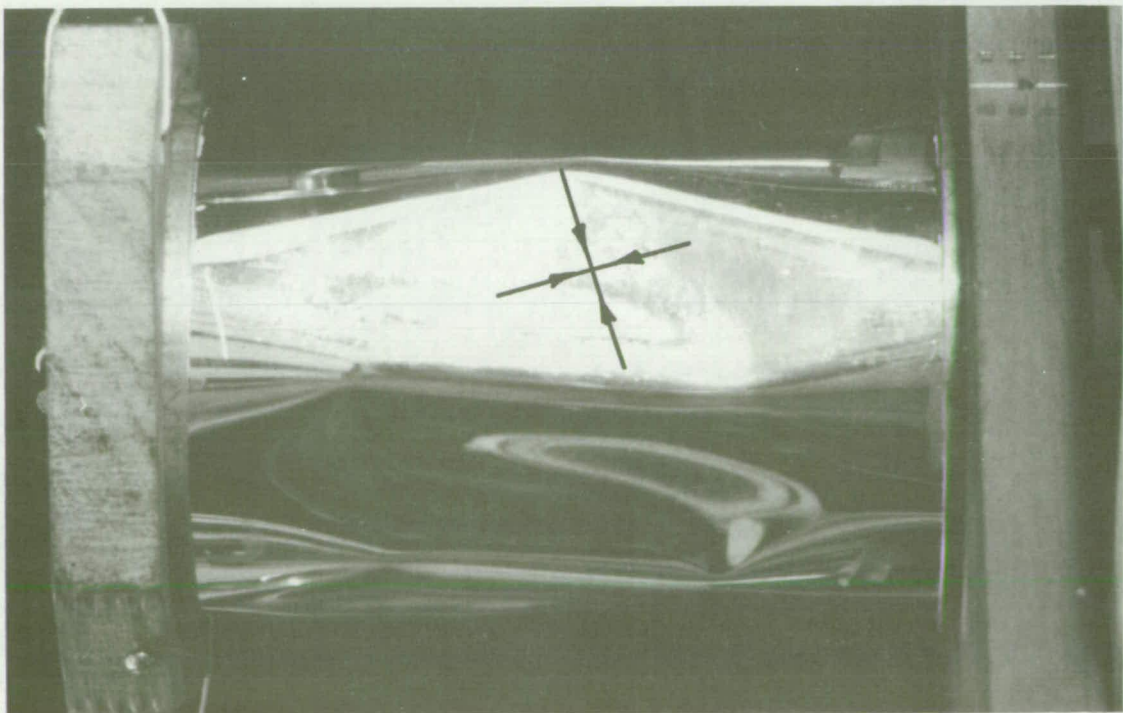
CYLINDER									STRESSES AT COLLAPSE								
	MATERIAL	E	$\nu$	R	T	L	R/T	L/R	AXIAL COMPRESSION			TORSION			EXTERNAL PRESSURE		
									ROARK	BAKER	MEASURED	ROARK	BAKER	MEASURED	ROARK	BAKER	MEASURED
		GPa		mm.	mm.	mm.			MPa	MPa	MPa	MPa	MPa	MPa	MPa	MPa	MPa
1	MELANEX	5.6	0.35*	44.5	0.1	127	445	2.85	3.10	2.62	1.16	0.82	0.91	0.98	0.19	0.16	0.23
	INTERNALLY PRESSURISED								----	1.53**	1.95	----	1.01**	1.76	----	----	----
2	MELANEX	5.6	0.35*	44.5	0.1	127	445	2.85	3.10	2.62	1.89	0.82	0.91	1.34	0.19	0.16	0.31
3	BRASS	106	0.32	44.5	0.025	125	1780	2.81	16.7	5.81	4.77	2.69	2.45	2.38	0.43	0.39	1.13
4	BRASS	106	0.32	44.5	0.075	125	593	2.81	43.6	31.6	9.24	----	----	----	----	----	----
5	BRASS	106	0.32	44.5	0.025	125	1780	2.81	16.7	5.81	4.20	2.69	2.45	1.77	0.43	0.39	1.22
6	MELANEX	5.6	0.35*	23.4	0.05	133	468	5.68	2.95	2.43	2.56	0.90	0.60	0.75	0.076	0.074	0.18
7	MELANEX	5.6	0.35*	23.4	0.05	133	468	5.68	2.95	2.43	1.63	0.90	0.60	0.69	0.076	0.074	0.18
8	MELANEX	5.6	0.35*	44.5	0.05	125	890	2.81	1.55	0.93	1.07	0.58	0.36	0.38	0.055	0.063	0.21
9	MELANEX	5.6	0.35*	44.5	0.05	125	890	2.81	1.55	0.93	1.10	0.58	0.36	0.46	0.055	0.063	0.20
10	NYLAR	5.6	0.35*	44.5	0.15	125	297	2.81	4.65	4.65	2.93	----	----	----	----	----	----
11	MELANEX	5.6	0.35*	44.5	0.05	54	890	1.21	1.55	0.93	1.33	0.90	0.54	0.51	----	----	----
12	MELANEX	5.6	0.35*	44.5	0.05	54	890	1.21	1.55	0.93	1.09	0.90	0.54	0.68	0.13	0.14	0.27
13	MELANEX	5.6	0.35*	44.5	0.05	54	890	1.21	1.55	0.93	1.19	0.90	0.54	0.68	0.13	0.14	0.26
14	MELANEX	5.6	0.35*	44.5	0.1	54	445	1.21	3.10	2.62	3.17	2.17	1.39	1.80	0.44	0.40	0.60
15	MELANEX	5.6	0.35*	23.4	0.05	133	468	5.68	2.95	2.43	2.59	0.90	0.60	0.96	0.076	0.074	0.15

\* Value guessed as being similar to Perspex and Araldite because of the difficulty in measurement and relative unimportance in calculation. All other values measured.

\*\* Measured critical stresses used as the basis for these calculations.



A.  $\sigma_a = -0.86 \text{ MPa}$ ,  $\sigma_h = 0$   $\tau = 0.39 \text{ MPa}$ .

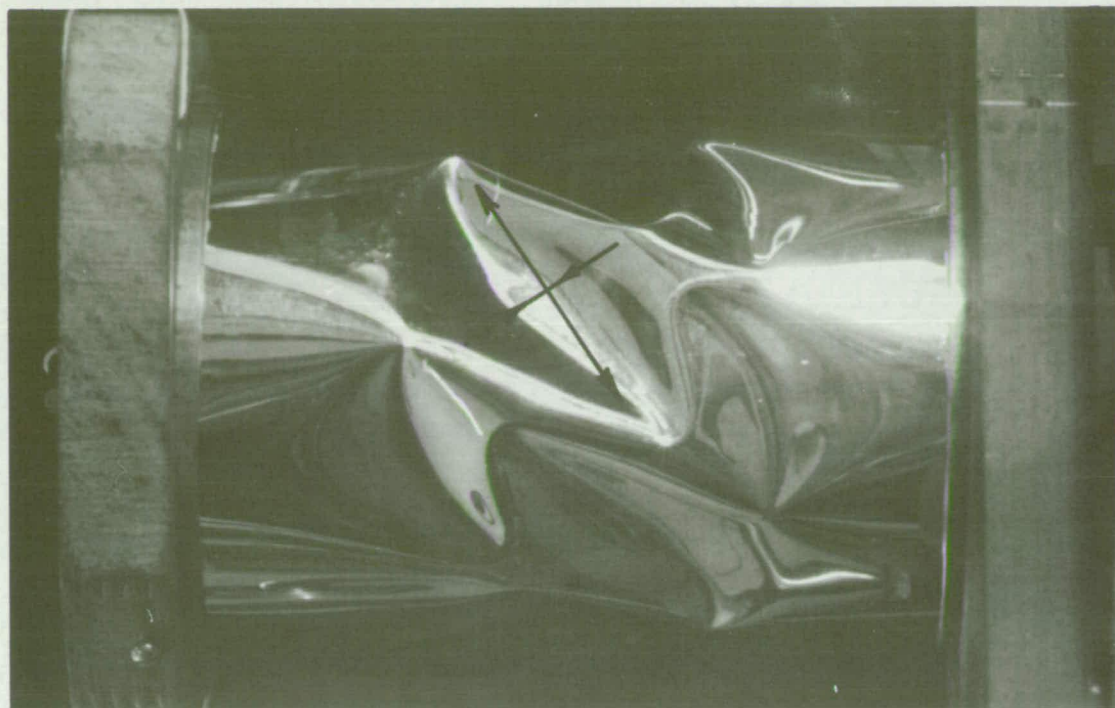


B.  $\sigma_a = -0.68 \text{ MPa}$ ,  $\sigma_h = -0.148 \text{ MPa}$ ,  $\tau = 0.19 \text{ MPa}$ .

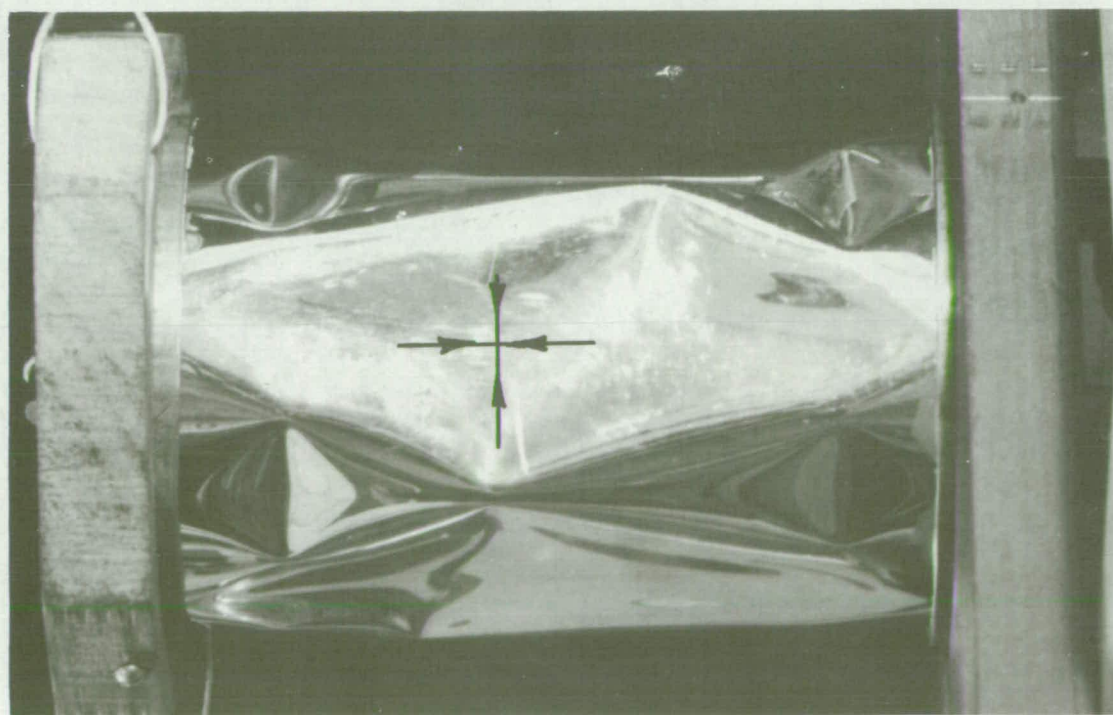
FIGURE 1.8

MELANEX CYLINDER—COMBINED LOADING





C.  $\sigma_a = -0.68 \text{ MPa}$ .  $\sigma_h = -0.044 \text{ MPa}$ .  $\tau = 0.78 \text{ MPa}$ .

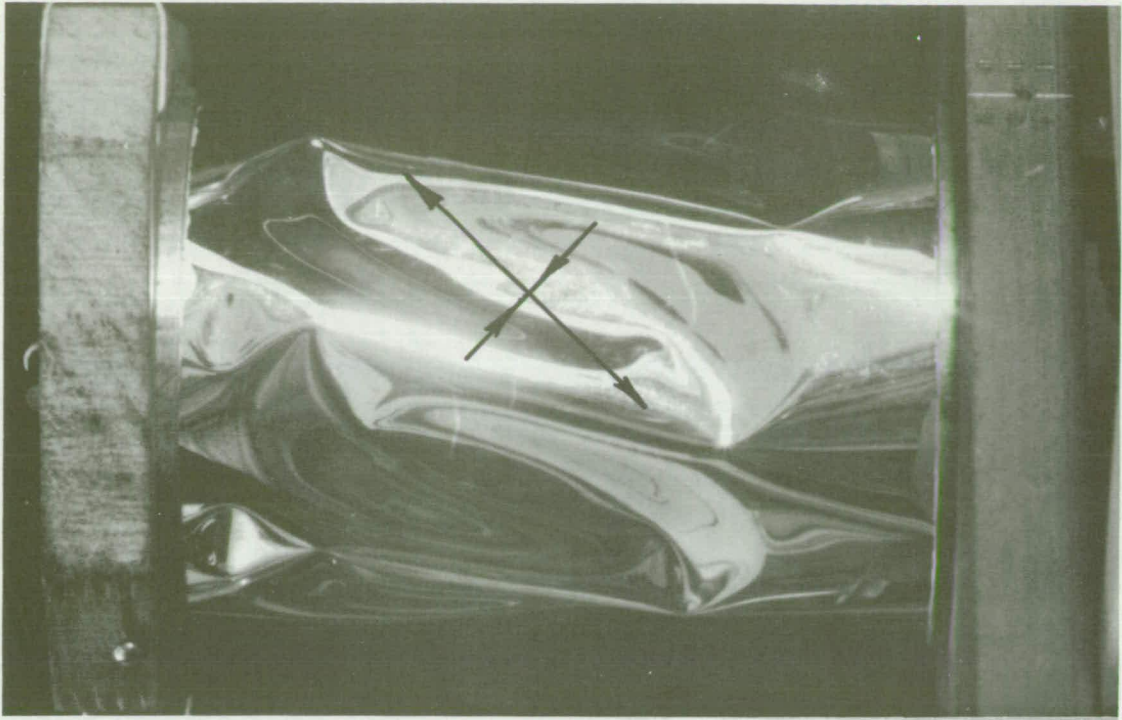


D.  $\sigma_a = -0.68 \text{ MPa}$ .  $\sigma_h = -0.201 \text{ MPa}$ .  $\tau = 0$

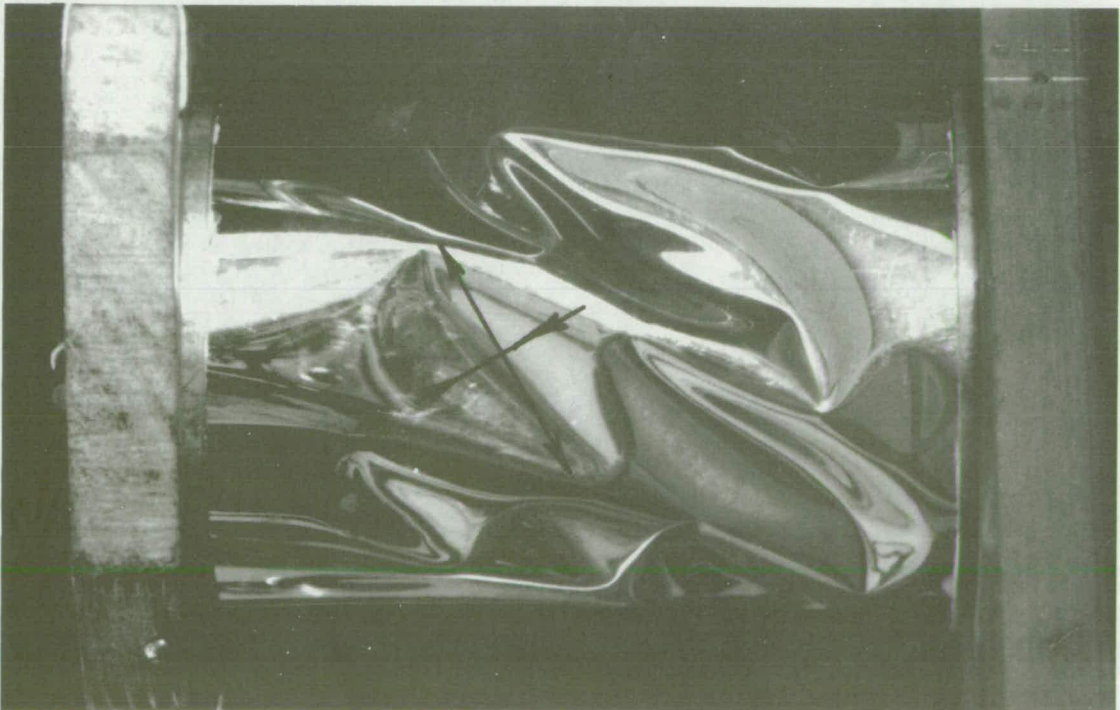
FIGURE 1.8

MELANEX CYLINDER—COMBINED LOADING





E.  $\sigma_a = -0.05 \text{ MPa}$ .  $\sigma_h = -0.113 \text{ MPa}$ .  $\tau = 0.88 \text{ MPa}$ .



F.  $\sigma_a = -1.17 \text{ MPa}$ .  $\sigma_h = +0.179 \text{ MPa}$ .  $\tau = 1.17 \text{ MPa}$ .

FIGURE 1.8

MELANEX CYLINDER—COMBINED LOADING



TABLE 1.3

NOMINAL STRESSES AT COLLAPSE FOR CYLINDER NO.1

$\sigma_a$	$\sigma_h$	$\tau$	$A_1$	$A_2$	$A_3$	$A_4$
MPa	MPa	MPa				
-1.16	0	0	1.00	1.00	1.00	1.00
-0.88	0	0.19	0.79	0.84	0.79	0.84
-0.86	0	0.39	0.89	0.99	0.89	0.99
-0.75	0	0.58	0.98	1.10	0.98	1.10
-0.44	0	0.78	0.99	1.09	0.99	1.09
-0.05	0	0.98	1.00	1.00	1.00	1.00
-0.05	-0.231	0	1.00	1.00	1.00	1.00
-0.96	-0.144	0	1.04	1.04	1.16	1.16
-0.68	-0.148	0.19	0.90	0.95	1.01	1.06
-0.68	-0.144	0.39	1.01	1.11	1.11	1.20
-0.68	-0.096	0.58	1.05	1.17	1.13	1.24
-0.68	-0.044	0.78	1.22	1.33	1.25	1.35
-0.68	-0.201	0	1.05	1.05	1.17	1.17
-0.40	-0.201	0	0.94	0.94	1.01	1.01
-0.40	-0.192	0.19	0.94	0.99	1.01	1.06
-0.40	-0.166	0.39	0.95	1.05	1.02	1.11
-0.40	-0.153	0.58	1.08	1.20	1.15	1.26
-0.40	-0.105	0.78	1.18	1.28	1.23	1.33
-0.05	-0.231	0.19	1.04	1.09	1.04	1.09
-0.05	-0.205	0.39	1.04	1.14	1.05	1.14
-0.05	-0.179	0.58	1.11	1.23	1.12	1.23
-0.05	-0.135	0.78	1.19	1.30	1.20	1.30
-0.05	-0.113	0.88	1.27	1.34	1.27	1.34
-1.95	+0.179	0	-----	-----	-----	-----
-1.74	+0.179	0.39	-----	-----	-----	-----
-1.67	+0.179	0.78	-----	-----	-----	-----
-1.17	+0.179	1.17	-----	-----	-----	-----
-0.82	+0.179	1.56	-----	-----	-----	-----
-0.12	+0.179	1.76	-----	-----	-----	-----

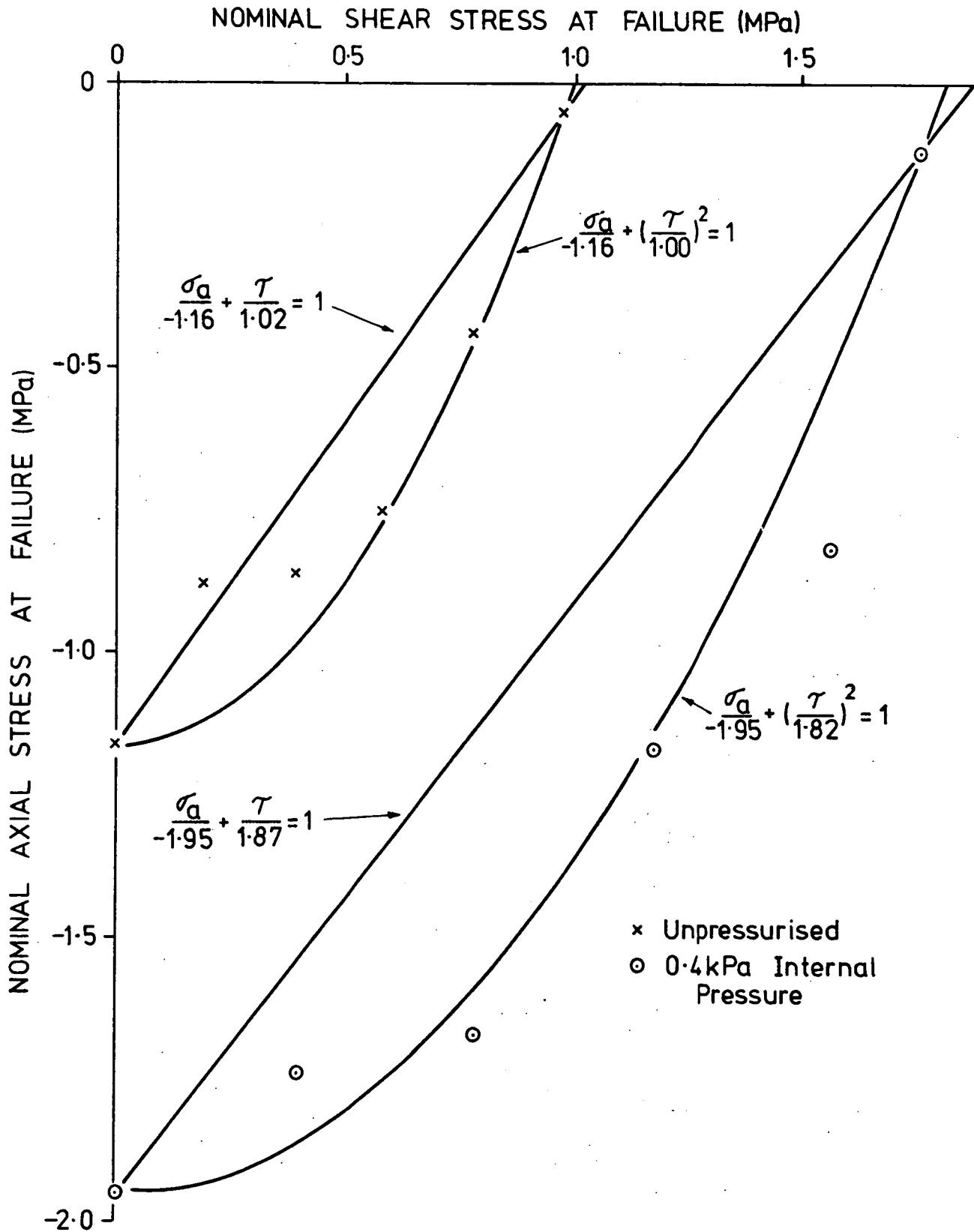
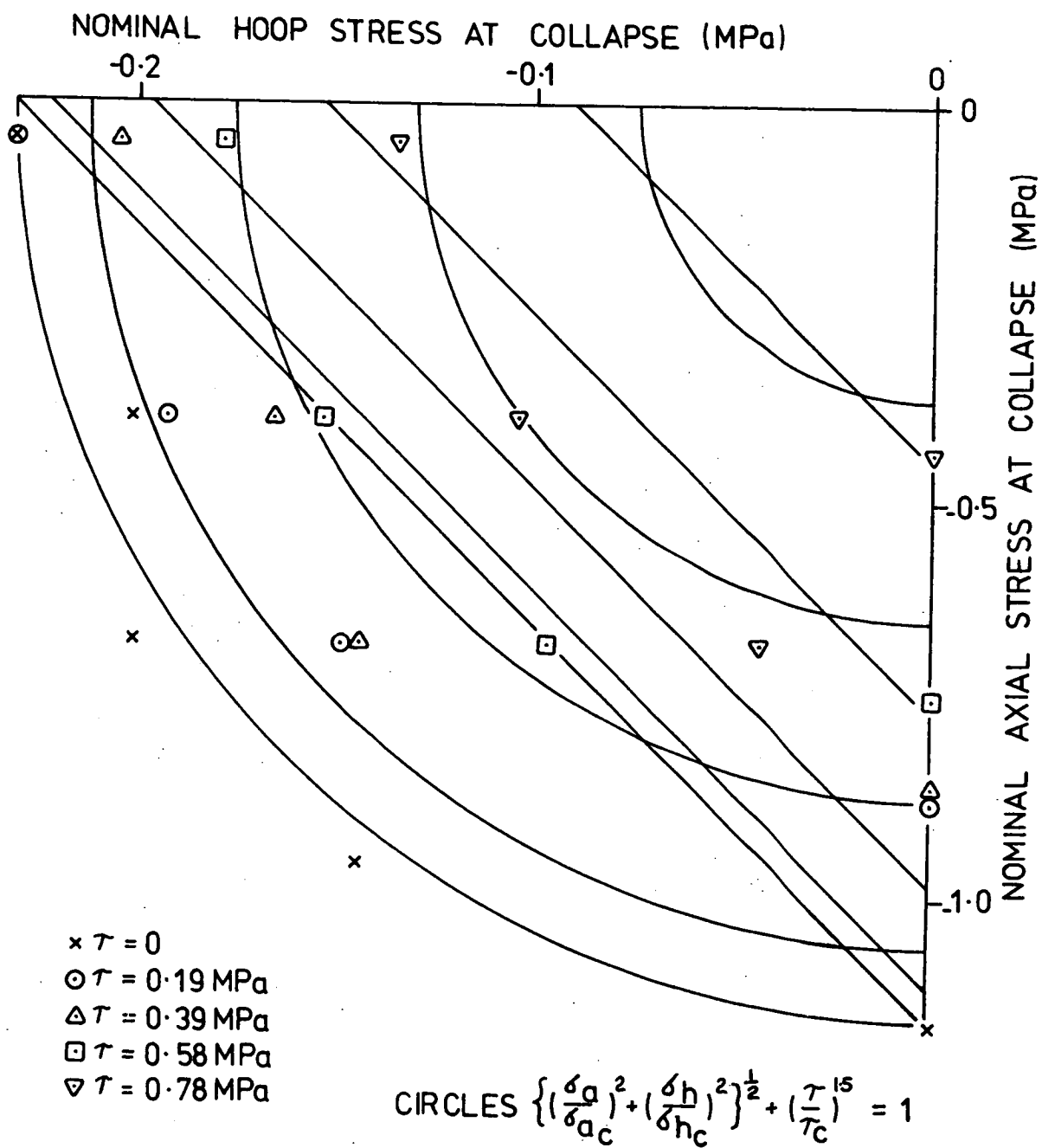


FIGURE 1.9

BUCKLING STRESS STATE DIAGRAM FOR AXIAL  
COMPRESSION - TORSION INTERACTION IN FIRST  
MELANEX CYLINDER



**FIGURE 1-10**  
**BUCKLING STRESS STATE DIAGRAM**  
**INTERACTION OF BUCKLING MODES - CYLINDER No 1**

Equation 1.3 is plotted as the curved line in figure 1.9 for both the unpressurised and the pressurised conditions. Immediately, it is apparent that some of the test points were well inside this curve. Thus it was considered that perhaps the formula 1.3 may not be completely safe. In figure 1.10 the combination of equations 1.3 and 1.4 given below was plotted as the series of straight lines.

$$\frac{\sigma_a}{\sigma_{a_c}} + \left(\frac{\tau}{\tau_c}\right)^2 + \frac{\sigma_h}{\sigma_{h_c}} = 1 \text{ ----- 1.5}$$

Here it can be seen that the only test points to fail this condition are those on the Y axis, i.e. those that had already failed the condition given by equation 1.3. Thus it was apparent that for this cylinder at least, equation 1.5<sup>5</sup> was very conservative. In plotting this and all other curves  $\sigma_{a_c}$  was taken as the value measured in axial compression alone.  $\sigma_{h_c}$  and  $\tau_c$  were based on the values measured with internal vacuum combined with the weight of the crosshead only and the combination of crosshead weight and torsion loading.

So as to more nearly represent the actual combined loading conditions the following relations were considered.

$$\left\{ \left(\frac{\sigma_a}{\sigma_{a_c}}\right)^2 + \left(\frac{\sigma_h}{\sigma_{h_c}}\right)^2 \right\}^{\frac{1}{2}} + \left(\frac{\tau}{\tau_c}\right)^2 = A1 \text{ ----- 1.6}$$

$$\left\{ \left(\frac{\sigma_a}{\sigma_{a_c}}\right)^2 + \left(\frac{\sigma_h}{\sigma_{h_c}}\right)^2 \right\}^{\frac{1}{2}} + \left(\frac{\tau}{\tau_c}\right)^{1.5} = A2 \text{ ----- 1.7}$$

$$\left\{ \left( \frac{\sigma_a}{\sigma_{a_c}} \right)^{1.5} + \left( \frac{\sigma_h}{\sigma_{h_c}} \right)^{1.5} \right\}^{0.667} + \left( \frac{\tau}{\tau_c} \right)^2 = A3 \text{ --- } 1.8$$

$$\left\{ \left( \frac{\sigma_a}{\sigma_{a_c}} \right)^{1.5} + \left( \frac{\sigma_h}{\sigma_{h_c}} \right)^{1.5} \right\}^{0.667} + \left( \frac{\tau}{\tau_c} \right)^{1.5} = A4 \text{ --- } 1.9$$

In these equations the quantities A1, A2, A3 and A4 represent the goodness of fit of the relation to the actual loading condition. If the relation was to truly represent the buckling state in the combined mode then the value of the constant would be unity. Because of the doubt observed in the square law relation for torsion axial compression interaction it was necessary to consider a relation with a lower index. Similarly, the linear relation for axial compression- hoop compression interaction was observed to be very conservative. Thus higher power relations were considered necessary. These considerations account for the four equations given above. Equation 1.7 is plotted as a series of circles in figure 1.10 for A2 equal to unity. Clearly this relation is not an unrealistic relation for the combined loading conditions. In table 1.3 the values of A1, A2, A3 and A4 are given for each of the collapse conditions measured.

Because of the apparent discrepancy between measured conditions and published information several more cylinders were made and tested in the combined load state. Details of these cylinders and the collapse loads in the independent buckling modes are listed in table 1.2.

For all the remaining cylinders an attempt was made at manufacturing more nearly perfect cylinders than the first cylinder tested. In the case of cylinders nos. 2 to 9 the seam was made again as a butt joint with cellulose adhesive tape overlapping the ends. However the material was first wrapped around a mandrel to keep the edges flat and straight and avoid obvious wrinkles along the seam. For cylinders nos. 10 to 15 another important improvement was made in that instead of a butt joint a small overlap of cylinder material was provided and covered with cellulose adhesive tape. Because of the method of fixing the cylinder to the brass end support rings it was found to be impossible to provide a satisfactory glued longitudinal seam. Three materials were used although it is understood that mylar and melanex are different trade names for effectively the same product. Because melanex was considered to be a less than ideal test material (low Young's modulus and low creep resistance) some cylinders were also made from brass shim. These brass cylinders were found to be even less satisfactory in practice though useful results were obtained from them. The shim as supplied had a large number of wrinkles forming rather severe imperfections. With the first collapse of these cylinders some permanent damage was observed which appeared to increase the size of the imperfections and reduce the buckling load when the cylinder was retested. However after several applications of load, the load carrying capacity stabilised and it is this stabilised figure that is given in table 1.2. These

cylinders were loaded first in axial compression and then in torsion. The same type of phenomenon was observed in torsion but subsequent loading in axial compression appeared to be unaffected. A similar effect was also detected with hoop compression. Thus it would seem that the permanent damage sustained by the cylinder served to increase the size of the initial imperfections but the imperfections controlling each buckling mode appeared to be independent.

Cylinder no. 4 (the thick brass cylinder) and cylinder no. 10 (the mylar cylinder, i.e. thickest plastic) were both so severely damaged after the first loading that no further testing was possible.

An interesting phenomenon was observed with the melanex cylinders. Sometimes the results appeared to be a little suspect, as though the cylinder had suffered a small amount of permanent damage. In such cases the tests could be repeated after a short interval because the melanex was able to recover its initial shape.

From table 1.2 it can be seen that it would be wise not to use the formulae from Roark for design in axial compression or torsion. Both Roark and Baker, Kovalevsky and Rish appear to be satisfactory in hoop compression. In torsion the design criterion of Baker, Kovalevsky and Rish appears to be satisfactory although two cylinders failed at loads less than the design figure.

These were the brass cylinders which had already undergone some permanent damage so it is not surprising that they failed at a lower figure. In axial compression the Baker, Kovalevsky and Rish design condition was not always met. It is interesting to note, however, that for the later cylinders where the manufacturing technique had improved their criterion was satisfied. This indicates the importance of the magnitude of the imperfections.

The results of the collapse tests on these cylinders are summarised in tables A1 to A12 (Appendix A). Figures A1, A2 and A3 show the axial compression-torsion interaction for the three basically different length to radius ratios. From these graphs it can be seen that <sup>for the cylinders investigated</sup> length has virtually no effect on the collapse condition. Also some doubt must exist about the square law relation. The power index of 1.5 appears to be a more satisfactory relation though it seems that different cylinders could possibly follow different rules. An explanation for this may be in the measurement of the pure axial compression load and pure torsion load. However, these loads and the hoop compression load were checked many times throughout the duration of the test on each cylinder so that they would be well established. This procedure ensured that these values were established in the worst case to within 5%. However, combined load measurements in some cases may have been in error by up to about 10% of the independent critical load.



The combined axial compression, torsion and hoop compression buckling conditions are presented for these cylinders as figures A4 to A14. As well as cylinders nos. 4 and 10 which were permanently damaged on first loading, there is no combined loading graph for cylinder no. 11. This was because cylinder no. 11 also suffered some severe damage before hoop compression tests could be conducted. Cylinder no. 6 also suffered some permanent damage early in the testing cycle thus severely limiting its usefulness. In all these graphs circles are drawn representing the square relationship between hoop compression and axial compression. In some of them the relation for a power law with index of 1.5 is also plotted.

Some interesting observations can be made from these graphs.

1. The linear relation between the two compression modes as recommended by Baker, Kovalevsky and Rish is obviously very conservative and design savings can be achieved over their criterion when combined loading is present.

2. The square-square relation (equations 1.6 and 1.7) appeared to be satisfactory for some cylinders but not for others where the index of 1.5 was more satisfactory. This change appeared to be concerned with the cylinder behaviour as a whole and not just with a scatter of results. It is possible that the quality of the seam may have had something to do with this change. The situation also appeared to occur to a lesser extent with axial compression, torsion interaction (see figure A3 in particular).

3. Cylinder no.15 was perhaps the best manufactured cylinder and by this time the testing procedure was also well established so that good reliable results were obtained. It is interesting to note that in figure A14 the test points appear to follow a distinct pattern which is slightly conservative when compared to a square-square relation. In fact it is possible to infer from figure A14 that two separate conditions could exist providing two intersecting curves. These conditions correspond to basically an axial compression failure with the collapse load modified by the hoop compression and vice versa. At about the point that these two conditions would intersect on the graph a physical change in the buckling mode was detected during the test. Having observed this phenomenon with cylinder no.15 a review of the remaining graphs showed that a similar trend may have occurred earlier (see in particular graphs A6,A7,A11 and A12 ). No attempt has been made to statistically analyse these test results. Such an analysis would be meaningless because of the basic change in the nature of the interaction conditions between cylinders.

These tests on cylinder collapse in combined loading serve to illustrate the difficulties associated with this topic. A great deal of the scatter is associated with shape imperfections in the cylinders. It was also pointed out earlier in the chapter that the Von Karman and Tsien approach was inappropriate. In the ensuing chapters

theory is developed in an attempt to satisfactorily describe the collapse of cylinders in axial compression and to correlate this theory with laboratory measurements. The investigation here is limited to axial compression only. Combined loading conditions must be considered as scope for further expansion of the work.

NOTATION--CHAPTER 1

$E$	Young's modulus.
$L$	Cylinder length.
$R$	Cylinder radius.
$T$	Wall thickness.
$\nu$	Poisson's ratio.
$\sigma_a$	Nominal axial stress at collapse in combined mode.
$\sigma_h$	Nominal hoop stress at collapse in combined mode.
$\tau$	Nominal shear stress at collapse in combined mode.
$\sigma_{a_c}$	Nominal axial stress at collapse when loaded solely in axial compression.
$\sigma_{h_c}$	Nominal hoop stress at collapse when loaded solely in hoop compression.
$\tau_c$	Nominal shear stress at collapse when loaded solely in torsion.

# CHAPTER 2

## A NEW THEORY

## CHAPTER 2

### A NEW THEORY FOR THE BUCKLING OF THIN CYLINDERS IN AXIAL COMPRESSION

In the preceding discussion it was pointed out that the usual Von Karman and Tsien approach to the solution of the buckling problem was found by Hoff, Madsen and Mayers to be inappropriate. For many years a large number of researchers have endeavoured to find a satisfactory description of the collapse behaviour of cylinders in this mode but all efforts have been in vain. Esslinger and Geier (ref. 13) sum up the situation when they state.

"The history of the investigations on the postbuckling behaviour of thin walled cylindrical shells under axial load can be compared to that of the days of

Gold Rush in Wild West, with seekers of El Dorado finding some small prize amidst much disappointment but with unshakable hope."

In spite of this background a new theory is advanced in this chapter for the buckling of cylinders in axial compression. This theory appears to offer a satisfactory explanation of a great deal of the buckling (and postbuckling) behaviour of thin walled cylindrical shells loaded in axial compression. It was developed primarily from a consideration of the geometry of the Yoshimura buckle pattern and achieved through the manufacture of a number of models folded from sheets of paper. The development of this theory is an excellent example of the importance of models in an engineering investigation.

When a sheet of paper is folded into the shape of a Yoshimura pattern the model obtained is very definitely a structure capable of sustaining a substantial axial load. This observation is contrary to the conclusions reached by Hoff, Madsen and Mayers. One explanation for the discrepancy that has (in the past) been proposed is that the folds in the Yoshimura pattern have a certain bending rigidity and it is this action that supports the load. Certainly the bending action, by itself, cannot support the load since if a piece of paper is folded into a Yoshimura pattern with two lobes around the circumference the model shown in figure 2.1 is obtained. This model can easily be interpreted as a series of tetrahedra joined by

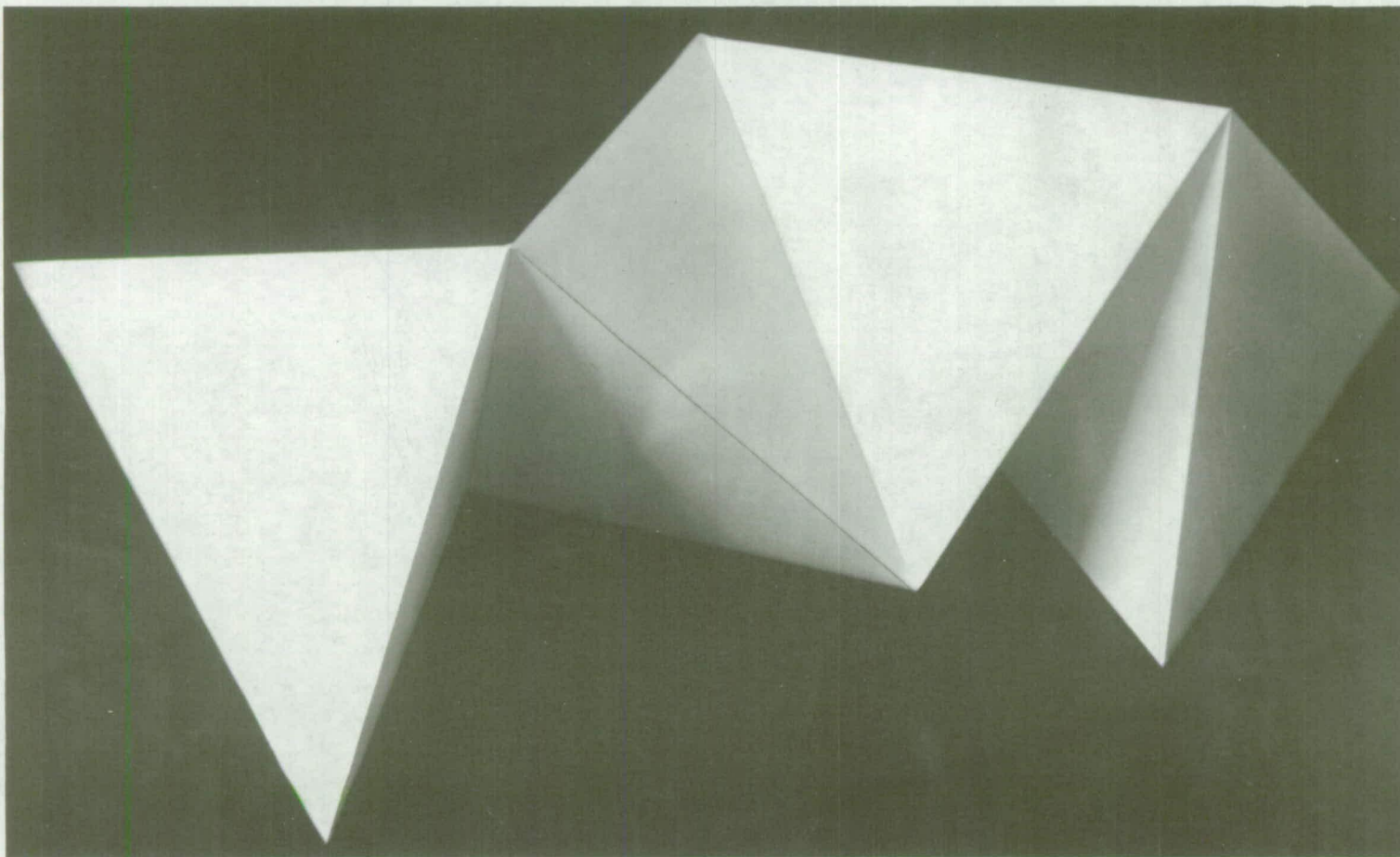


FIGURE 2.1  
YOSHIMURA PATTERN WITH  $N=2$



hinges. The hinges have almost no strength in bending but the tetrahedra themselves are reasonably robust structures. Thus shell bending does not explain the load carrying capacity in the postbuckled shape.

In a cylinder buckled into a true Yoshimura pattern and carrying some axial load each of the flat facets will have some stress distribution. If we consider any two adjacent facets then any stress in one facet perpendicular to the common fold will be matched by a similar stress in the adjacent facet. Thus a net radial force would exist along the fold and this force could only be supported if the two facets were considered collectively as an extremely wide flanged beam in bending. Clearly, the structure could not support a substantial load in this manner so we can conclude that the stress in the facets perpendicular to the folds is negligible.

Obviously, if there is very small stress in the facets perpendicular to the folds then the load must be carried by stresses parallel to the folds. Some distance away from the fold these stresses would be relieved due to the flexibility of the shell. Thus the load is carried principally along the folds and the structure can be considered as a space frame with slender members located along these folds (figure 2.2). The members would be wide flanged angles effectively pin-jointed with the load applied through the corner of the angle. It has already been demonstrated that the folds have very small strength in bending (figure 2.1) so the assumption of pin ends is reasonable.

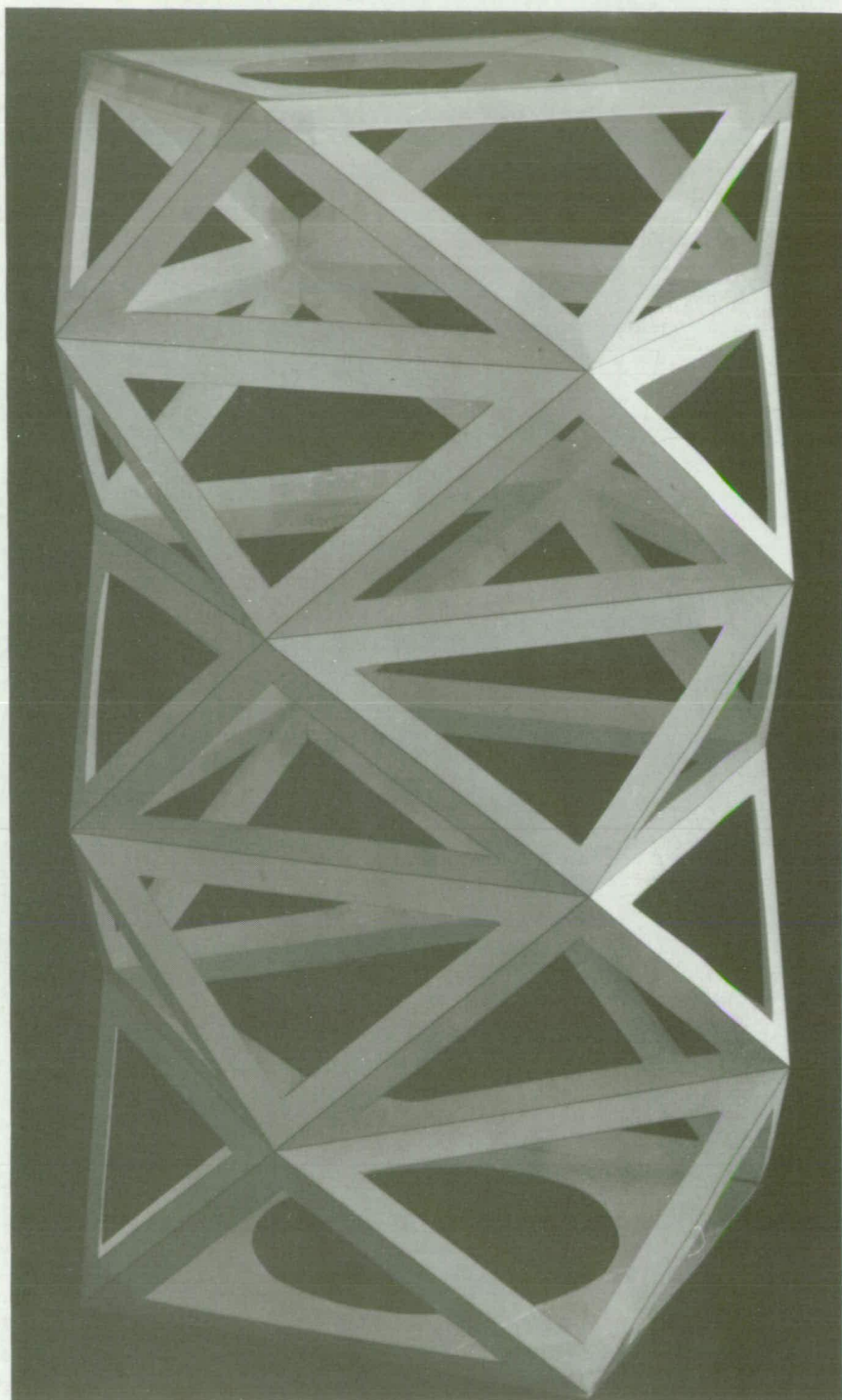


FIGURE 2.2  
SPACE FRAME MODEL

The geometry of the space frame is illustrated in figure 2.3 and from this geometry the following relations can be derived.

$$\phi = \frac{2\pi}{N} \text{-----} 2.1$$

$$\begin{array}{l} \text{Axial length of} \\ \text{facet (DE)} \end{array} = L_2 \left\{ 1 - \left( \frac{L_1}{2 \cdot L_2} \right)^2 \frac{(1 - \cos(\phi/2))}{(1 + \cos(\phi/2))} \right\}^{\frac{1}{2}} \text{--} 2.2$$

$$\begin{array}{l} \text{Axial deflection} \\ \text{(unloaded)} \end{array} = L_2 - L_2 \left\{ 1 - \left( \frac{L_1}{2 \cdot L_2} \right)^2 \frac{(1 - \cos(\phi/2))}{(1 + \cos(\phi/2))} \right\}^{\frac{1}{2}} \text{-----} 2.3$$

The angle ( $\theta$ ) between adjacent facets along the diagonal can be shown to be

$$\theta = 2 \cdot \cos^{-1} \left[ \frac{\sin(\phi/2)}{2 \cdot \cos(\phi/4)} \left\{ 1 + \left( \frac{L_1}{2 \cdot L_2} \right)^2 \right\}^{\frac{1}{2}} \right] \text{-----} 2.4$$

From a consideration of axial equilibrium we can calculate the force in the diagonal members.

$$P_1 = \frac{P}{2 \cdot N} \left\{ \frac{1 + \left( \frac{L_1}{2 \cdot L_2} \right)^2}{1 - \left( \frac{L_1}{2 \cdot L_2} \right)^2 \frac{(1 - \cos(\phi/2))}{(1 + \cos(\phi/2))}} \right\}^{\frac{1}{2}} \text{---} 2.5$$

And from radial equilibrium at a node we obtain.

$$P_2 = \frac{-P_1}{(1 + \cos(\phi/2)) \left\{ \left( \frac{L_2}{L_1} \right)^2 + \frac{1}{4} \right\}^{\frac{1}{2}}} \text{-----} 2.6$$

Thus for a given axial load on the cylinder (P) the load in the diagonal member ( $P_1$ ) is of the same sign (both compressive in a buckling situation) while the

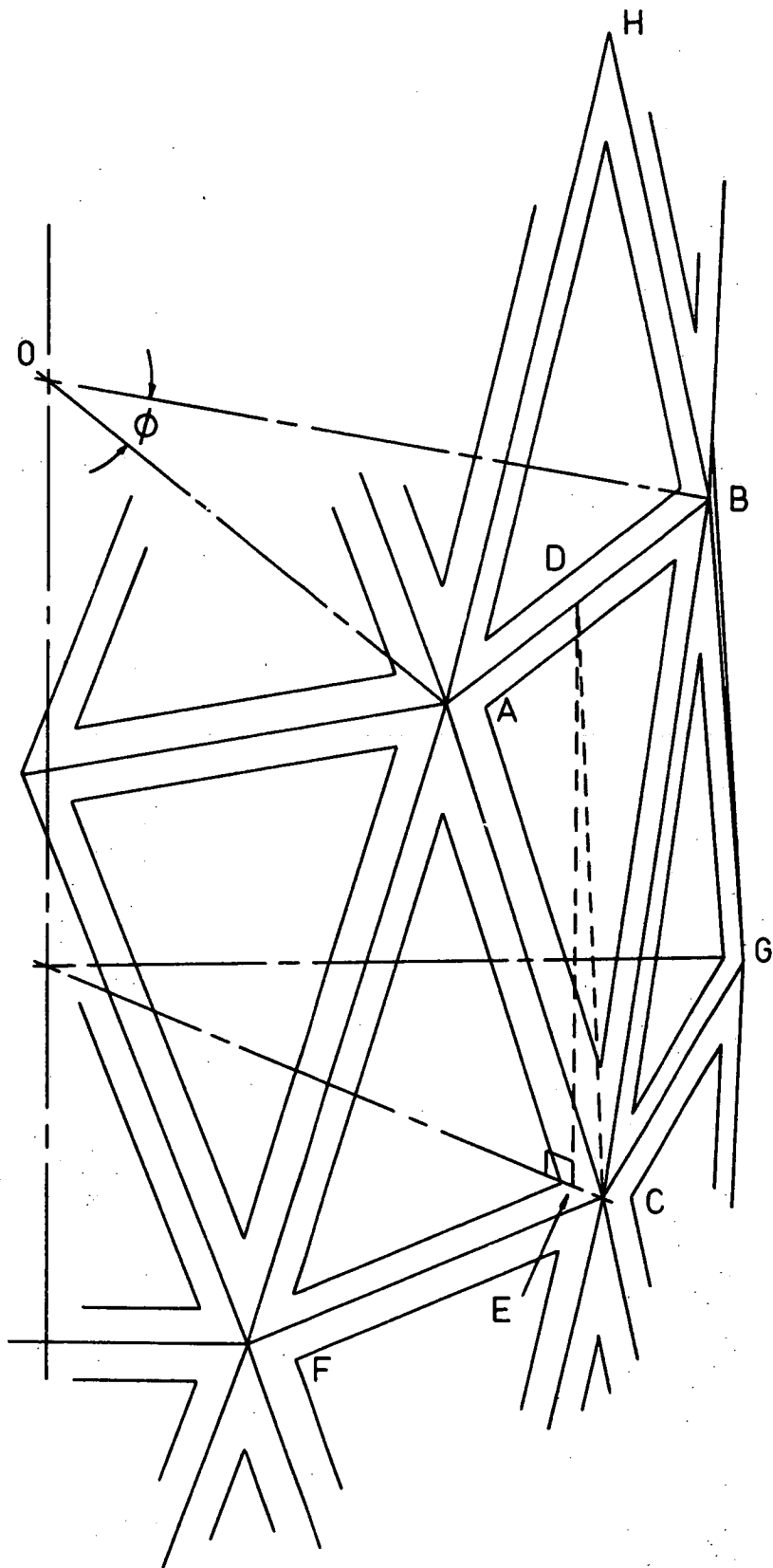


FIGURE 2.3  
SPACE FRAME REPRESENTATION OF  
YOSHIMURA PATTERN

load in the tangential member is opposite in sign. Since the space frame has compression members these may in turn collapse through buckling. Suppose AC (figure 2.3) is to collapse through buckling then all the other members remain somewhat in their original positions but AC vanishes and in its place there is a new member FB. The angle between the facets HAB and ABC becomes  $180^\circ$  so that this member also vanishes and we are left with another form of Yoshimura pattern with larger facets ( a second buckling mode ). The members HF and HB are compressive members and both can be shown to support the same load and both have the same angle between the facets. The tensile member is FF. Figure 2.4 shows a series of paper models. On the left is the conventional Yoshimura pattern with  $N=16$ . The second model is the corresponding second buckling mode assuming the entire cylinder collapses into this shape. Obviously the compression members in this second mode can buckle but since both carry the same load the long member will collapse first. The resulting buckled shape is similar to the first form but with half as many facets. The procedure can be repeated until complete collapse has been achieved. In this case  $N=2$  which is flat because  $L_1=2.L_2$ .

Two significant changes in geometry occur in the formation of this second mode. Firstly, the cross section of the pattern is no longer a regular polygon. In collapsing member AC (figure 2.3), A and C both move closer to the axis of the cylinder and points F and B move outwards.



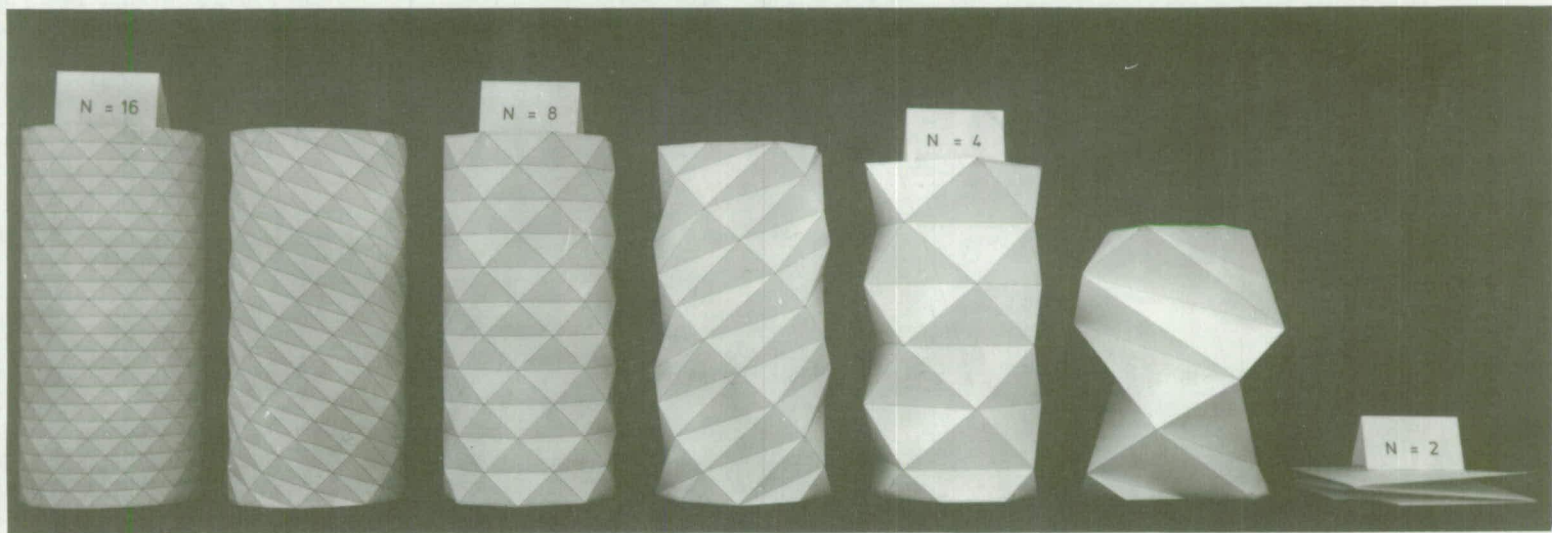


FIGURE 2.4

PAPER MODELS OF PROGRESSIVE COLLAPSE N=16 TO N=2



Secondly, there is a rotation of one end of the cylinder relative to the other. In the case of the second and sixth models in figure 2.4, this rotation is clockwise when viewed from on top.

In general, the second mode described here is not observed when testing cylinders in axial compression. However some evidence of its forming does exist. Esslinger and Geier (ref. 13) report that in testing very short cylinders with the ends free to rotate a pattern was obtained of this form (their Kreutzberg pattern). In heavily deforming cylinders it is common to see the diagonal tension member between two facets. In figure 2.5 two such diagonals are evident in a shell made from melanex. Clearly, the shell has been restrained from overall rotation so that a clockwise rotation in one section of the shell must be balanced by a corresponding anticlockwise rotation in another. To test this principle further, several models of the Yoshimura pattern were made from melanex and dead weight loaded. Typical of the results obtained is the buckle pattern shown in figure 2.6. Here, both the second buckling mode and the next standard Yoshimura pattern have formed on one side of the structure. This has led to a tilting of the free end. Thus it would seem that cylinders which are not restrained to move axially must fall over sideways once buckling has commenced.

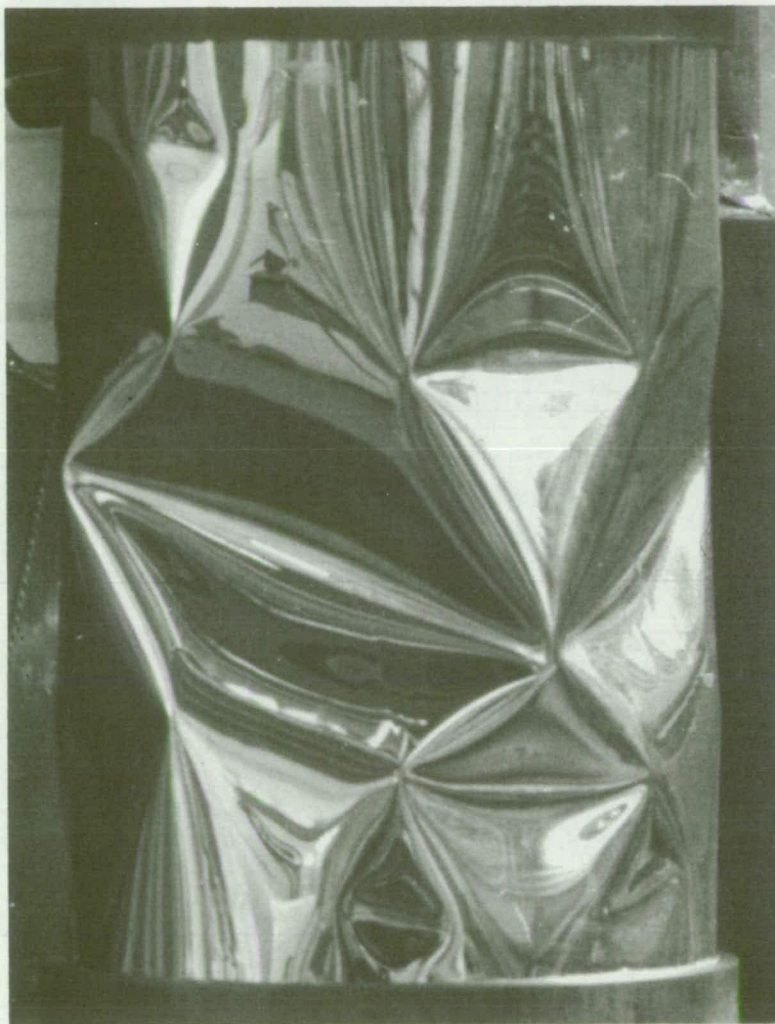


FIGURE 2.5

BUCKLED MELANEX CYLINDER  
WITH DIAGONALLY ORIENTED FACETS



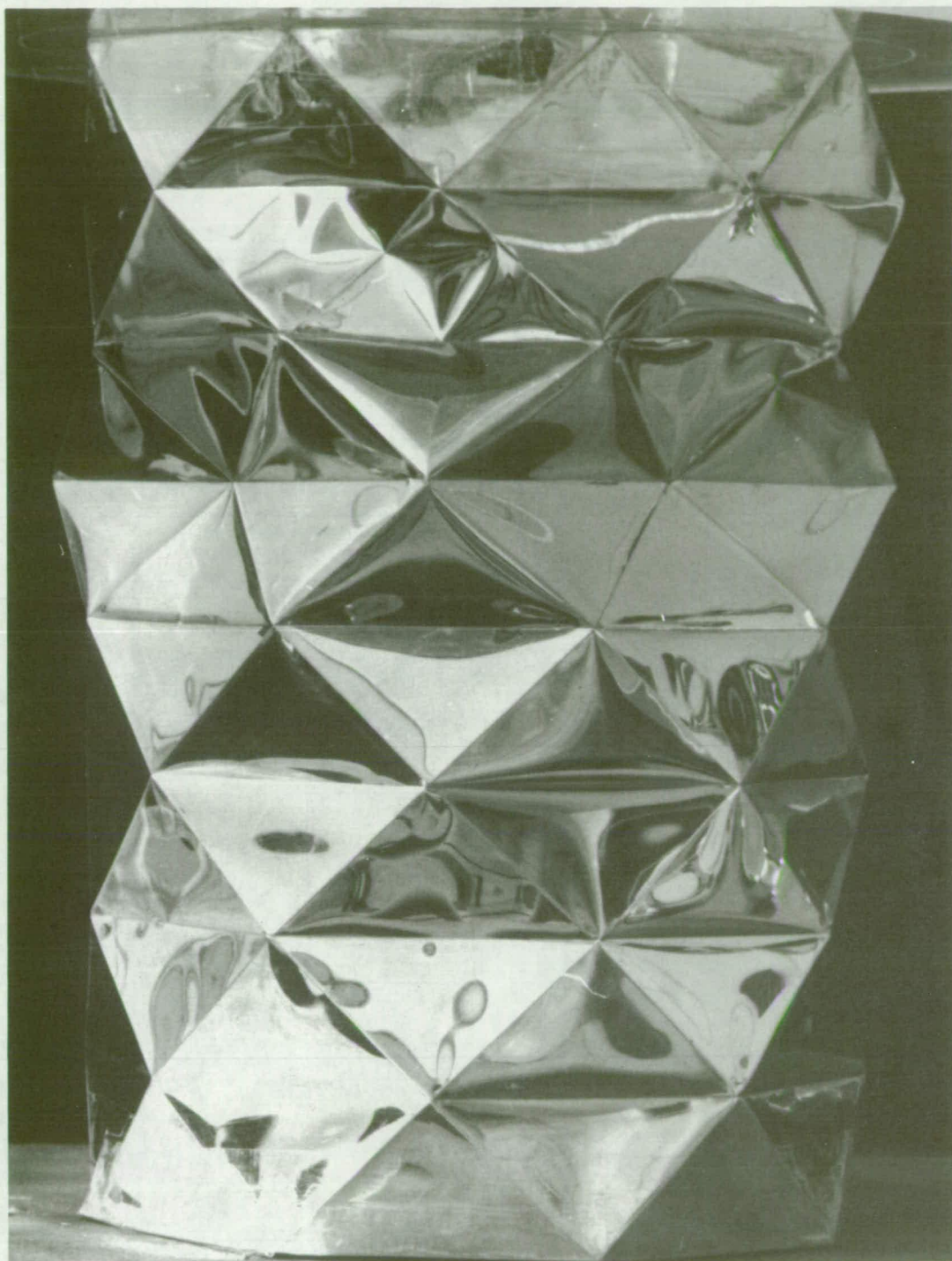


FIGURE 2.6

COLLAPSED MELANEX MODEL  
OF YOSHIMURA PATTERN

So far this discussion has centered about the collapse of structures which are true Yoshimura patterns. It is possible to consider a cylinder as a Yoshimura pattern with a very large number of facets and a corresponding large number of links in the space frame, each with a very short length. The collapse of these links could continue until we have the pattern that is so readily recognised. Unfortunately, boundary conditions on the cylinder do not permit such an idealised picture. The ends of the cylinder are usually restrained to be approximately circular and some transition is necessary between the Yoshimura pattern that may develop in the centre and the circular ends. Two possibilities for this transition are shown in figure 2.7, both of which can be seen in practical situations.

On the left of figure 2.7 is shown a paper model which has been folded so that there are four lobes in the buckled pattern at the centre of the tube, with a transition to eight, sixteen and thirty-two. This type of pattern is often seen in cylinders that have been substantially compressed after buckling has been first observed.

The model on the right of figure 2.7 illustrates a condition that occurs with somewhat less compression though still substantially more than is required to buckle the cylinder. The transition here is directly from  $N=4$  to  $N=32$ . It can be seen that there is a



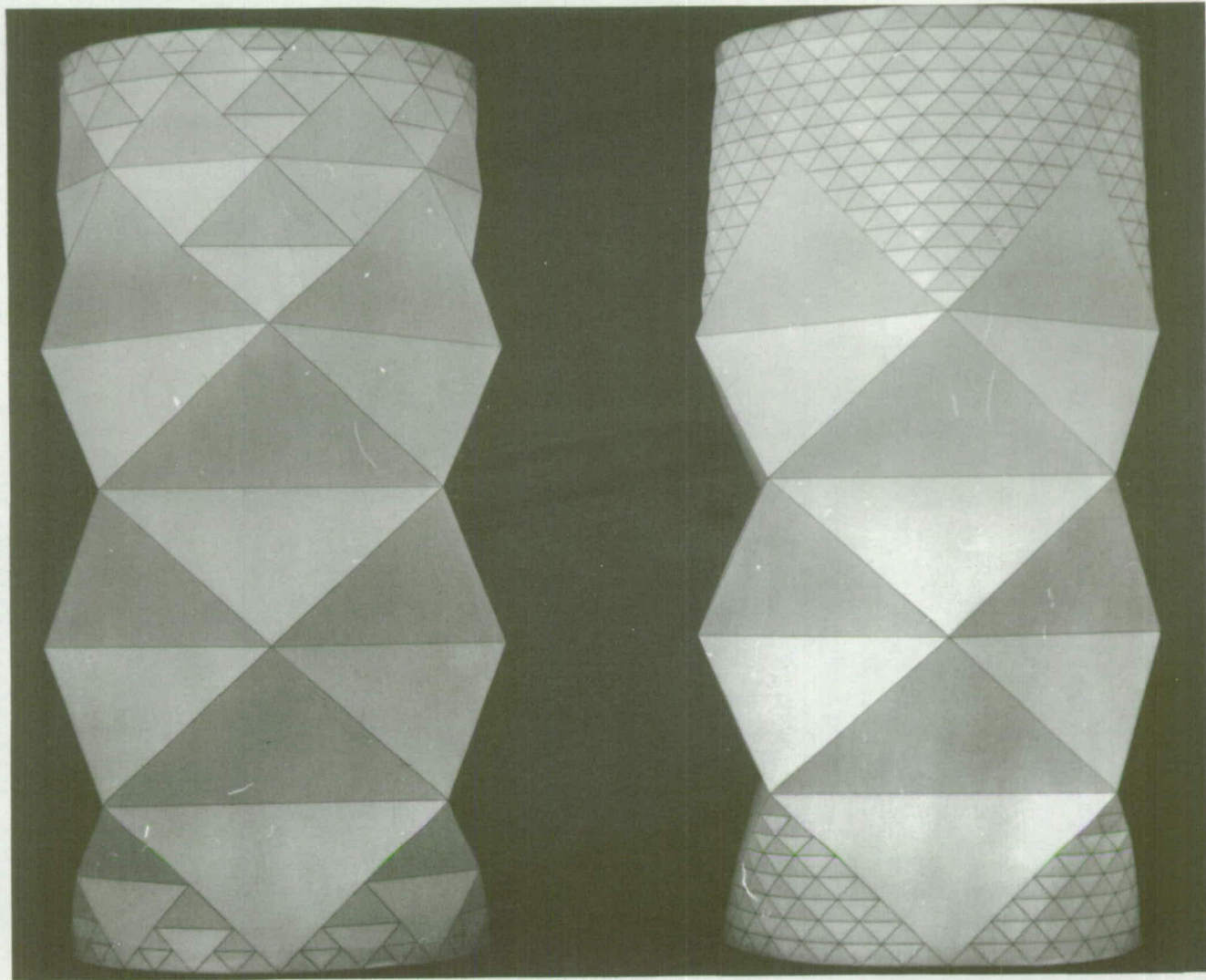


FIGURE 2.7  
TRANSITION FROM N=4 TO N=32

flattening of the small facets near the end of the large facets. Thus the small facets would be more susceptible to collapse in this area. Also, in this free form model, the ends are not flat. It is actually sitting on four points equally spaced between the apexes of the larger lobes. The corresponding increase in load in these areas would promote collapse of the small facets between the larger ones. Thus it is possible to infer that once the buckle pattern has been formed it can grow to cover the entire cylinder.

The discussion to this point has been concerned with Yoshimura patterns spread over the entire cylinder and the simultaneous collapse of a number of column members in the resulting space frame. Obviously, the loading on the cylinder would not be completely uniform and one member would collapse before the remainder. Should this collapse be inelastic then the dimple so formed would remain fixed in position and the remaining compression members would progressively collapse away from that location. Thus the buckle pattern could be seen to grow from an initial dimple. In the case of an elastic collapse of the compression member the dimple pattern can move around on the cylinder and take up a position of lower energy before any more diagonals collapse. Apparently this lower energy position would be with all dimples of equal size and with the dimples moving away from the fixed boundary (i.e. the ends).



For this reason a cylinder with a buckle pattern of, say 16 lobes would not collapse directly to a pattern of 8 lobes but would collapse progressively through 15,14,13 etc. Also, a buckle pattern with  $N$  lobes in it would in general require less effort to collapse the diagonal compression member than to extend the buckle pattern over the rest of the surface. Thus once a column member has been elastically collapsed a buckle pattern generally forms in the centre of the cylinder which has a length such that there is only one diagonal compression member. This type of pattern is illustrated by the very familiar model shown on the left of figure 2.8 (paper model) and in figure 2.9 (melanex cylinder with  $N=12$ ). Esslinger and Geier term this type of buckle pattern a two tier pattern. In fact it has a length corresponding to just one compression member (and two tension members). Since we are concerned with the collapse of the compression member it would seem to be preferable to call this a one tier pattern. Their interpretation of a one tier pattern is actually a pattern where the buckling interferes with the fixed boundary, i.e. it is a pattern controlled by the boundary (see figure 2.10).

If the collapse of the diagonal compression member is considered in this model then the situation shown on the right of figure 2.8 can be envisaged. Here a diagonal tension member has been formed and the compression members appear to have vanished. Thus the corners joined

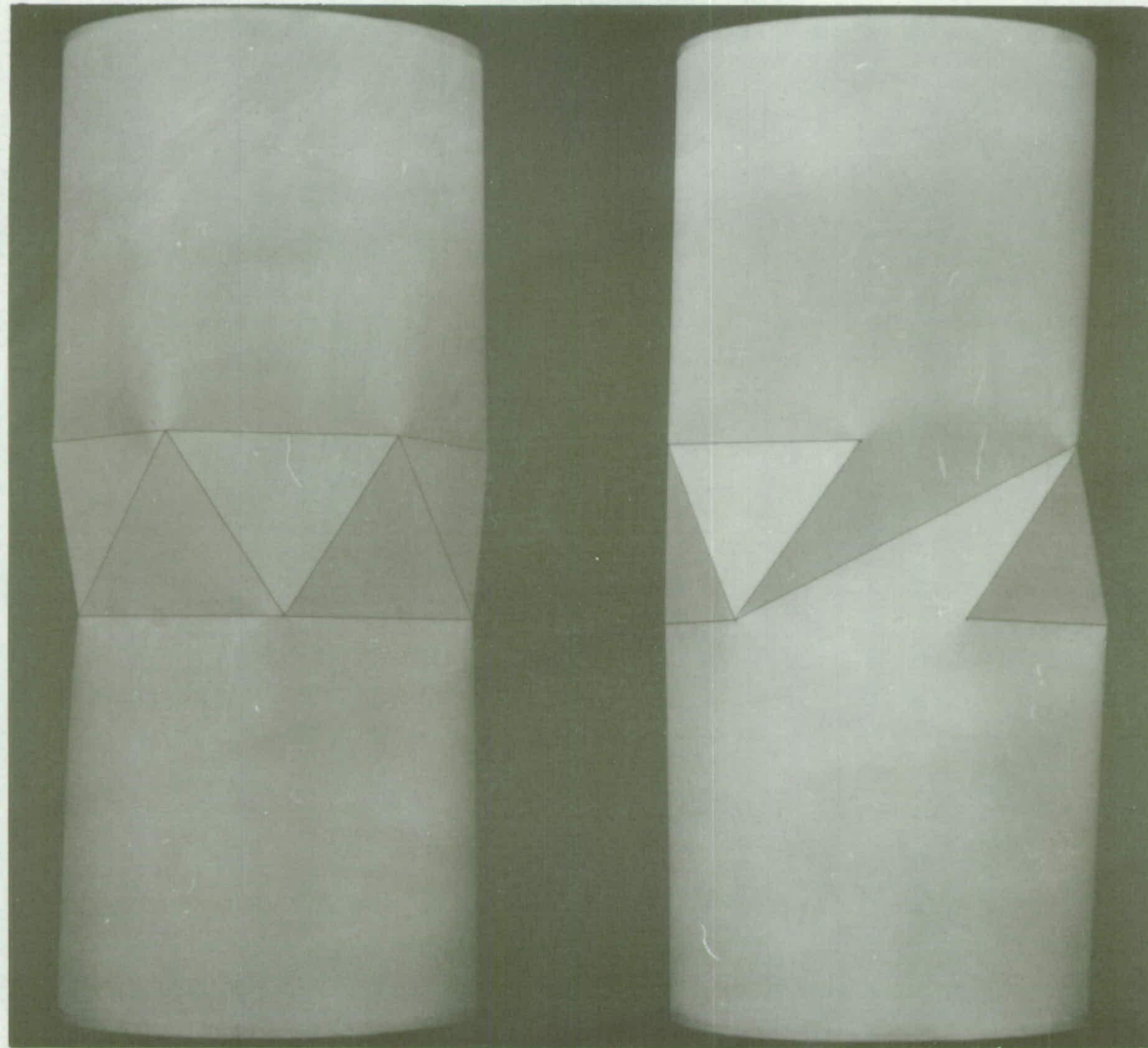


FIGURE 2-8  
PAPER MODELS OF USUAL FORM OF COLLAPSE IN CYLINDERS



FIGURE 2.9  
BUCKLED MELANEX CYLINDER



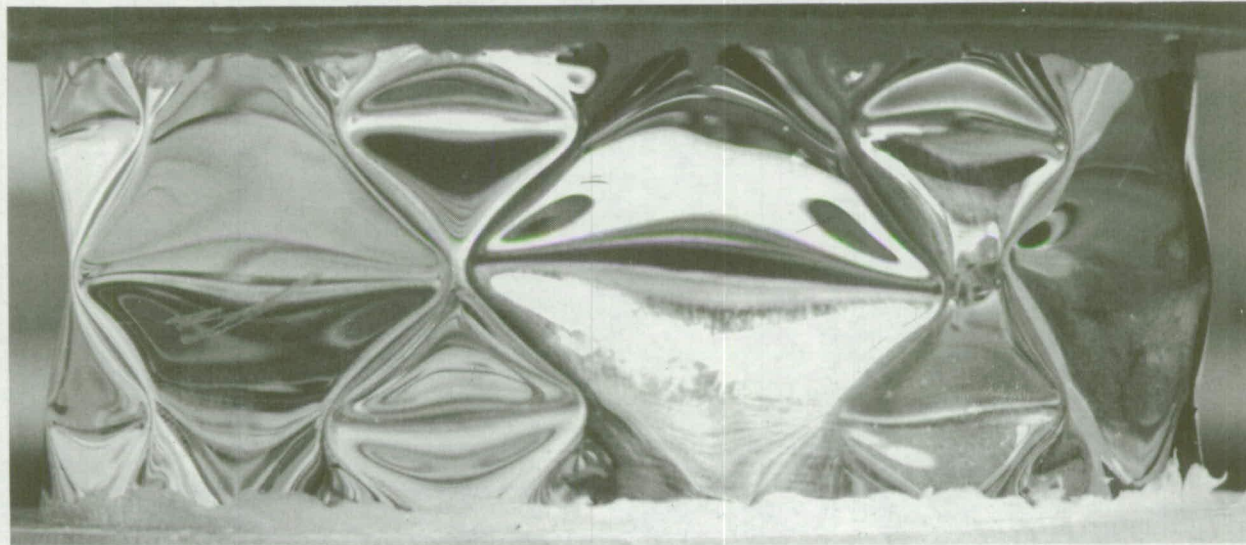


FIGURE 2.10

ESSLINGER AND GEIER'S ONE TIER PATTERN

by the tension member would be quickly brought together. If the collapse is elastic then the height difference would be evened out and a similar pattern formed with one less lobe. However, should the cylinder be relatively short then on bringing the two corners together, the buckle pattern would interfere with the end boundary and be somewhat inelastic. The result would be that the pattern would spiral around the cylinder; this situation is also often seen in shortish cylinders. Figures 2.11 and 2.12 show buckle patterns from advanced stages of collapse. In figure 2.11 ( $N=6$ ) an extra facet has formed adjacent to the main buckle pattern which is the first stage of spreading of the pattern. In figure 2.12 (a very advanced stage of collapse) the buckle pattern is spiralling around the cylinder. There are also smaller facets present at the ends which are approximately half the size of the facets in the main body of the pattern.

Obviously, in considering true Yoshimura patterns and these paper models, the buckled shape is a stable configuration and one has to consider load reversal rather than unloading. The major difference between real cylinders and the models in this case is probably due to the small amount of bending rigidity at the corners.

In compressing a Yoshimura pattern it has been demonstrated that there are diagonal compression members and tangential tension members. In reversing the



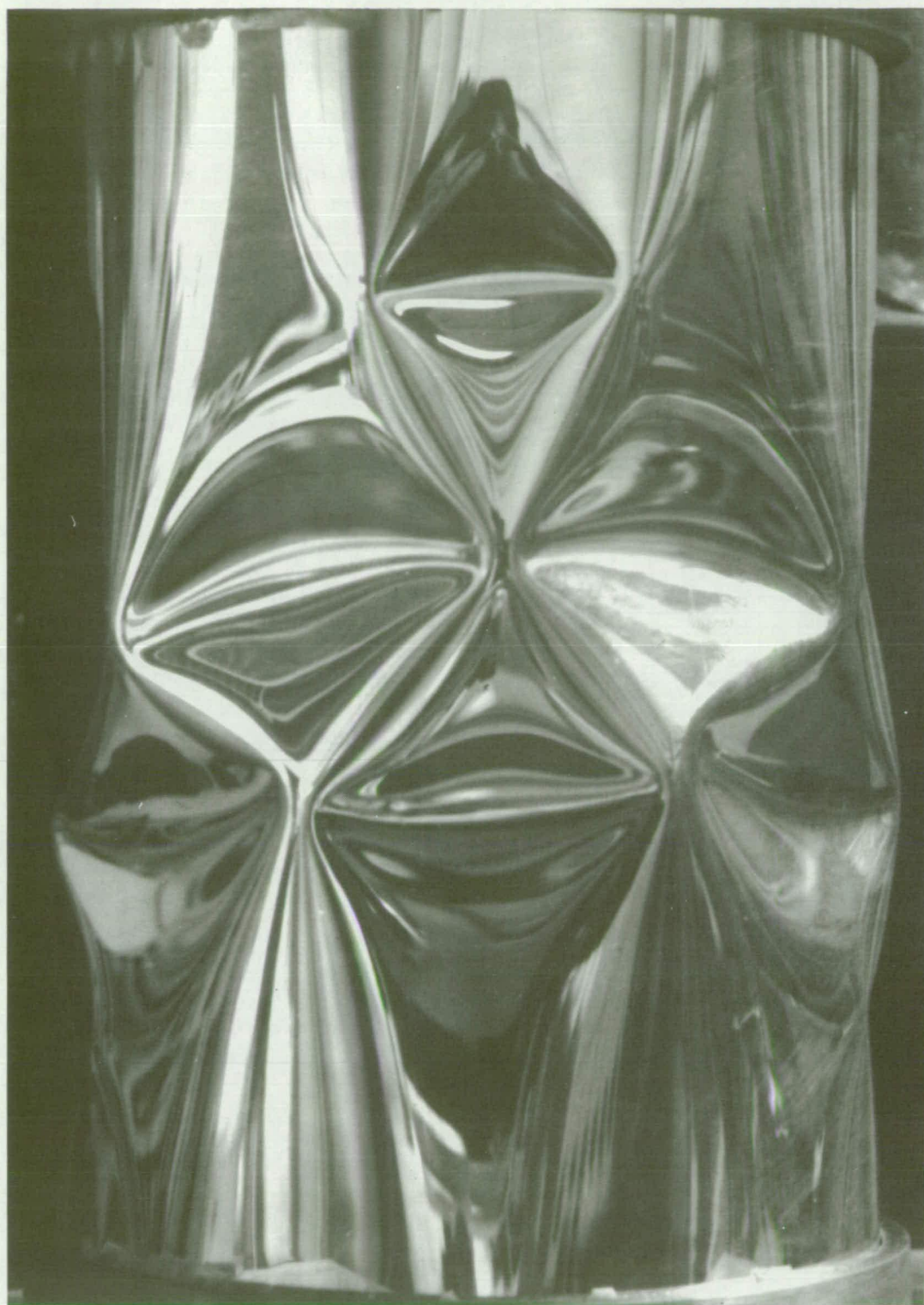


FIGURE 2.11

PROGRESSIVE BUCKLING IN  
MELANEX CYLINDER





FIGURE 2-12

HEAVILY DEFORMED MELANEX CYLINDER

load the diagonals become tension members and the tangential members are in compression. Thus the tangential member can collapse as a column in buckling and the situation shown in figure 2.13 can arise (here shown as a pure Yoshimura pattern). The sequence of models in this photograph are  $N=8$ , second buckling mode,  $N=4$  and a model representing the collapse of the tangential members. This last model has been folded to form a regular octagonal prism (for clarity) but obviously, it would in fact revert directly to a cylinder. In an actual cylinder the bending rigidity of the shell could force an intermediate pattern into the shell with a higher number of lobes.

Now that the buckling behaviour of an axially compressed cylinder has been explained qualitatively by reference to a space frame it remains to quantitatively estimate the buckling loads of the space frame and hence the cylinder. However, the collapse of a diagonal member is not that of a simple Euler column. When the member AC (in figure 2.14) starts to buckle then the diagonal member FB begins to form. Although FB eventually becomes a tension member when the second mode is achieved, at the start of transverse deformation in AC there is a compressive force in FB. Thus it seems that a reasonable model for the collapse of the Yoshimura buckle pattern is to consider the column members as pin jointed angles loaded through the corner of the angle and with a central spring restraining the deformation. This model ensures that the deformation of AC is always inwards.



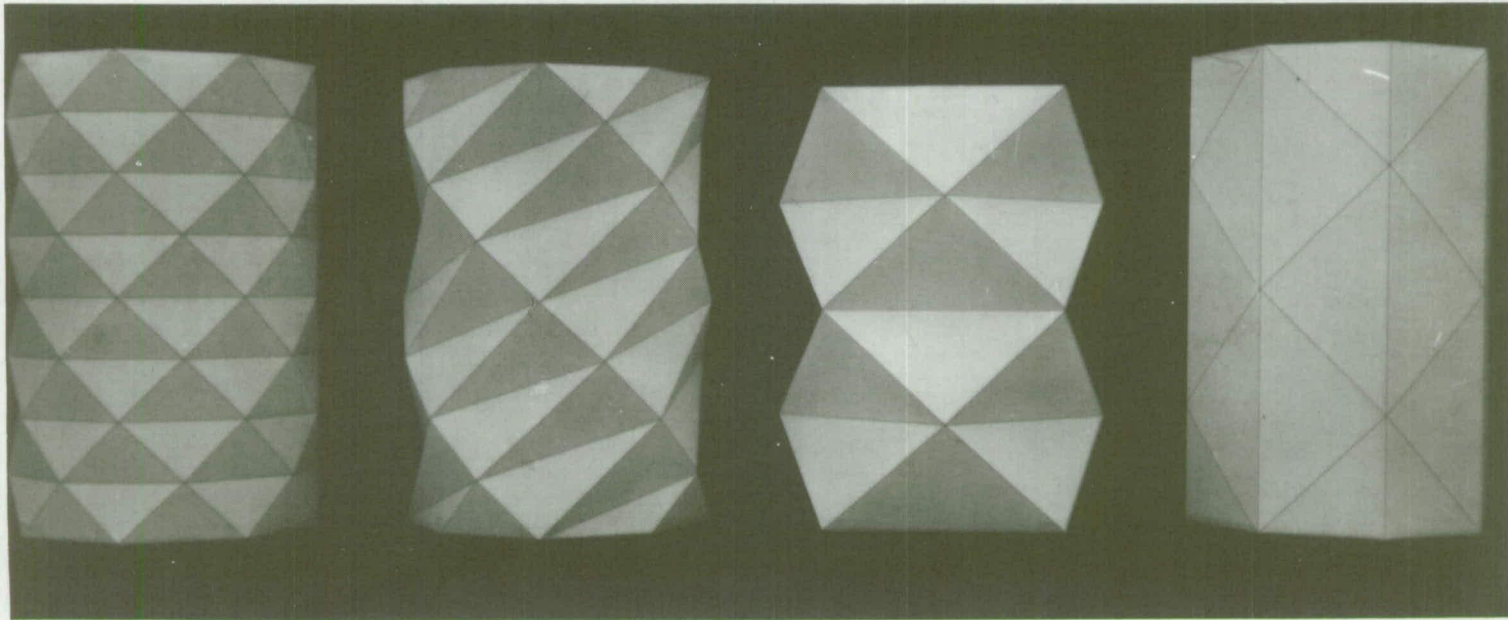


FIGURE 2-13

LOAD REVERSAL ON YOSHIMURA PATTERN

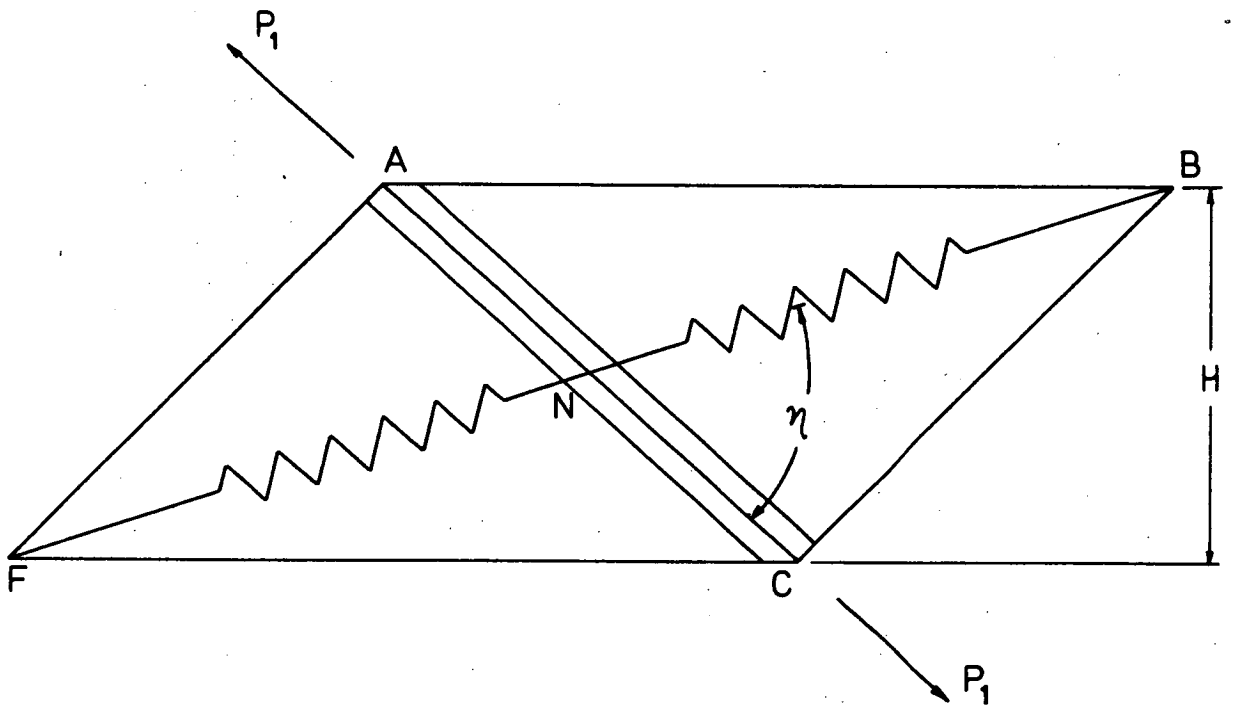
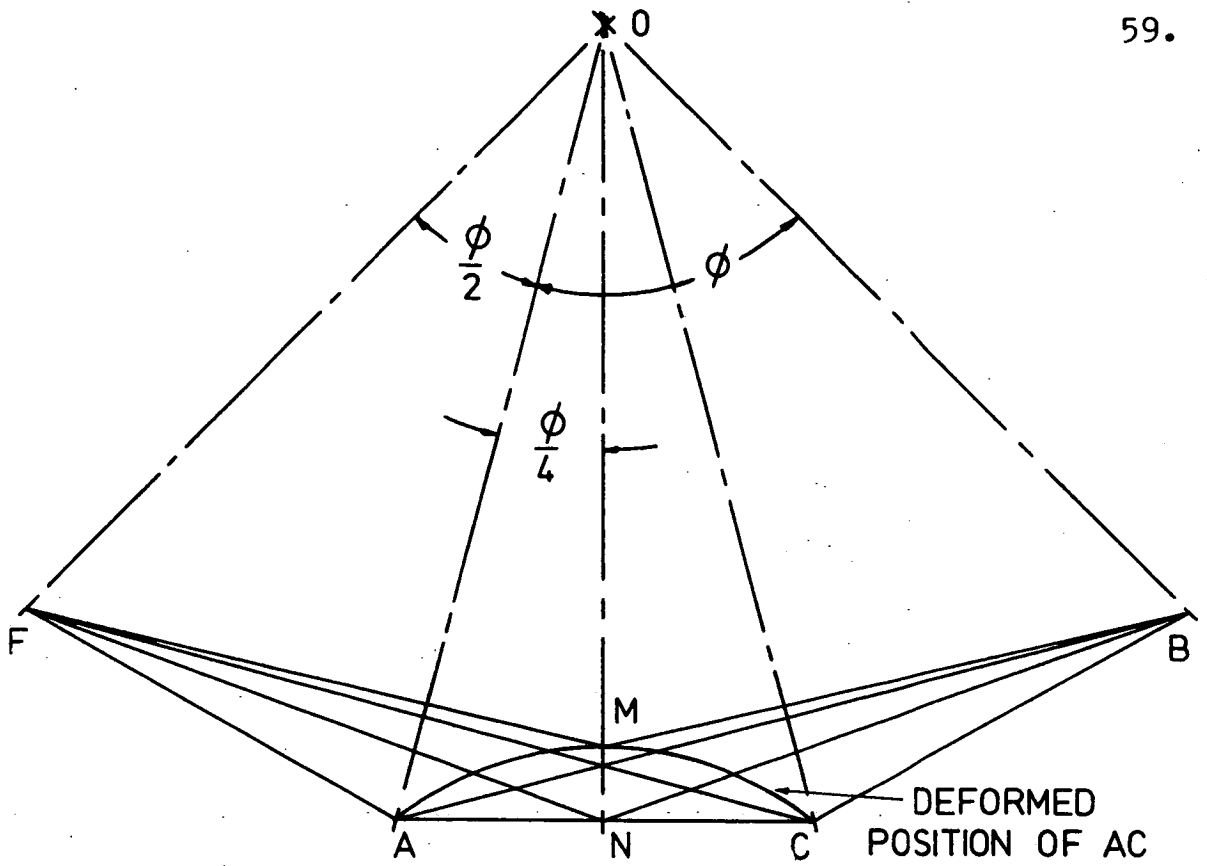


FIGURE 2-14  
MODEL FOR COLLAPSE OF COMPRESSION MEMBER

Some justification for including the member FN as a spring can be qualitatively obtained by building two identical paper Yoshimura models. In one some of the facets can be removed leaving a strip along each of the folds only. In the second model the member FN can also be left. Observation shows that the second model will support a substantially greater load than the first and sometimes the additional members will buckle.

During collapse of the member AC both points A and C move radially inwards while points F and B move outwards. In fact there appears to be very little of this movement before the collapse load has been reached so that for the purpose of investigating the collapse of AC, the relative movement of the corners can be ignored. However, when an axial load is supported by the cylinder without buckling, the column members AF, AC and BC shorten and the tension members AB and FC stretch. This change in geometry has been taken into account in the following theory.

From figure 2.14 the following geometrical relations are obtained.

$$H = \left\{ AF^2 - \frac{AB^2}{2(1+\cos(\phi/2))} \right\}^{\frac{1}{2}} \text{-----} 2.7$$

$$OA = \frac{AB}{2.\sin(\phi/2)} \text{-----} 2.8$$

$$ON = \frac{AB.\cos(\phi/4)}{2.\sin(\phi/2)} \text{-----} 2.9$$

$$\begin{aligned}
 FM &= \{OA^2 + (ON-MN)^2 - 2.OA.(ON-MN).\cos(\frac{3\phi}{4})\}^{\frac{1}{2}} \\
 &= \{OA^2 + ON^2 - 2.ON.MN \\
 &\quad - 2.OA.(ON-MN).\cos(\frac{3\phi}{4})\}^{\frac{1}{2}} \\
 &= \frac{1}{2}\{AF^2 + 2.AB^2 - 8.AB.MN.\sin(\phi/4)\}^{\frac{1}{2}} \text{ --- 2.10} \\
 MN &= \frac{1}{2}\{L_2^2 + (\frac{3.L_1}{2})^2\}^{\frac{1}{2}} \text{ ----- 2.11} \\
 &\quad \text{(unloaded condition)}
 \end{aligned}$$

Thus the strain in FM is

$$\epsilon = \left\{ \frac{AF^2 + 2.AB^2 - 8.AB.MN.\sin(\phi/4)}{L_2^2 + (\frac{3.L_1}{2})^2} \right\}^{\frac{1}{2}} - 1 \text{ --- 2.12}$$

Consequently, the restraining force on the centre of the column is.

$$\begin{aligned}
 P_3 &= 2.E.W.T. \left[ \left\{ \frac{AF^2 + 2.AB^2 - 8.AB.MN.\sin(\phi/4)}{L_2^2 + (\frac{3.L_1}{2})^2} \right\}^{\frac{1}{2}} \right. \\
 &\quad \left. - 1 \right] \text{ ----- 2.13}
 \end{aligned}$$

Also

$$AF = (1 + \frac{P_1}{2.T.E.W}).K \text{ ----- 2.14}$$

$$AB = L_1.(1 + \frac{P_2}{2.T.E.W}) \text{ ----- 2.15}$$

and since

$$P_2 = \frac{-P_1}{(1+\cos(\phi/2))\left\{(\frac{L_2}{L_1})^2 + \frac{1}{4}\right\}^{\frac{1}{2}}} \text{ ----- (2.6)}$$

then

$$AB = L_1 \left[ 1 - \frac{P_1}{2TEW(1+\cos(\phi/2))\left\{(\frac{L_2}{L_1})^2 + \frac{1}{4}\right\}^{\frac{1}{2}}} \right] \text{ --- 2.16}$$

Substituting in the above, we have;-

62.

$$P_3 = \frac{-8.L_1.MN.T.W.T.\sin(\phi/4)}{\left\{L_2^2 + \left(\frac{3.L_1}{2}\right)^2\right\}} + \frac{P_1\left\{K^2 - \frac{2.L_1^3}{(1+\cos(\phi/2))K}\right\}}{\left\{L_2^2 + \left(\frac{3.L_1}{2}\right)^2\right\}} \quad \text{-----} \quad 2.17$$

The angle  $\eta$  between the restraining force and the column is given by.

$$\cos\eta = \frac{-L_2^2 + \frac{3.L_1^2}{4}}{K\left\{L_2^2 + \left(\frac{3.L_1}{2}\right)^2\right\}^{\frac{1}{2}}} \quad \text{-----} \quad 2.18$$

Having determined the transverse restraining force we can isolate the member AC and treat it as a buckling pin ended column as illustrated in figure 2.15. At any point "X" in the column the moment is given by.

$$\begin{aligned} M &= P_1(Y + \frac{1}{2}W.\cos(\theta/2)) - P_3.\sin\eta.\cos(\theta/2).(K/2-X) \\ &= E.I.\frac{d^2Y}{dx^2} \quad \text{-----} \quad 2.19 \end{aligned}$$

$$\text{and } I = \frac{T.W^3.\cos^2(\theta/2)}{6}$$

$$\begin{aligned} \text{Thus } Y &= C_1.\sin(J.X) + C_2.\cos(J.X) - \frac{1}{2}W.\cos(\theta/2) \\ &\quad + \frac{P_3}{P_1}\sin\eta.\cos(\theta/2).(K/2-X) \quad \text{-----} \quad 2.20 \end{aligned}$$

$$\text{where } J^2 = -\frac{P_1}{E.I}$$

The constants of integration  $C_1$  and  $C_2$  are found from the boundary conditions which are zero slope at the centre ( $X=0$ ) and zero deflection at the end ( $X=K/2$ ).



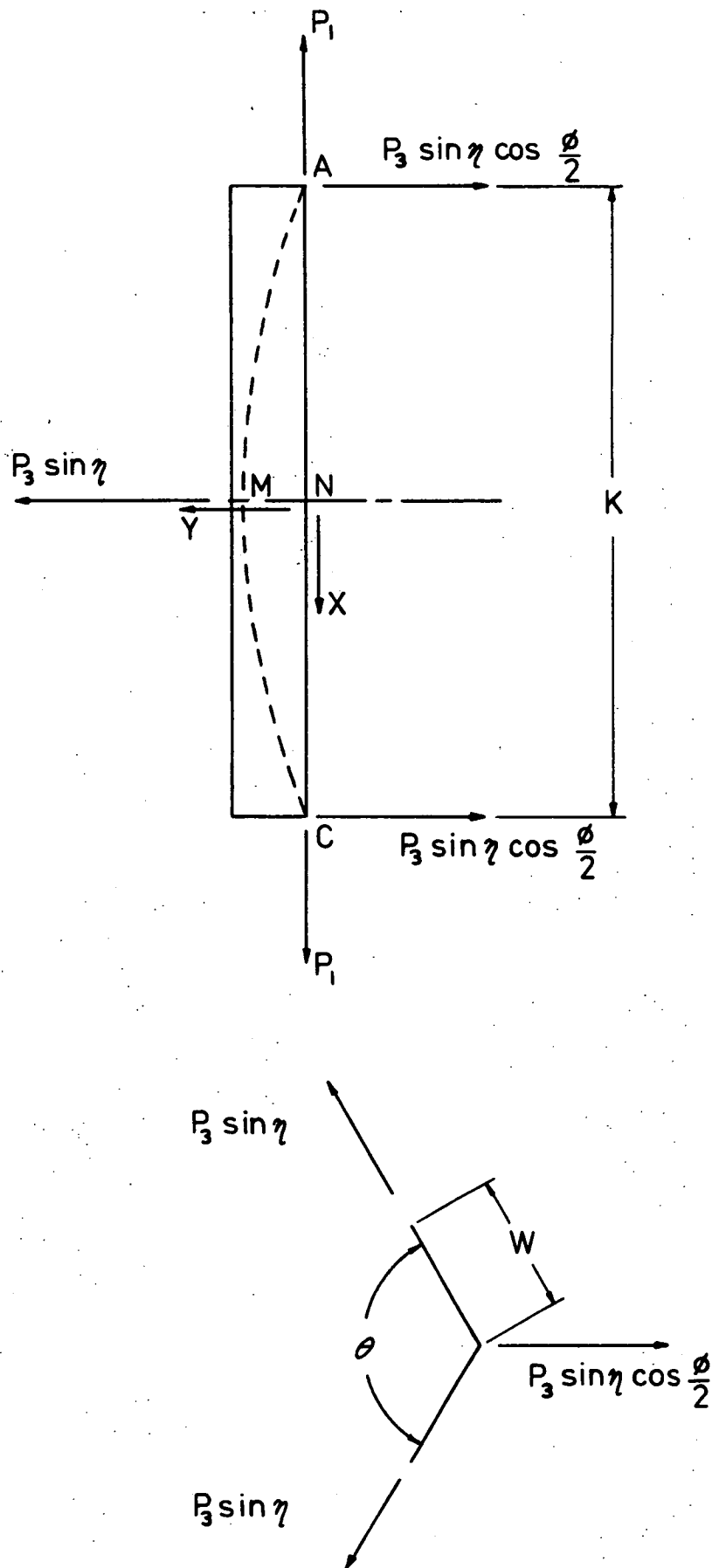


FIGURE 2-15  
LOADING SYSTEM ON COLUMN MEMBER

$$\begin{aligned} \text{Thus } C_1 &= \frac{P_3 \cdot \sin \gamma \cdot \cos(\theta/2)}{P_1 \cdot J} \quad \text{-----} \quad 2.21 \\ \text{and } C_2 &= \frac{\frac{1}{2}W \cdot \cos(\theta/2) - \frac{P_3 \cdot \sin \gamma \cdot \cos(\theta/2) \cdot \sin(J \cdot K/2)}{P_1 \cdot J}}{\cos(J \cdot K/2)} \quad \text{-----} \quad 2.22 \end{aligned}$$

at the centre,

$$\begin{aligned} Y &= MN \\ &= C_2 - \frac{1}{2}W \cdot \cos(\theta/2) + \frac{P_3 \cdot K}{2 \cdot P_1} \sin \gamma \cdot \cos(\theta/2) \quad \text{---} \quad 2.23 \end{aligned}$$

Substituting for  $C_2$  and  $P_3$  we obtain,

$$\begin{aligned} MN &\left[ 1 + \frac{8 \cdot L_1 \cdot E \cdot W \cdot T \cdot \sin(\phi/4) \cdot \sin \gamma \cdot \cos(\theta/2)}{P_1 \left\{ L_2^2 + \left( \frac{3 \cdot L_1}{2} \right)^2 \right\}} (K/2 - \tan(J \cdot K/2)/J) \right] \\ &= \frac{\sin \gamma \cdot \cos(\theta/2) \left\{ K^2 - \frac{2L_1^3}{(1 + \cos(\phi/2))K} \right\} \left( \frac{K}{2} - \frac{\tan(\frac{J \cdot K}{2})}{J} \right)}{\left\{ L_2^2 + \left( \frac{3 \cdot L_1}{2} \right)^2 \right\}} \\ &\quad + \frac{1}{2}W \cdot \cos(\theta/2) \left\{ \frac{1}{\cos(J \cdot K/2)} - 1 \right\} \quad \text{-----} \quad 2.24 \end{aligned}$$

Now, as the critical load of the column is approached the central deflection grows very large and we have in the limit that,

$$\begin{aligned} 1 + \frac{8 \cdot L_1 \cdot E \cdot W \cdot T \cdot \sin(\phi/4) \cdot \sin \gamma \cdot \cos(\theta/2)}{P_1 \left\{ L_2^2 + \left( \frac{3 \cdot L_1}{2} \right)^2 \right\}} (K/2 - \tan(J \cdot K/2)/J) \\ = 0 \quad \text{-----} \quad 2.25 \end{aligned}$$

Solution of equation 2.25 leads to an evaluation of the compressive load carried by a diagonal member in the Yoshimura pattern at the point of collapse. The total load supported by the structure is readily found since,

$$P = 2.N.P_1 \left[ \frac{1 - \left(\frac{L_1}{2.L_2}\right)^2 \frac{(1 - \cos(\phi/2))}{(1 + \cos(\phi/2))}}{1 + \left(\frac{L_1}{2.L_2}\right)^2} \right]^{\frac{1}{2}} \text{----- 2.26}$$

The solution is multivalued. Figure 2.16 is a plot of the value of this function for changing load ( $P_1$  or  $P$ ). It can be seen that there is a root for no axial load. This root corresponds to a rigid body translation of the column member. The next root is the solution desired while higher roots relate to higher buckling modes (of the column only). Thus to solve equation 2.25 by a trial and error method it is necessary to guess an initial value which is high enough to prevent the solution converging on zero. It must also be low enough that the solution will not converge to a higher mode. The general shape of this curve also highlights another problem with the solution. If, for example, we were to assume a diagonal member load of 7 Newtons for this cylinder and apply the Newton-Raphson convergence criterion then the solution would follow the dotted line shown. The next guess would be about  $15\frac{1}{2}$  Newtons and the solution would converge to some higher buckling mode. To overcome this problem it is necessary to apply a convergence factor (less than unity) to the Newton-Raphson technique to ensure convergence to the correct value. This solution was performed on a Digital PDP8 computer using the language FOCAL. A listing of the programme together with typical output is given in Appendix C. As well as giving the buckling load the printout includes the important geometrical

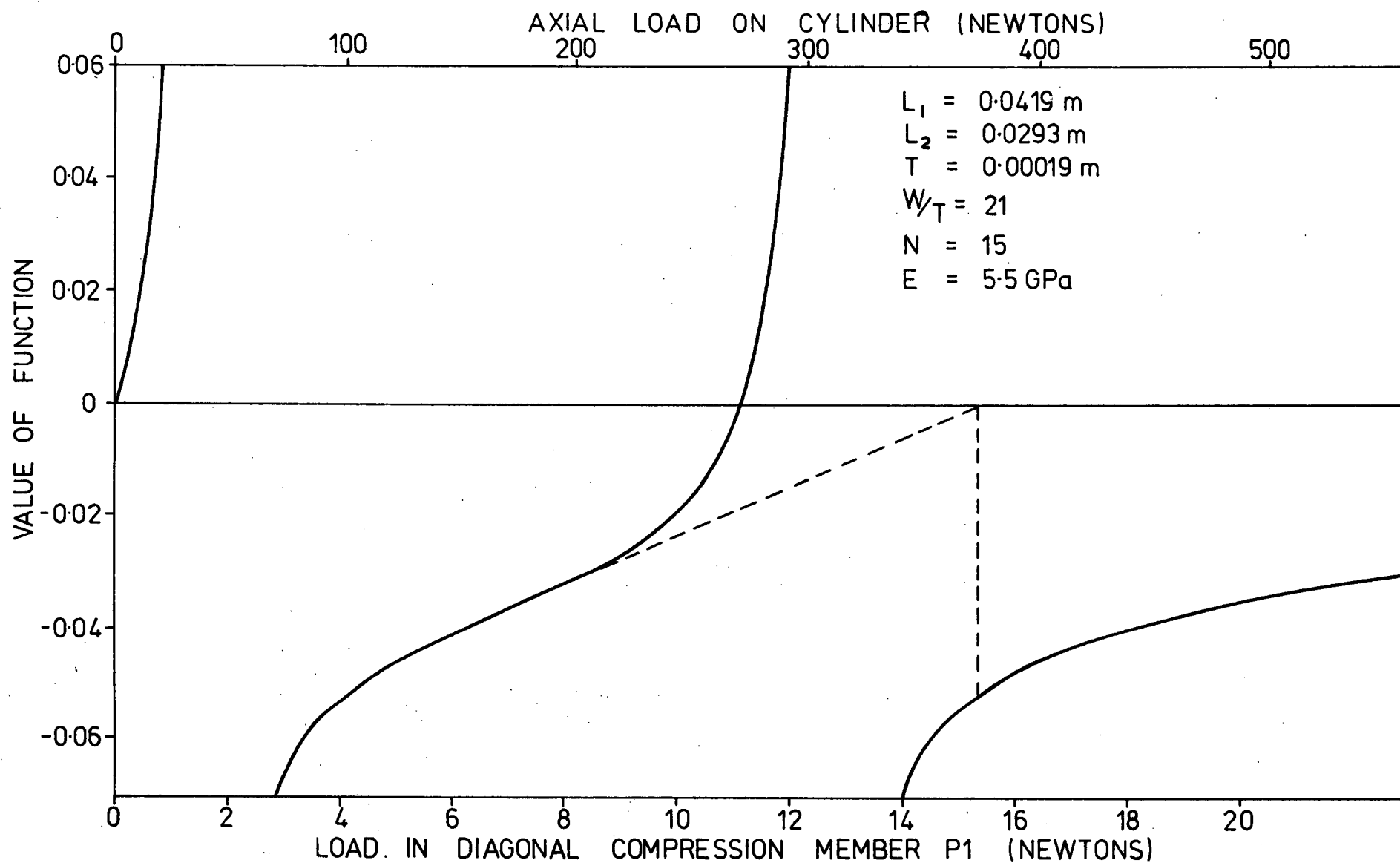


**FIGURE 2.16**

Plot of  $P_1 [L_2^2 + (3L_1/2)^2] + 8L_1 E W T \sin \phi/4 \sin^2 \phi/2 \cos \phi/2 [K/2 - 1/2 \tan (JK/2)]$

properties of the first buckling mode(normal Yoshimura pattern) and the second mode (pattern with inclined tension members).

The expression for calculating the critical load can be non-dimensionalised by using the following ratios,

$$\rho = \frac{P_1}{E.L_2^2} \quad \text{-----} \quad 2.27$$

$$\lambda = \frac{L_2}{L_1} \quad \text{-----} \quad 2.28$$

$$\omega = \frac{W}{T} \quad \text{-----} \quad 2.29$$

$$\text{and } \tau = \frac{T}{L_2} \quad \text{-----} \quad 2.30$$

Hence,

$$2 \left\{ \left( 1 + \left( \frac{3}{2\lambda} \right)^2 \right)^3 \right\}^{\frac{1}{2}} \rho + \frac{16.\omega.\tau^2.\sin^2(\phi/4)}{\lambda^2} \left[ \left\{ 1 + \left( \frac{1}{2\lambda} \right)^2 \right\}^{\frac{1}{2}} \right. \\ \left. - \frac{2.\tan\left\{ \frac{1}{2} \left( \frac{6\rho}{\tau^4\omega^3\sin^2(\phi/4)} \right)^{\frac{1}{2}} \right\}}{\left\{ \frac{6\rho}{\tau^4\omega^3\sin^2(\phi/4). \left( 1 + \left( \frac{1}{2\lambda} \right)^2 \right)} \right\}} \right] = 0 \quad \text{-----} \quad 2.31$$

In developing the theory to this point the author had become aware that a cylinder would have several buckling loads of differing values. Thus a load deflection curve would not have one peak ( as Von Karman and Tsien proposed ) but have several corresponding to the collapse of each mode. Within a couple of weeks of the author's realisation of this point Esslinger and Geir's book (ref.13) appeared on the shelves of the University of Tasmania

library. On page 105 of this book is a graph reproduced here as figure 2.17 which shows these multiple peaks obtained experimentally. This is the only reference that the author has found to show this property. All others have indicated a curve of the Von Karman and Tsien type. It appears to be a serious shortcoming in the published data which has at last been rectified.

It was decided to use the data from figure 2.17 to test the validity of the present theory. The only missing information was an estimate of the aspect ratio of the facets. To obtain this ratio several cylinders were manufactured from melanex with various combinations of radius, thickness and length. It was found that with these cylinders the aspect ratio ( $L_2/L_1$ ) was about 0.7 except where the pattern was seen to interfere with the end of the cylinder. The other unknown variable in the equation was the width of the flange of the angle member ( $W$ ). This width was manipulated until for  $N=15$  (the first post-buckling condition) the calculated collapse load coincided with the published data. A width of 21 times the thickness was found to be necessary. This width was then used to calculate the subsequent collapse loads and these loads are presented in table 2.1 together with the values read from the published curve for comparison. The agreement appears to be excellent in this range.



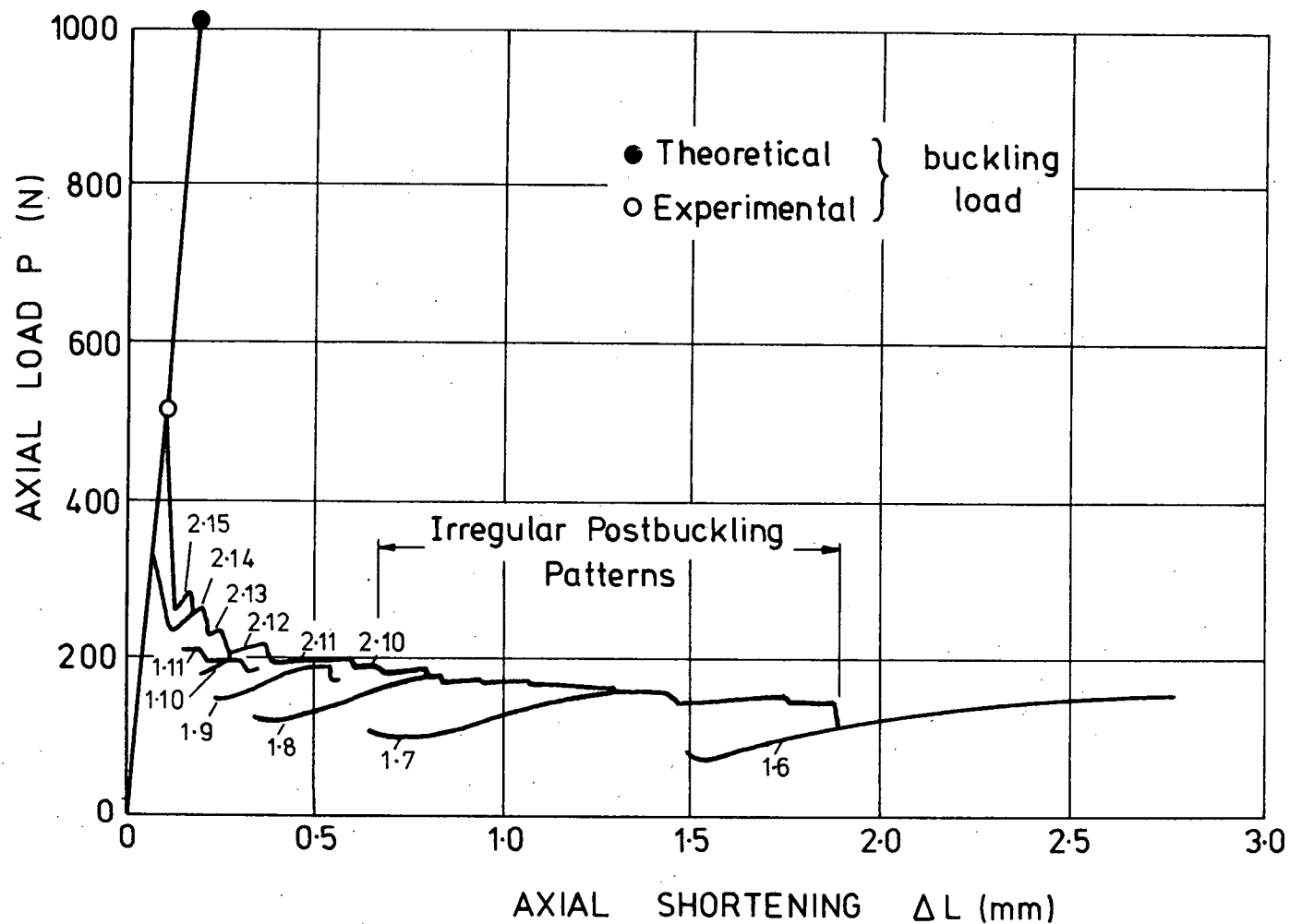


**FIGURE 2.17**

LOAD-SHORTENING CURVES MYLAR CYLINDER  $E = 5.5 \text{ GPa}$ ,  $R = 100 \text{ mm}$ ,  
 $T = 0.19 \text{ mm}$ ,  $L = 100 \text{ mm}$ . SOURCE ESSLINGER AND GEIER (REFERENCE 13)

TABLE 2.1

COMPARISON OF CALCULATED AND MEASURED POST-BUCKLING CRITICAL LOADS

R = 100mm.

T = 0.19mm.

W/T = 21

Number of Lobes	Critical Loads	
	Calculated	Measured (Esslinger and Geier)
	N	N
15	278	275
14	254	260
13	236	235
12	218	215
11	200	200
10	181	185

The variation in critical load with number of lobes is plotted as figure 2.18 for an extended range of values of  $N$ . The interesting point about this graph is that there is a maximum with 38 facets of 518N. Esslinger and Geier's cylinder buckled at a load of approximately 520N. It is also interesting to note that by using high speed photography Almroth, Holmes and Brush (ref.14) observed an initial buckle pattern with facets about half the size of the final pattern. Perhaps these smaller dimples correspond to the peak of the curve in figure 2.18 which corresponds to just over twice the number of lobes finally obtained.

When a short cylinder is loaded in axial compression, then it is impossible to maintain the same aspect ratio as in a freely formed pattern. Firstly the buckles start to interfere with the ends and it is found that the pattern spirals around the cylinder. It tends to break down completely over a considerable section until a different kind of pattern evolves - Esslinger and Geir's one tier pattern. This type of pattern can not be properly represented by the simple space frame model presented here. However, if the length of the facet ( $L_2$ ) is limited to half the length of the cylinder and the preceding theory used to predict buckling loads, then an indication of the behaviour of the cylinder is obtained. The two additional curves on the left of figure 2.18 are based on this approximation. It will be seen that the intersection

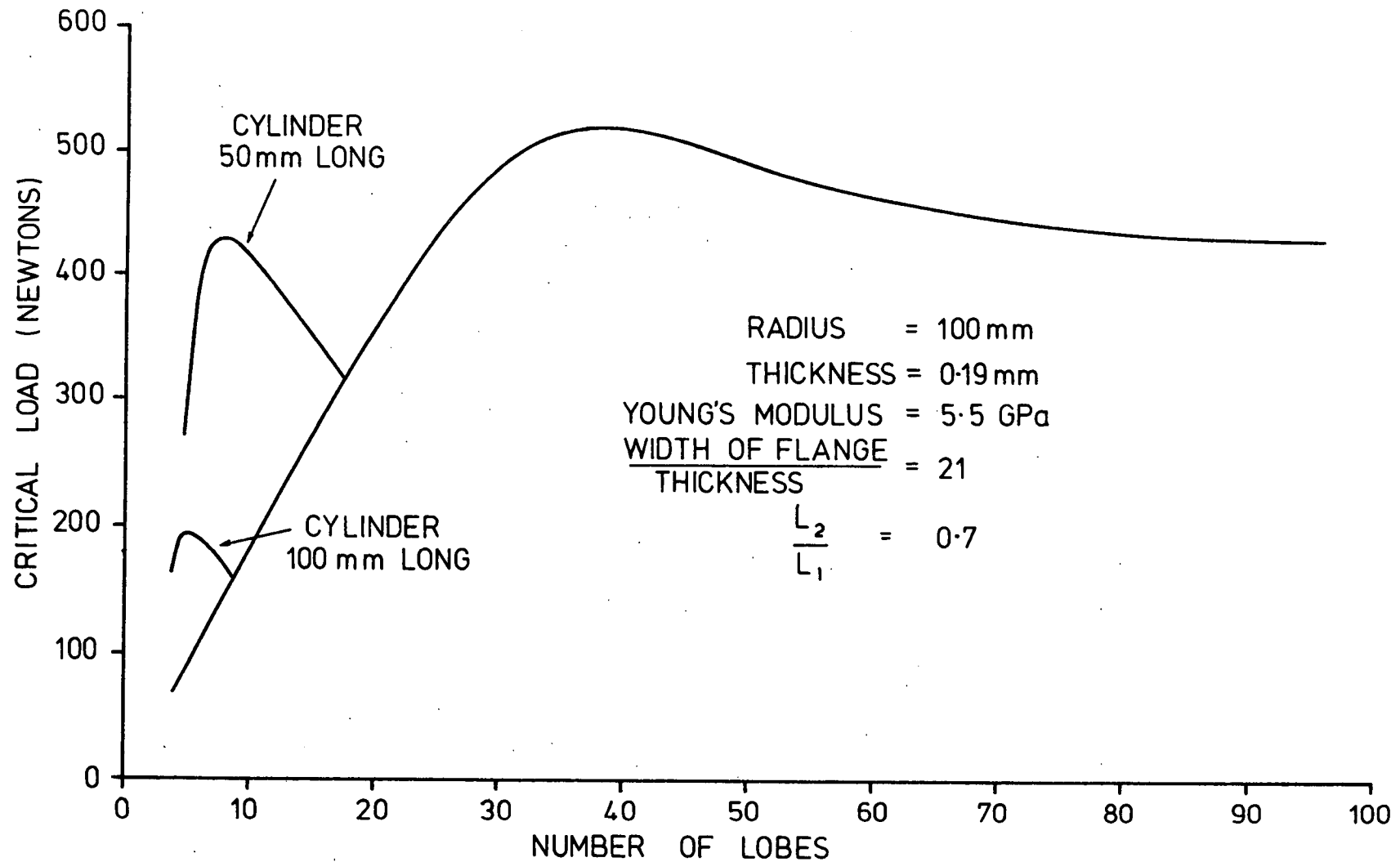


FIGURE 2-18  
VARIATION OF CRITICAL LOAD WITH YOSHIMURA PATTERN  
GEOMETRY

of this curve for a 100mm. long cylinder with the principal buckling curve for the cylinder occurs at about the position that the buckling pattern becomes irregular. Further compression beyond this point appears to create a combination of buckling modes, one of which is approximated by the short cylinder branch and the other by the aspect ratio of 0.7. When all the compression members with this higher aspect ratio are buckled we are left with the regular buckle pattern that Esslinger and Geier call the one tier pattern.

Seeing that the collapse loads for Esslinger and Geier's cylinder have been satisfactorily calculated by this method it remains to estimate the corresponding deflections and complete a load deformation graph. Unfortunately, the calculation of deflection is not as satisfactory because the geometry is not that of a simple Yoshimura pattern. Apparently the bending rigidity of the shell restricts the pattern from forming completely with the result that the actual shell is a little longer than would be predicted by the simple Yoshimura geometry.

Even with this known limitation a reasonable load deformation graph can be drawn (figure 2.19) purely by considering the simple Yoshimura geometry. For this calculation the buckle pattern was approximated by a Yoshimura pattern with a length such that there was one diagonal member only. This pattern was considered to be connected to the ends by a regular cylinder covering the



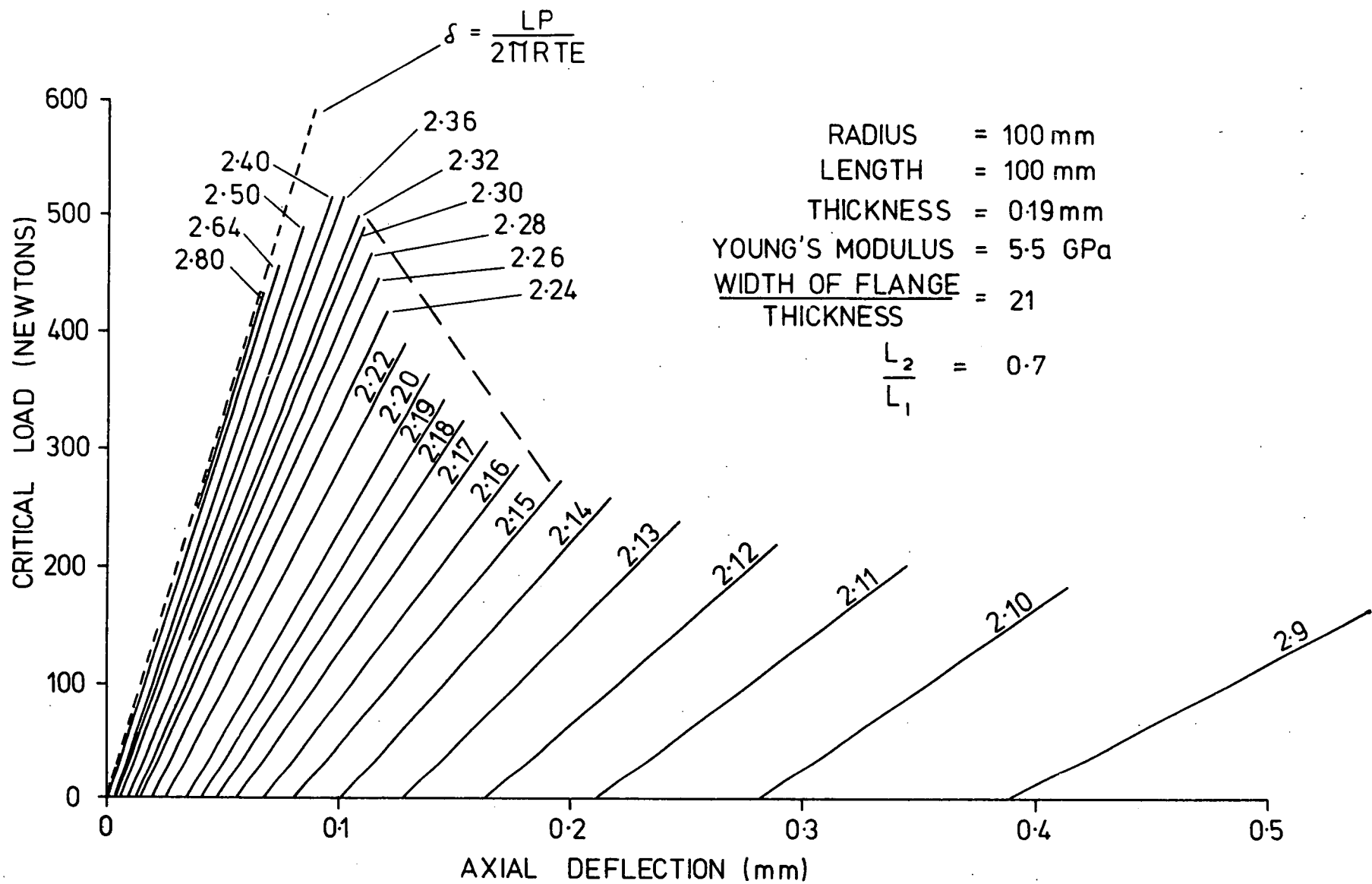


FIGURE 2.19  
THEORETICAL LOAD DEFORMATION DIAGRAM FOR MYLAR CYLINDER

remainder of the length. Using this model meant that at each node there were two tangential members and two diagonal compression members instead of the four in the complete pattern. Thus the force in the tangential member was half that previously calculated. The axial deflection was estimated from the following expression.

$$\delta = L - H - (L - L_2) \left( 1 + \frac{P}{2 R.T.E} \right) \text{ ----- } 2.32$$

(P negative in compression)

This expression is linear and is represented in figure 2.19 by a straight line for each mode shape. The nomenclature ( 2,15 for example) is that adopted by Esslinger and Geier. It refers to a mode shape that has a Yoshimura pattern length corresponding to one diagonal member (2 tangential members) and 15 lobes around the circumference. Calculated deflections at collapse are within about 15% of the measured values.

One would expect that in loading the cylinder in a rigid testing machine a load deformation curve would reach a peak and immediately drop without increasing the axial deformation. Thus in considering the collapse according to figure 2.19 it would appear that the collapse would progress through every mode shape after the peak has been reached. The concept of a rigid machine applies only to the cylinder as a whole. We have been discussing the collapse as a local phenomenon and in fact the buckling compression member must see the

remainder of the cylinder as a somewhat flexible machine. Thus the combination of cylinder and machine stiffnesses would produce a load release characteristic of the form represented by the dotted line in figure 2.19. In this cylinder it was known that the first post-buckling mode had 15 lobes. Allowing for the fact that the deflections are over-estimated as explained earlier, it is reasonable to expect a pattern of about 15 lobes from this diagram. The dotted line indicates the combined machine and cylinder characteristic necessary to achieve 15 lobes in the buckled shape according to this load deformation diagram.

Changing the length of the cylinder has no effect on the critical loads since these are only dependent on the local buckling of the diagonal strut at the centre of the cylinder. However, increasing the overall length of the cylinder increases the length of the section that is not collapsing. This portion is still deforming so that the buckle pattern has a smaller overall relative effect on the deformation. Figure 2.20 is a load deformation diagram for a cylinder of similar proportions to that used in deriving figure 2.19 except that the length has been quadrupled to 400 mm. By assuming the same cylinder-machine stiffness as in the previous case ( the dotted line ) a post-buckled shape with 10 lobes would be anticipated. However the extra length of the cylinder would mean that the combined machine-cylinder stiffness would probably be considerably less than previously encountered and an even smaller number of lobes could occur.

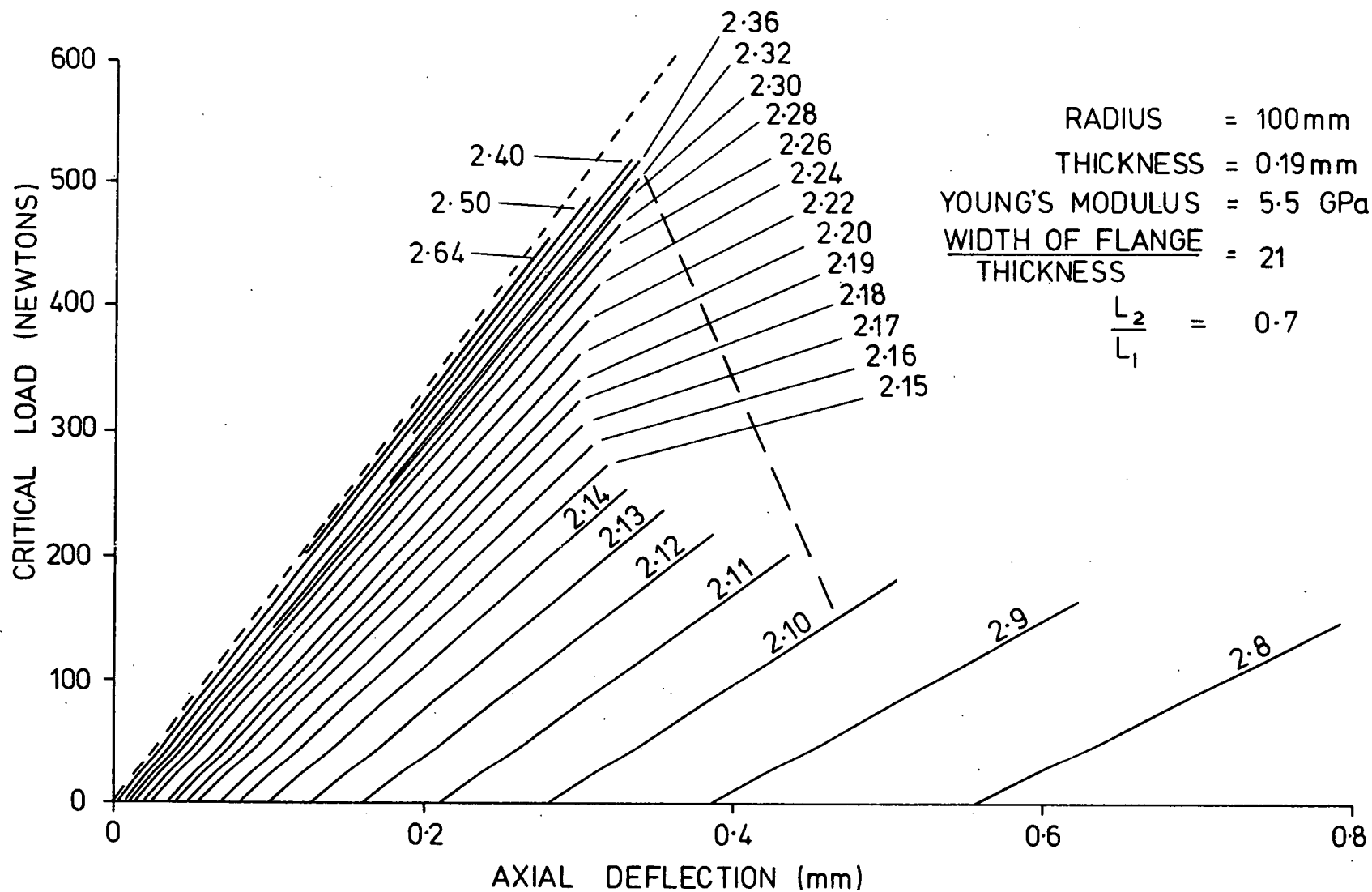


FIGURE 2.20  
THEORETICAL LOAD DEFORMATION DIAGRAM FOR MYLAR CYLINDER

Even with this very simple model excellent agreement with the published data has been obtained. By a consideration of the variations in cylinder geometry from the Yoshimura pattern refinements should be able to be made to the theory to improve its validity. Some of the additional properties that could be included are;-

1.               The edges of the Yoshimura pattern are not angular but are bent to a fairly sharp radius. The radius of curvature varying with position.
2.               Because the radius of curvature varies along the length of the compression member this member is not initially straight. These two considerations are discussed in chapter 5. In that chapter it is shown that the addition of these two properties does not assist the analysis. In fact, their inclusion necessitates so many additional assumptions that the analysis becomes useless.
3.               The mechanism used in the calculations assumed that all the corners remained in the same relative position during the collapse. In fact the corners at the end of the collapsing diagonal move inwards and the adjacent corners outwards. This movement is also reflected in the corners further away but to a lesser extent.
4.               In collapsing one member the load carried by that member is reduced. This results in an increase in load in the adjacent members with a consequent shortening and an overall effect of bending the cylinder.



If a cylinder is not perfect but has a defect of finite magnitude then loading will not be along the dotted line shown in figures 2.19 and 2.20. It will follow one of the full lines corresponding to the size of the defect.e.g. should the defect cover one twelfth of the circumference then the line marked 2,12 would be followed until the collapse load for 12 lobes is obtained. For small defects (less than  $1/38$  of the circumference for Esslinger and Geier's cylinder) the cylinder appears to behave as though it were perfect.

E	Young's Modulus.
H	Axial length of half facet, i.e. collapsed length corresponding to $L_2$ .
I	Moment of inertia of column member.
K	Length of diagonal compression member.
L	Length of cylinder.
$L_1$	Length of facet in circumferential direction.
$L_2$	Half developed axial length of facet.
M	Moment.
N	Number of circumferential facets.
P	Axial load on cylinder.
$P_1$	Axial load in diagonal member.      Tension positive.
$P_2$	Axial load in tangential member.
$P_3$	Load in member being formed.
T	Shell thickness.
W	Effective width of flange on angle member.
$\epsilon$	Strain in member being formed.
$\delta$	Axial deflection of cylinder.
$\eta$	Angle between collapsing diagonal member and member being formed.
$\phi$	Angle subtended at axis of cylinder by each facet.
$\theta$	Angle between adjacent facets along the diagonal member.
$\rho$	$\frac{P_1}{E \cdot L_2^2}$
$\lambda$	$\frac{L_2}{L_1}$ Non-dimensional quantities.
$\omega$	$\frac{W}{T}$
$\tau$	$\frac{T}{L_2}$

# CHAPTER 3

## CONVENTIONAL

## SOLUTION

### CHAPTER 3

#### AN EXAMINATION OF THE CONVENTIONAL SOLUTION METHOD FOR THE AXIAL BUCKLING PROBLEM.

It has already been indicated that Hoff, Madsen and Mayers (ref. 7) found the usual Von Karman and Tsien approach (ref.3) to be inappropriate. Before proceeding further with the current theory it is worthwhile to contemplate this much tried and apparently inadequate theory.

For the shell element shown in figure 3.1, Donnell's equations can be expressed in the following form.

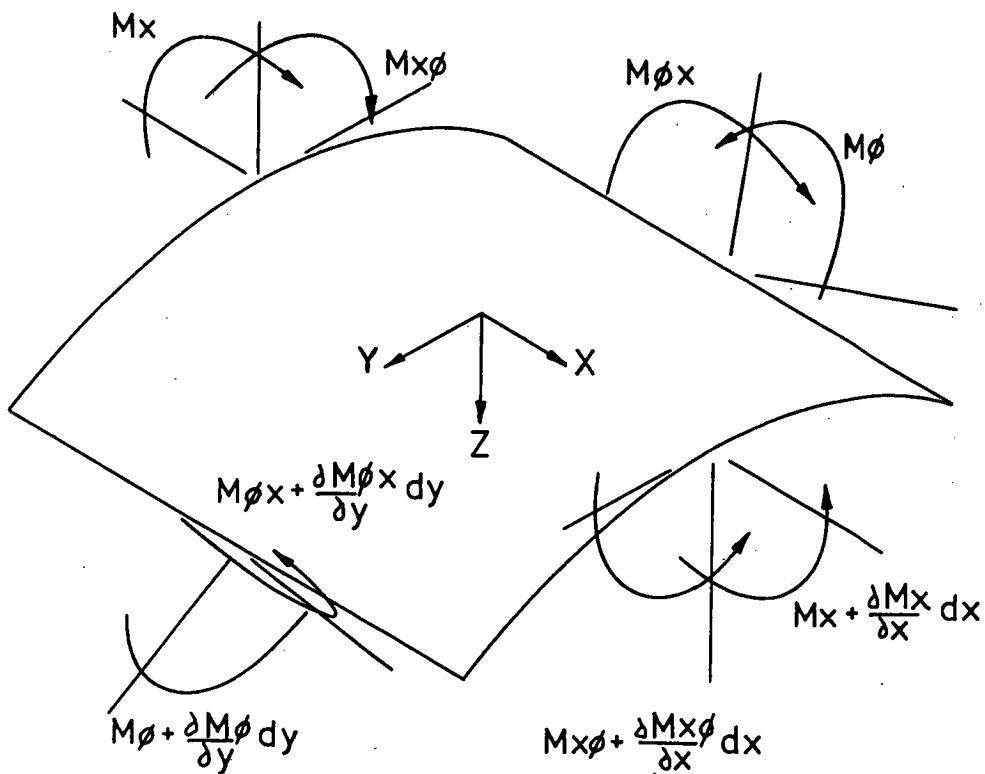
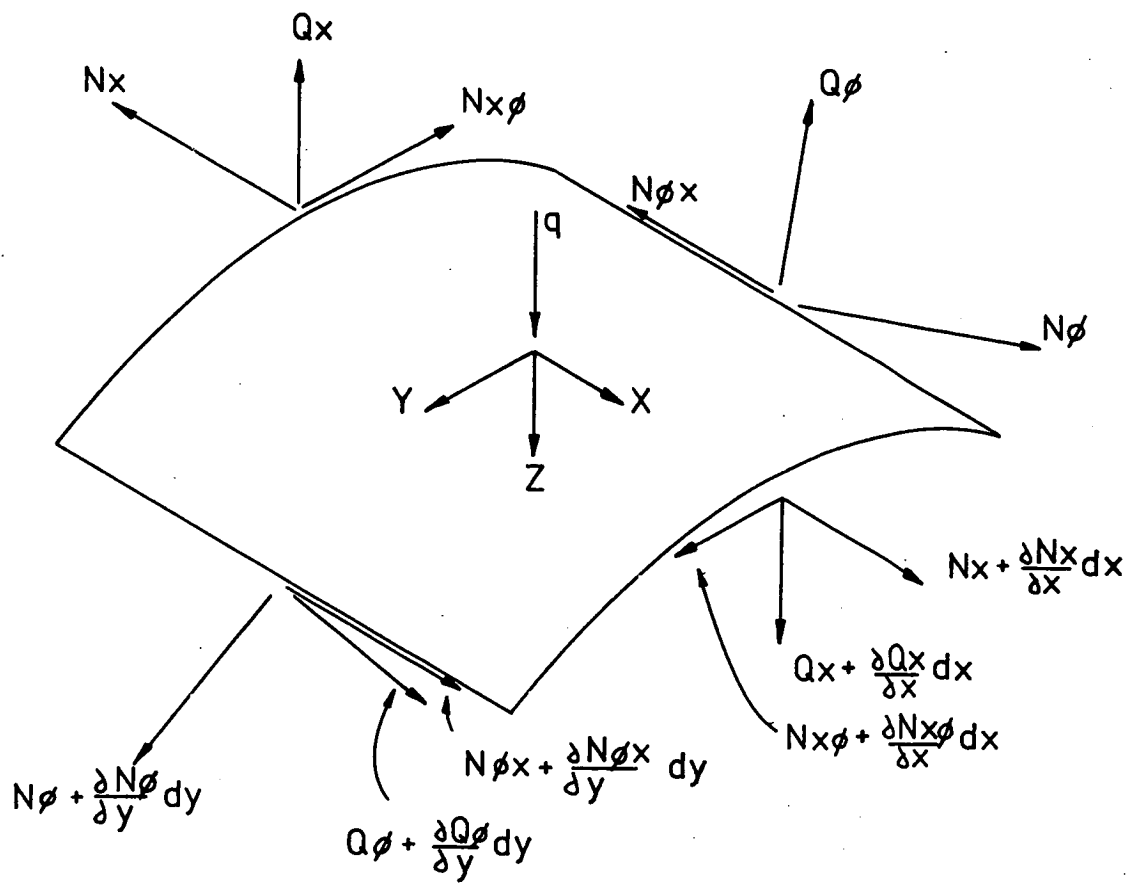


**FIGURE 3.1**  
**ELEMENT OF CYLINDER**



$$\frac{\partial N_x}{\partial x} + \frac{\partial N_{\phi x}}{\partial s} = 0 \quad \text{-----} \quad 3.1$$

$$\frac{\partial N_{x\phi}}{\partial x} + \frac{\partial N_{\phi}}{\partial s} = 0 \quad \text{-----} \quad 3.2$$

$$\begin{aligned} \text{and} \quad & \frac{\partial^2 M_x}{\partial x^2} + 2 \frac{\partial^2 M_{\phi x}}{\partial x \partial s} + \frac{\partial^2 M_{\phi}}{\partial s^2} + \frac{N_{\phi}}{R} + N_x \frac{\partial^2 w}{\partial x^2} + 2 \cdot N_{x\phi} \frac{\partial^2 w}{\partial x \partial \phi} \\ & + N_{\phi} \frac{\partial^2 w}{\partial s^2} = -q \quad \text{-----} \quad 3.3 \end{aligned}$$

$$\text{also} \quad R\phi = s \quad \text{-----} \quad 3.4$$

Of these equations, 3.1 and 3.2 represent equations of axial equilibrium and tangential equilibrium. Equation 3.3 is a combination of the moment equilibrium equation and radial equilibrium. In their paper Von Karman and Tsien refer to the first two of these equations as being "generally accepted". This author finds it difficult to accept these equations as they stand. Equations 3.1 and 3.2 are in fact the flat plate conditions. They would apply to cylindrical shells provided the radii of curvature of the shell were large relative to the thickness. Unfortunately in the post-buckled shape of the shell, to which Donnell's equations are meant to apply, the cylinder is heavily deformed and the radii of curvature quite small. This author believes the misalignment of forces should be taken into account in considering the membrane equilibrium conditions of the element.

The solution of any strength of materials problem requires the establishment of three separate sets of equations namely, force equations, geometrical or compatibility equations and material properties (e.g. Hooke's law). In shell theory it is conventional to solve these equations by what can be considered as a deformation method. Equations 3.1, 3.2 and 3.3 are three equations of equilibrium, i.e. they are three simultaneous equations in forces. The compatibility equations and material properties are usually combined together to form what are commonly called stress resultants.

In Donnell's theory the stress resultants are given by the following expressions (in the sign convention of figure 3.1)

$$\begin{aligned}
 N_{\theta} &= D \left[ \frac{1}{R} \frac{\partial v}{\partial \theta} + \frac{1}{2R^2} \left( \frac{\partial w}{\partial \theta} \right)^2 - \frac{w}{R} + \nu \left\{ \frac{\partial u}{\partial x} \right. \right. \\
 &\quad \left. \left. + \frac{1}{2} \left( \frac{\partial w}{\partial x} \right)^2 \right\} \right] \\
 N_x &= D \left[ \frac{\partial u}{\partial x} + \frac{1}{2} \left( \frac{\partial w}{\partial x} \right)^2 + \nu \left\{ \frac{1}{R} \frac{\partial v}{\partial \theta} + \frac{1}{2R^2} \left( \frac{\partial w}{\partial \theta} \right)^2 \right. \right. \\
 &\quad \left. \left. - \frac{w}{R} \right\} \right] \\
 N_{x\theta} &= N_{\theta x} = \frac{D(1-\nu)}{2} \left[ \frac{1}{R} \frac{\partial u}{\partial \theta} + \frac{\partial v}{\partial x} + \frac{1}{R} \frac{\partial w}{\partial x} \frac{\partial w}{\partial \theta} \right]
 \end{aligned}
 \quad \text{--- 3.5}$$

$$\left. \begin{aligned}
 M_{\phi} &= -K \left( \frac{1}{R^2} \cdot \frac{\partial^2 w}{\partial \phi^2} + \nu \frac{\partial^2 w}{\partial x^2} \right) \\
 M_x &= -K \left( \frac{\partial^2 w}{\partial x^2} + \frac{\nu}{R^2} \cdot \frac{\partial^2 w}{\partial \phi^2} \right) \\
 M_{x\phi} &= -M_{\phi x} = \frac{K(1-\nu)}{R} \cdot \frac{\partial^2 w}{\partial x \partial \phi}
 \end{aligned} \right] \text{-----} 3.6$$

Where D is the extensional rigidity and K is the flexural rigidity.

$$D = \frac{E \cdot T}{1 - \nu^2} \text{-----} 3.7$$

$$K = \frac{E \cdot T^3}{12(1 - \nu^2)} \text{-----} 3.8$$

In obtaining these stress resultants Donnell has ignored higher order terms in curvature. Apparently this omission produces an error of the order of  $\frac{1}{N^2}$  where N is the number of circumferential facets and could in general be ignored.

Equations 3.5 take account of the effect that changes in slope of the middle surface of the shell have on the strains. Thus they can be used where surface slopes are high. A useful comparison can be made between the Donnell equations and the Euler collapse of a simple column. In the case of a column it is usual in determining the collapse load to consider only a moment equilibrium equation which allows for the fact that the axial force is not aligned with the column section. In the first approximation a simple moment -curvature relation is used and the Euler load is obtained. A better approximation is made by considering the change in slope of the column in calculating

strains. Donnell has partly considered the misalignment of the forces with the shell element in equation 3.3. He has taken into account only the effect membrane forces have on the radial equilibrium. These are obviously the most important conditions to be included. Neglecting misalignment of forces completely in equations 3.1 and 3.2 has some analogy to column buckling. In calculating the collapse load of a column we consider only the axial force as constant. This is the equivalent statement to equation 3.1. However, in shells, transverse shears are also present and have components in the plane of the middle surface of the shell.

Donnell's equations can be further examined as follows. Suppose we consider deformations where the cylinder has buckled into a shape containing a relatively large number of lobes, then the surface slopes would still be quite small and the terms containing products of slopes would be negligible. In such a case the radial deflection "w" would also be small in comparison to the radius "R" but surface curvatures around the buckle could be considerable. If we neglect the terms in products of slopes and  $w/R$  in equations 3.5 we are left with a pair of equations in "u" and "v" only. The conclusion that can be drawn from this statement is that the membrane conditions in such a case are virtually independent of the radial deflections. In the preceding chapter it was shown that the load in such a buckled cylinder is essentially carried along the folds.

Thus where buckling deformations are encountered in a cylinder it is probably not wise to ignore the interaction terms in the membrane equations. Certainly, Donnell's equations would provide results much closer to the truth than simple small deflection theory but they do not appear to go far enough for the case of post-buckling deformations.

Timoshenko and Woinowsky Krieger (ref.15) provide us with the expanded equilibrium conditions which are.

Axial equilibrium.

$$\begin{aligned} R \frac{\partial N_x}{\partial x} + \frac{\partial N_{\phi x}}{\partial \phi} - R \cdot Q_x \frac{\partial^2 w}{\partial x^2} - R \cdot N_{x\phi} \frac{\partial^2 v}{\partial x^2} - Q_{\phi} \left( \frac{\partial v}{\partial x} + \frac{\partial^2 w}{\partial x \partial \phi} \right) \\ - N_{\phi} \left( \frac{\partial^2 v}{\partial x \partial \phi} - \frac{\partial w}{\partial x} \right) = 0 \end{aligned} \quad 3.9$$

Tangential equilibrium.

$$\begin{aligned} \frac{\partial N_{\phi}}{\partial \phi} + R \frac{\partial N_{x\phi}}{\partial x} + R \cdot N_x \frac{\partial^2 v}{\partial x^2} - Q_x \left( \frac{\partial v}{\partial x} + \frac{\partial^2 w}{\partial x \partial \phi} \right) + N_{\phi x} \left( \frac{\partial^2 v}{\partial x \partial \phi} - \frac{\partial w}{\partial x} \right) \\ - Q_{\phi} \left( 1 + \frac{1}{R} \cdot \frac{\partial v}{\partial \phi} + \frac{1}{R} \cdot \frac{\partial^2 w}{\partial \phi^2} \right) = 0 \end{aligned} \quad 3.10$$

Radial equilibrium.

$$\begin{aligned} R \frac{\partial Q_x}{\partial x} + \frac{\partial Q_{\phi}}{\partial \phi} + N_{x\phi} \left( \frac{\partial v}{\partial x} + \frac{\partial^2 w}{\partial x \partial \phi} \right) + R \cdot N_x \frac{\partial^2 w}{\partial x^2} + N_{\phi} \left( 1 + \frac{1}{R} \cdot \frac{\partial v}{\partial \phi} \right. \\ \left. + \frac{1}{R} \cdot \frac{\partial^2 w}{\partial \phi^2} \right) + N_{\phi x} \left( \frac{\partial v}{\partial x} + \frac{\partial^2 w}{\partial x \partial \phi} \right) + q \cdot R = 0 \end{aligned} \quad 3.11$$

Moment equilibrium about "X" axis.

$$\begin{aligned} R \frac{\partial M_{x\phi}}{\partial x} - \frac{\partial M_{\phi}}{\partial \phi} - R \cdot M_x \frac{\partial^2 v}{\partial x^2} - M_{\phi x} \left( \frac{\partial^2 v}{\partial x \partial \phi} - \frac{\partial w}{\partial x} \right) + R \cdot Q_{\phi} \\ = 0 \end{aligned} \quad 3.12$$

Moment equilibrium about "Y" axis.

$$\begin{aligned} \frac{\partial M_{\phi x}}{\partial \phi} + R \frac{\partial M_x}{\partial x} + R \cdot M_{x\phi} \frac{\partial^2 v}{\partial x^2} - M_{\phi} \left( \frac{\partial^2 v}{\partial x \partial \phi} - \frac{\partial w}{\partial x} \right) - R \cdot Q_x \\ = 0 \end{aligned} \quad 3.13$$

Moment equilibrium about "Z" axis.

$$\begin{aligned} M_x \left( \frac{\partial v}{\partial x} + \frac{\partial^2 w}{\partial x \partial \phi} \right) + R \cdot M_{x\phi} \frac{\partial^2 w}{\partial x^2} + M_{\phi x} \left( 1 + \frac{1}{R} \cdot \frac{\partial v}{\partial \phi} + \frac{1}{R} \cdot \frac{\partial^2 w}{\partial \phi^2} \right) \\ - M_{\phi} \left( \frac{\partial v}{\partial x} + \frac{\partial^2 w}{\partial x \partial \phi} \right) + R(N_{x\phi} - N_{\phi x}) = 0 \end{aligned} \quad 3.14$$

If we look closely at these equations we see that they contain many terms in the derivatives of "v" and "w". In practice "in plane" deflections are much smaller than "out of plane" deflections and we can neglect all the derivatives of "v" in equations 3.9 to 3.14. Thus, these equilibrium equations can be rewritten as follows.

$$R \frac{\partial N_x}{\partial x} + \frac{\partial N_{\phi x}}{\partial \phi} - R \cdot Q_x \frac{\partial^2 w}{\partial x^2} - Q_{\phi} \frac{\partial^2 w}{\partial x \partial \phi} + N_{\phi} \frac{\partial w}{\partial x} = 0 \quad 3.15$$

$$\frac{\partial N_{\phi}}{\partial \phi} + R \frac{\partial N_{x\phi}}{\partial x} - Q_x \frac{\partial^2 w}{\partial x \partial \phi} - N_{\phi x} \frac{\partial w}{\partial x} - Q_{\phi} \left( 1 + \frac{1}{R} \cdot \frac{\partial^2 w}{\partial \phi^2} \right) = 0 \quad 3.16$$

$$\begin{aligned} R \frac{\partial Q_x}{\partial x} + \frac{\partial Q_{\phi}}{\partial \phi} + N_{x\phi} \frac{\partial^2 w}{\partial x \partial \phi} + R \cdot N_x \frac{\partial^2 w}{\partial x^2} + N_{\phi} \left( 1 + \frac{1}{R} \cdot \frac{\partial^2 w}{\partial \phi^2} \right) \\ + N_{\phi x} \frac{\partial^2 w}{\partial x \partial \phi} + q \cdot R = 0 \end{aligned} \quad 3.17$$



$$R \frac{\partial M_{x\phi}}{\partial x} - \frac{\partial M_\phi}{\partial \phi} + M_{\phi x} \frac{\partial w}{\partial x} + R \cdot Q_\phi = 0 \quad \text{-----} \quad 3.18$$

$$\frac{\partial M_{\phi x}}{\partial \phi} + R \frac{\partial M_x}{\partial x} + M_\phi \frac{\partial w}{\partial x} - R \cdot Q_x = 0 \quad \text{-----} \quad 3.19$$

$$\begin{aligned} \text{and} \quad M_x \frac{\partial^2 w}{\partial x \partial \phi} + R \cdot M_{x\phi} \frac{\partial^2 w}{\partial x^2} + M_{\phi x} \left(1 + \frac{1}{R} \cdot \frac{\partial^2 w}{\partial \phi^2}\right) - M_\phi \frac{\partial^2 w}{\partial x \partial \phi} \\ + R(N_{x\phi} - N_{\phi x}) = 0 \quad \text{-----} \quad 3.20 \end{aligned}$$

Now, from equation 3.18.

$$Q_\phi = - \frac{\partial M_{x\phi}}{\partial x} + \frac{1}{R} \cdot \frac{\partial M_\phi}{\partial \phi} - \frac{M_{\phi x} \cdot \partial w}{R \cdot \partial x} \quad \text{-----} \quad 3.21$$

$$\begin{aligned} \text{and} \quad \frac{\partial Q_\phi}{\partial \phi} = - \frac{\partial^2 M_{x\phi}}{\partial x \partial \phi} + \frac{1}{R} \cdot \frac{\partial^2 M_\phi}{\partial \phi^2} - \frac{1}{R^2} \cdot \frac{\partial M_\phi}{\partial \phi} \cdot \frac{\partial R}{\partial \phi} - \frac{1}{R} \cdot \frac{\partial M_{\phi x}}{\partial \phi} \cdot \frac{\partial w}{\partial x} \\ + M_{\phi x} \left( \frac{1}{R^2} \cdot \frac{\partial w}{\partial x} \cdot \frac{\partial R}{\partial \phi} - \frac{1}{R} \cdot \frac{\partial^2 w}{\partial x \partial \phi} \right) \quad \text{-----} \quad 3.22 \end{aligned}$$

And from equation 3.19.

$$Q_x = \frac{1}{R} \cdot \frac{\partial M_{\phi x}}{\partial \phi} + \frac{\partial M_x}{\partial x} + \frac{M_\phi \cdot \partial w}{R \cdot \partial x} \quad \text{-----} \quad 3.23$$

$$\begin{aligned} \text{and} \quad \frac{\partial Q_x}{\partial x} = \frac{1}{R} \cdot \frac{\partial^2 M_{\phi x}}{\partial x \partial \phi} - \frac{1}{R^2} \cdot \frac{\partial M_{\phi x}}{\partial \phi} \cdot \frac{\partial R}{\partial x} + \frac{\partial^2 M_x}{\partial x^2} + \frac{1}{R} \cdot \frac{\partial M_\phi}{\partial x} \cdot \frac{\partial w}{\partial x} \\ + M_\phi \left( \frac{1}{R} \cdot \frac{\partial^2 w}{\partial x^2} - \frac{1}{R^2} \cdot \frac{\partial w}{\partial x} \cdot \frac{\partial R}{\partial x} \right) \quad \text{-----} \quad 3.24 \end{aligned}$$

Substituting in equation 3.15. (axial equilibrium).

$$\begin{aligned}
 & R \frac{\partial N_x}{\partial x} + \frac{\partial N_{\phi x}}{\partial \phi} - R \frac{\partial^2 w}{\partial x^2} \left( \frac{1}{R} \cdot \frac{\partial M_{\phi x}}{\partial \phi} + \frac{\partial M_x}{\partial x} + \frac{M}{R} \cdot \frac{\partial w}{\partial x} \right) + N_{\phi x} \frac{\partial w}{\partial x} \\
 & - \frac{\partial^2 w}{\partial x \partial \phi} \left( - \frac{\partial M_{\phi x}}{\partial x} + \frac{1}{R} \cdot \frac{\partial M_{\phi}}{\partial \phi} - \frac{M}{R} \cdot \frac{\partial w}{\partial x} \right) = 0 \\
 \text{or} \quad & R \frac{\partial N_x}{\partial x} + \frac{\partial N_{\phi x}}{\partial \phi} - \frac{\partial M_{\phi x}}{\partial \phi} \cdot \frac{\partial^2 w}{\partial x^2} - R \frac{\partial M_x}{\partial x} \cdot \frac{\partial^2 w}{\partial x^2} - M \frac{\partial^2 w}{\partial x^2} \cdot \frac{\partial w}{\partial x} + N_{\phi x} \frac{\partial w}{\partial x} \\
 & + \frac{\partial M_{\phi x}}{\partial x} \cdot \frac{\partial^2 w}{\partial x \partial \phi} - \frac{1}{R} \cdot \frac{\partial M_{\phi}}{\partial \phi} \cdot \frac{\partial^2 w}{\partial x \partial \phi} + \frac{M}{R} \cdot \frac{\partial w}{\partial x} \cdot \frac{\partial^2 w}{\partial x \partial \phi} = 0 \quad \text{--- 3.25}
 \end{aligned}$$

Substituting in equation 3.16. (tangential equilibrium).

$$\begin{aligned}
 & \frac{\partial N_{\phi}}{\partial \phi} + R \frac{\partial N_{\phi x}}{\partial x} - \frac{\partial^2 w}{\partial x \partial \phi} \left( \frac{1}{R} \cdot \frac{\partial M_{\phi x}}{\partial \phi} + \frac{\partial M_x}{\partial x} + \frac{M}{R} \cdot \frac{\partial w}{\partial x} \right) - N_{\phi x} \frac{\partial w}{\partial x} \\
 & - \left( 1 + \frac{1}{R} \cdot \frac{\partial^2 w}{\partial \phi^2} \right) \left( - \frac{\partial M_{\phi x}}{\partial x} + \frac{1}{R} \cdot \frac{\partial M_{\phi}}{\partial \phi} - \frac{M}{R} \cdot \frac{\partial w}{\partial x} \right) = 0 \\
 \text{or} \quad & \frac{\partial N_{\phi}}{\partial \phi} + R \frac{\partial N_{\phi x}}{\partial x} - \frac{1}{R} \cdot \frac{\partial M_{\phi x}}{\partial \phi} \cdot \frac{\partial^2 w}{\partial x \partial \phi} - \frac{\partial M_x}{\partial x} \cdot \frac{\partial^2 w}{\partial x \partial \phi} - \frac{M}{R} \cdot \frac{\partial w}{\partial x} \cdot \frac{\partial^2 w}{\partial x \partial \phi} \\
 & - N_{\phi x} \frac{\partial w}{\partial x} + \frac{\partial M_{\phi x}}{\partial x} \left( 1 + \frac{1}{R} \cdot \frac{\partial^2 w}{\partial \phi^2} \right) - \frac{1}{R} \cdot \frac{\partial M_{\phi}}{\partial \phi} \left( 1 + \frac{1}{R} \cdot \frac{\partial^2 w}{\partial \phi^2} \right) \\
 & + \frac{M}{R} \cdot \frac{\partial w}{\partial x} \left( 1 + \frac{1}{R} \cdot \frac{\partial^2 w}{\partial \phi^2} \right) = 0 \quad \text{----- 3.26}
 \end{aligned}$$

It can be seen that equations 3.25 and 3.26 are very similar to equations 3.1 and 3.2 but each contain many additional terms. These extra terms are small when deflections are small but some, if not all, should probably

be included once buckling has commenced. The radial equilibrium equation can be treated in a similar manner.

$$\begin{aligned}
 & R \left( \frac{1}{R} \cdot \frac{\partial^2 M}{\partial x \partial \phi} - \frac{1}{R^2} \cdot \frac{\partial M}{\partial \phi} \cdot \frac{\partial R}{\partial x} + \frac{\partial^2 M_x}{\partial x^2} + \frac{1}{R} \cdot \frac{\partial M}{\partial x} \cdot \frac{\partial w}{\partial x} + \frac{M}{R} \cdot \frac{\partial^2 w}{\partial x^2} \right. \\
 & \left. - \frac{M}{R^2} \cdot \frac{\partial w}{\partial x} \cdot \frac{\partial R}{\partial x} \right) - \frac{\partial^2 M_{x\phi}}{\partial x \partial \phi} + \frac{1}{R} \cdot \frac{\partial^2 M}{\partial \phi^2} - \frac{1}{R^2} \cdot \frac{\partial M}{\partial \phi} \cdot \frac{\partial R}{\partial \phi} - \frac{1}{R} \cdot \frac{\partial M}{\partial \phi} \cdot \frac{\partial w}{\partial x} \\
 & - \frac{M}{R} \cdot \frac{\partial^2 w}{\partial x \partial \phi} + \frac{M}{R^2} \cdot \frac{\partial w}{\partial x} \cdot \frac{\partial R}{\partial \phi} + N_{x\phi} \frac{\partial^2 w}{\partial x \partial \phi} + R \cdot N_x \frac{\partial^2 w}{\partial x^2} \\
 & + N_\phi \left( 1 + \frac{1}{R} \cdot \frac{\partial^2 w}{\partial \phi^2} \right) + N_{\phi x} \frac{\partial^2 w}{\partial x \partial \phi} + q \cdot R = 0
 \end{aligned}$$

or

$$\begin{aligned}
 & N_{x\phi} \frac{\partial^2 w}{\partial x \partial \phi} + R \cdot N_x \frac{\partial^2 w}{\partial x^2} + N_\phi \left( 1 + \frac{1}{R} \cdot \frac{\partial^2 w}{\partial \phi^2} \right) + N_{\phi x} \frac{\partial^2 w}{\partial x \partial \phi} + R \frac{\partial^2 M_x}{\partial x^2} \\
 & + M_\phi \left( \frac{\partial^2 w}{\partial x^2} - \frac{1}{R} \cdot \frac{\partial w}{\partial x} \cdot \frac{\partial R}{\partial x} \right) + \frac{\partial M}{\partial x} \cdot \frac{\partial w}{\partial x} - \frac{1}{R^2} \cdot \frac{\partial M}{\partial \phi} \cdot \frac{\partial R}{\partial \phi} + \frac{1}{R} \cdot \frac{\partial^2 M}{\partial \phi^2} \\
 & - \frac{\partial^2 M_{x\phi}}{\partial x \partial \phi} + \frac{M}{R} \left( \frac{1}{R} \cdot \frac{\partial w}{\partial x} \cdot \frac{\partial R}{\partial \phi} - \frac{\partial^2 w}{\partial x \partial \phi} \right) + \frac{\partial^2 M_{\phi x}}{\partial x \partial \phi} \\
 & - \frac{1}{R} \cdot \frac{\partial M}{\partial \phi} \cdot \frac{\partial R}{\partial x} \left( \frac{\partial R}{\partial x} + \frac{\partial w}{\partial x} \right) + q \cdot R = 0 \quad \text{-----} \quad 3.27
 \end{aligned}$$

Again, equation 3.27 is very similar to Donnell's equation (3.3) but has many additional terms. Some of these terms could be important when surface curvatures are large. It is interesting to note that Donnell has used terms in the products of surface slopes in his stress resultants and yet there are terms in the

product of slope and rate of change of moment in the above equation which are not included. These terms could be expected to be significant. In the membrane equations (3.25 and 3.26) there are also terms of slope with force or moment and these would also be expected to be important.

Flügge (ref.5,p.463) makes the statement that shape imperfections can be accommodated by replacing "w" with "w + B" in the equilibrium equations, where "B" is the radial difference between a true cylinder and the actual undeformed cylinder.

Thus, if  $R_1$  is the radius of the true cylinder,

$$R = R_1 - B$$

$$\frac{\partial R}{\partial \phi} = - \frac{\partial B}{\partial \phi}$$

and 
$$\frac{\partial R}{\partial x} = - \frac{\partial B}{\partial x}$$

And if  $B \ll R$  then  $R \doteq R_1$  and equations 3.25, 3.26 and 3.27 can be rewritten as.

Axial equilibrium.

$$\begin{aligned} & R \frac{\partial N_x}{\partial x} + \frac{\partial N_{\phi x}}{\partial \phi} + N_{\phi} \left( \frac{\partial w}{\partial x} + \frac{\partial B}{\partial x} \right) - M_{\phi} \left( \frac{\partial^2 w}{\partial x^2} + \frac{\partial^2 B}{\partial x^2} \right) \left( \frac{\partial w}{\partial x} + \frac{\partial B}{\partial x} \right) \\ & + \frac{M_{\phi x}}{R} \left( \frac{\partial^2 w}{\partial x \partial \phi} + \frac{\partial^2 B}{\partial x \partial \phi} \right) \left( \frac{\partial w}{\partial x} + \frac{\partial B}{\partial x} \right) - R \frac{\partial M_x}{\partial x} \left( \frac{\partial^2 w}{\partial x^2} + \frac{\partial^2 B}{\partial x^2} \right) \\ & - \frac{1}{R} \frac{\partial M_{\phi}}{\partial \phi} \left( \frac{\partial^2 w}{\partial x \partial \phi} + \frac{\partial^2 B}{\partial x \partial \phi} \right) - \frac{\partial M_{\phi x}}{\partial \phi} \left( \frac{\partial^2 w}{\partial x^2} + \frac{\partial^2 B}{\partial x^2} \right) + \frac{\partial M_{x\phi}}{\partial x} \left( \frac{\partial^2 w}{\partial x \partial \phi} + \frac{\partial^2 B}{\partial x \partial \phi} \right) \\ & \frac{\partial^2 B}{\partial x \partial \phi} = 0 \end{aligned} \quad \text{-----} \quad 3.28$$

Tangential equilibrium.

$$\begin{aligned}
 & \frac{\partial F}{\partial \phi} + R \frac{\partial N_{x\phi}}{\partial x} - N_{\phi x} \left( \frac{\partial w}{\partial x} + \frac{\partial B}{\partial x} \right) - \frac{M}{R} \left( \frac{\partial w}{\partial x} + \frac{\partial B}{\partial x} \right) \left( \frac{\partial^2 w}{\partial x \partial \phi} + \frac{\partial^2 B}{\partial x \partial \phi} \right) \\
 & + \frac{M_{\phi x}}{R} \left( \frac{\partial w}{\partial x} + \frac{\partial B}{\partial x} \right) \left( 1 + \frac{1}{R} \frac{\partial^2 w}{\partial \phi^2} + \frac{1}{R} \frac{\partial^2 B}{\partial \phi^2} \right) - \frac{\partial M_x}{\partial x} \left( \frac{\partial^2 w}{\partial x \partial \phi} + \frac{\partial^2 B}{\partial x \partial \phi} \right) \\
 & - \frac{1}{R} \frac{\partial M}{\partial \phi} \left( 1 + \frac{1}{R} \frac{\partial^2 w}{\partial \phi^2} + \frac{1}{R} \frac{\partial^2 B}{\partial \phi^2} \right) - \frac{1}{R} \frac{\partial M_{\phi x}}{\partial \phi} \left( \frac{\partial^2 w}{\partial x \partial \phi} + \frac{\partial^2 B}{\partial x \partial \phi} \right) \\
 & + \frac{\partial M_{x\phi}}{\partial x} \left( 1 + \frac{1}{R} \frac{\partial^2 w}{\partial \phi^2} + \frac{1}{R} \frac{\partial^2 B}{\partial \phi^2} \right) = 0 \quad \text{-----} \quad 3.29
 \end{aligned}$$

Radial equilibrium.

$$\begin{aligned}
 & N_{x\phi} \left( \frac{\partial^2 w}{\partial x \partial \phi} + \frac{\partial^2 B}{\partial x \partial \phi} \right) + R \cdot N_x \left( \frac{\partial^2 w}{\partial x^2} + \frac{\partial^2 B}{\partial x^2} \right) + N_{\phi} \left( 1 + \frac{1}{R} \frac{\partial^2 w}{\partial \phi^2} + \right. \\
 & \left. \frac{1}{R} \frac{\partial^2 B}{\partial \phi^2} \right) + N_{\phi x} \left( \frac{\partial^2 w}{\partial x \partial \phi} + \frac{\partial^2 B}{\partial x \partial \phi} \right) + R \frac{\partial^2 M_x}{\partial x^2} + M_{\phi} \left( \frac{1}{R} \frac{\partial w}{\partial x} \frac{\partial B}{\partial x} + \right. \\
 & \left. \frac{1}{R} \left( \frac{\partial B}{\partial x} \right)^2 + \frac{\partial^2 w}{\partial x^2} + \frac{\partial^2 B}{\partial x^2} \right) + \frac{\partial M}{\partial x} \left( \frac{\partial w}{\partial x} + \frac{\partial B}{\partial x} \right) + \frac{1}{R^2} \frac{\partial M}{\partial \phi} \frac{\partial B}{\partial \phi} \\
 & + \frac{1}{R} \frac{\partial^2 M}{\partial \phi^2} - \frac{\partial^2 M_{x\phi}}{\partial x \partial \phi} - \frac{M_{\phi x}}{R} \left( \frac{\partial^2 w}{\partial x \partial \phi} + \frac{\partial^2 B}{\partial x \partial \phi} \right) + \frac{1}{R} \frac{\partial B}{\partial \phi} \frac{\partial w}{\partial x} + \frac{1}{R} \frac{\partial B}{\partial \phi} \frac{\partial B}{\partial x} \\
 & + \frac{\partial^2 M_{\phi x}}{\partial x \partial \phi} - \frac{1}{R} \frac{\partial M_{\phi x}}{\partial \phi} \frac{\partial w}{\partial x} + q \cdot R = 0 \quad \text{-----} \quad 3.30
 \end{aligned}$$

Flügge (p.214) also gives wider expressions for the stress resultants as follows.

$$\begin{aligned}
 N_{\phi} &= D\left(\frac{1}{R} \cdot \frac{\partial v}{\partial \phi} - \frac{w}{R} + \nu \frac{\partial u}{\partial x}\right) - \frac{K}{R^2}\left(\frac{w}{R} + \frac{1}{R} \cdot \frac{\partial^2 w}{\partial \phi^2}\right) \\
 N_x &= D\left(\frac{\partial u}{\partial x} + \frac{\nu}{R} \cdot \frac{\partial v}{\partial \phi} - \frac{\nu}{R} \cdot \frac{w}{R}\right) + \frac{K}{R} \cdot \frac{\partial^2 w}{\partial x^2} \\
 N_{\phi x} &= \frac{D(1-\nu)}{2} \left(\frac{1}{R} \cdot \frac{\partial u}{\partial \phi} + \frac{\partial v}{\partial x}\right) + \frac{K}{R^2} \cdot \frac{(1-\nu)}{2} \left(\frac{1}{R} \cdot \frac{\partial u}{\partial \phi} \right. \\
 &\quad \left. - \frac{\partial^2 w}{\partial x \partial \phi}\right) \\
 N_{x\phi} &= \frac{D(1-\nu)}{2} \left(\frac{1}{R} \cdot \frac{\partial u}{\partial \phi} + \frac{\partial v}{\partial x}\right) + \frac{K(1-\nu)}{2R^2} \left(\frac{\partial v}{\partial x} \right. \\
 &\quad \left. + \frac{\partial^2 w}{\partial x \partial \phi}\right)
 \end{aligned}
 \quad \text{--- 3.31}$$

$$\begin{aligned}
 M_{\phi} &= -K\left(\frac{w}{R^2} + \frac{1}{R^2} \cdot \frac{\partial^2 w}{\partial \phi^2} + \nu \frac{\partial^2 w}{\partial x^2}\right) \\
 M_x &= -K\left(\frac{\partial^2 w}{\partial x^2} + \frac{\nu}{R^2} \cdot \frac{\partial^2 w}{\partial \phi^2} + \frac{1}{R} \cdot \frac{\partial u}{\partial x} + \frac{\nu}{R^2} \cdot \frac{\partial v}{\partial \phi}\right) \\
 M_{\phi x} &= \frac{K}{R}(1-\nu) \left(-\frac{\partial^2 w}{\partial x \partial \phi} + \frac{1}{2R} \cdot \frac{\partial u}{\partial \phi} - \frac{1}{2} \cdot \frac{\partial v}{\partial x}\right) \\
 M_{x\phi} &= \frac{K}{R}(1-\nu) \left(\frac{\partial^2 w}{\partial x \partial \phi} + \frac{\partial v}{\partial x}\right)
 \end{aligned}
 \quad \text{--- 3.32}$$

$$\text{N.B. } \frac{K}{R^2} = \frac{T^2 D}{12R^2}$$

For most practical purposes  $\frac{K}{R^2}$  is much smaller than  $D$  and can be neglected where both appear in the one relation. Thus the first four stress resultants can be rewritten as,



$$\begin{aligned}
 N_{\phi} &= D \left( \frac{1}{R} \cdot \frac{\partial v}{\partial \phi} - \frac{w}{R} + \nu \frac{\partial u}{\partial x} \right) \\
 N_x &= D \left( \frac{\partial u}{\partial x} + \frac{\nu}{R} \frac{\partial v}{\partial \phi} - \frac{\nu}{R} w \right) \\
 N_{x\phi} &= N_{\phi x} = \frac{D(1-\nu)}{2} \left( \frac{1}{R} \frac{\partial u}{\partial \phi} + \frac{\partial v}{\partial x} \right)
 \end{aligned}
 \quad \text{----- 3.33}$$

Flügge ignores additional terms in the expressions for moments which are even less significant. The third reference is the ever faithful book by Timoshenko and Woinowsky Krieger (ref.15). Their membrane stresses are those given by equation 3.33 while the moments are slightly different, namely,

$$\begin{aligned}
 M_x &= -K \left( \frac{\partial^2 w}{\partial x^2} + \frac{\nu}{R^2} \frac{\partial v}{\partial \phi} + \frac{\nu}{R^2} \frac{\partial^2 w}{\partial \phi^2} \right) \\
 M_{\phi} &= -K \left( \frac{1}{R^2} \frac{\partial v}{\partial \phi} + \frac{1}{R^2} \frac{\partial^2 w}{\partial \phi^2} + \nu \frac{\partial^2 w}{\partial x^2} \right) \\
 M_{x\phi} &= -M_{\phi x} = \frac{K(1-\nu)}{R} \left( \frac{\partial v}{\partial x} + \frac{\partial^2 w}{\partial x \partial \phi} \right)
 \end{aligned}
 \quad \text{----- 3.34}$$

The difference between these equations and the Flügge equations is only small. The change occurs by considering the fact that the cross-sectional area on which the stresses act is not rectangular but is wider on the outside than on the inside. Thus, for the remainder of this discussion the Flügge stress resultants will be ignored. The additional terms used in the Timoshenko moment resultants which do not appear in the Donnell

resultants are all derivatives of in plane displacements. These are small in comparison to derivatives of out of plane displacements and will also be ignored for this discussion. Thus Timoshenko and Woinowsky Krieger's moment resultants reduce to the same as those used by Donnell. The inclusion of the slope terms in Donnell's membrane forces is necessary for post-buckling deformations so that this discussion will also consider the combination of Donnell's resultants and Timoshenko's equilibrium conditions. Thus the following combinations arise.

1. The Donnell equilibrium equations (3.1, 3.2 and 3.3) with his resultants (3.5 and 3.6).
2. The modified Timoshenko and Woinowsky Krieger equilibrium equations (3.28, 3.29 and 3.30) with their resultants (3.33 and 3.6).
3. The modified Timoshenko and Woinowsky Krieger equilibrium equations (3.28, 3.29 and 3.30) with Donnell's resultants (3.5 and 3.6).

From equations 3.5 we can obtain the following derivatives.

$$\begin{aligned}
 \frac{\partial N_x}{\partial x} &= D \left[ \frac{\partial^2 u}{\partial x^2} + \frac{\partial w}{\partial x} \frac{\partial^2 w}{\partial x^2} + \nu \left( \frac{1}{R} \frac{\partial^2 v}{\partial x \partial \phi} + \frac{1}{R^2} \frac{\partial w}{\partial \phi} \frac{\partial^2 w}{\partial x \partial \phi} \right. \right. \\
 &\quad \left. \left. - \frac{1}{R} \frac{\partial w}{\partial x} \right) \right] \\
 \frac{\partial N_{\phi x}}{\partial \phi} &= \frac{\partial N_{x\phi}}{\partial \phi} = \frac{D(1-\nu)}{2} \left( \frac{1}{R} \frac{\partial^2 u}{\partial \phi^2} + \frac{\partial^2 v}{\partial x \partial \phi} \right. \\
 &\quad \left. + \frac{1}{R} \frac{\partial^2 w}{\partial x \partial \phi} \frac{\partial w}{\partial \phi} + \frac{1}{R} \frac{\partial w}{\partial x} \frac{\partial^2 w}{\partial \phi^2} \right)
 \end{aligned}
 \tag{3.35}$$

$$\begin{aligned}
\frac{\partial N_{\phi x}}{\partial x} &= \frac{\partial N_{x\phi}}{\partial x} = \frac{D(1-\nu)}{2} \left( \frac{1}{R} \frac{\partial^2 u}{\partial x \partial \phi} + \frac{\partial^2 v}{\partial x^2} \right. \\
&\quad \left. + \frac{1}{R} \frac{\partial^2 w}{\partial x^2} \frac{\partial w}{\partial \phi} + \frac{1}{R} \frac{\partial w}{\partial x} \frac{\partial^2 w}{\partial x \partial \phi} \right) \\
\frac{\partial N_{\phi}}{\partial \phi} &= D \left[ \frac{1}{R} \frac{\partial^2 v}{\partial \phi^2} + \frac{1}{R^2} \frac{\partial w}{\partial \phi} \frac{\partial^2 w}{\partial \phi^2} - \frac{1}{R} \frac{\partial w}{\partial \phi} \right. \\
&\quad \left. + \nu \left( \frac{\partial^2 u}{\partial x \partial \phi} + \frac{\partial w}{\partial x} \frac{\partial^2 w}{\partial x \partial \phi} \right) \right]
\end{aligned}$$

The alternative derivatives using equations 3.33 are.

$$\begin{aligned}
\frac{\partial N_x}{\partial x} &= D \left( \frac{\partial^2 u}{\partial x^2} + \frac{\nu}{R} \frac{\partial^2 v}{\partial x \partial \phi} - \frac{\nu}{R} \frac{\partial w}{\partial x} \right) \\
\frac{\partial N_{\phi x}}{\partial \phi} &= \frac{\partial N_{x\phi}}{\partial \phi} = \frac{D(1-\nu)}{2} \left( \frac{1}{R} \frac{\partial^2 u}{\partial \phi^2} + \frac{\partial^2 v}{\partial x \partial \phi} \right) \\
\frac{\partial N_{\phi x}}{\partial x} &= \frac{\partial N_{x\phi}}{\partial x} = \frac{D(1-\nu)}{2} \left( \frac{1}{R} \frac{\partial^2 u}{\partial x \partial \phi} + \frac{\partial^2 v}{\partial x^2} \right) \\
\frac{\partial N_{\phi}}{\partial \phi} &= D \left( \frac{1}{R} \frac{\partial^2 v}{\partial \phi^2} - \frac{1}{R} \frac{\partial w}{\partial \phi} + \nu \frac{\partial^2 u}{\partial x \partial \phi} \right)
\end{aligned}
\quad \text{----- 3.36}$$

Also, from equations 3.6 the following derivatives of the moments are required.

$$\begin{aligned}
\frac{\partial M_x}{\partial x} &= -K \left( \frac{\partial^3 w}{\partial x^3} + \frac{\nu}{R^2} \frac{\partial^3 w}{\partial x \partial \phi^2} \right) \\
\frac{\partial M_{\phi}}{\partial \phi} &= -K \left( \frac{1}{R^2} \frac{\partial^3 w}{\partial \phi^3} + \nu \frac{\partial^3 w}{\partial x^2 \partial \phi} \right) \\
\frac{\partial M_{\phi}}{\partial x} &= -K \left( \frac{1}{R^2} \frac{\partial^3 w}{\partial x \partial \phi^2} + \nu \frac{\partial^3 w}{\partial x^3} \right) \\
\frac{\partial M_{\phi x}}{\partial \phi} &= -\frac{K(1-\nu)}{R} \frac{\partial^3 w}{\partial x \partial \phi^2} \\
\frac{\partial M_{x\phi}}{\partial x} &= \frac{K(1-\nu)}{R} \frac{\partial^3 w}{\partial x^2 \partial \phi}
\end{aligned}
\quad \text{----- 3.37}$$

And.

$$\left. \begin{aligned} \frac{\partial^2 M_x}{\partial x^2} &= -K \left( \frac{\partial^4 w}{\partial x^4} + \frac{\nu}{R^2} \frac{\partial^4 w}{\partial x^2 \partial \phi^2} \right) \\ \frac{\partial^2 M_{\phi x}}{\partial x \partial \phi} &= -\frac{K(1-\nu)}{R} \frac{\partial^4 w}{\partial x^2 \partial \phi^2} \\ \frac{\partial^2 M_{\phi}}{\partial \phi^2} &= -K \left( \frac{1}{R^2} \frac{\partial^4 w}{\partial \phi^4} + \nu \frac{\partial^4 w}{\partial x^2 \partial \phi^2} \right) \end{aligned} \right] \text{-----} 3.38$$

Now, returning to Donnell's equations we can substitute for the stress resultants and allow for initial imperfections as follows.

$$\begin{aligned} D \left( \frac{\partial^2 u}{\partial x^2} + \frac{\partial w}{\partial x} \frac{\partial^2 w}{\partial x^2} + \frac{\nu}{R} \frac{\partial^2 v}{\partial x \partial \phi} + \frac{\nu}{R^2} \frac{\partial w}{\partial \phi} \frac{\partial^2 w}{\partial x \partial \phi} - \frac{\nu}{R} \frac{\partial w}{\partial x} \right) \\ + \frac{D(1-\nu)}{2R} \left( \frac{1}{R} \frac{\partial^2 u}{\partial \phi^2} + \frac{\partial^2 v}{\partial x \partial \phi} + \frac{1}{R} \frac{\partial^2 w}{\partial x \partial \phi} \frac{\partial w}{\partial \phi} + \frac{1}{R} \frac{\partial w}{\partial x} \frac{\partial^2 w}{\partial \phi^2} \right) = 0 \end{aligned}$$

i.e.

$$\begin{aligned} \frac{\partial^2 u}{\partial x^2} + \frac{(1-\nu)}{2R^2} \frac{\partial^2 u}{\partial \phi^2} &= -\frac{\partial w}{\partial x} \frac{\partial^2 w}{\partial x^2} - \frac{(1+\nu)}{2R} \frac{\partial^2 v}{\partial x \partial \phi} + \frac{\nu}{R} \frac{\partial w}{\partial x} \\ &- \frac{(1+\nu)}{2R^2} \frac{\partial w}{\partial \phi} \frac{\partial^2 w}{\partial x \partial \phi} - \frac{(1-\nu)}{2R^2} \frac{\partial w}{\partial x} \frac{\partial^2 w}{\partial \phi^2} \text{-----} 3.39 \end{aligned}$$

$$\begin{aligned} \frac{D(1-\nu)}{2} \left( \frac{1}{R} \frac{\partial^2 u}{\partial x \partial \phi} + \frac{\partial^2 v}{\partial x^2} + \frac{1}{R} \frac{\partial^2 w}{\partial x^2} \frac{\partial w}{\partial \phi} + \frac{1}{R} \frac{\partial w}{\partial x} \frac{\partial^2 w}{\partial x \partial \phi} \right) \\ \frac{D}{R} \left( \frac{1}{R} \frac{\partial^2 v}{\partial \phi^2} + \frac{1}{R^2} \frac{\partial w}{\partial \phi} \frac{\partial^2 w}{\partial \phi^2} - \frac{1}{R} \frac{\partial w}{\partial \phi} + \nu \frac{\partial^2 u}{\partial x \partial \phi} + \nu \frac{\partial w}{\partial x} \frac{\partial^2 w}{\partial x \partial \phi} \right) = 0 \end{aligned}$$

i.e.

$$\begin{aligned} \frac{1}{R^2} \frac{\partial^2 v}{\partial \phi^2} + \frac{(1-\nu)}{2} \frac{\partial^2 v}{\partial x^2} &= -\frac{(1+\nu)}{2R} \frac{\partial^2 u}{\partial x \partial \phi} - \frac{(1+\nu)}{2R} \frac{\partial w}{\partial x} \frac{\partial^2 w}{\partial x \partial \phi} \\ &+ \frac{1}{R^2} \frac{\partial w}{\partial \phi} - \frac{(1-\nu)}{2R} \frac{\partial w}{\partial \phi} \frac{\partial^2 w}{\partial x^2} - \frac{1}{R^3} \frac{\partial w}{\partial \phi} \frac{\partial^2 w}{\partial \phi^2} \text{-----} 3.40 \end{aligned}$$

and.

$$\begin{aligned}
 & K \left( \frac{\partial^4 w}{\partial x^4} + \frac{\nu}{R^2} \cdot \frac{\partial^4 w}{\partial x^2 \partial \phi^2} \right) + \frac{2K(1-\nu)}{R^2} \cdot \frac{\partial^4 w}{\partial x^2 \partial \phi^2} + \frac{K}{R^2} \left( \frac{1}{R^2} \cdot \frac{\partial^4 w}{\partial \phi^4} \right. \\
 & \left. + \nu \frac{\partial^4 w}{\partial x^2 \partial \phi^2} \right) = \frac{N}{R} \phi + N_x \left( \frac{\partial^2 w}{\partial x^2} + \frac{\partial^2 B}{\partial x^2} \right) \\
 & + \frac{2N_x \phi}{R} \left( \frac{\partial^2 w}{\partial x \partial \phi} + \frac{\partial^2 B}{\partial x \partial \phi} \right) + \frac{N}{R^2} \left( \frac{\partial^2 w}{\partial \phi^2} + \frac{\partial^2 B}{\partial \phi^2} \right) \\
 \text{i.e. } & \frac{\partial^4 w}{\partial x^4} + \frac{2}{R^2} \cdot \frac{\partial^4 w}{\partial x^2 \partial \phi^2} + \frac{1}{R^4} \cdot \frac{\partial^4 w}{\partial \phi^4} = \frac{N}{K \cdot R} + \frac{N_x}{K} \cdot \frac{\partial^2 w}{\partial x^2} + \frac{N_x}{K} \cdot \frac{\partial^2 B}{\partial x^2} \\
 & + \frac{2N_x \phi}{K \cdot R} \cdot \frac{\partial^2 w}{\partial x \partial \phi} + \frac{2N_x \phi}{K \cdot R} \cdot \frac{\partial^2 B}{\partial x \partial \phi} + \frac{N}{K \cdot R^2} \cdot \frac{\partial^2 w}{\partial \phi^2} + \frac{N}{K \cdot R^2} \cdot \frac{\partial^2 B}{\partial \phi^2} \quad \text{--- 3.41}
 \end{aligned}$$

$$\text{N.B. } \frac{D}{K} = \frac{12}{T^2} \quad \text{----- 3.42}$$

Equations 3.39, 3.40 and 3.41 are Donnell's equations reduced to three simultaneous partial differential equations in deflections. Solution of these equations will give the deformations according to his theory. The modified Timoshenko equations can be treated in a similar manner.

From equation 3.28.

$$\begin{aligned}
 & D \left( \frac{\partial^2 u}{\partial x^2} + \frac{\nu}{R} \cdot \frac{\partial^2 v}{\partial x \partial \phi} - \frac{\nu}{R} \cdot \frac{\partial w}{\partial x} \right) + \frac{D(1-\nu)}{2R} \left( \frac{1}{R} \cdot \frac{\partial^2 u}{\partial \phi^2} + \frac{\partial^2 v}{\partial x \partial \phi} \right) \\
 & = - \frac{N}{R} \left( \frac{\partial w}{\partial x} + \frac{\partial B}{\partial x} \right) + \frac{M}{R} \left( \frac{\partial^2 w}{\partial x^2} + \frac{\partial^2 B}{\partial x^2} \right) \left( \frac{\partial w}{\partial x} + \frac{\partial B}{\partial x} \right) - \frac{M}{R^2} \phi x \left( \frac{\partial^2 w}{\partial x \partial \phi} \right. \\
 & \left. + \frac{\partial^2 B}{\partial x \partial \phi} \right) \left( \frac{\partial w}{\partial x} + \frac{\partial B}{\partial x} \right) + \frac{\partial M_x}{\partial x} \left( \frac{\partial^2 w}{\partial x^2} + \frac{\partial^2 B}{\partial x^2} \right) + \frac{1}{R^2} \cdot \frac{\partial M}{\partial \phi} \left( \frac{\partial^2 w}{\partial x \partial \phi} + \frac{\partial^2 B}{\partial x \partial \phi} \right) \\
 & + \frac{1}{R} \cdot \frac{\partial M}{\partial \phi} \phi x \left( \frac{\partial^2 w}{\partial x^2} + \frac{\partial^2 B}{\partial x^2} \right) - \frac{1}{R} \cdot \frac{\partial M_x}{\partial x} \phi \left( \frac{\partial^2 w}{\partial x \partial \phi} + \frac{\partial^2 B}{\partial x \partial \phi} \right)
 \end{aligned}$$

$$\begin{aligned}
\text{i.e. } \frac{\partial^2 u}{\partial x^2} + \frac{(1-\nu)}{2R^2} \cdot \frac{\partial^2 u}{\partial \rho^2} &= - \frac{N}{R \cdot D} \left( \frac{\partial w}{\partial x} + \frac{\partial B}{\partial x} \right) + \frac{M}{R \cdot D} \left( \frac{\partial^2 w}{\partial x^2} + \right. \\
&\left. \frac{\partial^2 B}{\partial x^2} \right) \left( \frac{\partial w}{\partial x} + \frac{\partial B}{\partial x} \right) - \frac{M}{R^2 D} \left( \frac{\partial^2 w}{\partial x \partial \rho} + \frac{\partial^2 B}{\partial x \partial \rho} \right) \left( \frac{\partial w}{\partial x} + \frac{\partial B}{\partial x} \right) + \\
&\frac{1}{D} \cdot \frac{\partial M_x}{\partial x} \left( \frac{\partial^2 w}{\partial x^2} + \frac{\partial^2 B}{\partial x^2} \right) + \frac{1}{R^2 D} \cdot \frac{\partial M}{\partial \rho} \left( \frac{\partial^2 w}{\partial x \partial \rho} + \frac{\partial^2 B}{\partial x \partial \rho} \right) + \\
&\frac{1}{R \cdot D} \cdot \frac{\partial M_x}{\partial \rho} \left( \frac{\partial^2 w}{\partial x^2} + \frac{\partial^2 B}{\partial x^2} \right) - \frac{1}{R \cdot D} \cdot \frac{\partial M_x}{\partial x} \left( \frac{\partial^2 w}{\partial x \partial \rho} + \frac{\partial^2 B}{\partial x \partial \rho} \right) + \\
&\frac{\nu \cdot \partial w}{R \partial x} - \frac{(1+\nu)}{2R} \cdot \frac{\partial^2 v}{\partial x \partial \rho} \quad \text{-----} \quad 3.43
\end{aligned}$$

From equation 3.29.

$$\begin{aligned}
D \left( \frac{1}{R} \cdot \frac{\partial^2 v}{\partial \rho^2} - \frac{1}{R} \cdot \frac{\partial w}{\partial \rho} + \nu \frac{\partial^2 u}{\partial x \partial \rho} \right) + D \cdot R \frac{(1-\nu)}{2} \left( \frac{1}{R} \cdot \frac{\partial^2 u}{\partial x \partial \rho} + \frac{\partial^2 v}{\partial x^2} \right) \\
= \frac{N}{R} \left( \frac{\partial w}{\partial x} + \frac{\partial B}{\partial x} \right) + \frac{M}{R} \left( \frac{\partial w}{\partial x} + \frac{\partial B}{\partial x} \right) \left( \frac{\partial^2 w}{\partial x \partial \rho} + \frac{\partial^2 B}{\partial x \partial \rho} \right) - \\
\frac{M}{R} \left( \frac{\partial w}{\partial x} + \frac{\partial B}{\partial x} \right) \left( 1 + \frac{1}{R} \cdot \frac{\partial^2 w}{\partial \rho^2} + \frac{1}{R} \cdot \frac{\partial^2 B}{\partial \rho^2} \right) + \frac{\partial M_x}{\partial x} \left( \frac{\partial^2 w}{\partial x \partial \rho} + \frac{\partial^2 B}{\partial x \partial \rho} \right) + \\
\frac{1}{R} \cdot \frac{\partial M}{\partial \rho} \left( 1 + \frac{1}{R} \cdot \frac{\partial^2 w}{\partial \rho^2} + \frac{1}{R} \cdot \frac{\partial^2 B}{\partial \rho^2} \right) + \frac{1}{R} \cdot \frac{\partial M_x}{\partial \rho} \left( \frac{\partial^2 w}{\partial x \partial \rho} + \frac{\partial^2 B}{\partial x \partial \rho} \right) - \\
\frac{\partial M_x}{\partial x} \left( 1 + \frac{1}{R} \cdot \frac{\partial^2 w}{\partial \rho^2} + \frac{1}{R} \cdot \frac{\partial^2 B}{\partial \rho^2} \right)
\end{aligned}$$

$$\begin{aligned}
\text{i.e. } \frac{1}{R^2} \cdot \frac{\partial^2 v}{\partial \rho^2} + \frac{(1-v)}{2} \cdot \frac{\partial^2 v}{\partial x^2} &= \frac{N}{R \cdot D} \left( \frac{\partial w}{\partial x} + \frac{\partial B}{\partial x} \right) + \frac{M}{D \cdot R^2} \left( \frac{\partial w}{\partial x} + \right. \\
&\left. \frac{\partial B}{\partial x} \right) \left( \frac{\partial^2 w}{\partial x \partial \rho} + \frac{\partial^2 B}{\partial x \partial \rho} \right) - \frac{M}{D \cdot R^2} \left( \frac{\partial w}{\partial x} + \frac{\partial B}{\partial x} \right) \left( 1 + \frac{1}{R} \cdot \frac{\partial^2 w}{\partial \rho^2} + \frac{1}{R} \cdot \frac{\partial^2 B}{\partial \rho^2} \right) + \\
&\frac{1}{R \cdot D} \cdot \frac{\partial^M}{\partial x} \left( \frac{\partial^2 w}{\partial x \partial \rho} + \frac{\partial^2 B}{\partial x \partial \rho} \right) + \frac{1}{D \cdot R^2} \cdot \frac{\partial^M}{\partial \rho} \left( 1 + \frac{1}{R} \cdot \frac{\partial^2 w}{\partial \rho^2} + \frac{1}{R} \cdot \frac{\partial^2 B}{\partial \rho^2} \right) + \\
&\frac{1}{D \cdot R^2} \cdot \frac{\partial^M}{\partial \rho} \left( \frac{\partial^2 w}{\partial x \partial \rho} + \frac{\partial^2 B}{\partial x \partial \rho} \right) - \frac{1}{R \cdot D} \cdot \frac{\partial^M}{\partial x} \left( 1 + \frac{1}{R} \cdot \frac{\partial^2 w}{\partial \rho^2} + \frac{1}{R} \cdot \frac{\partial^2 B}{\partial \rho^2} \right) + \\
&\frac{1}{R^2} \cdot \frac{\partial w}{\partial \rho} - \frac{(1+v)}{2R} \cdot \frac{\partial^2 u}{\partial x \partial \rho} \quad \text{-----} \quad 3.44
\end{aligned}$$

And from equation 3.30.

$$\begin{aligned}
&- R \cdot K \left( \frac{\partial^4 w}{\partial x^4} + \frac{v}{R^2} \cdot \frac{\partial^4 w}{\partial x^2 \partial \rho^2} \right) - \frac{K}{R} \left( \frac{1}{R^2} \cdot \frac{\partial^4 w}{\partial \rho^4} + \frac{\partial^4 w}{\partial x^2 \partial \rho^2} \right) - \\
&\frac{2K(1-v)}{R} \cdot \frac{\partial^4 w}{\partial x^2 \partial \rho^2} = - N_{x\rho} \left( \frac{\partial^2 w}{\partial x \partial \rho} + \frac{\partial^2 B}{\partial x \partial \rho} \right) - R \cdot N_x \left( \frac{\partial^2 w}{\partial x^2} + \frac{\partial^2 B}{\partial x^2} \right) - \\
&N_\rho \left( 1 + \frac{1}{R} \cdot \frac{\partial^2 w}{\partial \rho^2} + \frac{1}{R} \cdot \frac{\partial^2 B}{\partial \rho^2} \right) - N_{\rho x} \left( \frac{\partial^2 w}{\partial x \partial \rho} + \frac{\partial^2 B}{\partial x \partial \rho} \right) - M_\rho \left( \frac{1}{R} \cdot \frac{\partial w}{\partial x} \cdot \frac{\partial B}{\partial x} + \right. \\
&\left. \frac{1}{R} \left( \frac{\partial B}{\partial x} \right)^2 + \frac{\partial^2 w}{\partial x^2} + \frac{\partial^2 B}{\partial x^2} \right) - \frac{\partial^M}{\partial x} \left( \frac{\partial w}{\partial x} + \frac{\partial B}{\partial x} \right) - \frac{1}{R^2} \cdot \frac{\partial^M}{\partial \rho} \cdot \frac{\partial B}{\partial \rho} + \\
&\frac{M}{R} \rho_x \left( \frac{\partial^2 w}{\partial x \partial \rho} + \frac{\partial^2 B}{\partial x \partial \rho} + \frac{1}{R} \cdot \frac{\partial B}{\partial \rho} \cdot \frac{\partial w}{\partial x} + \frac{1}{R} \cdot \frac{\partial B}{\partial \rho} \cdot \frac{\partial B}{\partial x} \right) + \frac{1}{R} \cdot \frac{\partial^M}{\partial \rho} \rho_x \left( \frac{\partial w}{\partial x} + \right. \\
&\left. 2 \frac{\partial B}{\partial x} \right) - q \cdot R
\end{aligned}$$



$$\text{i.e. } \frac{\partial^4 w}{\partial x^4} + \frac{1}{R^4} \cdot \frac{\partial^4 w}{\partial \phi^4} + \frac{2}{R^2} \cdot \frac{\partial^4 w}{\partial x^2 \partial \phi^2} = \frac{N_x \phi}{R \cdot K} \left( \frac{\partial^2 w}{\partial x \partial \phi} + \frac{\partial^2 B}{\partial x \partial \phi} \right) +$$

$$\frac{N_x}{K} \left( \frac{\partial^2 w}{\partial x^2} + \frac{\partial^2 B}{\partial x^2} \right) + \frac{N_\phi}{R \cdot K} \left( 1 + \frac{1}{R} \cdot \frac{\partial^2 w}{\partial \phi^2} + \frac{1}{R} \cdot \frac{\partial^2 B}{\partial \phi^2} \right) + \frac{N_{\phi x}}{R \cdot K} \left( \frac{\partial^2 w}{\partial x \partial \phi} + \right.$$

$$\left. \frac{\partial^2 B}{\partial x \partial \phi} \right) + \frac{M_\phi}{R \cdot K} \left( \frac{1}{R} \cdot \frac{\partial w}{\partial x} \cdot \frac{\partial B}{\partial x} + \frac{1}{R} \left( \frac{\partial B}{\partial x} \right)^2 + \frac{\partial^2 w}{\partial x^2} + \frac{\partial^2 B}{\partial x^2} \right) +$$

$$\frac{1}{R \cdot K} \cdot \frac{\partial M_\phi}{\partial x} \left( \frac{\partial w}{\partial x} + \frac{\partial B}{\partial x} \right) + \frac{1}{K \cdot R^3} \cdot \frac{\partial M_\phi}{\partial \phi} \cdot \frac{\partial B}{\partial \phi} - \frac{M_{\phi x}}{K \cdot R^2} \left( \frac{\partial^2 w}{\partial x \partial \phi} + \frac{\partial^2 B}{\partial x \partial \phi} + \right.$$

$$\left. \frac{1}{R} \cdot \frac{\partial B}{\partial \phi} \cdot \frac{\partial w}{\partial x} + \frac{1}{R} \cdot \frac{\partial B}{\partial \phi} \cdot \frac{\partial B}{\partial x} \right) - \frac{1}{K \cdot R^2} \cdot \frac{\partial M_{\phi x}}{\partial \phi} \left( \frac{\partial w}{\partial x} + 2 \frac{\partial B}{\partial x} \right) + \frac{q}{K} \quad \text{--- 3.45}$$

In the third case where a combination of the Timoshenko and Woinowsky Krieger equilibrium equations are used with the Donnell resultants, similar equations arise. In fact, the radial equilibrium equation appears the same as equation 3.45. The only difference between the two equations is in the magnitude of the resultants. For the axial equilibrium and tangential equilibrium conditions small changes occur, namely.

$$\begin{aligned}
 \frac{\partial^2 u}{\partial x^2} + \frac{(1-\nu)}{2R^2} \cdot \frac{\partial^2 u}{\partial \rho^2} &= - \frac{N}{R \cdot D} \left( \frac{\partial w}{\partial x} + \frac{\partial B}{\partial x} \right) + \frac{M}{R \cdot D} \left( \frac{\partial^2 w}{\partial x^2} + \frac{\partial^2 B}{\partial x^2} \right) \left( \frac{\partial w}{\partial x} + \right. \\
 \frac{\partial B}{\partial x} \Big) - \frac{M}{D \cdot R^2} \left( \frac{\partial^2 w}{\partial x \partial \rho} + \frac{\partial^2 B}{\partial x \partial \rho} \right) \left( \frac{\partial w}{\partial x} + \frac{\partial B}{\partial x} \right) + \frac{1}{D} \cdot \frac{\partial M}{\partial x} \left( \frac{\partial^2 w}{\partial x^2} + \frac{\partial^2 B}{\partial x^2} \right) + \\
 \frac{1}{D \cdot R^2} \cdot \frac{\partial M}{\partial \rho} \left( \frac{\partial^2 w}{\partial x \partial \rho} + \frac{\partial^2 B}{\partial x \partial \rho} \right) + \frac{1}{R \cdot D} \cdot \frac{\partial M}{\partial \rho} \left( \frac{\partial^2 w}{\partial x^2} + \frac{\partial^2 B}{\partial x^2} \right) - \\
 \frac{1}{R \cdot D} \cdot \frac{\partial M}{\partial x} \left( \frac{\partial^2 w}{\partial x \partial \rho} + \frac{\partial^2 B}{\partial x \partial \rho} \right) + \frac{\nu}{R} \cdot \frac{\partial w}{\partial x} - \frac{(1+\nu)}{2R} \cdot \frac{\partial^2 v}{\partial x \partial \rho} - \frac{\partial w}{\partial x} \cdot \frac{\partial^2 w}{\partial x^2} - \\
 \frac{(1+\nu)}{2R^2} \cdot \frac{\partial w}{\partial \rho} \cdot \frac{\partial^2 w}{\partial x \partial \rho} - \frac{(1-\nu)}{2R^2} \cdot \frac{\partial w}{\partial x} \cdot \frac{\partial^2 w}{\partial \rho^2} & \text{-----} 3.46
 \end{aligned}$$

Tangential equilibrium.

$$\begin{aligned}
 \frac{1}{R^2} \cdot \frac{\partial^2 v}{\partial \rho^2} + \frac{(1-\nu)}{2} \cdot \frac{\partial^2 v}{\partial x^2} &= \frac{N}{R \cdot D} \left( \frac{\partial w}{\partial x} + \frac{\partial B}{\partial x} \right) + \frac{M}{D \cdot R^2} \left( \frac{\partial w}{\partial x} + \right. \\
 \frac{\partial B}{\partial x} \Big) \left( \frac{\partial^2 w}{\partial x \partial \rho} + \frac{\partial^2 B}{\partial x \partial \rho} \right) - \frac{M}{D \cdot R^2} \left( \frac{\partial w}{\partial x} + \frac{\partial B}{\partial x} \right) \left( 1 + \frac{1}{R} \cdot \frac{\partial^2 w}{\partial \rho^2} + \frac{1}{R} \cdot \frac{\partial^2 B}{\partial \rho^2} \right) + \\
 \frac{1}{R \cdot D} \cdot \frac{\partial M}{\partial x} \left( \frac{\partial^2 w}{\partial x \partial \rho} + \frac{\partial^2 B}{\partial x \partial \rho} \right) + \frac{1}{D \cdot R^2} \cdot \frac{\partial M}{\partial \rho} \left( 1 + \frac{1}{R} \cdot \frac{\partial^2 w}{\partial \rho^2} + \frac{1}{R} \cdot \frac{\partial^2 B}{\partial \rho^2} \right) + \\
 \frac{1}{D \cdot R^2} \cdot \frac{\partial M}{\partial \rho} \left( \frac{\partial^2 w}{\partial x \partial \rho} + \frac{\partial^2 B}{\partial x \partial \rho} \right) - \frac{1}{R \cdot D} \cdot \frac{\partial M}{\partial x} \left( 1 + \frac{1}{R} \cdot \frac{\partial^2 w}{\partial \rho^2} + \frac{1}{R} \cdot \frac{\partial^2 B}{\partial \rho^2} \right) + \\
 \frac{1}{R^2} \cdot \frac{\partial w}{\partial \rho} - \frac{(1+\nu)}{2R} \cdot \frac{\partial^2 u}{\partial x \partial \rho} - \frac{(1+\nu)}{2R} \cdot \frac{\partial w}{\partial x} \cdot \frac{\partial^2 w}{\partial x \partial \rho} - \frac{(1-\nu)}{2R} \cdot \frac{\partial w}{\partial \rho} \cdot \frac{\partial^2 w}{\partial x^2} - \\
 \frac{1}{R^3} \cdot \frac{\partial w}{\partial \rho} \cdot \frac{\partial^2 w}{\partial \rho^2} & \text{-----} 3.47
 \end{aligned}$$

The three groups of equations 3.39 with 3.40 and 3.41; 3.43 with 3.44 and 3.45 and 3.46 with 3.47 and 3.45 each are three simultaneous equations in the three displacement components. Solution of each set of equations constitutes a boundary value problem and provides the three components of deflections at all points over the entire middle surface of the shell. It will be seen that corresponding equations in each of the groups have been arranged such that the same expression appears on the left hand side. In the case of the axial equilibrium equation it is an expression in axial deflection ( $u$ ). The tangential equilibrium equation contains terms in tangential deflection ( $v$ ) and the radial equilibrium equation has terms in radial deflection ( $w$ ). Thus each of the three sets of equations can be written in a simplified form as follows,

$$\frac{\partial^2 u}{\partial x^2} + \frac{(1-\nu) \cdot \partial^2 u}{2R^2 \partial \phi^2} = \text{R.H.S. (1)} \text{ ----- 3.48}$$

$$\frac{1}{R^2} \cdot \frac{\partial^2 v}{\partial \phi^2} + \frac{(1-\nu) \cdot \partial^2 v}{2 \partial x^2} = \text{R.H.S. (2)} \text{ ----- 3.49}$$

$$\frac{\partial^4 w}{\partial x^4} + \frac{2}{R^2} \cdot \frac{\partial^4 w}{\partial x^2 \partial \phi^2} + \frac{1}{R^4} \cdot \frac{\partial^4 w}{\partial \phi^4} = \text{R.H.S. (3)} \text{ ----- 3.50}$$

Solution of the three equations can be either approximate, by assuming a deflected shape or more accurately by simultaneous solution. Although the approximate method is far quicker the second method was chosen for this comparative study of the three theories. It was anticipated that by choosing a deflected shape real differences between the theoretical relations may have been masked. Details of the solution are presented in the next chapter (Chapter 4).

B	Magnitude of imperfections.	
D	Extensional rigidity.	$D = \frac{E.T}{(1-\nu^2)}$
E	Young's modulus.	
K	Flexural rigidity.	$K = \frac{E.T^3}{12(1-\nu^2)}$
$M_x$	} Moments per unit length.	
$M_\phi$		
$M_{x\phi}$		
$M_{\phi x}$		
$N_x$	} Membrane forces per unit length.	
$N_\phi$		
$N_{x\phi}$		
$Q_x$	} Shear forces per unit length.	
$Q_\phi$		
q	Radial pressure.	
R	Cylinder radius.	
T	Wall thickness.	
u	Deflection in the axial (x) direction.	
v	Deflection in the tangential ( $\phi$ or s) direction.	
w	Deflection in the radial (z) direction.	
$\nu$	Poisson's ratio.	

# CHAPTER 4

## SOLUTION OF

## PARTIAL

## DIFFERENTIAL

## EQUATIONS

## CHAPTER 4

### FINITE DIFFERENCE SOLUTION OF THE PARTIAL DIFFERENTIAL EQUATIONS.

It was shown in the previous chapter that for each of the three theories discussed the partial differential equations could be expressed briefly in the same simple form (equations 3.48, 3.49 and 3.50). The three equations represent conditions of axial equilibrium, tangential equilibrium and radial equilibrium. The axial equilibrium equation has been expressed in terms of axial deflections, tangential equilibrium in terms of tangential displacements and for the radial equilibrium equation, radial deflections have been considered. The equations have been arranged in this manner because these deflections predominate in their respective equations.

No explicit form of solution is available for any of the three sets of equations. Thus to obtain a solution it is necessary to resort to some approximate technique. Von Karman and Tsien, in their solution of Donnell's equations used a guessed shape approximating the diamond buckled pattern as a starting point. They then minimised energy to obtain values of certain parameters. This procedure is the one that has generally been followed by subsequent researchers. However, in the type of investigation carried out here such a procedure may not show the differences between the three theories. It was considered that in this case an alternative procedure would be more suitable, namely direct approximation of the equations. Two techniques are available for this approximation-finite differences and finite elements. The two techniques are essentially variations on a theme, the choice of one or the other depending on the boundaries and the ease of manipulation. In this case the choice was made for finite differences with the form of relaxation technique known as successive approximation. In this technique guesses are made as to the deflection values at a number of points within the boundary. From these guesses the equations are solved at each point to obtain better estimates and these used in turn to obtain better guesses still until the deflection values converge onto those that satisfy the differential equations. There are three deflections at each point and we have three partial differential equations. Thus for each point on the middle



surface of the shell we solve for the three values in turn using equation 3.48 to obtain better estimates of axial deflection; 3.49 for tangential deflections and 3.50 for radial deflections. This procedure is very slow and would not normally be used in solving the equations for design purposes. Rather, it is a research tool useful for gaining an understanding of the behaviour of the cylinder.

Originally the solution was tried in Algol on a Burroughs B6700 computer but difficulties with the availability of the machine for such a long running program prevented the work being completed on this machine. Instead a Digital PDP 11 was available with floppy disk storage and 16K word memory. Programs were written for this machine in Fortran and the computer was left to run unattended overnight. The speed of solution on this machine was about one tenth of the speed on the Burroughs and to obtain one solution it was necessary to operate the machine for several nights. Thus it was essential to organise the program so that it could be interrupted at any time without losing the benefit of the previous work. The solution was therefore subdivided into several parts. For each part a separate program was written and listings of these programs are given in Appendix D. The organisation and sequence of use of the programs is illustrated in figure 4.1. Essentially the main finite difference procedure was conducted in one

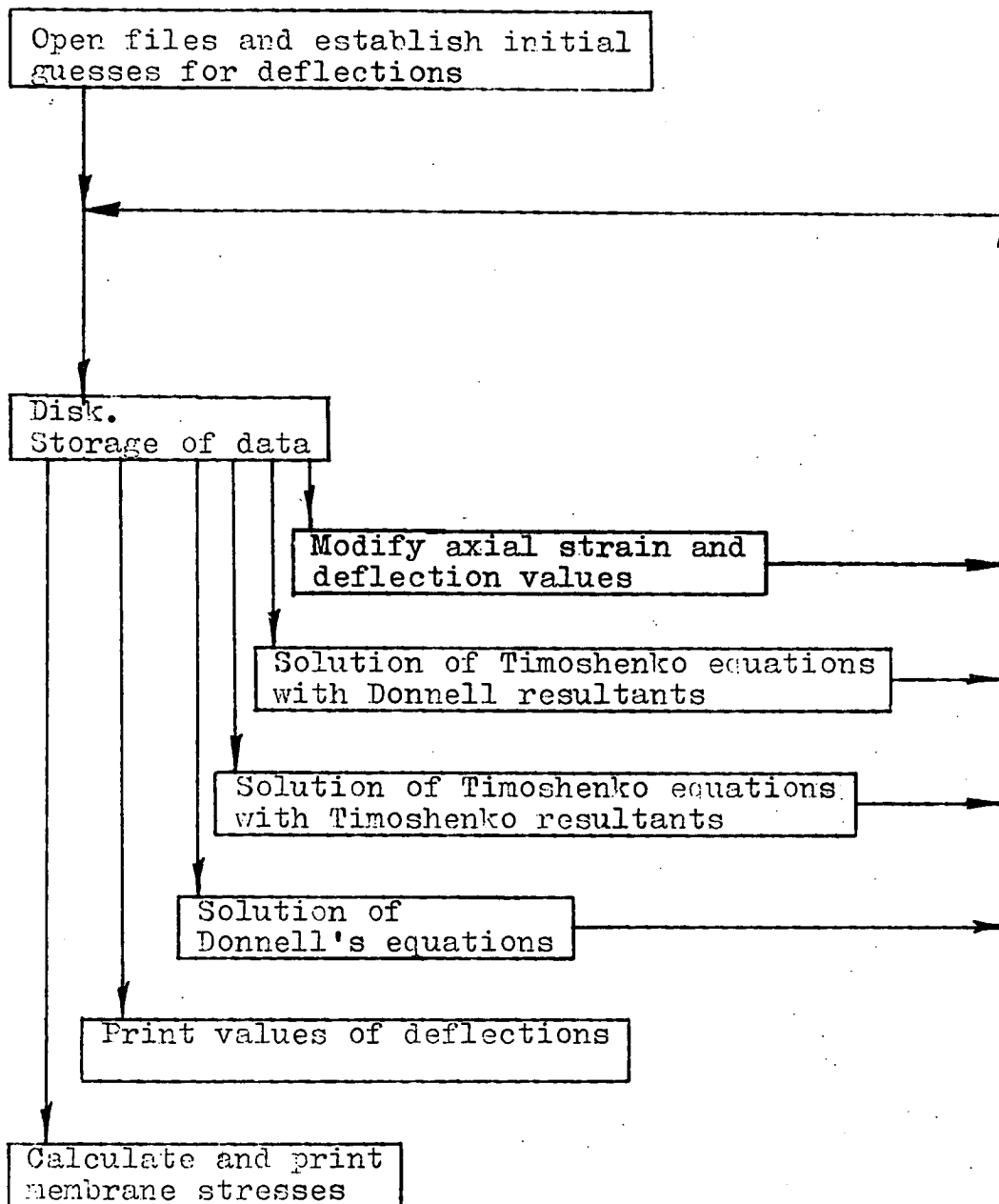


FIGURE 4.1

COMPUTER ORGANISATION

program with a separate program for each theory. Thus when the solution was obtained for one theory these values could be used as initial guesses for the other theories. All other programs acted as service programs to these three. The service programs included the following.

1. A program to open the necessary files on disk and establish initial values.
2. A program to print out values of deflections.
3. A program to calculate and print membrane stresses.
4. A program to modify the value of the axial strain and deflection values proportional to the change in strain.

No cylinder can be made which is completely circular. Instead there would be small defects in shape. These imperfections control the buckling behaviour of the cylinder and so should be considered in any investigation. From the observations made in chapters 1 and 2 it seems likely that diamond shaped defects would have most effect on the buckling of a cylinder. Thus it was considered that a shape defect of approximately that form should be considered. A simple way in which a defect of approximately this shape can be considered is illustrated in figure 4.2. Essentially, it comprises a plane intersecting a cylinder. Thus we have two planes of symmetry and we need only work on one quarter of the defect. We also need to investigate

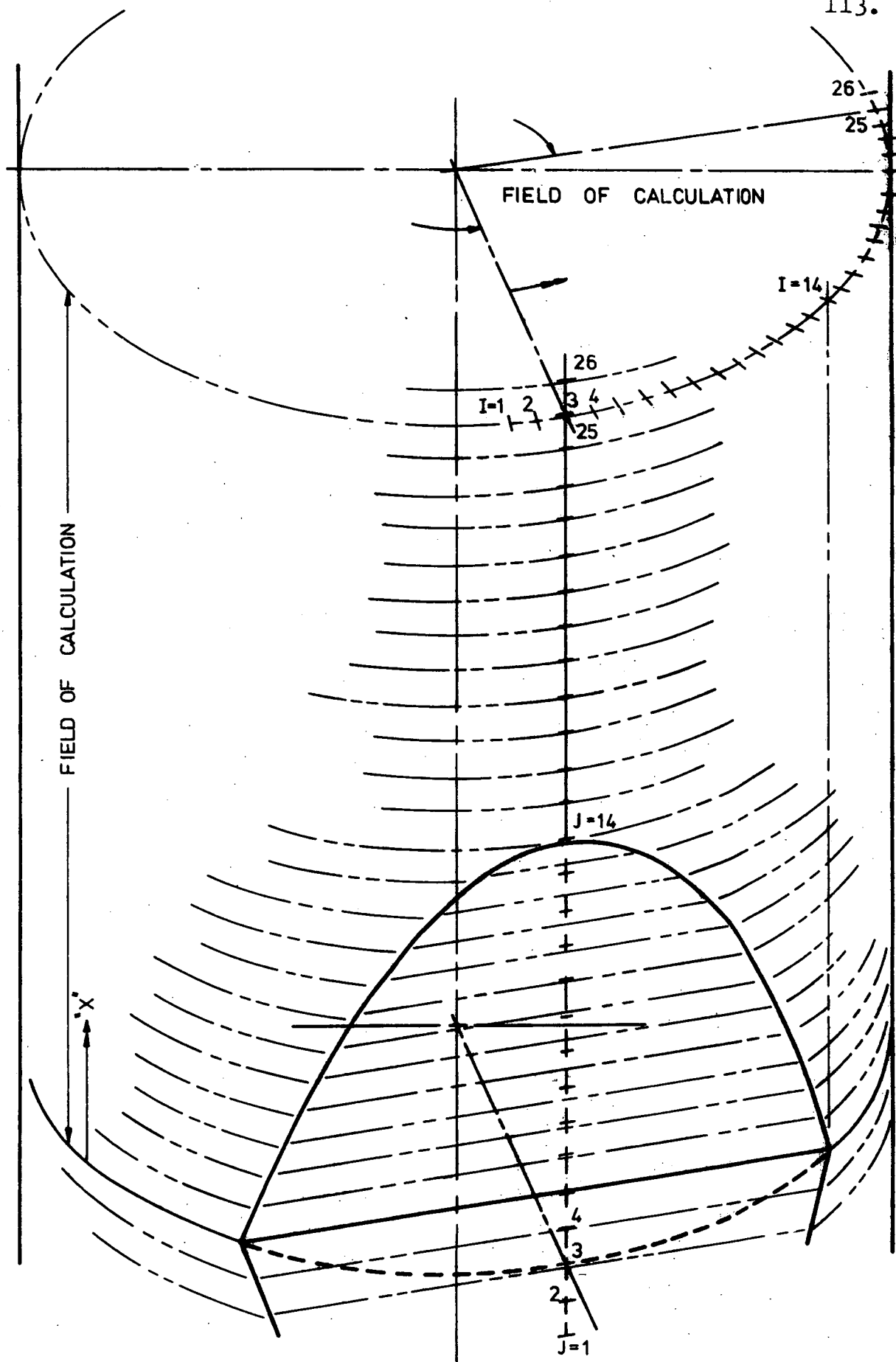


FIGURE 4.2  
CYLINDER WITH DEFECT

the section of the cylinder adjacent to the imperfection. Thus the solution was conducted over the portion of the cylinder bounded by lines twice the width of the defect and twice the length. It was assumed that the defect would have minimal effect outside this area. A grid of points was used 23X23 which was the limit that could be manipulated in the memory of the PDP 11. A larger grid could be accommodated by accessing a row of points at a time but this process slowed down the solution to such an extent that it became impractical.

The central difference technique was adopted because it offered the greatest accuracy of solution. Thus, for the grid of points illustrated in figure 4.2 we can write the following relations for the derivatives of the radial deflection "w".

$$\begin{aligned}
 \frac{\partial w}{\partial x} &= \frac{1}{2(\delta x)}(w(i, j+1) - w(i, j-1)) \\
 \frac{\partial^2 w}{\partial x^2} &= \frac{1}{(\delta x)^2}(w(i, j+1) - 2w(i, j) + w(i, j-1)) \\
 \frac{\partial^3 w}{\partial x^3} &= \frac{1}{2(\delta x)^3}(w(i, j+2) - 2w(i, j+1) + 2w(i, j-1) - w(i, j-2)) \quad \text{---4.1} \\
 \frac{\partial^4 w}{\partial x^4} &= \frac{1}{(\delta x)^4}(w(i, j+2) - 4w(i, j+1) + 6w(i, j) - 4w(i, j-1) \\
 &\quad + w(i, j-2)) \\
 \frac{\partial w}{\partial \theta} &= \frac{1}{2(\delta x)}(w(i+1, j) - w(i-1, j))
 \end{aligned}$$

$$\frac{\partial^2 w}{\partial \phi^2} = \frac{1}{(\delta \phi)^2} (w(i+1, j) - 2w(i, j) + w(i-1, j))$$

$$\frac{\partial^3 w}{\partial \phi^3} = \frac{1}{2(\delta \phi)^3} (w(i+2, j) - 2w(i+1, j) + 2w(i-1, j) - w(i-2, j))$$

$$\frac{\partial^4 w}{\partial \phi^4} = \frac{1}{(\delta \phi)^4} (w(i+2, j) - 4w(i+1, j) + 6w(i, j) - 4w(i-1, j) + w(i-2, j))$$

$$\frac{\partial^2 w}{\partial x \partial \phi} = \frac{1}{4(\delta x)(\delta \phi)} (w(i+1, j+1) - w(i+1, j-1) - w(i-1, j+1) + w(i-1, j-1))$$

$$\frac{\partial^3 w}{\partial x^2 \partial \phi} = \frac{1}{2(\delta x)^2(\delta \phi)} (w(i+1, j+1) - 2w(i+1, j) + w(i+1, j-1) - w(i-1, j+1) + 2w(i-1, j) - w(i-1, j-1))$$

$$\frac{\partial^3 w}{\partial x \partial \phi^2} = \frac{1}{2(\delta x)(\delta \phi)^2} (w(i+1, j+1) - 2w(i, j+1) + w(i-1, j+1) - w(i+1, j-1) + 2w(i, j-1) - w(i-1, j-1))$$

and.

$$\frac{\partial^4 w}{\partial x^2 \partial \phi^2} = \frac{1}{(\delta x)^2(\delta \phi)^2} (w(i+1, j+1) - 2w(i+1, j) + w(i+1, j-1) - 2w(i, j+1) + 4w(i, j) - 2w(i, j-1) + w(i-1, j+1) - w(i-1, j) + w(i-1, j-1))$$

In a similar manner we can also write the derivatives we require of  $u, v$  and  $B$ . Thus the three partial differential equations (3.48, 3.49, and 3.50) were rewritten in finite difference form as follows.

$$\begin{aligned} -\frac{2u(i, j)}{(\delta x)^2} - \frac{(1-\nu)}{R^2} \cdot \frac{u(i, j)}{(\delta \phi)^2} = & \text{R.H.S. (1)} - \frac{1}{(\delta x)^2} (u(i, j+1) \\ & + u(i, j-1)) - \frac{(1-\nu)}{2R^2(\delta \phi)^2} (u(i+1, j) + u(i-1, j)) \end{aligned}$$

$$\begin{aligned}
-\frac{2v(i,j)}{R^2(\delta\phi)^2} - \frac{(1-\nu)v(i,j)}{(\delta x)^2} = \text{R.H.S. (2)} - \frac{1}{R^2(\delta\phi)^2}(v(i+1,j) \\
+v(i-1,j)) - \frac{(1-\nu)}{2(\delta x)^2}(v(i,j+1)+v(i,j-1)) \text{ ----- 4.3}
\end{aligned}$$

and.

$$\begin{aligned}
\frac{6w(i,j)}{(\delta x)^4} + \frac{8w(i,j)}{R^2(\delta x)^2(\delta\phi)^2} + \frac{6w(i,j)}{R^4(\delta\phi)^4} = \text{R.H.S. (3)} \\
- \frac{1}{(\delta x)^4}(w(i,j+2)-4w(i,j+1)-4w(i,j-1)+w(i,j-2)) \\
- \frac{2}{R^2(\delta x)^2(\delta\phi)^2}(w(i+1,j+1)-2w(i+1,j)+w(i+1,j-1) \\
-2w(i,j+1)-2w(i,j-1)+w(i-1,j+1)-2w(i-1,j)+w(i-1,j-1)) \\
- \frac{1}{R^4(\delta\phi)^4}(w(i+2,j)-4w(i+1,j)-4w(i-1,j)+w(i-2,j)) \\
\text{----- 4.4}
\end{aligned}$$

From these equations it can be seen that if we have approximate values of the deflection components  $u, v$ , and  $w$  at all points on the middle surface of the shell then better approximations can be obtained by solving equations 4.2, 4.3 and 4.4 for that point. The deflections at that point are then obtained in terms of the deflections at adjacent points. This procedure is not always numerically stable so that a convergence factor was used on each of the calculations. Thus the "better approximation" at the point in question was not set at the newly calculated value but was made equal to the old value together with a proportion of the difference between old and new.

The section of the cylinder over which the calculation was carried out was bounded by two longitudinal boundaries and two circumferential boundaries. On these boundaries the following conditions applied.

At  $x = 0, j = 3$  i.e. central circumferential boundary

$$u(i,3) = 0$$

$$\frac{\partial u}{\partial x} = \text{constant} \quad \therefore u(i,2) = -u(i,4)$$

also there is symmetry for  $w$  and  $v$

$$\text{i.e. } v(i,2) = v(i,4)$$

$$w(i,2) = w(i,4)$$

$$w(i,1) = w(i,5)$$

At the remote circumferential boundary,  $j = 25$

$$u(i,25) = 2 \cdot \epsilon_x \cdot (\text{defect half length})$$

$$v(i,25) = 0$$

$$w(i,25) = w(i,26) = \nu \cdot \epsilon_x \cdot R$$

At  $\phi = 0, i = 3$  i.e. central axial boundary

$$v(3,j) = 0$$

$$\frac{\partial v}{\partial \phi} = \text{constant} \quad \therefore v(2,j) = -v(4,j)$$

also there is symmetry for  $w$  and  $u$

$$\text{i.e. } u(2,j) = u(4,j)$$

$$w(2,j) = w(4,j)$$

$$w(1,j) = w(5,j)$$



and along the remote longitudinal boundary,  $i=25$

$$u(25,j) = \epsilon_x \cdot (j-3) \cdot \delta x$$

$$v(25,j) = 0$$

$$w(25,j) = w(26,j) = \nu \cdot \epsilon_x \cdot R$$

The shape of the defect was accounted for by calculating the radial difference between the true cylinder and the intersecting plane and allowing for the fact that this dimension can not be negative.

$$\text{i.e. } B = R - \frac{(R^2 - \frac{A^2}{4})^{\frac{1}{2}} + \frac{j-3}{11}(R - (R^2 - \frac{A^2}{4})^{\frac{1}{2}})}{\cos((i-3) \cdot \delta \phi)} \quad \text{---- 4.5}$$

The solution was obtained by firstly selecting a value for nominal axial strain and from that value calculating the deflection components. This procedure was adopted because the solution was known to be multivalued in load but it may have been single valued in axial deflection, particularly if the defect was large (see figure 1.3). A multivalued solution would almost certainly lead to numerical instability whereas the solution may be stable with a single valued solution. The aim of this investigation was to determine, if possible, the load deformation relations over the peak load for a rather large defect. The comparison between results would then indicate if the additional terms in the equations were necessary. For this reason the chief comparison was between Donnell's equations and the modified Timoshenko and Woinowsky-Krieger equations with the resultants containing the slope product terms. The solution without the slope terms was included for comparison in the pre-buckled range.

The variables chosen for the investigation were;-

Cylinder radius	= 0.1 m.
Wall thickness	= <del>0.019</del> 0.19 m.m.
Poisson's ratio	= 0.35
Imperfection width	= 0.04 m.
Aspect ratio	= 0.7

The calculated results for this cylinder with a defect are summarised in figures B1 to B35. In figures B1 to B21 the comparison is made in the form of contour maps of the various calculated quantities over the surface between the boundaries selected. Figures B22 to B24 show the stress trajectories and figures B26 to B35 comparative cross sections through the contours. In figure B25 the comparison is made of the load-deformation relations for the three conditions. All other curves are plotted for the maximum deformation condition calculated which was for a nominal axial strain of  $300\mu\epsilon$ . Although there is no indication in figure B25 that the maximum load had been reached or even approached, all attempts to calculate deformations at nominal axial strains greater than  $300\mu\epsilon$  met with disaster. In every case the solution was numerically unstable.

In examining all the contour maps it is immediately apparent that a section of cylinder of twice the dimension of the defect is not sufficient to permit the calculation to be satisfactorily completed within the

boundary. There are shear stresses along the external boundaries. Thus the calculations do not actually relate to the deformations of a cylinder. They do, however, provide theoretical deflection values for a cylindrical panel twice the width of the defect and twice the length with ~~built in edge beams~~ <sup>edges constrained to the Poisson expansion.</sup> The relations should hold equally as well for this case as for a complete cylinder. Thus it is justifiable to consider the conclusions from this examination as applying to a complete cylinder.

As anticipated, the solutions to all three theoretical relations are similar in nature. This is evidenced by the fact that the contour maps of any variable appear to be similar in each case and the sections through the contours are of the same form. There was, however, a substantial difference between the magnitudes of the deformations calculated. Generally, this difference was greatest between the solution to Donnell's equations and the solution to the modified Timoshenko and Woinowsky-Krieger equations using Donnell's resultants. The solution to the Timoshenko and Woinowsky-Krieger equations with the shortened form of resultants usually lay between the other two but surprisingly closer to the Donnell solution. In the case of radial deflections the maximum variation between the theories was of the order of 15 - 20% of the maximum deflection. This was considerably more than was anticipated considering that the solution was only for pre-buckling deformations. It showed the importance of the additional terms.

The load-deformation relations (fig. B25) are drawn as the difference between a condition based solely on Young's modulus with an axial load and the calculated conditions. If the condition illustrated by "B" in figure 1.3 was to be achieved then the curves in figure B25 would have ever increasing slope until the collapse load had been reached. In fact, Donnell's solution is a straight line which could be reasonably accepted as an alternative to the increasing slope. Both of the other two lines show a section of increasing slope followed by a section with decreasing slope. This latter section corresponds to a stiffening of the shell. It is well known that flat plates exhibit such a stiffening effect in buckling. Thus it seems likely that the behaviour in this region can be attributed to the stiffening of the facet. An excellent account of this stiffening effect was given by Kremmer (ref.20) for flat plates in shear. The stiffening is not present in Donnell's solution which would indicate that perhaps his equations do not allow the load to flow around the corners of the Yoshimura pattern adequately. In order to achieve this flow it appears necessary to include the terms in surface curvature which are present in the other relations discussed here.

Another interesting point to be deduced from all the contour plots and stress trajectories is that there is definitely a flow of stress as anticipated in the space frame theory. However, with the lack of symmetry along the edge of the defect this stress concentration is not

directed along the sharp edge of the defect. Instead the panel behaves as though the defect were effectively about  $1\frac{1}{2}$  times its actual size. Thus in anticipating the results of any experimental investigation a defect of measurable size may make the cylinder collapse as though it had a Yoshimura pattern in it of somewhat larger dimensions. Once the buckle pattern has been established, however, the symmetry of the pattern would ensure that the load concentration would be along the diagonals.

It was stated earlier that the reason for considering the modified Timoshenko and Woinowsky-Krieger equations was the effect of the curvature terms. In fact these equations contain several other terms as well. Thus it was decided that a further computation would be made with only the curvature terms added to Donnell's equations. The results were extremely encouraging in that there was no discernable difference between this solution and the solution of the previously modified Timoshenko and Woinowsky-Krieger equations. Thus it seems that in shell buckling analysis the following set of equations should replace Donnell's equations as the governing equations.

$$\begin{aligned} \frac{\partial N_x}{\partial x} + \frac{1}{R} \cdot \frac{\partial N_{\phi x}}{\partial \phi} - \frac{1}{R} \cdot \frac{\partial M_{\phi x}}{\partial \phi} \cdot \frac{\partial^2 w}{\partial x^2} - \frac{\partial M_x}{\partial x} \cdot \frac{\partial^2 w}{\partial x^2} + \frac{1}{R^2} \cdot \frac{\partial M_{x\phi}}{\partial \phi} \cdot \frac{\partial^2 w}{\partial x \partial \phi} \\ - \frac{1}{R^2} \cdot \frac{\partial M_{\phi}}{\partial \phi} \cdot \frac{\partial^2 w}{\partial x \partial \phi} = 0 \end{aligned} \quad \text{-----} \quad 4.6$$

$$\begin{aligned}
& \frac{1}{R} \frac{\partial N}{\partial \phi} + \frac{\partial N_x}{\partial x} - \frac{1}{R^2} \frac{\partial M}{\partial \phi} \frac{\partial^2 w}{\partial x \partial \phi} - \frac{1}{R} \frac{\partial M_x}{\partial x} \frac{\partial^2 w}{\partial x \partial \phi} - \frac{1}{R^3} \frac{\partial M}{\partial \phi} \frac{\partial^2 w}{\partial \phi^2} \\
& + \frac{1}{R^2} \frac{\partial M_x}{\partial x} \frac{\partial^2 w}{\partial \phi^2} = 0 \quad \text{-----} \quad 4.7
\end{aligned}$$

And

$$\begin{aligned}
& \frac{\partial^2 M_x}{\partial x^2} + \frac{2}{R} \frac{\partial^2 M}{\partial x \partial \phi} + \frac{1}{R^2} \frac{\partial^2 M}{\partial \phi^2} + \frac{N}{R} + N_x \frac{\partial^2 w}{\partial x^2} + \frac{2 \cdot N_x}{R} \frac{\partial^2 w}{\partial x \partial \phi} \\
& + \frac{N}{R^2} \frac{\partial^2 w}{\partial \phi^2} = 0 \quad \text{-----} \quad 4.8
\end{aligned}$$

This last equation is exactly the same as that suggested by Donnell. It is only the in plane equilibrium conditions that have been altered.

Since a finite difference procedure has been used for the calculation some doubt must exist about the validity of the representation of the derivatives in finite difference form. This would be particularly true near the edge of the defect. Two types of error are normally encountered, namely increment errors and roundoff errors. In this case roundoff errors (the accuracy of the machine) appear to account for errors in the solution of the order of one part in 1,000. Increment errors were not so easily treated. In general the derivatives were power series fits to the shape. At the edge of the defect this could only be considered as a rough approximation to the value at the point. In fact the finite difference procedure

had the effect of rounding the interface between cylinder and defect. Thus increment changes would have a significant effect on the result. The usual method of checking for increment errors is to compare the computed results with the desired increment with the results obtained when the increment is reduced to say, half the size, then a quarter of the size etc. This should give a converging solution and an indication of the error involved. Unfortunately, this procedure was quite impossible here because the increment chosen was the smallest that would allow a solution in the computer used. Any smaller increment would require more storage than was available. The grid used for the computation was  $23 \times 23$ . To obtain some idea of increment errors the grid was reduced to  $19 \times 19$  for one computation. Unfortunately, this move tended to promote numerical instability but a solution was obtained. As could be expected, increasing the increment length had the effect of averaging the calculations. By enforcing a change in increment length of 18 % there was a change in calculated values of about 3 % of the range of oscillation in each variable. The form of the plot was identical in each case but the amplitude of the variation was reduced. Thus increment length can not be considered as the reason for the variation between the theories. However, the actual values of deflections and stresses at any point must be somewhat different from those presented in figures B1 to B35. It seems likely that the range of variation in the calculated values would be at least 10 % greater than those calculated. In fact the variation would probably be greater when the curvature terms were included since they would be very susceptible to averaging effects.

A Width of defect.

B Amplitude of defect.

$M_x$	}	Moments per unit length.
$M_{\phi x}$		
$M_{x\phi}$		
$M_{\phi}$		

$N_x$	}	Membrane forces per unit length.
$N_{\phi x}$		
$N_{x\phi}$		
$N_{\phi}$		

R Cylinder radius.

u Deflection in the axial (x) direction.

v Deflection in the tangential ( $\phi$ ) direction.

w Deflection in the radial (z) direction.



CHAPTER 5

EXTENSIONS TO

SPACE FRAME

THEORY

## CHAPTER 5

### EXTENSIONS TO THE SPACE FRAME MODEL FOR THE COLLAPSE OF CYLINDERS LOADED IN AXIAL COMPRESSION

In the concluding section of chapter 2 it was stated that a possible improvement could be made to the model for collapse by not considering the folds in a Yoshimura pattern as straight sharp bends. From observation of cylinders collapsed in axial compression it was realised that the shape of the fold was essentially the shape that would be obtained by bending a rhomboidal sheet across the short diagonal into two triangles with all four edges held straight. Thus the model shown in figure 5.1A and 5.1B was proposed for the analysis. The reason for the rectangular

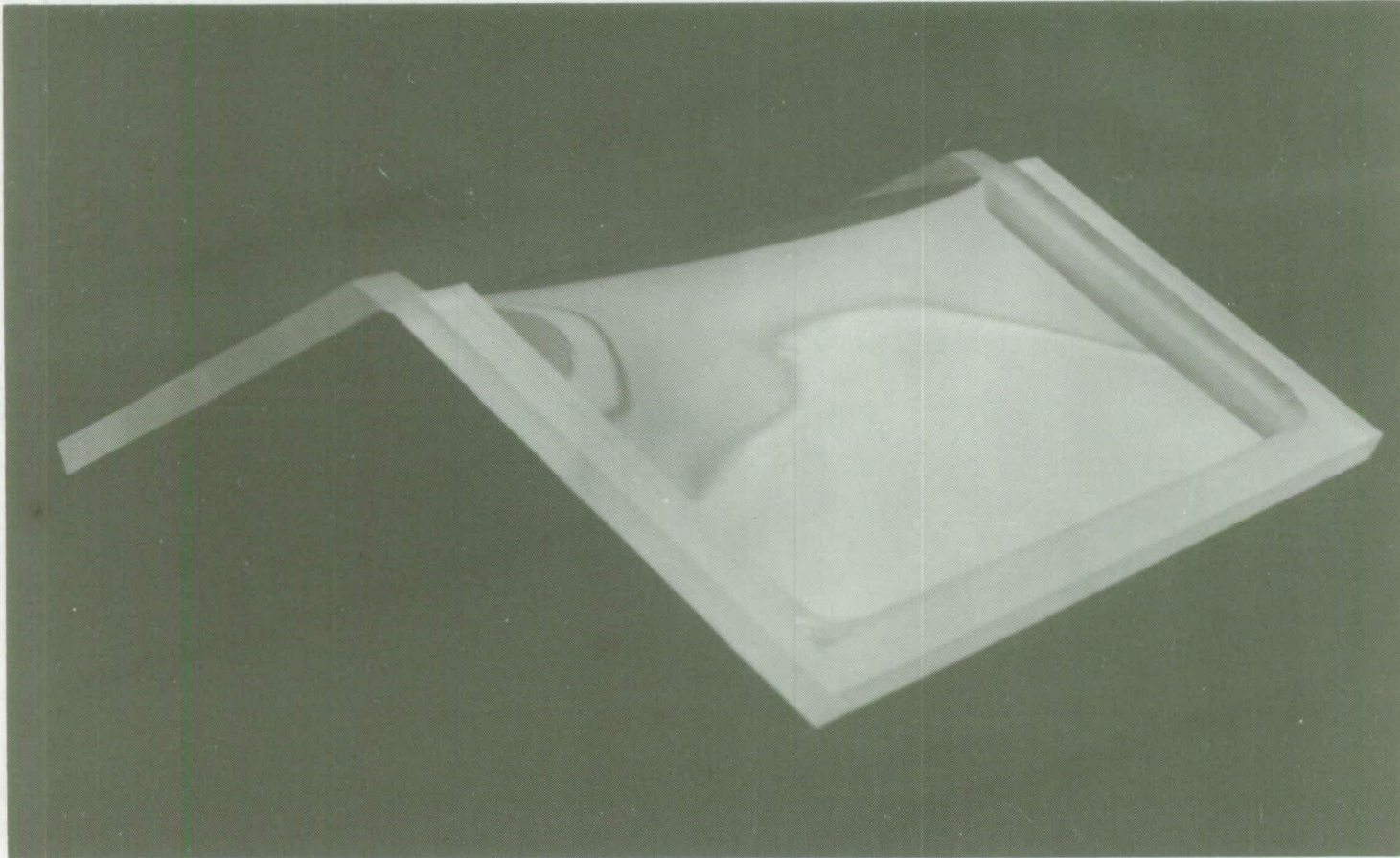


FIGURE 5.1A

MODEL FOR SHAPE OF SHELL ALONG FOLD LINE

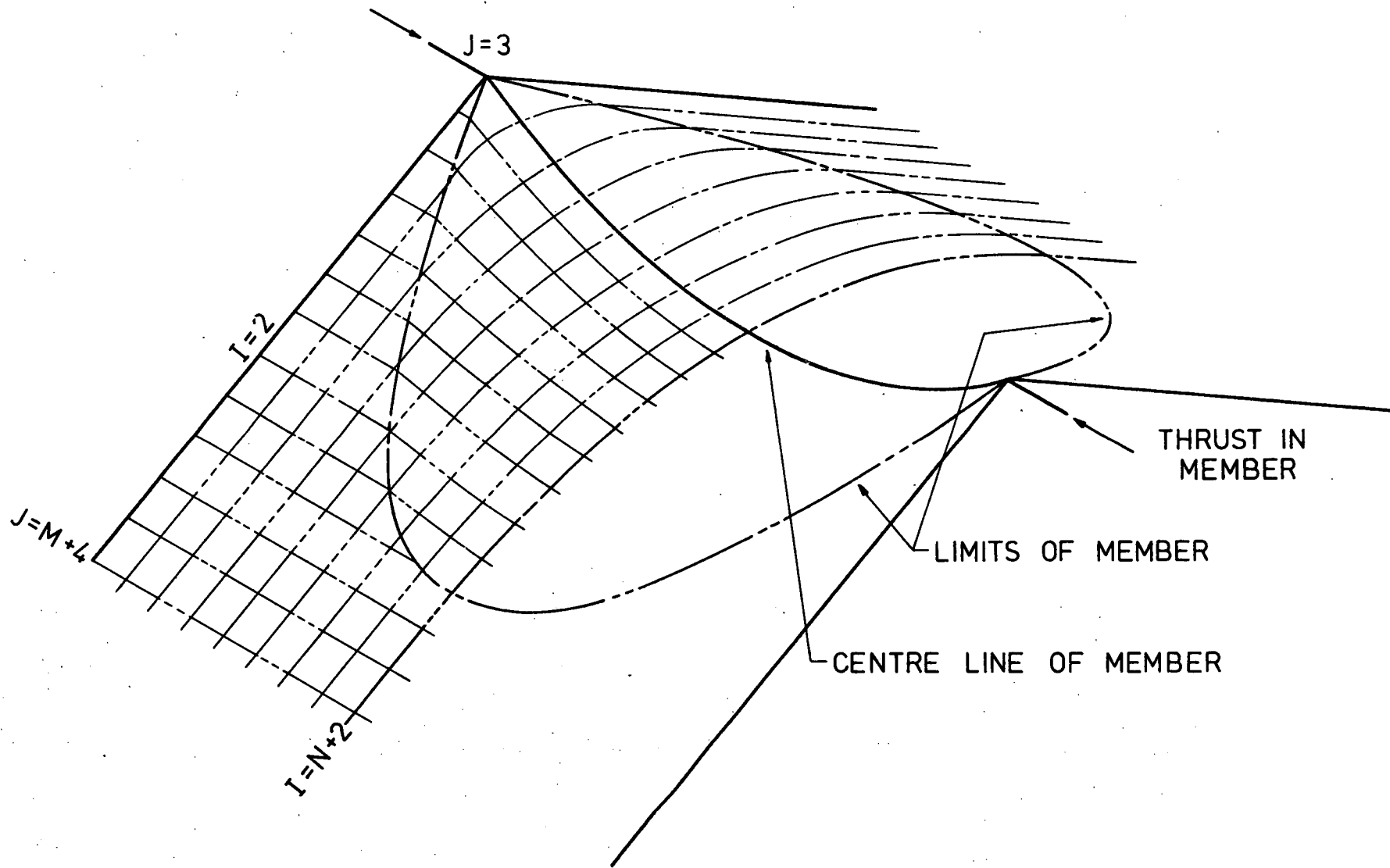


FIGURE 5.1B  
MODEL FOR SHAPE OF SHELL ALONG FOLD LINE

shape instead of triangular was for ease of calculation. It would also represent a condition where the width of the facet perpendicular to the fold was infinite. Thus the effective width of the bend could be easily **determined**.

The analysis of the bend could be achieved either experimentally or theoretically (or both). In fact both methods were tried but the theoretical analysis was found to be inadequate. This theoretical analysis was similar in nature to the finite difference procedure used in chapter 4. There were two axes of symmetry in the model so that only one quadrant was necessary for the analysis. The M long by N wide grid point layout for the finite difference procedure is illustrated in figure 5.1B.

As a first approximation and for the condition where the angle between the facets approaches  $180^\circ$  then membrane stresses and surface slopes would be negligible. Therefore, in the first instance the out of plane deformations can be reasonably approximated by the bi-harmonic equation. In the absence of transverse pressure this equation can be written as.

$$\frac{\partial^4 w}{\partial x^4} + \frac{\partial^4 w}{\partial y^4} + 2 \frac{\partial^4 w}{\partial x^2 \partial y^2} = 0 \quad \text{-----} \quad 5.1$$

The in plane displacements (u and v) could be considered as **zero** and the required boundary conditions were as follows.

Along the fold line and at the mid point of the fold there was symmetry.

Thus.

$$w(i,1) = w(i,5)$$

$$w(i,2) = w(i,4)$$

$$w(N+3,j) = w(N+1,j)$$

and  $w(N+4,j) = w(N,j)$

Along the grid lines  $i=1, i=2, j=N+3$  and  $j=N+4$  the value of the out of plane deflection was that given by the initial guess.

$$w(i,j) = (j-3) \cdot \delta y \cdot \cos\left(\frac{\theta}{2}\right)$$

The programmes used for this calculation are listed in Appendix E together with typical output. Although these programmes calculated a shape of fold that was of the correct general form they were completely useless in that the calculated central deflection was approximately three times the actual measured value. Because of this discrepancy it was thought that membrane conditions may have played a more significant role and should have been included. Thus the programmes were rewritten to include membrane stresses. The listing of these revised programmes together with typical output is given in Appendix F. The additional boundary conditions needed were as follows.

Symmetry for  $u$  along  $i=N+2$  and for  $v$  along  $j=3$ .

i.e.  $u(N+3,j) = -u(N+1,j)$

$$v(i,2) = -v(i,4)$$

Zero shear strain along the axes of symmetry.

$$\begin{aligned} \text{i.e. } u(i,2) &= u(i,4) \\ v(N+3,j) &= v(N+1,j) \end{aligned}$$

And along the external boundaries there was no in plane displacement.

$$\text{i.e. } u(3,j) = v(3,j) = u(i,j+2) = v(i,j+2) = 0$$

In setting up these programmes it was decided to use the equivalent to the Donnell equations (3.1, 3.2 and 3.3) as the governing equations. For flat plates any term with a reciprocal of the radius vanishes and since we know that surface slopes are not large the terms in the product of surface slopes can also be ignored. Thus Donnell's equations for a flat plate reduce to the well known Von Karman equations which (with small surface slopes) can be written as,

$$\frac{\partial^2 u}{\partial x^2} + \frac{(1-\nu)}{2} \cdot \frac{\partial^2 u}{\partial y^2} + \frac{(1+\nu)}{2} \cdot \frac{\partial^2 v}{\partial x \partial y} = 0 \quad \text{-----} \quad 5.2$$

$$\frac{\partial^2 v}{\partial y^2} + \frac{(1-\nu)}{2} \cdot \frac{\partial^2 v}{\partial x^2} + \frac{(1+\nu)}{2} \cdot \frac{\partial^2 u}{\partial x \partial y} = 0 \quad \text{-----} \quad 5.3$$

and

$$\begin{aligned} \frac{\partial^4 w}{\partial x^4} + \frac{\partial^4 w}{\partial y^4} + 2 \frac{\partial^4 w}{\partial x^2 \partial y^2} &= \frac{12}{T^2} \cdot \frac{\partial^2 w}{\partial x^2} \left( \frac{\partial u}{\partial x} + \nu \frac{\partial v}{\partial y} \right) \\ &+ \frac{12}{T^2} \cdot \frac{\partial^2 w}{\partial y^2} \left( \frac{\partial v}{\partial y} + \nu \frac{\partial u}{\partial x} \right) + \frac{12}{T^2} (1-\nu) \left( \frac{\partial u}{\partial y} + \frac{\partial v}{\partial x} \right) \frac{\partial^2 w}{\partial x \partial y} \end{aligned}$$

----- 5.4

Clearly equations 5.2 and 5.3 are the membrane conditions and are independent of the out of plane displacement "w". If these equations are used in the finite difference procedure then the result is to find that the initial guesses of zero for the in-plane displacements remain unaltered and thus the membrane stresses are zero. The solution thus reverts to the solution of the simple bi-harmonic equation. This solution further helps to highlight the weakness in the Donnell equations. Perhaps a more satisfactory set of equations can be obtained by considering equations 3.25, 3.26 and 3.27, the Timoshenko and Woinowsky Krieger equations. If all terms in the reciprocal of R are eliminated in these equations then the following set are obtained.

$$\frac{\partial N_x}{\partial x} + \frac{\partial N_{yx}}{\partial y} + \left( \frac{\partial M_{xy}}{\partial x} - \frac{\partial M_y}{\partial y} \right) \frac{\partial^2 w}{\partial x \partial y} - \left( \frac{\partial M_{yx}}{\partial y} + \frac{\partial M_x}{\partial x} \right) \frac{\partial^2 w}{\partial x^2} = 0 \quad \text{-----} \quad 5.5$$

$$\frac{\partial N_y}{\partial y} + \frac{\partial N_{xy}}{\partial x} - \left( \frac{\partial M_{yx}}{\partial y} + \frac{\partial M_x}{\partial x} \right) \frac{\partial^2 w}{\partial x \partial y} - \left( \frac{\partial M_{xy}}{\partial x} + \frac{\partial M_y}{\partial y} \right) \frac{\partial^2 w}{\partial y^2} = 0 \quad \text{-----} \quad 5.6$$

and

$$\frac{\partial^2 M_x}{\partial x^2} + 2 \frac{\partial^2 M_{yx}}{\partial x \partial y} + \frac{\partial^2 M_y}{\partial y^2} + N_x \frac{\partial^2 w}{\partial x^2} + N_y \frac{\partial^2 w}{\partial y^2} + 2 N_{xy} \frac{\partial^2 w}{\partial x \partial y} = 0 \quad \text{-----} \quad 5.7$$



These three equations were the three used in the numerical solution. Their combined effect was to reduce the value of the out of plane deflection at the centre by about 1 % when the angle between the facets was  $173.9^{\circ}$ . This was insignificant when compared to the factor of approximately three between these calculated values and the experimental results.

Apparently, the large difference between calculation and measurement could be attributed to the severity of the singular point at the end of the fold line. To investigate the effect this sharp point had on the calculation the increment length was halved. The result was that the central deflection was reduced by some 5 %. This, at least, was a step in the right direction but only a start. Associated with this improvement was an increase in solution time from about 10 hours to about 120 hours. Clearly, a considerable improvement could still be obtained by taking a much smaller increment near the singularity and varying the increment size. However, to gain a sufficient improvement in the solution the increment would apparently have to be so small that round off errors would predominate. Therefore this theoretical procedure was abandoned in favour of a purely experimental approach.

The experimental analysis was based on the Ligtenberg moiré technique (ref.16). In this method a set of parallel grid lines are reflected off the test

model which must have a reflective surface and a photographic image made of the lines. The model is then deformed and a double exposure made. Moiré patterns on this photograph represent contours of constant change in surface slope. To obtain curvatures Ligtenberg and others have plotted curves of slope against position and differentiated this curve or mechanically shifted the image to obtain secondary moiré fringes. In fact, it is important to realise that absolute curvatures can be obtained directly from a single exposure photograph without having to resort to the rather inaccurate technique of graphical differentiation or the severe averaging effect of mechanically shifting the image. This technique is not new. It is essentially adapting the original idea from which Ligtenberg developed his method. It does not, however, appear to be described in the literature.

If a Ligtenberg screen with a line spacing of "f" is placed at a distance "Q" from the model and the surface is tilted an angle " $\alpha$ " in a direction perpendicular to the lines, then it can be easily shown that,

$$\alpha = \frac{n \cdot f}{2Q} \text{ ----- } 5.8$$

Here "n" is the fringe order of the reflected pattern. If the complete surface is tilted by " $\alpha$ " then the grid pattern will appear unaltered in the reflection except for a translation. The lines will still appear on the model at a spacing of  $\frac{f}{2}$ . Now, when the surface of the model is bent, there will be a change in line spacing since there is a change in slope between adjacent points. If " $f_1$ " is the line spacing on the model after it has been curved then the following relation is valid.

Curvature normal to the grid lines

$$= \frac{1}{Q} \left( \frac{f}{2f_1} - 1 \right) \text{ ---- } 5.9$$

Thus if one photograph is taken of the reflected grid lines it is possible to obtain values of slope normal to the lines by observing grid line movement (provided a datum is known) as well as curvatures by observing grid line spacing. The accuracy of the measurement is limited to the accuracy of measurement of the line spacing. This measurement technique was the one used in the experimental analysis. In fact using the conventional moiré technique in this instance was found to be misleading and quite inaccurate.

The model shown in figure 5.1A was made from a rectangular piece of melanex bonded to a perspex frame with cuts in the frame at the midpoints of the sides. The model was bent at these cuts forming the fold line of the member and photographs were taken of the grid lines reflected off the surface. The "cats eyes" picture (figure 5.2) is typical of the pattern obtained when the grid lines were perpendicular to the fold while figure 5.3 shows the type of image obtained with grid lines parallel to the bend.

Obviously the slope along the member at the mid point was zero. Therefore, by observing the shift of the lines in figure 5.2 relative to this mid

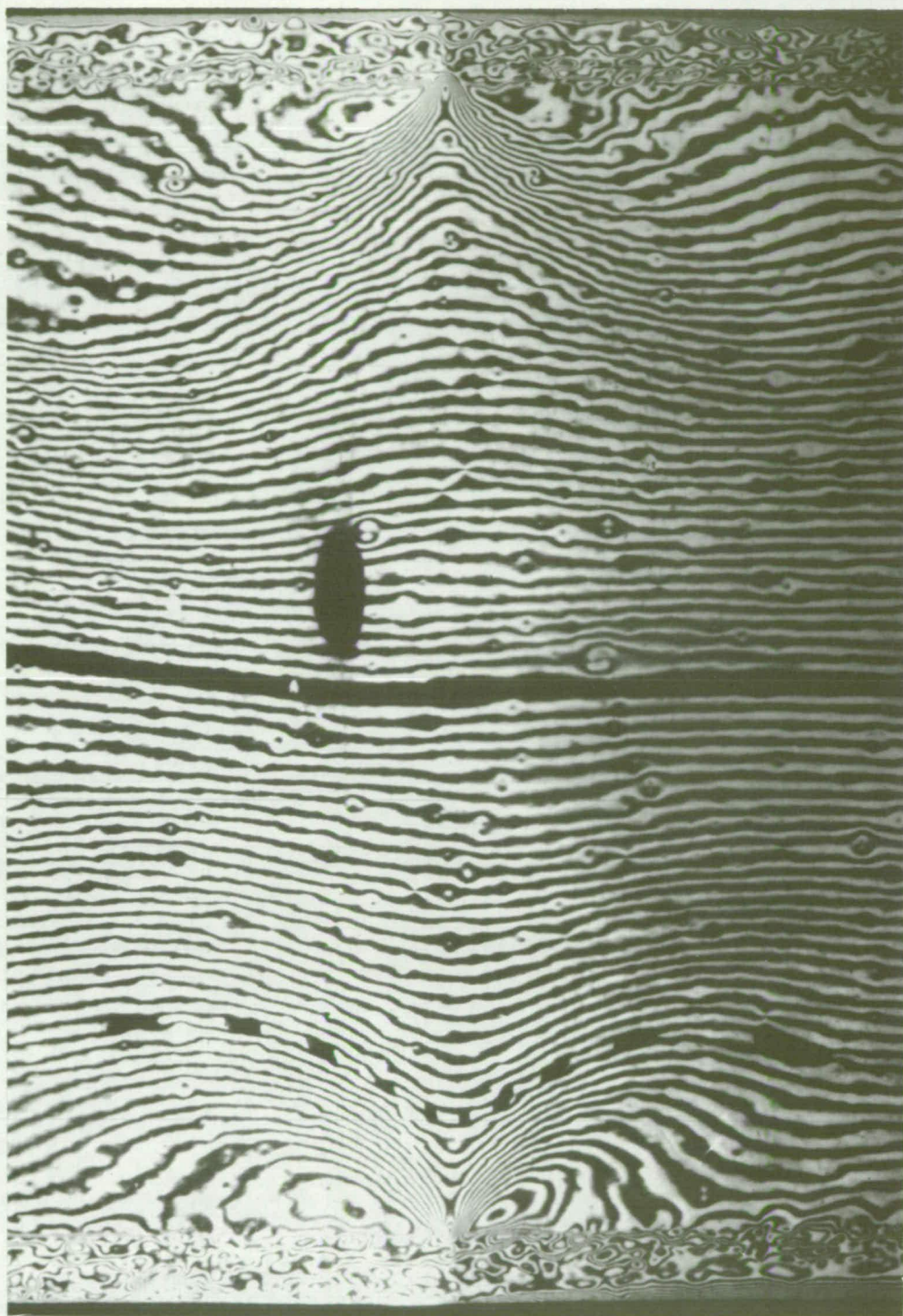


FIGURE 5.2

REFLECTED GRID LINE PATTERN WITH LINES  
PERPENDICULAR TO FOLD

$K = 150 \text{ m.m.}$

$T = 0.1 \text{ m.m.}$

$\theta = 173.9^\circ$



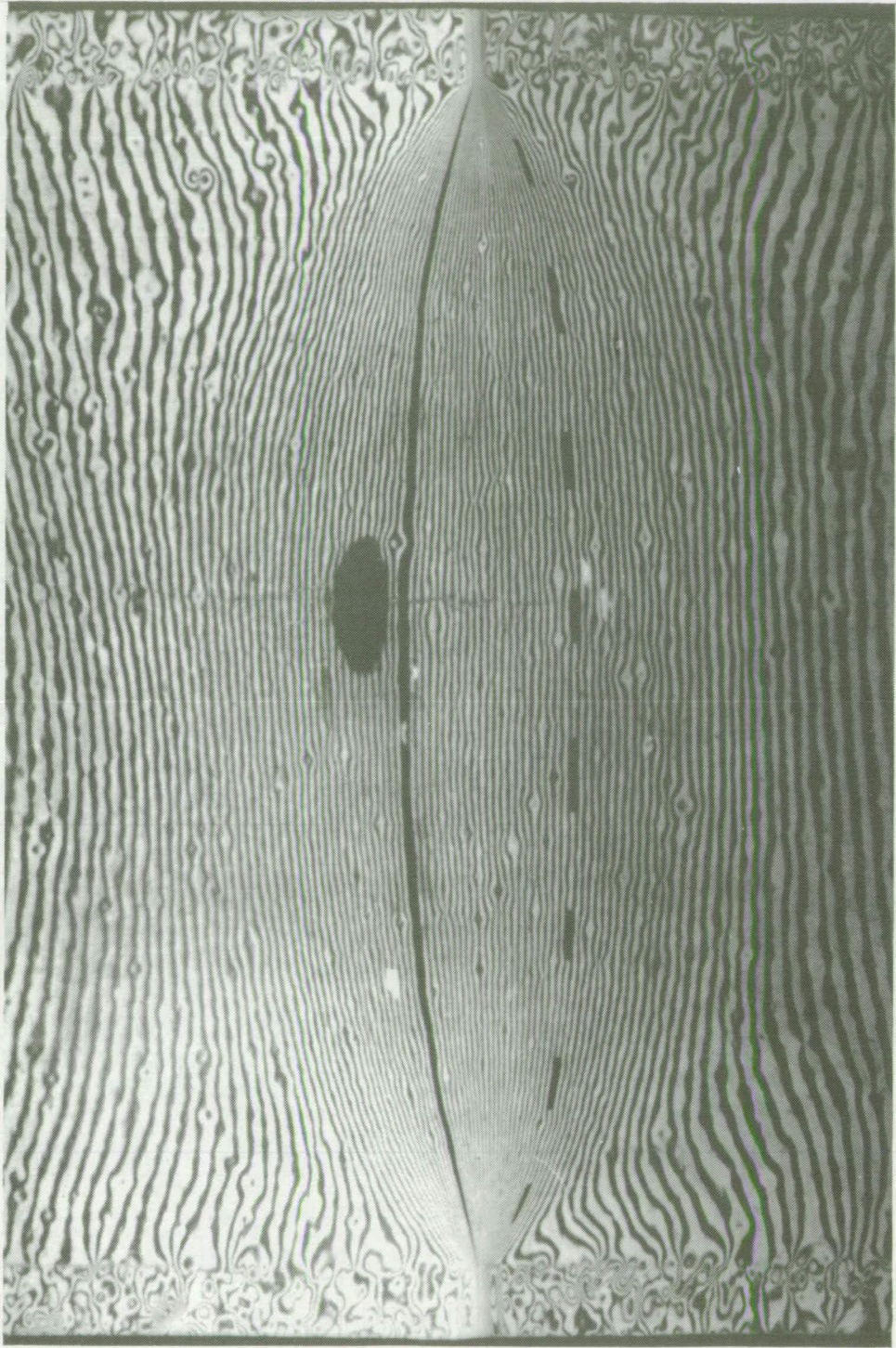


FIGURE 5.3

REFLECTED GRID LINE PATTERN WITH LINES  
PARALLEL TO FOLD

$$K = 150 \text{ m.m.}$$

$$T = 0.1 \text{ m.m.}$$

$$\theta = 173.9^\circ$$

point a curve of slope in the axial direction against position was plotted. Integration of this curve gave the deflection along the fold line as a function of position. From figure 5.3 the transverse curvature was measured for various positions. An interesting feature of figure 5.3 is that there is a reasonably well defined area where the curvature is significant. Outside this area the surface is essentially flat while within, the transverse curvature is almost constant for any given position along the fold. This area usually was about half as wide as the fold was long. Thus the proposed model would apply to diagonal compression member of the Yoshimura pattern provided the facet width perpendicular to the fold was greater than a quarter of the length of the fold. This stipulation would require a very short and sharp facet and would not normally be a limitation.

A summary of central deflection values is given in figure 5.4 for three different test specimens with varying angles between the facets. The three lines drawn are linear regression lines providing a line of best fit to the test results. The regression line for specimen no.1 was almost identical to the regression line for all points. From this graph it was very apparent that thinner members had, in general, a lesser central deflection than thick ones though the difference was small and only important at large changes in angle. This phenomenon could be attributed directly to membrane

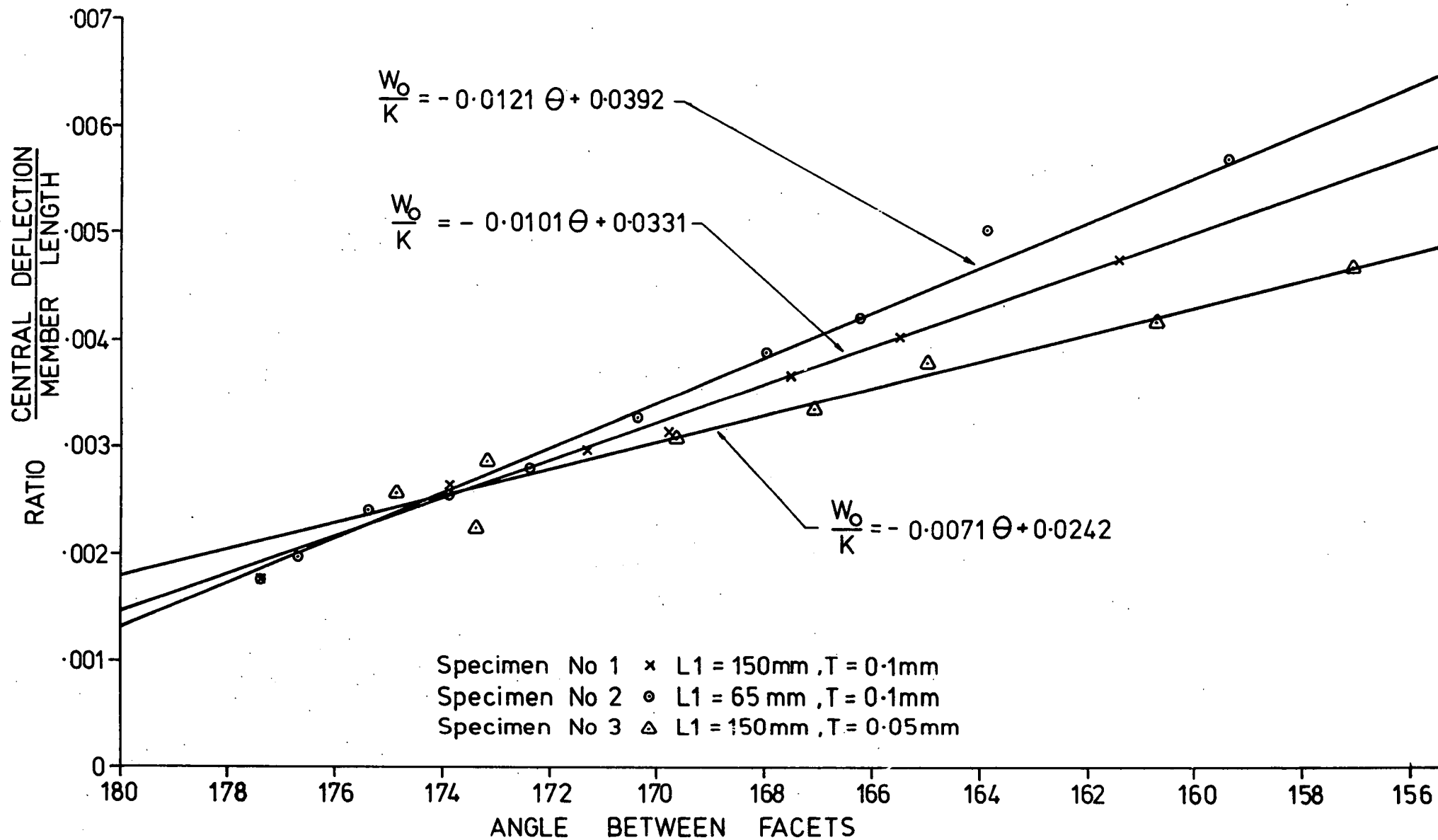


FIGURE 5.4

EFFECT OF ANGLE BETWEEN FACETS ON CENTRAL DEFLECTION



conditions. When the angle between the facets was  $174^{\circ}$  the difference was negligible which is the result obtained in the finite difference analysis. The range of conditions represented in figure 5.4 correspond to those that would exist in a buckled cylinder with a range of radius to thickness ratios of a few hundred to several thousand with a minimum of ten facets. Thus the results cover most of the range of interest.

In figure 5.5 the deflection on the member axis is plotted as a function of position. It was found that a least squares fit of a power curve with an index of 2.44 gave perhaps the best fit to the range of experimental results. It was hoped when the decision was made to investigate the shape of the fold that from the analysis the moment required to bend the sheet could be found. This moment in turn may have ultimately led to the establishment of the aspect ratio. However, with the sharp bend at the end of the member the moment at that point would be infinite and thus the calculated moment for bending the sheet would also be infinite. One possible way around the problem would be to use this model for the fold centre section and combine it with another shape at the end. Unfortunately, the problem cannot be simplified to that extent. In a buckled cylinder the size of this end section varies with load.



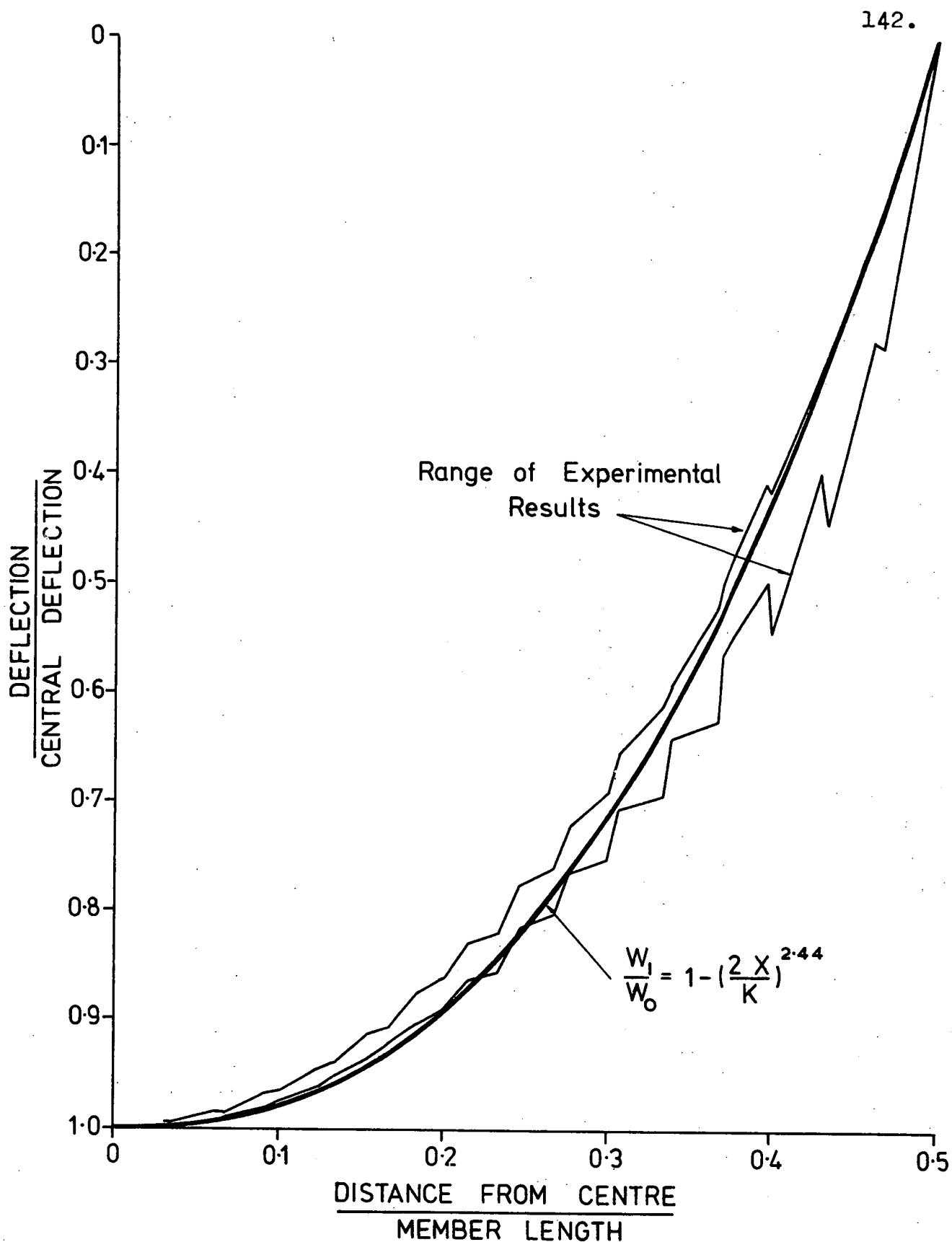


FIGURE 5.5  
LEAST SQUARES POWER CURVE FIT TO  
EXPERIMENTAL RESULTS

For figure 5.6, at three points along the member lines were drawn with constant curvature to intersect the axis at the value of deflection at the point. The curvatures used in the plot were the values measured from photographs similar to figure 5.3. Included in figure 5.6 is a line representing the slope of the facet. Clearly, if the fold was sharp then this line would also represent the facet. The curves in figure 5.6 became almost tangential to this line. In the actual bend the curved lines do, in fact, deflect further than this straight line but then converge on the line. This was logical since the measured curvature was the maximum but it reduced only slightly within the fold area. Thus a reasonable approximation to fold shape is that illustrated in figure 5.7. Likewise it is reasonable to assume that the member has resistance to bending only within the curved section. Therefore a finite area exists that can be considered as the member. This area is well illustrated in figure 5.1B.

The following mathematical relations describe the compression member deduced from the above argument.

$$\frac{w_1}{w_0} = 1 - \left(\frac{2x}{K}\right)^{2.44} \quad \text{-----} \quad 5.10$$

$$\frac{w_0}{K} = -0.0101.\theta + 0.0331 \quad \text{-----} \quad 5.11$$

(  $\theta$  in radians )

$$\therefore \frac{w_1}{K} = \left\{ 1 - \left(\frac{2x}{K}\right)^{2.44} \right\} ( 0.0331 - 0.0101.\theta ) \quad \text{--} \quad 5.12$$

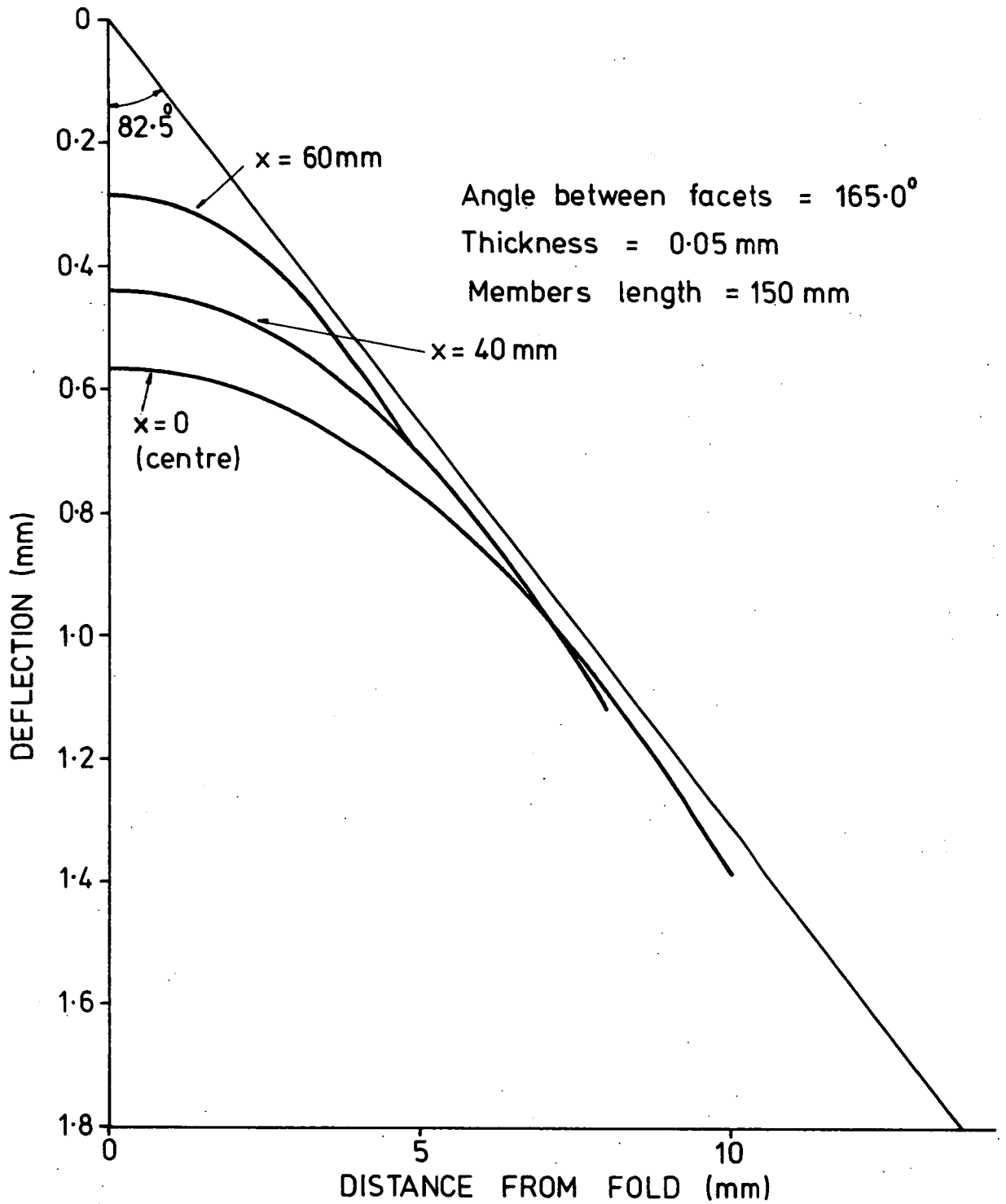


FIGURE 5.6  
APPROXIMATION TO TRANSVERSE SHAPE

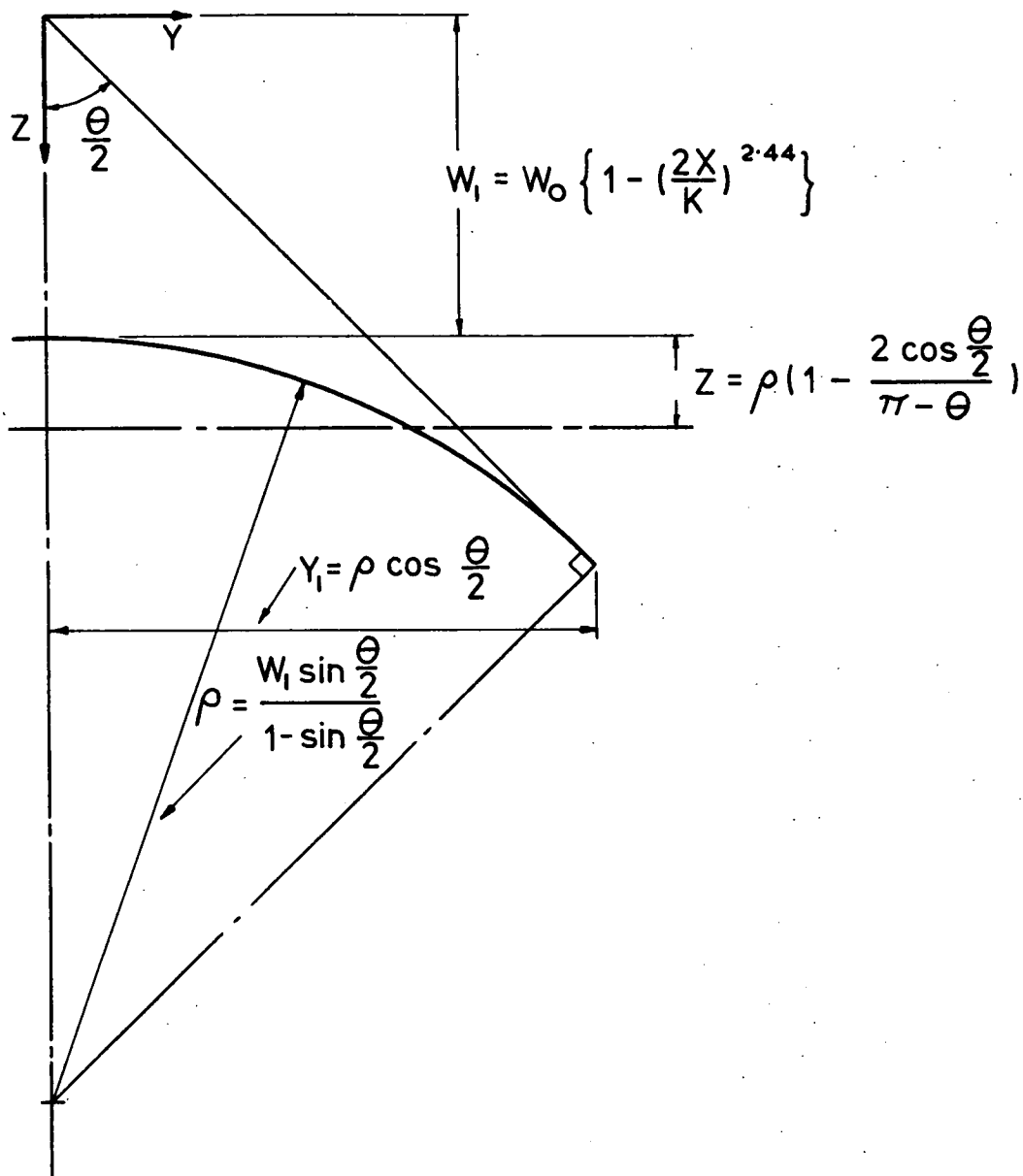


FIGURE 5.7  
FOLD SHAPE

$$\rho = \frac{w_1 \cdot \sin \frac{\theta}{2}}{(1 - \sin \frac{\theta}{2})} \quad \text{-----} \quad 5.13$$

The width of the member is given by

$$Y_1 = \rho \cdot \cos \frac{\theta}{2}$$

or

$$\frac{Y_1}{K} = \left\{ 1 - \left( \frac{2 \cdot X}{K} \right)^{2.44} \right\} (0.0331 - 0.0101 \cdot \theta) \frac{\sin \theta}{2(1 - \sin \frac{\theta}{2})}$$

----- 5.14

And the position of the neutral axis is given by.

$$Z = \rho \left( 1 - \frac{2 \cos \frac{\theta}{2}}{\pi - \theta} \right) \quad \text{-----} \quad 5.15$$

$$\text{also } I = \rho^3 T \left( \frac{\pi}{2} - \frac{\theta}{2} + \frac{\sin \theta}{2} - \frac{2 + 2 \cos \theta}{\pi - \theta} \right) \quad \text{-----} \quad 5.16$$

The collapse of the diagonal member was calculated in the same way as in chapter 2. For this purpose it was assumed that the member being formed during the collapse was straight and parallel with a half width of "w". Thus the collapse conditions were formulated in the same manner as in chapter 2 and figure 2.1<sup>4</sup> applied equally for this case.

$$\text{Now, as previously,}$$

$$H = \left\{ AF^2 - \frac{AB^2}{2(1 + \cos(\phi/2))} \right\}^{\frac{1}{2}} \quad \text{-----} \quad 5.17$$

$$OA = \frac{AB}{2 \sin(\phi/2)} \quad \text{-----} \quad 5.18$$

$$ON = \frac{AB \cdot \cos(\phi/4)}{2 \sin(\phi/2)} \text{ ----- 5.19}$$

$$FM = \frac{1}{2} \left\{ AF^2 + 2 \cdot AB^2 - 8 \cdot AB \cdot MN \cdot \sin(\phi/4) \right\}^{\frac{1}{2}} \text{ --- 5.20}$$

$$\text{and } FN = \frac{1}{2} \left\{ L_2^2 + \left( \frac{3 \cdot L_1}{2} \right)^2 \right\}^{\frac{1}{2}} \text{ ----- 5.21}$$

For the purpose of this analysis the deflection "FM" was considered as zero with no axial load. Thus the strain in FM was,

$$\epsilon = \left\{ \frac{AF^2 + 2 \cdot AB^2 - 8 \cdot AB \cdot MN \cdot \sin(\phi/4)}{L_2^2 + \left( \frac{3 \cdot L_1}{2} \right)^2} \right\}^{\frac{1}{2}} - 1 \text{ ----- 5.22}$$

And the resulting force exerted on the centre of the column was.

$$P_3 = 2 \cdot E \cdot W \cdot T \left[ \left\{ \frac{AF^2 + 2 \cdot AB^2 - 8 \cdot AB \cdot MN \cdot \sin(\phi/4)}{L_2^2 + \left( \frac{3 \cdot L_1}{2} \right)^2} \right\}^{\frac{1}{2}} - 1 \right] \text{ ----- 5.23}$$

It was also assumed that the tension member was straight and parallel with a half width of "W".

$$\text{Thus } AB = L_1 \left( 1 + \frac{P_2}{2 \cdot T \cdot E \cdot W} \right) \text{ ----- 5.24}$$

$$\text{and } P_2 = - \frac{2 \cdot P_1 \cdot L_1}{K} \text{ ----- 5.25}$$

$$AB = L_1 \left( 1 - \frac{P_1 \cdot L_1}{T \cdot E \cdot W \cdot K} \right) \text{ ----- 5.26}$$

The length of the loaded compression member was not so simply established since the member was not of uniform width but approached zero at the end. If one tries to compute the axial deflection of this member from an integration of strains then the calculated deflection would be infinite because of the singularity. Thus one has to approximate the situation further by calculating an average area of member.

$$\text{Area of member} = \rho \cdot \theta \cdot T$$

$$= \frac{.w_o \cdot \theta \cdot T \cdot \sin \frac{\theta}{2}}{(1 - \sin \frac{\theta}{2})} \left\{ 1 - \left( \frac{2 \cdot X}{K} \right)^{2.44} \right\}$$

$$\text{Average area} = \frac{2}{K} \int_0^{K/2} (\text{area of member}) dX$$

$$= \frac{0.709 \cdot \theta \cdot T \cdot w_o \cdot \sin \frac{\theta}{2}}{(1 - \sin \frac{\theta}{2})} \quad \text{-----} \quad 5.27$$

$$\text{Thus AF} = K + \frac{P_1 (1 - \sin \frac{\theta}{2})}{0.709 \cdot \theta \cdot T \cdot E \cdot w_o \cdot \sin \frac{\theta}{2}} \quad \text{-----} \quad 5.28$$

Substituting in equation 5.23, we have,

$$P_3 = \frac{\frac{2.82W \cdot P_1 (1 - \sin \frac{\theta}{2}) K^2}{\theta \cdot w_o \cdot \sin \frac{\theta}{2}} - \frac{4 \cdot P_1 \cdot L_1^3}{K} - 8 \cdot L_1 \cdot MN \cdot E \cdot W \cdot T \cdot \sin \frac{\theta}{4}}{L_2^2 + \left( \frac{3 \cdot L_1}{2} \right)^2} \quad \text{-----} \quad 5.29$$

Again, the angle that this force makes with the buckling member is given by,

$$\cos \eta = \frac{L_2^2 - \left(\frac{3 \cdot L_1}{2}\right)^2}{K \left\{ I_2^2 + \left(\frac{3 \cdot L_1}{2}\right)^2 \right\}^{\frac{1}{2}}} \quad \text{-----} \quad 5.30$$

We can also isolate the member as in Chapter 2 and determine the moment (see figure 2.14)

$$\begin{aligned} M &= P_1(Y + Z) - P_3 \cdot \sin \eta \cdot \cos\left(\frac{\theta}{2}\right) \left(\frac{K}{2} - x\right) \\ &= E \cdot I \cdot \frac{d^2 Y}{dx^2} \quad \text{-----} \quad 5.31 \end{aligned}$$

Since the moment of inertia "I" in this case was dependent on position "x" this equation was non-linear. A further approximation can be made by assuming the deflection of the column as a trigonometric function. The boundary conditions were zero deflection at the end ( $x = K/2$ ) and zero slope at the centre ( $x = 0$ ). Thus the deflection can be represented by the following,

$$Y = MN \cdot \cos\left(\frac{\pi \cdot x}{K}\right) \quad \text{-----} \quad 5.32$$

$$\frac{d^2 Y}{dx^2} = - \frac{MN \cdot \pi^2}{K^2} \cos\left(\frac{\pi \cdot x}{K}\right)$$

Substituting in equation 5.31, we have,



$$\begin{aligned}
& -E \left( \frac{w_1 \cdot \sin(\theta/2)}{1 - \sin(\theta/2)} \right)^3 \cdot T \cdot \left( \frac{\pi}{2} - \theta/2 + \frac{\sin \theta}{2} - \frac{2(1 + \cos \theta)}{\pi - \theta} \right) \cdot \frac{MN \cdot \pi^2}{K^2} \cos\left(\frac{\pi \cdot x}{K}\right) \\
& = P_1 \left( MN \cdot \cos\left(\frac{\pi \cdot x}{K}\right) + \frac{w_1 \cdot \sin(\theta/2)}{1 - \sin(\theta/2)} \left( 1 - \frac{2 \cdot \cos(\theta/2)}{\pi - \theta} \right) \right) \\
& \quad - \sin \gamma \cdot \cos(\theta/2) \left( \frac{K}{2} - x \right) \left[ \frac{2.82 \cdot W \cdot P_1 (1 - \sin(\theta/2)) K^2}{\frac{\theta \cdot w_0 \cdot \sin(\theta/2)}{L_2^2 + \left(\frac{3 \cdot L_1}{2}\right)^2} - \frac{4 \cdot P_1 \cdot L_1^3}{K}} \right. \\
& \quad \left. - \frac{8 \cdot L_1 \cdot MN \cdot E \cdot W \cdot T \cdot \sin(\phi/4)}{L_2^2 + \left(\frac{3 \cdot L_1}{2}\right)^2} \right] \text{----- 5.33}
\end{aligned}$$

At the centre of the column  $w_1 = w_0$  and  $x = 0$

Thus,

$$\begin{aligned}
& -\frac{E \cdot T \cdot MN \cdot \pi^2}{K^2} \left( \frac{w_0 \cdot \sin(\theta/2)}{1 - \sin(\theta/2)} \right)^3 \left( \frac{\pi}{2} - \theta/2 + \frac{\sin \theta}{2} - \frac{2(1 + \cos \theta)}{\pi - \theta} \right) \\
& = P_1 \left[ MN + \frac{w_0 \cdot \sin(\theta/2)}{1 - \sin(\theta/2)} \left( 1 - \frac{2 \cdot \cos(\theta/2)}{\pi - \theta} \right) \right. \\
& \quad \left. - \frac{K \cdot \sin \gamma \cdot \cos(\theta/2)}{2(L_2^2 + \left(\frac{3 \cdot L_1}{2}\right)^2)} \left\{ \frac{2.82 \cdot W \cdot (1 - \sin(\theta/2)) \cdot K^2}{\theta \cdot w_0 \cdot \sin(\theta/2)} - \frac{4 \cdot L_1^3}{K} \right\} \right. \\
& \quad \left. + \frac{K \cdot \sin \gamma \cdot \cos(\theta/2) \cdot 8 \cdot L_1 \cdot MN \cdot E \cdot W \cdot T \cdot \sin(\phi/4)}{2(L_2^2 + \left(\frac{3 \cdot L_1}{2}\right)^2)} \right]
\end{aligned}$$

Or,

$$\begin{aligned}
& P_1 \left[ MN + \frac{w_0 \cdot \sin(\theta/2)}{1 - \sin(\theta/2)} \left( 1 - \frac{2 \cdot \cos(\theta/2)}{\pi - \theta} \right) - \frac{\sin \gamma \cdot \cos(\theta/2)}{L_2^2 + \left(\frac{3 \cdot L_1}{2}\right)^2} \left\{ -2 \cdot L_1^3 \right. \right. \\
& \quad \left. \left. + \frac{1.41 \cdot W \cdot K^3 (1 - \sin(\theta/2))}{\theta \cdot w_0 \cdot \sin(\theta/2)} \right\} \right] \\
& = -MN \left[ \frac{E \cdot T \cdot \pi^2}{K^2} \left( \frac{w_0 \cdot \sin(\theta/2)}{1 - \sin(\theta/2)} \right)^3 \left( \frac{\pi}{2} - \theta/2 + \frac{\sin \theta}{2} - \frac{2(1 + \cos \theta)}{\pi - \theta} \right) \right. \\
& \quad \left. + \frac{4 \cdot K \cdot \sin \gamma \cdot \cos(\theta/2) \cdot L_1 \cdot E \cdot W \cdot T \cdot \sin(\phi/2)}{L_2^2 + \left(\frac{3 \cdot L_1}{2}\right)^2} \right] \text{----- 5.34}
\end{aligned}$$

Equation 5.34 is of the form,

$$P_1(MN+C) = -MN.D$$

Therefore, if  $P_1$  is plotted against  $MN$ , the curve is asymptotic to  $P_1 = -D$ . We can thus consider the value of  $-D$  as the critical load for the column.

$$\begin{aligned} \text{i.e. } P_{1_{cr}} &= - \frac{E.T.^2}{K^2} \left( \frac{w_o \cdot \sin(\theta/2)}{1 - \sin(\theta/2)} \right)^3 \left( \pi/2 - \theta/2 + \frac{\sin\theta}{2} \right. \\ &\quad \left. - \frac{2(1+\cos\theta)}{\pi - \theta} \right) - \frac{4.K.\sin^2 \gamma \cdot \cos(\theta/2) \cdot L_1 \cdot E.W.T.\sin(\phi/4)}{L_2^2 + \left( \frac{3.L_1}{2} \right)^2} \quad \text{---5.35} \end{aligned}$$

Apparently, the foregoing derivation has too many approximations to make it useful. If we use the previous cylinder of mylar ( $E=5.5\text{GPa}$ ) with a radius of 0.1 m. and thickness 0.19 mm. buckled into a pattern with 15 lobes and aspect ratio of 0.7 then an effective width of member of only 3.4 times the thickness is necessary to provide a buckling load of 272 N. The last term in equation 5.35 predominates and this term originates from the effect that the radial deflection of the buckling member has on the restraining force in the member being formed. It was in association with the establishment of this condition that perhaps the most serious approximations were made. Thus it seems that the so called refinement to the theory, allowing for the curved nature of the members was not a refinement at all but contributed greater inaccuracies. For this reason the rounded nature of the space frame members was not considered any further.

Up to this point the space frame analysis has centered about one condition of shell wall flexibility, i.e. one value of the ratio of radius to thickness. It would obviously be desirable to have the theory predict the collapse loads for cylinders of all proportions. However, before this complete picture can be obtained it is necessary to know how the aspect ratio varies with the radius to thickness ratio. The aspect ratio is very critical in determining the effective width of the space frame members. In Chapter 2 an approximate value of 0.7 was measured for the aspect ratio. While this value did provide a great deal of useful information about buckling loads it was later found to be inaccurate. The aspect ratio was also found to vary with the radius to thickness ratio and possibly with the number of facets in the buckled shape.

In attempting to calculate the aspect ratio it was realised that the simplest space frame model described in Chapter 2 was insufficient to fully describe the load carrying action of the buckled cylinder. In that chapter a true space frame was envisaged with compression members that could buckle and tension members. In fact there is no reason for the tension load to be concentrated near the fold. Instead, it could just as well be distributed through the triangular facet. By changing the tension load carrying mechanism to a uniform tension instead of an angle tension member there is no change to the calculation

of the collapse load. There is, however, a small change in the axial deflection calculated at collapse. The main advantage in treating the tension field in this way is that it enables a calculation to be made of the aspect ratio which appears satisfactory at least over part of the range of buckled cylinders.

If we consider each facet to have a uniform tangential stress ( $\sigma$ ) then by considering radial equilibrium as before we find that.

$$\sigma = \frac{-P.L_1.\cos(\phi/2)}{4.N.L_2^2.T(1+\cos(\phi/2))\left\{1 - \frac{L_1^2(1-\cos(\phi/2))}{4.L_2^2(1+\cos(\phi/2))}\right\}^{\frac{1}{2}}}$$

----- 5.36

Thus,

$$P_3 = \frac{P_1.K + 4.W.T.L_1^2.\sigma - 8.L_1.E.W.T.MN.\sin(\phi/4)}{L_2^2 + \left(\frac{3L_1}{2}\right)^2}$$

----- 5.37

and,

$$MN \left[ 1 + \frac{8.L_1.E.W.T.\sin(\phi/4)\sin\eta.\cos(\theta/2)\{K/2 - \tan(J.K/2)\}}{P_1 \left\{ L_2^2 + \left(\frac{3L_1}{2}\right)^2 \right\}} \right]$$

$$= \frac{(P_1.K^2 + 4WTL_1^2.\sigma)\sin\eta.\cos(\theta/2)\{K/2 - \tan(J.K/2)\}}{P_1 \left\{ L_2^2 + \left(\frac{3L_1}{2}\right)^2 \right\}}$$

$$+ \frac{1}{2}W.\cos(\theta/2)\left\{\frac{1}{\cos(J.K/2)} - 1\right\} \text{ ---- } 5.38$$

At the critical load,

$$0 = 1 + \frac{8L_1 EWT. \sin(\phi/4) \cdot \sin \lambda \cdot \cos(\theta/2) \{K/2 - \tan(J.K/2)\}}{P_1 \left\{ L_2^2 + \left( \frac{3L_1}{2} \right)^2 \right\}} \quad \text{-----} \quad 5.39$$

This equation for the load carrying capacity is exactly the same as equation 2.25. When a cylinder is buckled any further deformation will have a certain strain energy associated with the deformation. This strain energy has three components.

Strain energy in the end cylindrical sections

$$= \frac{P^2(L - L_2)}{4 \cdot \pi \cdot R \cdot T \cdot E} \quad \text{-----} \quad 5.40$$

Strain energy in 2N diagonal members.

$$= \frac{P^2 \cdot L_1 (\lambda^2 + \frac{1}{4})^{1.5}}{8 \cdot T \cdot E \cdot W \cdot N \left\{ \lambda^2 - \frac{(1 - \cos(\phi/2))}{4(1 + \cos(\phi/2))} \right\}} \quad \text{-----} \quad 5.41$$

And the strain energy due to the tension field in 2N triangular facets

$$= \frac{P^2 \cos^2(\phi/2)}{32 \cdot N \cdot T \cdot E \cdot \lambda (1 + \cos(\phi/2))^2 \left\{ \lambda^2 - \frac{(1 - \cos(\phi/2))}{4(1 + \cos(\phi/2))} \right\}} \quad \text{-----} \quad 5.42$$

Thus, total strain energy,

$$U = \frac{P^2}{2TE} \left[ \frac{L - L_2}{2\pi R} + \frac{L_1 (\lambda^2 + \frac{1}{4})^{1.5}}{4WN \left\{ \lambda^2 - \frac{(1 - \cos(\phi/2))}{4(1 + \cos(\phi/2))} \right\}} + \frac{\cos^2(\phi/2)}{16 \cdot N \cdot \lambda (1 + \cos(\phi/2))^2 \left\{ \lambda^2 - \frac{(1 - \cos(\phi/2))}{4(1 + \cos(\phi/2))} \right\}} \right] \quad \text{-----} \quad 5.43$$

We can then find an estimate of the aspect ratio by letting  $\frac{\partial U}{\partial \lambda} = 0$

$$\begin{aligned}
 \text{i.e. } 0 &= -1 + \frac{3L_1\lambda(\lambda^2 + \frac{1}{4})^{\frac{1}{2}}}{4W\left\{\lambda^2 - \frac{(1-\cos(\phi/2))}{4(1+\cos(\phi/2))}\right\}} \\
 &\quad - \frac{\lambda L_1(\lambda^2 + \frac{1}{4})^{1.5}}{2W\left\{\lambda^2 - \frac{(1-\cos(\phi/2))}{4(1+\cos(\phi/2))}\right\}^2} \\
 &\quad - \frac{\cos^2(\phi/2)}{8(1+\cos(\phi/2))^2\left\{\lambda^2 - \frac{(1-\cos(\phi/2))}{4(1+\cos(\phi/2))}\right\}^2} \\
 &\quad - \frac{\cos^2(\phi/2)}{16\lambda^2(1+\cos(\phi/2))^2\left\{\lambda^2 - \frac{(1-\cos(\phi/2))}{4(1+\cos(\phi/2))}\right\}} \\
 &\hspace{15em} \text{----- 5.44}
 \end{aligned}$$

To solve equation 5.44 it was necessary to have an estimate of "W" which was in turn set by the load carrying capacity of the cylinder. To establish this variable the 15 lobe failure of Esslinger and Geier's cylinder was again used. The result was that an effective width of flange 24.5 times the material thickness was necessary and the aspect ratio was estimated to be 0.918. Both of these values appear to be reasonable.

To test the condition further several cylinders were made and buckled. The construction of the cylinders was the same as previously described. 56 measurements were made by photographing the cylinder and measuring the aspect ratio and number of facets from the photograph. The measured values are listed in table 5.1 and plotted in figure 5.8. The number of facets was not necessarily

MEASURED ASPECT RATIOS OF BUCKLED CYLINDERS

R	T	L	R/T	L/R	$\lambda$	N
mm.	mm.	mm.				
70.0	0.05	260	1400	3.71	0.73	8.7
"	"	"	"	"	0.70	7.2
"	"	132	"	1.89	0.75	10.2
"	"	"	"	"	0.70	11.8
"	"	"	"	"	0.75	11.1
"	"	"	"	"	0.74	9.9
"	"	90	"	1.29	0.70	11.1
"	"	"	"	"	0.74	14.0
"	"	"	"	"	0.73	13.8
44.5	"	127	890	2.85	0.76	9.5
"	"	51	"	1.14	0.77	12.4
"	"	"	"	"	0.77	12.5
"	"	147	"	3.30	0.78	8.7
"	"	"	"	"	0.76	8.5
"	"	"	"	"	0.75	7.9
"	"	"	"	"	0.76	7.3
"	"	99	"	2.22	0.82	10.3
"	"	"	"	"	0.80	10.1
"	"	"	"	"	0.76	9.8
"	"	72	"	1.62	0.83	11.4
"	"	52	"	1.17	0.77	14.1
"	"	"	"	"	0.76	13.6
"	"	80	"	1.80	0.80	8.7
70.0	0.1	246	700	3.51	0.79	7.5
"	"	"	"	"	0.81	7.6
"	"	"	"	"	0.77	8.0
"	"	186	"	2.66	0.77	8.8
"	"	"	"	"	0.78	8.4
"	"	136	"	1.94	0.81	10.0
"	"	"	"	"	0.78	8.9

MEASURED ASPECT RATIOS OF BUCKLED CYLINDERS

R	T	L	R/T	L/R	$\lambda$	N
mm.	mm.	mm.				
23.4	0.05	133	468	5.68	0.89	7.8
"	"	80	"	3.42	0.85	7.1
"	"	100	"	4.27	0.89	7.0
"	"	"	"	"	0.86	6.6
"	"	"	"	"	0.92	7.2
"	"	61	"	2.61	0.86	8.4
"	"	"	"	"	0.85	8.4
"	"	"	"	"	0.89	8.1
44.5	0.1	143	445	3.21	0.89	7.5
"	"	"	"	"	0.90	7.7
"	"	101	"	2.27	0.92	9.2
"	"	"	"	"	0.87	9.0
"	"	80	"	1.80	0.89	11.7
23.4	"	159	234	6.79	0.98	5.3
"	"	"	"	"	0.91	4.9
"	"	92	"	3.93	0.95	6.7
"	"	"	"	"	0.96	6.8
"	"	65	"	2.78	0.94	7.8
"	"	"	"	"	0.95	7.9
"	"	"	"	"	0.91	7.6
"	"	44	"	1.88	0.92	9.4
15.0	"	107	150	7.13	0.97	4.6
"	"	"	"	"	1.05	5.2
"	"	"	"	"	0.96	5.2
"	"	"	"	"	1.02	4.9
"	"	74	"	4.93	0.92	5.1



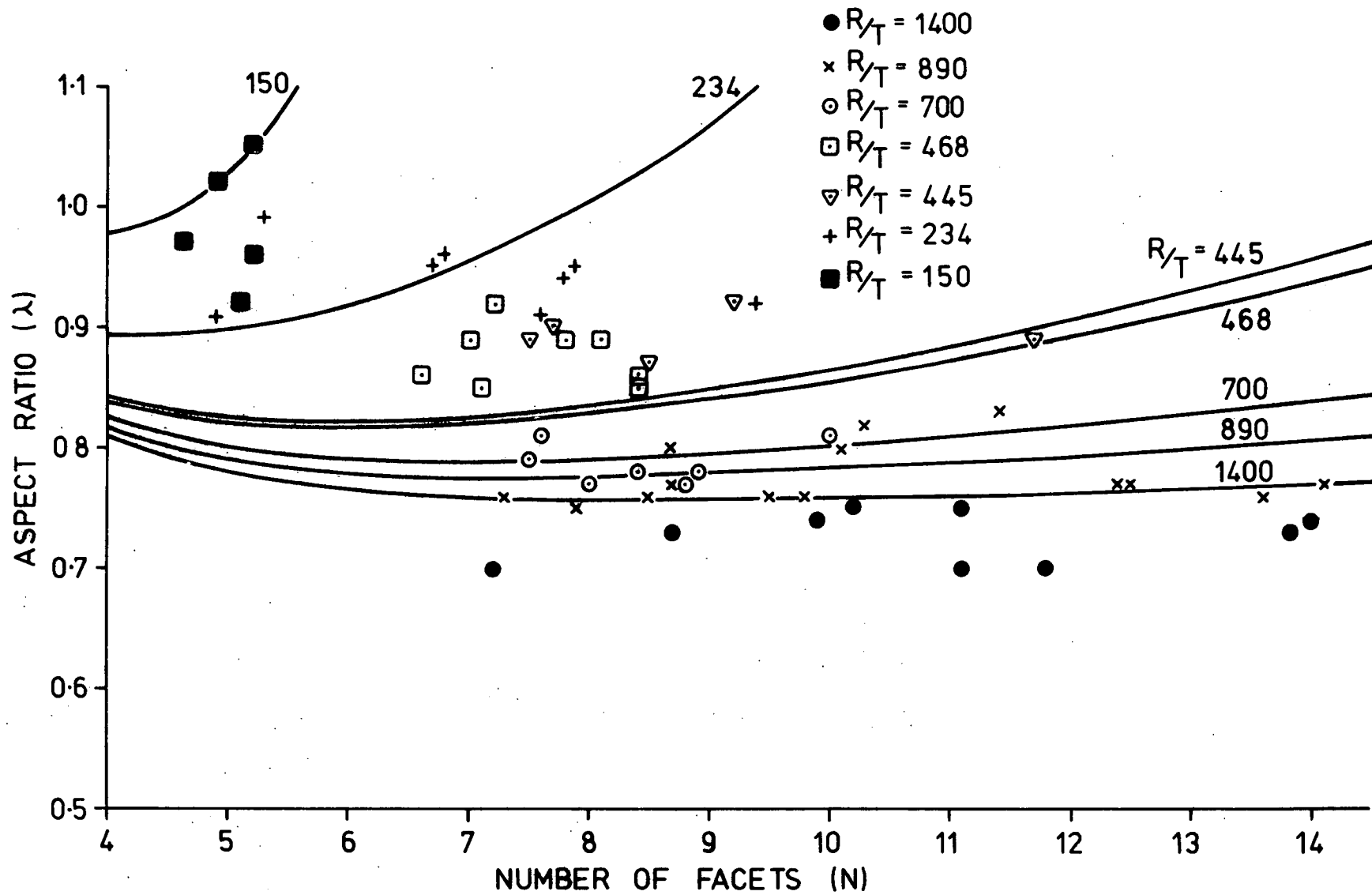


**FIGURE 5.8**  
**ASPECT RATIOS OF BUCKLED CYLINDERS**

a whole number since the loading was not completely uniform and the seam in the cylinder prevented a true <sup>uniform</sup> ~~asymmetric~~ pattern. This technique for measuring the aspect ratio can only be considered approximate and the repeatability of measurements was limited to about  $\pm 0.03$ .

Also plotted on figure 5.8 are curves representing the values calculated from equation 5.44. In the range covered by the graph there is much cause to celebrate the fit of the theory to experimental evidence. However, for larger values of N the calculated aspect ratio became very large with a consequent reduction in the load carrying capacity and thus equation 5.44 became unsatisfactory for calculating the aspect ratio. Thus the theoretically derived result was ignored for the remainder of the investigation.

Although the theory suggests a substantial change in aspect ratio with changing number of facets the measurements tend to show that any change in this direction was small and well within the scatter of results. Thus for figure 5.9 the range of values of  $\lambda$  together with the mean is plotted as a function of R/T. A linear regression line has been fitted to these results which provided the following relation.

$$\lambda = -0.121 \ln(R/T) + 1.606 \quad \text{-----} \quad 5.45$$

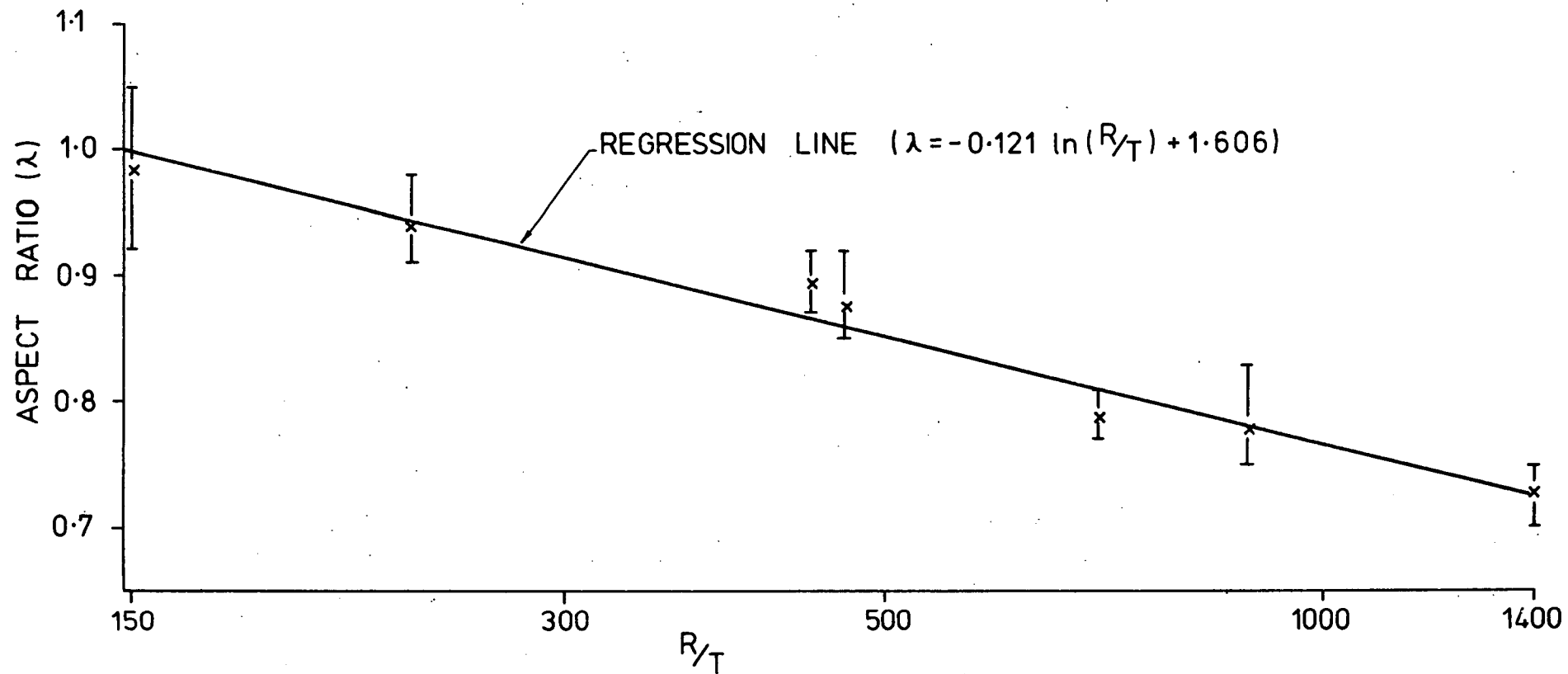


**FIGURE 5.9**  
**EFFECT OF RADIUS TO THICKNESS RATIO ON ASPECT RATIO**

A linear regression was chosen since any more elaborate a curve would be unreasonable with such a wide scatter of results. Equation 5.45 was then used as the condition governing the aspect ratio in all the subsequent work.

Now, incorporating equation 5.45 into the theory to account for shell wall flexibility and matching the 15 lobe failure in Esslinger and Geier's cylinder, an effective width of 23.5 times the thickness was obtained. Using this value with equation 5.45 a graph was drawn relating collapse load for a certain number of lobes with the radius to thickness ratio (figure 5.10). In this chart the ordinate is given as the proportion that the calculated collapse load is of the classical critical load.

Hart-Smith (ref. 19) gives a summary of published experimental buckling loads in a similar form of chart. In interpreting those results it is possible to infer that most lie within a fairly well defined band while only a small number are outside forming a much wider band. These two bands have been included in figure 5.10. The lower bound of the well defined band coincides with the design curve published by Baker, Kovalevsky and Rish (ref.11 pp.230). It seems that buckling strengths below this curve can usually be ignored. These cylinders would be those with large defects. The two higher bounds are not so easily treated but it is well known that hoop tension in a

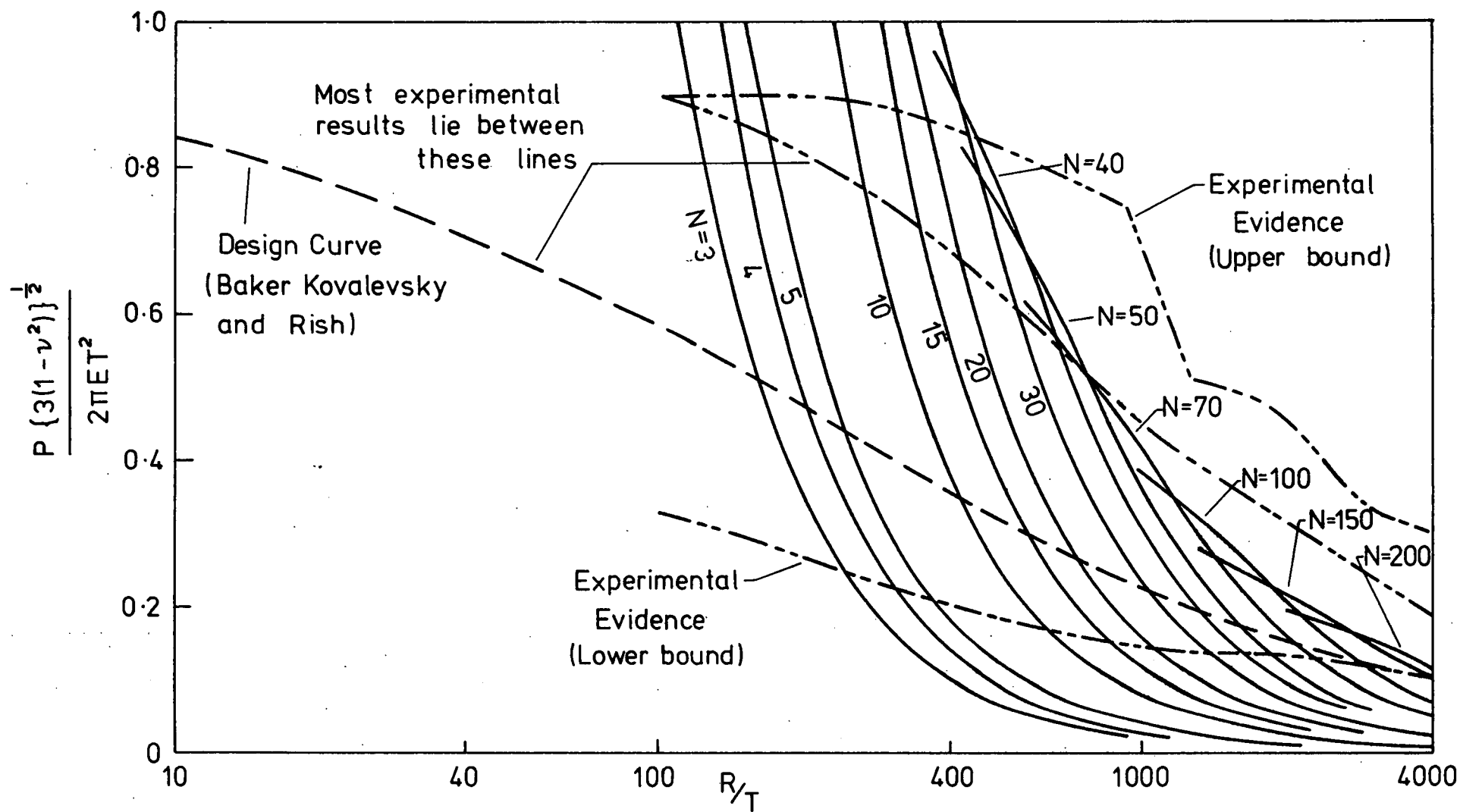


FIGURE 5.10  
PREDICTED COLLAPSE LOADS

cylinder will increase its axial buckling strength. One can not help but wonder if some of these experimental points may have been accidentally assisted by this cause, perhaps through air entrained in the cylinder or a hoop strain applied through the end boundary.

Whether these higher buckling strengths are included or not there appears to be a reasonable agreement between the experimental evidence and the collapse loads calculated for the substituted space frame. However, this graph should be treated with caution because it has been derived solely from one point on one experimentally obtained curve.

At low values of  $R/T$  it is known that a cylinder will buckle in the classical mode into ripples. Thus the curves representing the Yoshimura mode should exceed unity in this region. The drop in the design curve is due solely to yielding. It is interesting to note that a mild steel cylinder with  $R/T = 10$  will commence yielding on the surface at a load of only 7 % of the classical buckling load.

There is next a transition region where yielding still occurs and the mathematical model used here is inappropriate ( in the region of  $R/T = 100$ ). A further transition region occurs where yielding may or may not occur. In this section a well made cylinder may buckle into the axisymmetric pattern since its defects may only

cover a small section of the surface. The line representing the corresponding space frame would pass through the top of the chart at a point to the right of the particular  $R/T$  value. However, if the cylinder is poorly made then the curve representing the equivalent space frame passes to the left and the cylinder will buckle into the Yoshimura pattern.

In the last region, for high  $R/T$  values, the cylinder will buckle into the Yoshimura pattern. In this section none of the space frame curves passes through the line representing the classical mode. It is in this region that the greatest departure between prediction and experiment has occurred but then both have the same trend. The calculated values are in general somewhat lower for high values of  $R/T$  than the experimental evidence suggests. This situation could be improved considerably if the slope of the regression line in figure 5.9 were to be increased. Increasing the slope has the effect of increasing the collapse loads of the space frame for high  $R/T$  and moving the points of intersection of the curves with the top of the chart towards the left. Both of these corrections would appear to be desirable to make the chart more nearly reflect the practical situation. A close scrutiny of figure 5.9 would suggest that such a change may not be unreasonable particularly when it is realised that measurements of aspect ratio at low  $R/T$  were less reliable.

In the region of large  $R/T$  the number of facets at which the maximum load occurs increases with increasing  $R/T$ . Consequently, it would be expected that as the wall

thickness is reduced a larger number of facets would occur in the buckled shell. This is also a phenomenon observed in cylindrical shells.



E	Young's modulus.	
H	Axial length of half facet, i.e. collapsed length corresponding to $L_2$	
I	Moment of inertia of column member.	
K	Length of diagonal Compression member.	
L	Undeformed length of cylinder.	
$L_1$	Length of facet in the circumferential direction	
$L_2$	Half developed axial length of facet.	
$M_x$	} Moments per unit length.	
$M_y$		
$M_{xy}$		
N	Number of circumferential facets.	
$N_x$	} Membrane forces per unit length.	
$N_y$		
$N_{xy}$		
P	Axial load on cylinder.	} Tension positive
$P_1$	Axial load in diagonal member.	
$P_2$	Axial load in tangential member.	
$P_3$	Axial load in member being formed.	
Q	Distance Ligtenberg screen is placed away from the deformed model.	
R	Cylinder radius.	
T	Wall thickness.	
u	Deflection in a direction parallel to the axis of the compression member (x direction).	
v	Deflection in a direction normal to the axis of the compression member (y direction).	

$w$	Radial deflection.
$w_0$	Central deflection of unloaded compression member.
$w_1$	Unloaded deflection of any point on compression member.
$W$	Effective width of flange of remaining members.
$Y$	Transverse deflection of loaded compression member.
$Y_1$	Half width of curved compression member.
$Z$	Position of neutral axis of curved compression member.
$\delta$	Axial deflection of loaded space frame structure.
$\epsilon_1$	Strain in tangential member.
$\epsilon_2$	Strain in diagonal member.
$\eta$	Angle between collapsing diagonal member and member being formed.
$\theta$	Angle between adjacent facets along a diagonal member.
$\lambda$	Aspect ratio ( $\frac{L_2}{L_1}$ ).
$\nu$	Poisson's ratio.
$\rho$	Radius of curvature of cross section of compression member.
$\phi$	Angle subtended at axis of cylinder by each facet.
$\omega$	Ratio-effective width of flange to thickness( $W/T$ ).

# CHAPTER 6

## EXPERIMENTAL

## TECHNIQUE

## CHAPTER 6

### AN EXPERIMENTAL TECHNIQUE FOR MEASURING RADIAL DEFORMATIONS

A system was devised to measure radial deformations of the cylindrical shell based on the Ligtenberg moiré method (ref. 16). In the original Ligtenberg method a grid of equispaced lines was reflected off a model with a flat surface and photographed. The model was then deformed and a double exposure made of the grid lines. A moiré interference pattern was obtained between the grid lines photographed in the two load conditions and the fringes represented contours of constant slope perpendicular to the direction of the lines. Since two slopes are needed to define the condition at any point,

two double exposure photographs were needed. The grid lines for the second photograph were required to be rotated relative to their position for the first photograph.

An adaptation of the Ligtenberg method has been satisfactorily applied to the measurement of slope changes on the outside of cylindrical shell sections (ref.17). However, to determine the deflections of a complete cylinder it would be desirable to have one photograph describe the entire surface. One way in which all of the surface of the cylinder can be viewed at once is to use the internal surface. Thus, to utilise the Ligtenberg principle it is necessary to reflect a grid pattern off the inside of the cylinder and interfere the reflected pattern obtained in the undeformed state with that obtained after loading. By using the inside surface for measurement the outside is also left free for loading (e.g. pressure).

Figure 6.1 shows the system that was used to achieve this purpose. A cylindrical grid was reflected off the inside surface of the test cylinder and reflected again on the inside surface of a conically shaped mirror. Originally the grid pattern was then viewed by a special holosymmetrical camera (see ref. 18) that accepts only collimated light. Thus only light rays emerging parallel to the axis of the mirror were used in establishing the fringe pattern. This camera was subsequently found to be

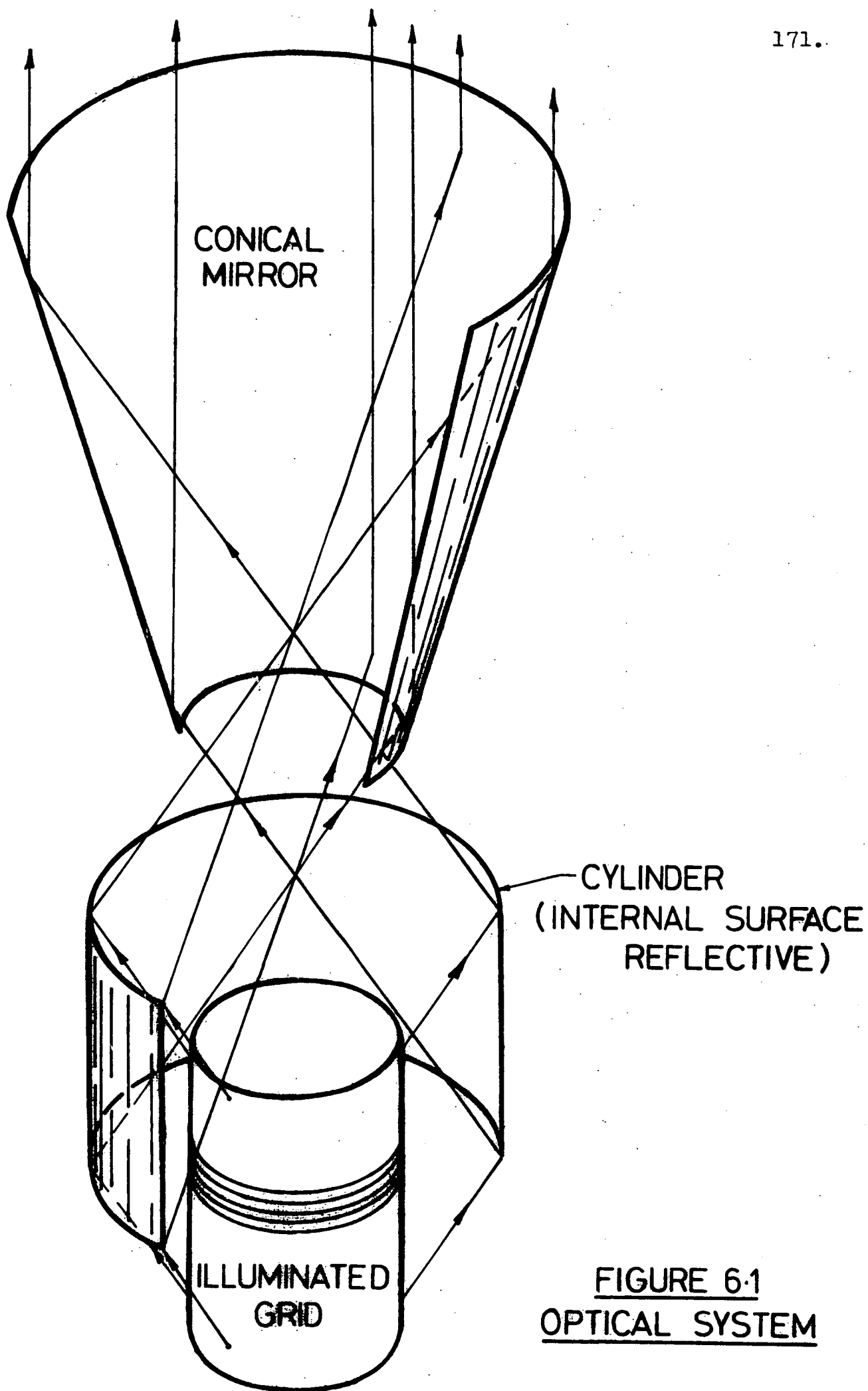


**FIGURE 6.1**  
**OPTICAL SYSTEM**

unsatisfactory because of insufficient depth of focus. It was replaced by an optic system comprising a large diameter very long focal length lens (2.27m. focal length and 130m.m. dia.). At the focal point of the lens the aperture of a camera was located, thus permitting only the collimated portion of the emerging rays to be photographed. This revised system had the minor disadvantage in that the image was no longer full size. Instead it was reduced considerably making resolution of the grid lines somewhat more difficult. The photographs made from this arrangement were flat and circular in nature. Grid lines oriented as in figure 6.1 (circumferential) were changed to concentric circles and longitudinal lines became radial lines. Thus the cylindrical co-ordinates of the test piece were transformed to polar co-ordinates by the optic system.

In the first instance the illuminated grid was a piece of a photographic negative wrapped around a miniature fluorescent tube. The test cylinder was an aluminium drink can (seamless) and the mirror was machined from a piece of aluminium alloy No. 2011. The test specimen was prepared by bonding the aluminium can into reinforcing rings with epoxy (Araldite AY103 with hardener HY951). The ends of the can were then removed and the inside polished to produce a reflective surface.

For reasons discussed later the grid was superseded while the aluminium can was changed for a fabricated melanex cylinder which would buckle elastically.

Figure 6.2 illustrates the geometry of the optical system. It is apparent from this diagram that for a given radius and cone angle ( $\theta$ ) the following relations hold.

$$X_2 = (R_2 - R_1) \cot 2\theta$$

$$X_3 = X_2 + X_1$$

$$X_4 = R_2 \cot 2\theta - \frac{X_1}{2}$$

The cylinder length  $X_1$  is limited because of interference of the reflected ray with the illuminated grid. The maximum value is.

$$\begin{aligned} X_{1_{\max.}} &= 2(R_2 - R_1) \cot 2\theta \\ &= 2X_2 \end{aligned}$$

The radius of the conical mirror at the small end has a minimum value, namely.

$$R_{5_{\min.}} = \frac{X_1}{2} \tan 2\theta$$

$$\text{also. } \frac{R_3 - R_5}{X_5 - X_4} = \tan \theta$$

$$\text{and } \frac{R_3 - R_{5_{\min.}}}{X_5 - X_4} = \tan 2\theta$$

$$\text{i.e. } R_3 = 2R_5 \cos^2 \theta - \frac{X_1}{2} \sin 2\theta$$



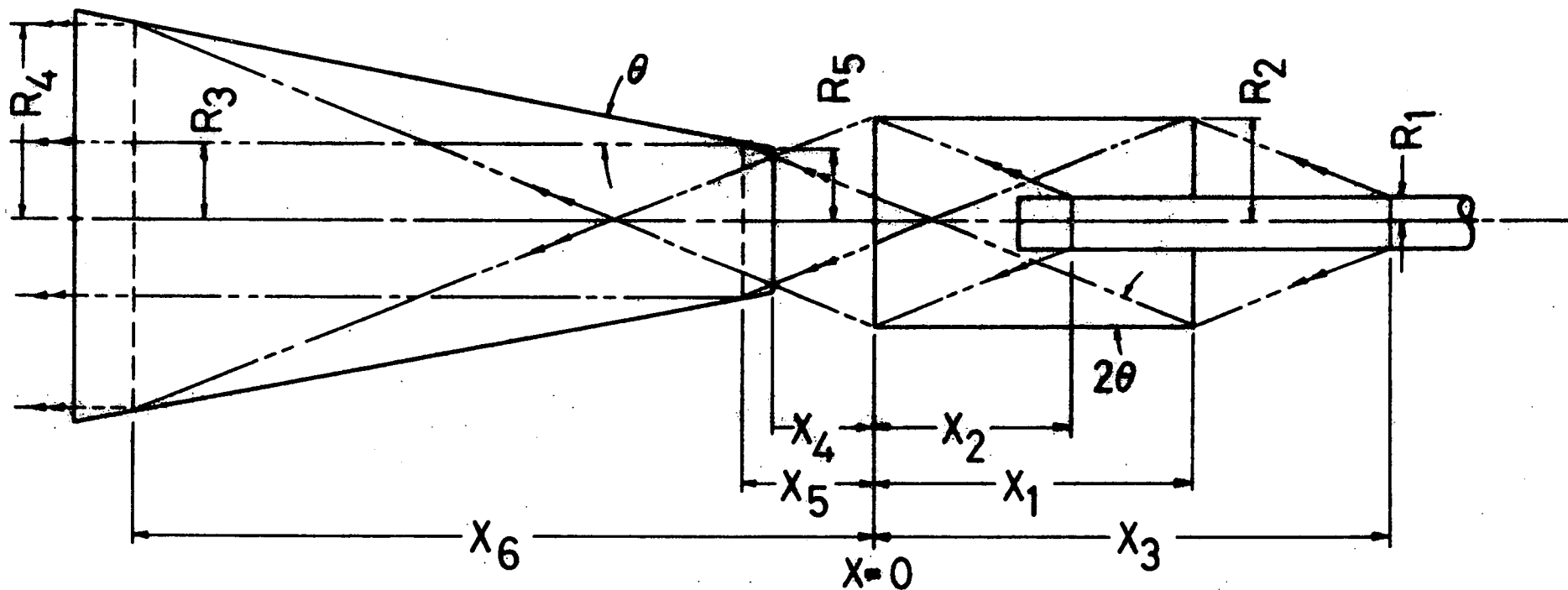


FIGURE 6.2  
GEOMETRY OF OPTIC SYSTEM

$$\text{and } X_5 = \frac{R_5 \cos 2\theta}{\tan \theta} - \frac{X_1 \cos 2\theta}{2} - \frac{R_2}{\tan 2\theta}$$

$$X_6 = X_5 + X_1(1 + \cos 2\theta)$$

$$R_4 = R_3 + X_1 \sin 2\theta$$

Circumferential grid lines spaced  $f_2$  apart will appear as concentric circles in the developed photograph spaced  $f_2 \sin 2\theta$  apart. Longitudinal grid lines with a line spacing of  $f_1$  will appear as radial lines on the photograph with a spacing of,

$$f = \frac{R}{R_1} f_1$$

Here  $f$  is the line spacing at radius  $R$  in the photograph. The minimum line spacing is.

$$f_{\min} = \frac{R_3}{R_1} f_1$$

When the cylinder deforms so that there is a change in slope in the tangential direction then the condition shown in figure 6.3 is established and,

$$\phi = \frac{nf_1}{R_1}$$

$$(AB)^2 = R_1^2 + (R_2 + r)^2 - 2R_1(R_2 + r)\cos\phi$$

$$\text{and } \frac{R_1}{\sin 2\delta_1} = \frac{AB}{\sin \phi}$$

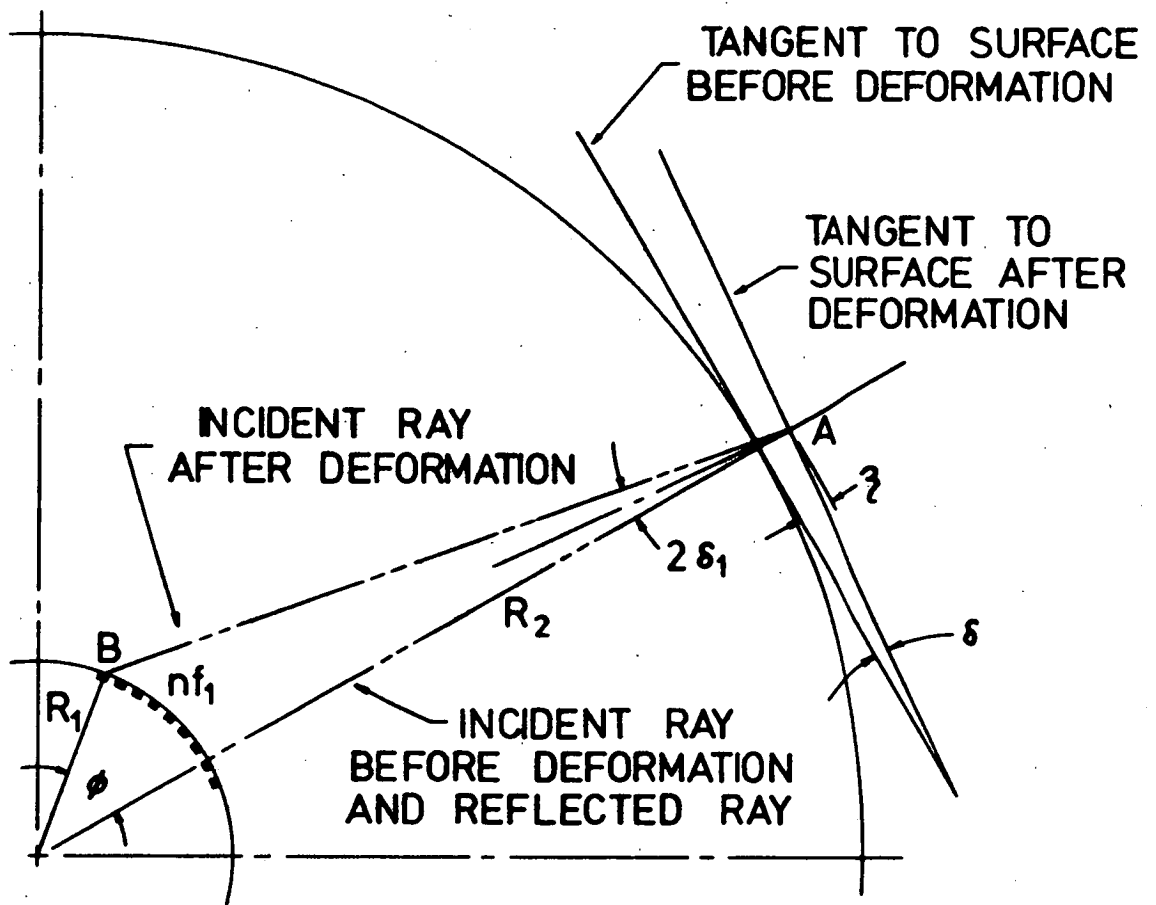


**FIGURE 6-3**

**EFFECT OF CHANGE OF SLOPE IN TANGENTIAL DIRECTION**

$$\text{i.e. } \sin 2\delta_1 = \frac{R_1 \sin\left(\frac{nf_1}{R_1}\right)}{\left\{R_1^2 + (R_2 + \gamma)^2 - 2R_1(R_2 + \gamma)\cos\left(\frac{nf_1}{R_1}\right)\right\}^{\frac{1}{2}}}$$

For the particular parameters adopted ( $R_1 = 8\text{mm.}$   
 $R_2 = 33\text{mm.}$ ) then.

$$\delta_1 = \frac{1}{2} \sin^{-1} \left[ \frac{8 \sin\left(\frac{nf_1}{8}\right)}{\left\{1153 + 66\gamma - 16(33 + \gamma)\cos\left(\frac{nf_1}{8}\right)\right\}^{\frac{1}{2}}} \right]$$

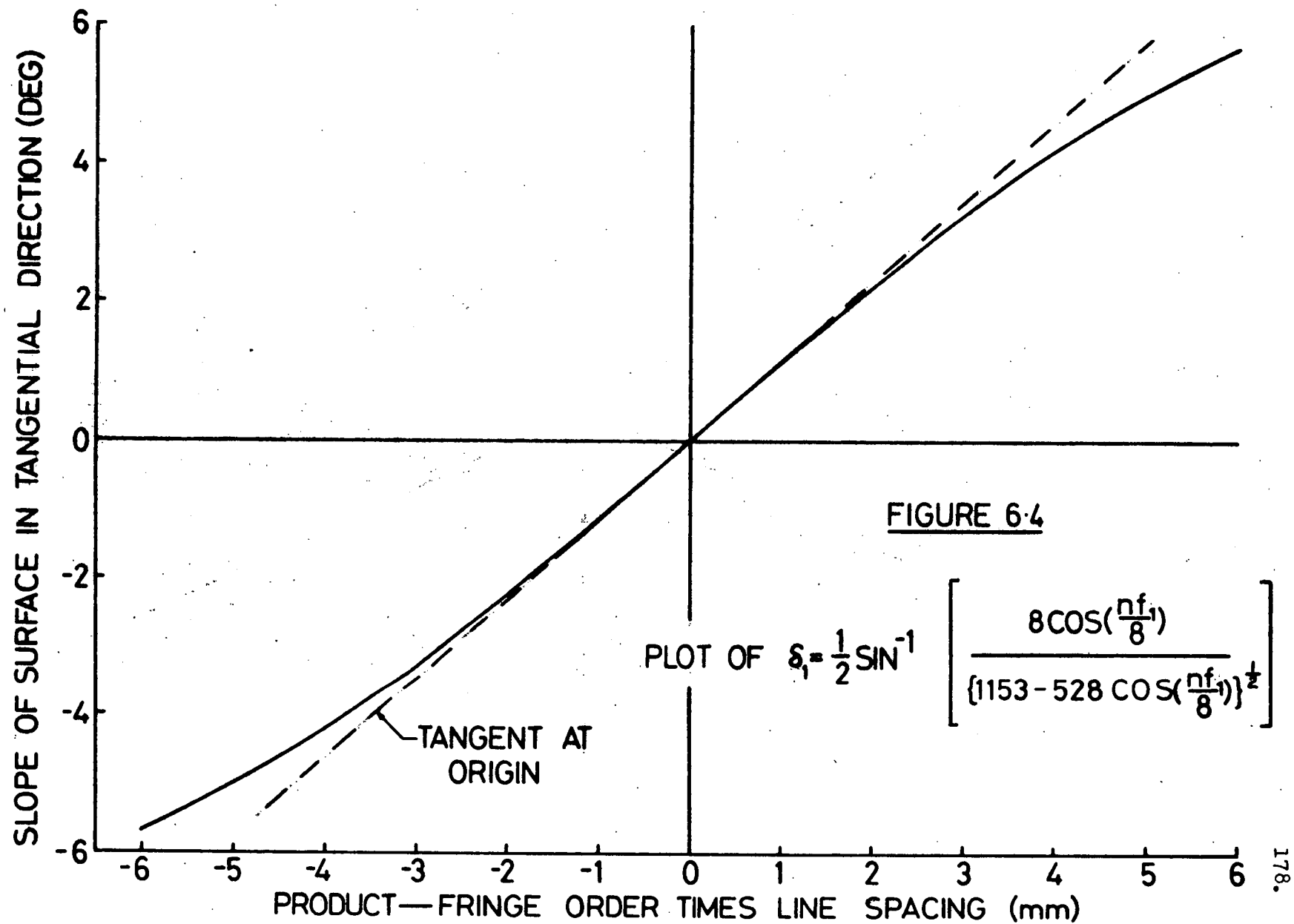
----- 6.1

Generally the finite deformation ( $\gamma$ ) is small and can be neglected in equation 6.1. Figure 6.4 is a plot of this relation for small  $\gamma$  together with the tangent at the origin which is given by.

$$\begin{aligned} \delta_1 &= 0.02nf_1 \text{ Rad.} \\ &= 1.146nf_1 \text{ Deg.} \end{aligned}$$

The relation is non-linear though the deviation from linearity is limited to about 2% with a  $2^\circ$  change in slope.

Figure 6.5 illustrates the condition that applies in measuring the change in slope in the axial direction. Unfortunately, changes in slope in the tangential direction also affect this measurement.



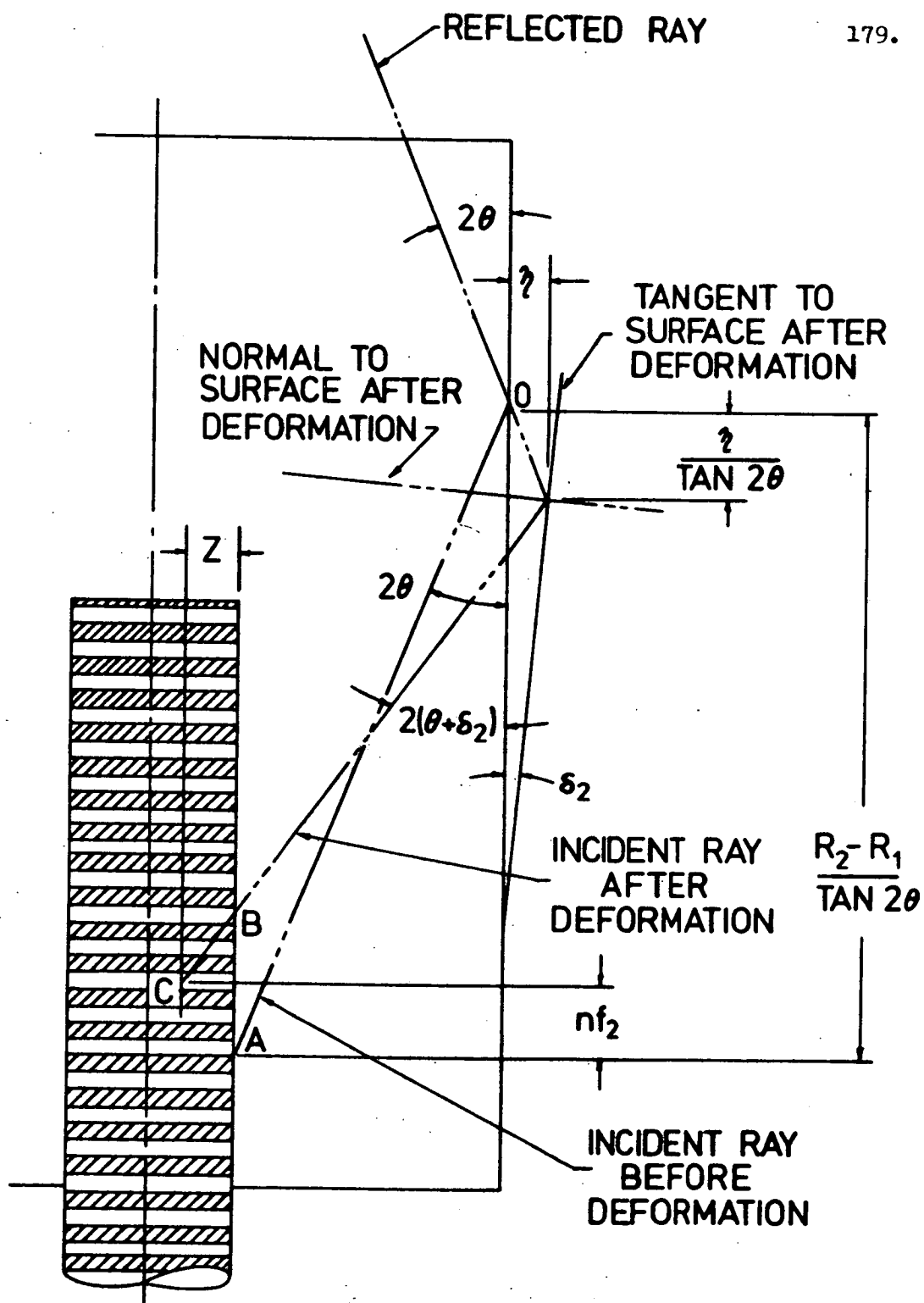


FIGURE 6.5  
EFFECT OF CHANGE OF SLOPE IN AXIAL DIRECTION

Before deformation the point "A" of the grid is seen in the reflection from the cylinder surface at "O". If there is a slope change in the axial direction then the point "B" will be seen at "O". A change in slope in the tangential direction will mean that the ray emerging from the grid will not come from a point on the same generator as "A" but will originate from a point to the side i.e. "C".

Now.

$$\frac{R_1}{\sin 2\delta_1} = \frac{\{R_1^2 + (R_2 + z)^2 - 2R_1(R_2 + z)\cos\phi\}^{\frac{1}{2}}}{\sin\phi}$$

$$\frac{R_1^2 \cdot \sin^2\phi}{\sin^2 2\delta_1} = R_1^2 + (R_2 + z)^2 - 2R_1(R_2 + z)\cos\phi$$

$$\begin{aligned} \text{i.e. } \frac{R_1^2}{\sin^2 2\delta_1} \cos^2\phi - 2R_1(R_2 + z)\cos\phi + R_1^2 + (R_2 + z)^2 \\ - \frac{R_1^2}{\sin^2 2\delta_1} = 0 \end{aligned}$$

$$\cos\phi = \frac{2R_1(R_2 + z) \pm \left\{ 4R_1^2(R_2 + z)^2 - \frac{4R_1^2}{\sin^2 2\delta_1} \left( R_1^2 + (R_2 + z)^2 - \frac{R_1^2}{\sin^2 2\delta_1} \right) \right\}^{\frac{1}{2}}}{\frac{2R_1^2}{\sin^2 2\delta_1}}$$

The positive sign gives the required root, therefore.

$$\cos\phi = \frac{(R_2 + z)\sin^2 2\delta_1}{R_1} + \left\{ (1 - \sin^2 2\delta_1) \left( 1 - \left( \frac{R_2 + z}{R_1} \right) \sin^2 2\delta_1 \right) \right\}^{\frac{1}{2}}$$

$$Z = R_1(1 - \cos\phi)$$

Now.

$$\tan 2(\theta + \delta_2) = \frac{R_2 - R_1 + Z + \eta}{\frac{R_2 - R_1}{\tan 2\theta} - nf_2 - \frac{\eta}{\tan 2\theta}}$$

or,

$$\tan 2\delta_2 = \frac{R_1(1 - \cos\phi) + nf_2 \tan 2\theta + 2\eta}{\frac{R_2 - R_1 - \eta}{\tan 2\theta} - nf_2 + \tan 2\theta(R_2 - R_1 \cos\phi + \eta)}$$

And for the particular design parameters adopted in the absence of large deformations this reduces to.

$$\cos\phi = 4.125 \sin^2 2\delta_1 + \{(1 - \sin^2 2\delta_1)(1 - 17.02 \sin^2 2\delta_1)\}^{\frac{1}{2}}$$

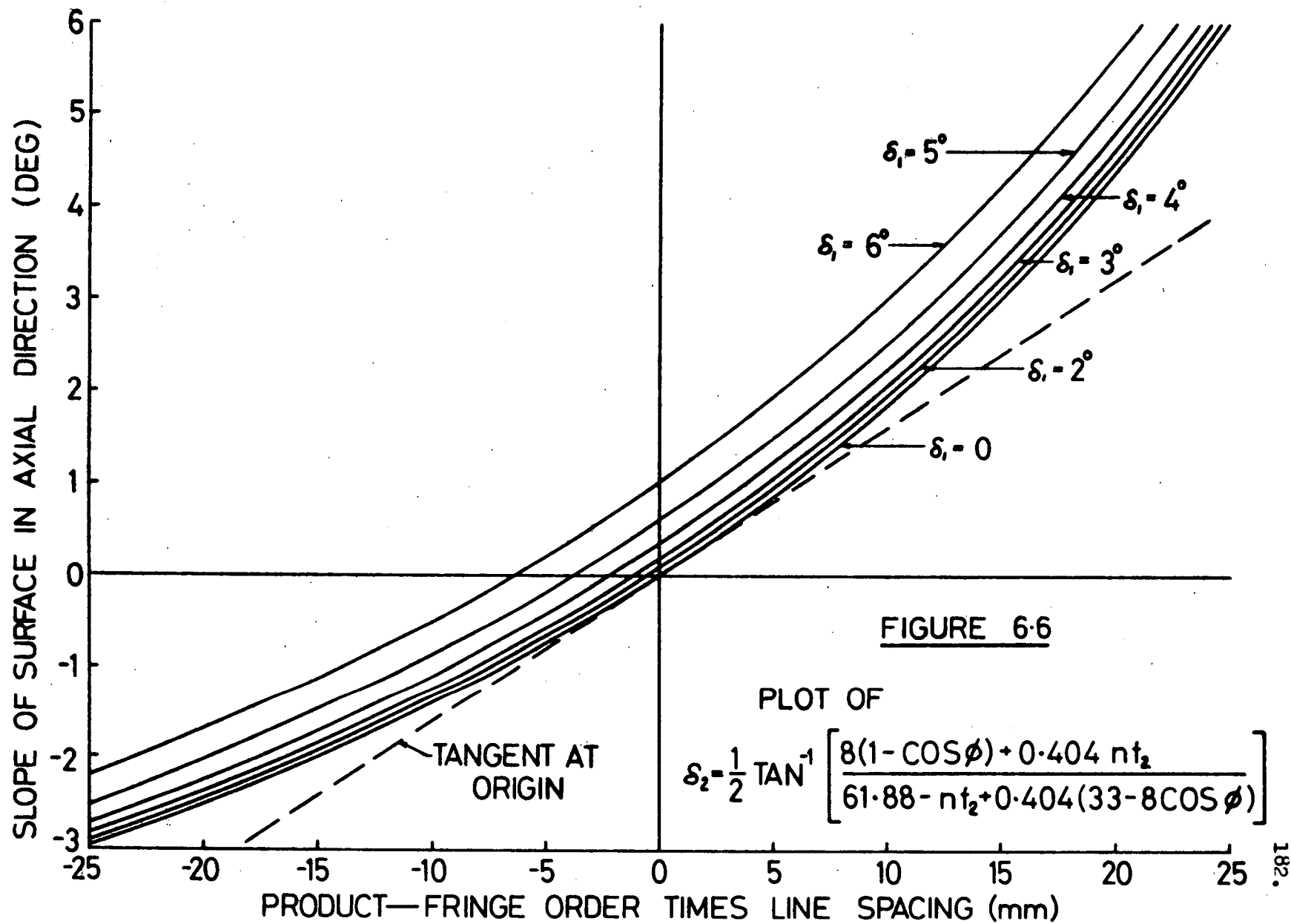
and,

$$\delta_2 = \frac{1}{2} \tan^{-1} \left\{ \frac{8(1 - \cos\phi) + 0.404nf_2}{61.88 - nf_2 + 0.404(33 - 8\cos\phi)} \right\} \text{ ---- 6.2}$$

Equation 6.2 is plotted as figure 6.6 and it can be seen that it is distinctly non-linear. Therefore, although a linearisation could be adopted when measuring slope changes in the tangential direction, it would be clearly inadvisable when determining slopes in the axial direction.

In using the Ligtenberg-moiré method it is common to obtain interference patterns for two grids at right angles and another pattern with the grid lines at some intermediate angle. It has already been shown that





slope changes in the tangential direction can be measured independently with axial grid lines but circumferential lines do not measure only the slope change in the axial direction. Interpreting fringe patterns obtained from a spiral grid would be even more difficult so that the use of this type of grid is not considered to be a worthwhile proposition.

In setting up the apparatus it was found that a reference specimen was necessary. For this purpose a cylinder was machined from brass to the same internal dimensions as the drink cans and internally polished. Alignment of grid, cylinder, mirror and camera was achieved when the images of all elements were concentric and the grid lines were either concentric circles or straight radial lines. Concentricity could be checked more accurately by observing the image in the camera than by measuring the relative positions of the optic elements.

To check the accuracy of the system a known tilt was applied to the cylinder and a moiré pattern obtained from a double exposure photograph taken of the grid lines at the two extreme positions. Figures 6.7 and 6.8 are the moiré patterns obtained.

Figure 6.7 was taken with the miniature fluorescent tube as the light source and it illustrates

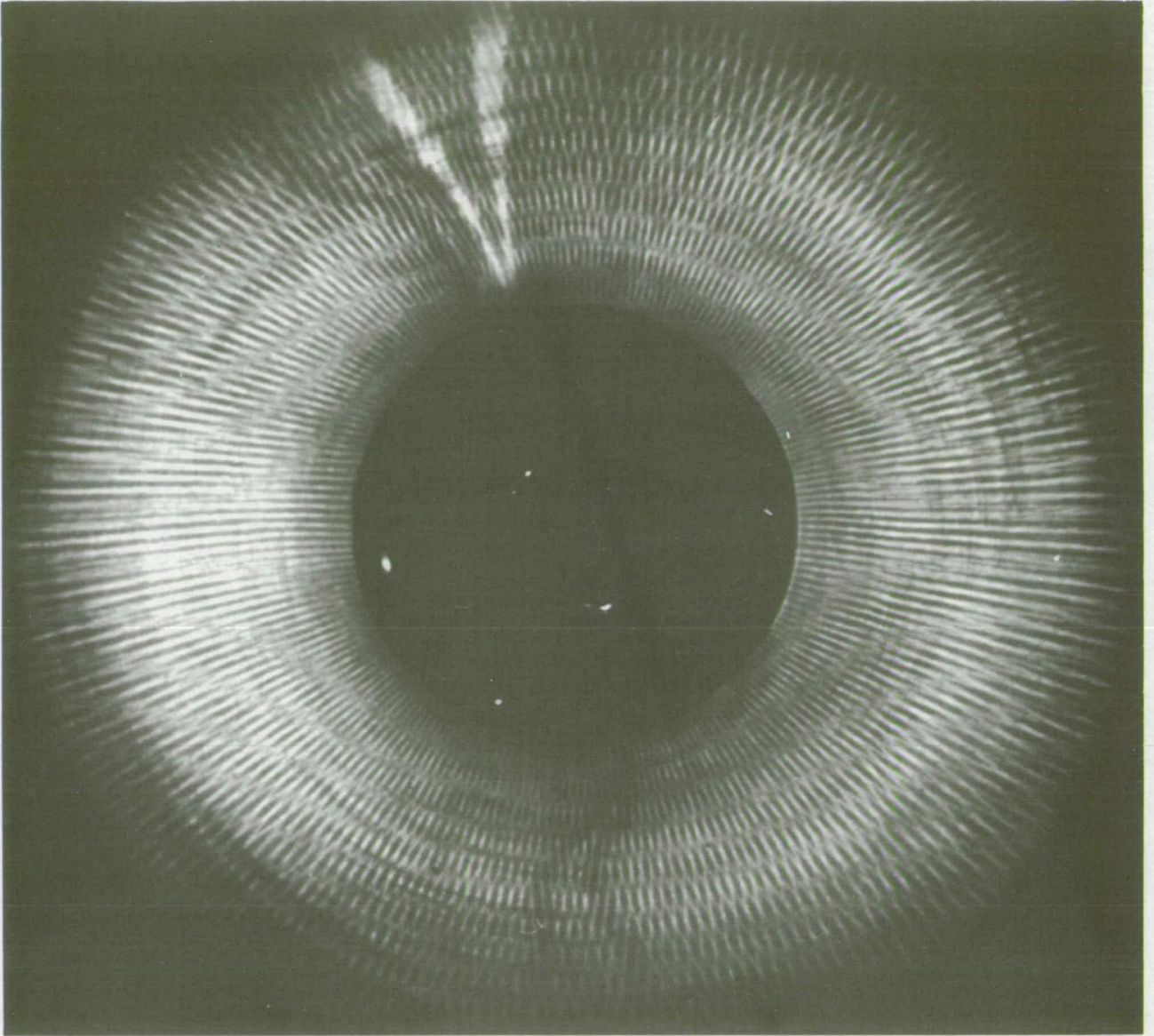


FIGURE 6.7

MOIRÉ PATTERN FROM BRASS CYLINDER  
WITH TILTED AXIS—AXIAL GRID LINES



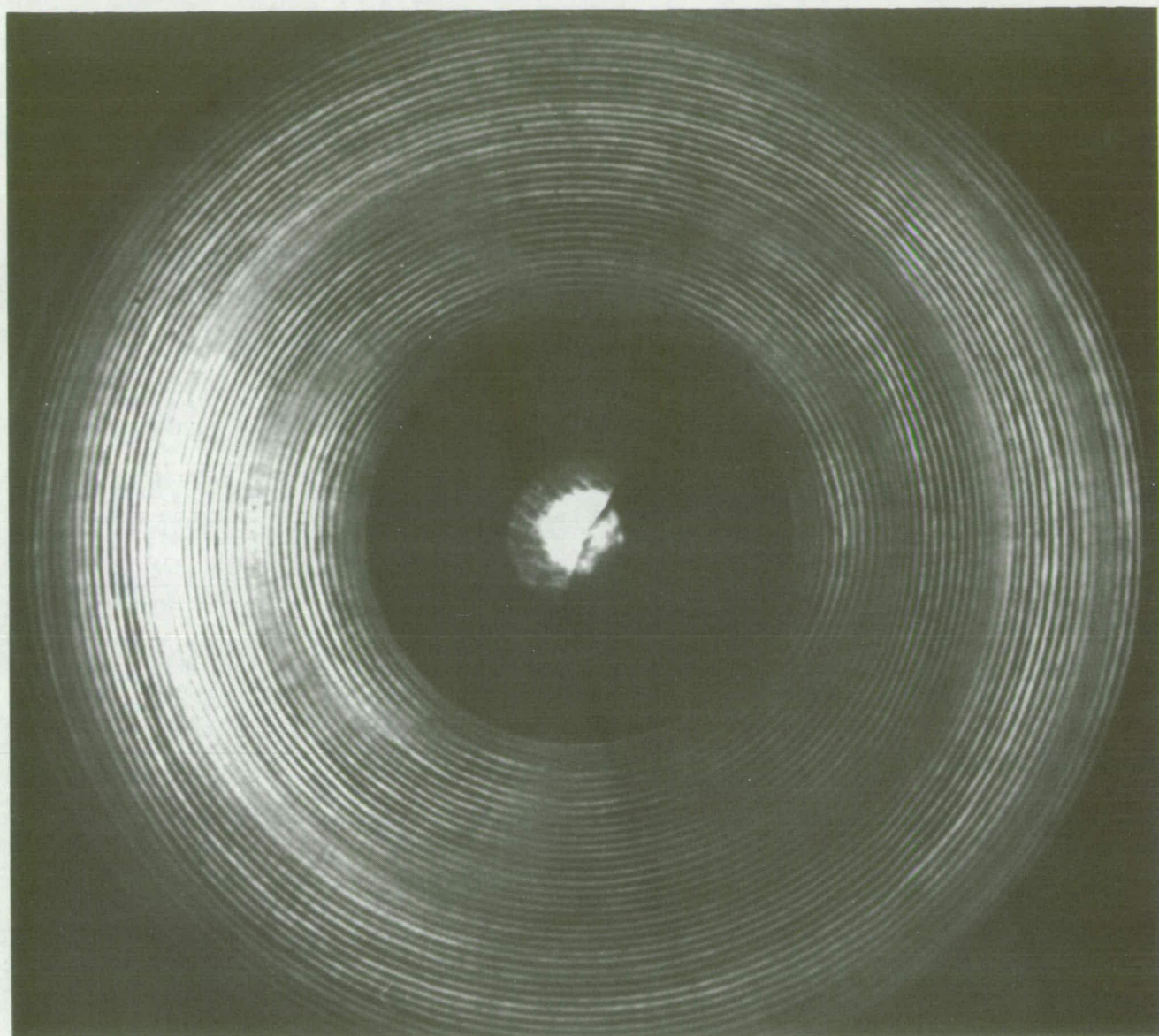


FIGURE 6·8

MOIRÉ PATTERN FROM BRASS CYLINDER  
WITH TILTED AXIS—TANGENTIAL GRID LINES

the shortcomings of this device. It will be seen that the image is very indistinct around the extremity. This is because the fluorescent tube tends to become dull at the end. The optical requirement of the system in this region is increased brightness. The lead wires required with the tube show on the image and blank out part of the grid (dark lines at top and bottom). The disadvantages of bonding a grid to the tube can also be seen in the photograph. The white lines at the top of the image are due to the join in the grid. Uneven patches of glue were also difficult to avoid. These showed as circular streaks in the photograph and tended to make the moiré pattern less distinct. These are most visible at the bottom of the photograph.

For figure 6.8 the fluorescent tube was replaced with a perspex bar with machined grooves progressively deeper towards the free end. Approximately collimated light was shone on the fixed end so that the grooves scattered the light forming bright bands and the intermediate sections were effectively internally reflective. The result was a considerably improved image. The unevenness of illumination was because the collimated light was not exactly parallel to the axis of the grid.

In figure 6.9 the fringes obtained from the two photographs (figures 6.7 and 6.8) are compared with fringes predicted from equations 1 and 2. Excellent agreement has been achieved. An insignificant discrepancy exists and appears to be due to improper alignment of all the optic elements at the time this test was made.

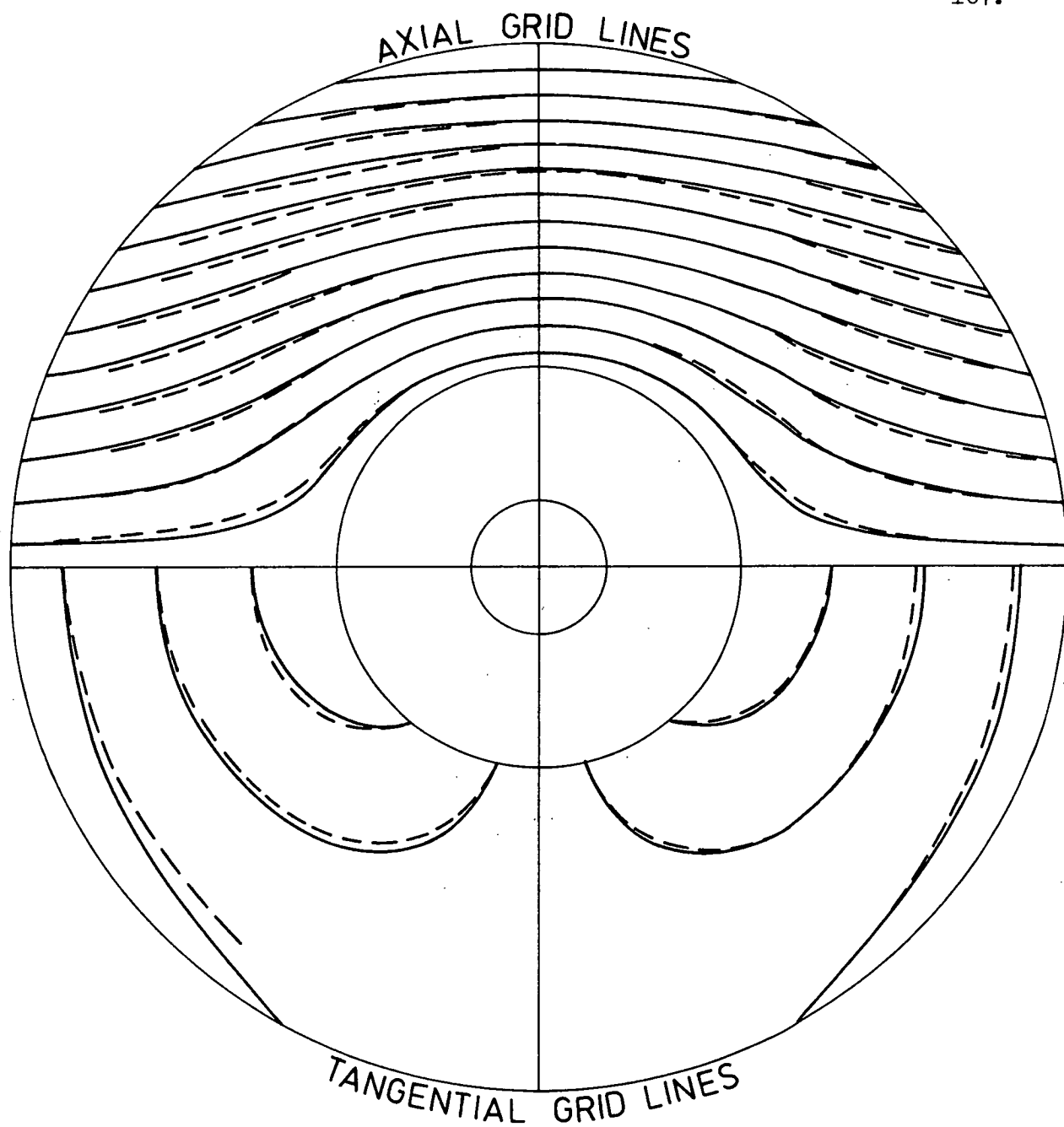


FIGURE 6.9  
COMPARISON OF FRINGES OBTAINED OPTICALLY  
WITH PREDICTED FRINGES  
FULL LINES – THEORETICAL FRINGES  
DOTTED LINES – OBSERVED FRINGES

The machined perspex bar is illustrated on the left hand side of figure 6.10. Also shown in figure 6.10 is the grid that replaced the fluorescent tube with axial grid lines. Both of the grids were made in a similar manner except that instead of turning grooves in the bar the grooves were made in a milling machine using a dividing head and the corner of a cutter. The patterns obtained with these two grids of the inside of the brass reference cylinder after final alignment of the optic elements are shown in figure 6.11. The variation in thickness of the radial grid lines occurs because the dividing head was running slightly out of true when the grid was manufactured.



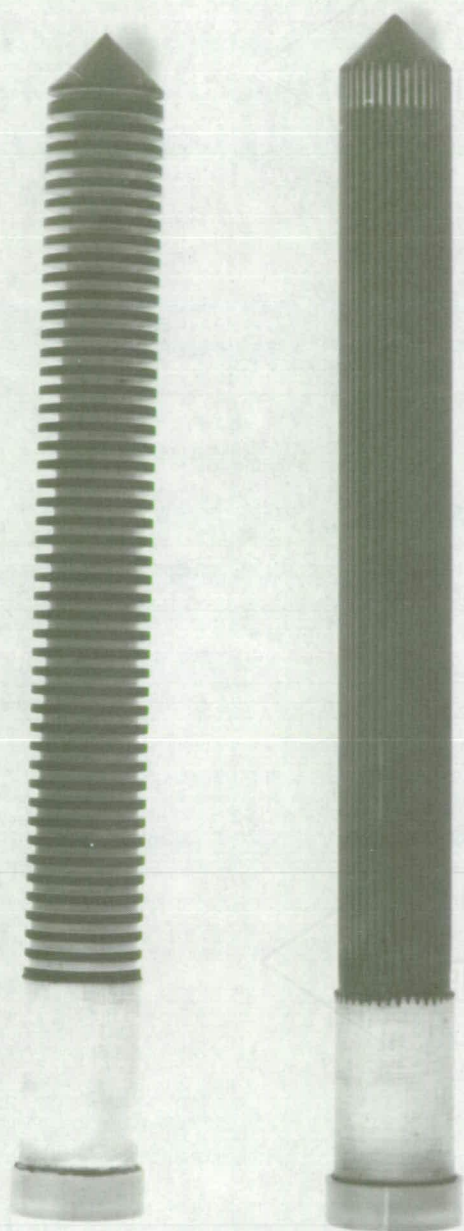


FIGURE 6.10  
PERSPEX GRIDS



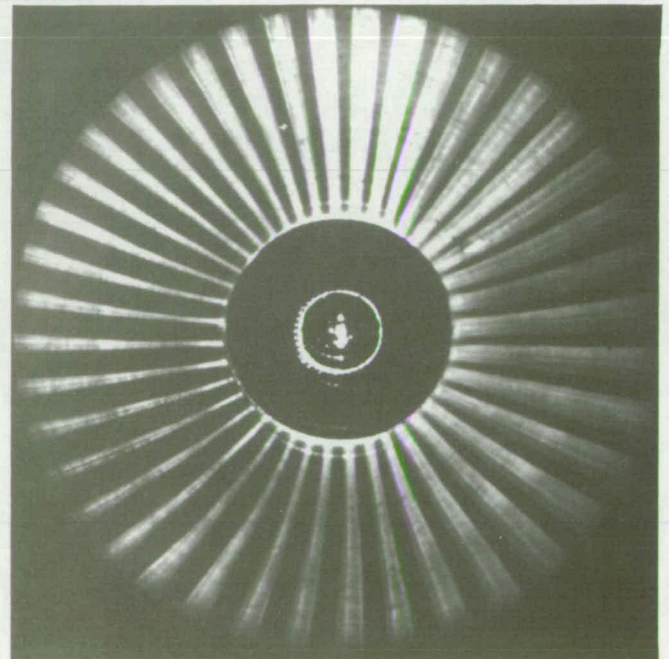
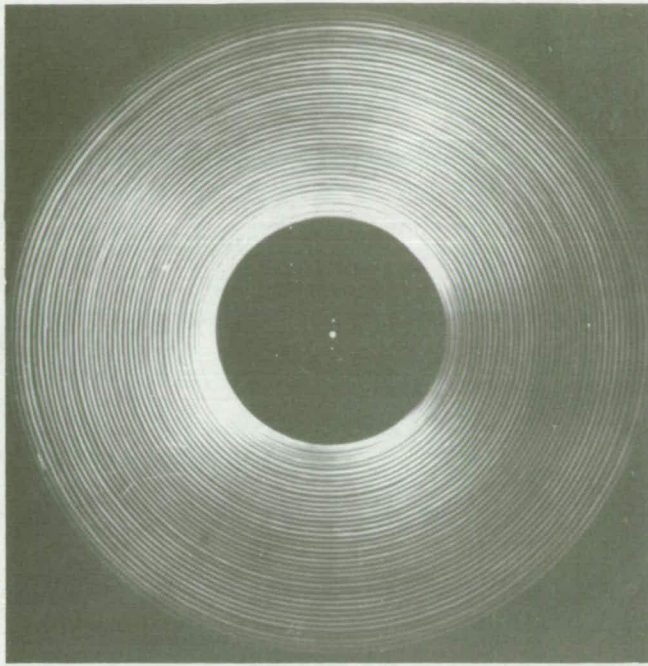


FIGURE 6.11  
GRID PATTERNS FROM BRASS REFERENCE  
CYLINDER

NOTATION

$f_1$	Pitch of lines on grid in tangential direction.
$f_2$	Pitch of lines on grid in axial direction.
$n$	Fringe order.
$R_1$	Radius of illuminated grid.
$R_2$	Internal radius of cylinder.
$R_3$	Internal radius of interference pattern.
$R_4$	External radius of interference pattern.
$R_5$	Radius of conical mirror at small end.
$X_1$	Length of cylinder.
$X_2$	Axial length between point of reflection of a light ray on the cylinder and its intersection with the illuminated grid.
$X_3$	Axial distance between end of cylinder nearest the mirror and the origin of the longest light ray.
$X_4$	Separation of mirror and cylinder.
$X_5$	Separation, end of cylinder to point of reflection on mirror of inner edge of interference pattern.
$X_6$	Separation, end of cylinder to point of reflection on mirror of outer edge of interference pattern.
$\delta_1$	Slope change in cylinder in tangential direction during deformation.
$\delta_2$	Slope change in cylinder in axial direction during deformation.
$\theta$	Cone angle of mirror.

# CHAPTER 7

## TEST RESULTS

## CHAPTER 7

### EXPERIMENTAL EVIDENCE TO SUPPORT THE SPACE FRAME THEORY.

The experimental technique explained in the previous chapter was developed with the Ligtenberg moiré technique in mind. However, it was quickly discovered that the alternative technique of obtaining line movement was a far superior method in this case. The earlier work in this thesis had shown that in considering the buckling of cylindrical shells it would be desirable to detect a defect and observe how that defect changed with load. Thus, some prediction of the buckling load could be made with the knowledge of the defect behaviour. Arbocz and Babcock (ref.21) have previously tried measuring defects. Their technique was to use a scanning capacitance transducer to measure the air gap between the test cylinder and a

generated cylindrical reference surface. They then fitted a Fourier series to the contour map obtained and observed the growth of the Fourier co-efficients with load. Such a technique is rather cumbersome and the fourier series represents the global condition. Since buckling appears to rely on local defects it would be desirable if the measuring system could measure local effects. Perhaps the real shortcoming in their work was that the imaging process they used could have masked the important deformation growth.

The current system appears to offer some advantages over their method. Since we are observing the line shift, a defect will show as a short deviation in the line, either from a circle or a straight radial line. Such a deviation is relatively easy to see and the local size of the defect can be readily measured. Although it is possible to measure slope and hence deflection by observing line movement it appears that for cylinder buckling such measurements are unnecessary. It seems that the width of the defect in particular and perhaps the length are important and these can be measured directly from the photograph with a minimum of effort. Perhaps the greatest difficulty is in selecting which of the defects present is the one controlling the collapse. This can be found by comparing two photographs at different loads and finding where the lines have changed position. The greatest shortcoming of the technique is that for a

particular conical mirror only a very narrow range of cylinder diameters is possible. In this case the cylinder diameter was limited to values around 66 mm.

To deform the cylinder a special loading frame was made. The loading arrangement in this frame is shown in figure 7.1. Axial compression was applied to a crosshead attached to the free end of the cylinder by two stainless steel wire cables and the load in these cables was equalised by a pivoting support bar. Torsion could be introduced by adding another pair of balanced load cables while some bending could be added by shifting the pivot point position on the equalising bar. In hindsight this last provision was probably unwise since it meant that the loading crosshead had to be freely floating. In chapter 2 it was shown that a buckling cylinder would fall over unless it was restrained. Not only did they fall over but it was impossible to straighten them up under load. Thus, the post-buckling investigations were very limited. Parallel moving plattens would have been more satisfactory for this purpose. The test apparatus arranged for axial compression measurements is shown in figure 7.2. As well as measuring the axial load with a strain gauged proving ring and a Bruel and Kjaer bridge (type 1526), the axial displacement was measured by summing the output of two Hewlett Packard differential current displacement transducers. The transducers were located on either side of the crosshead. A load-deformation graph was then

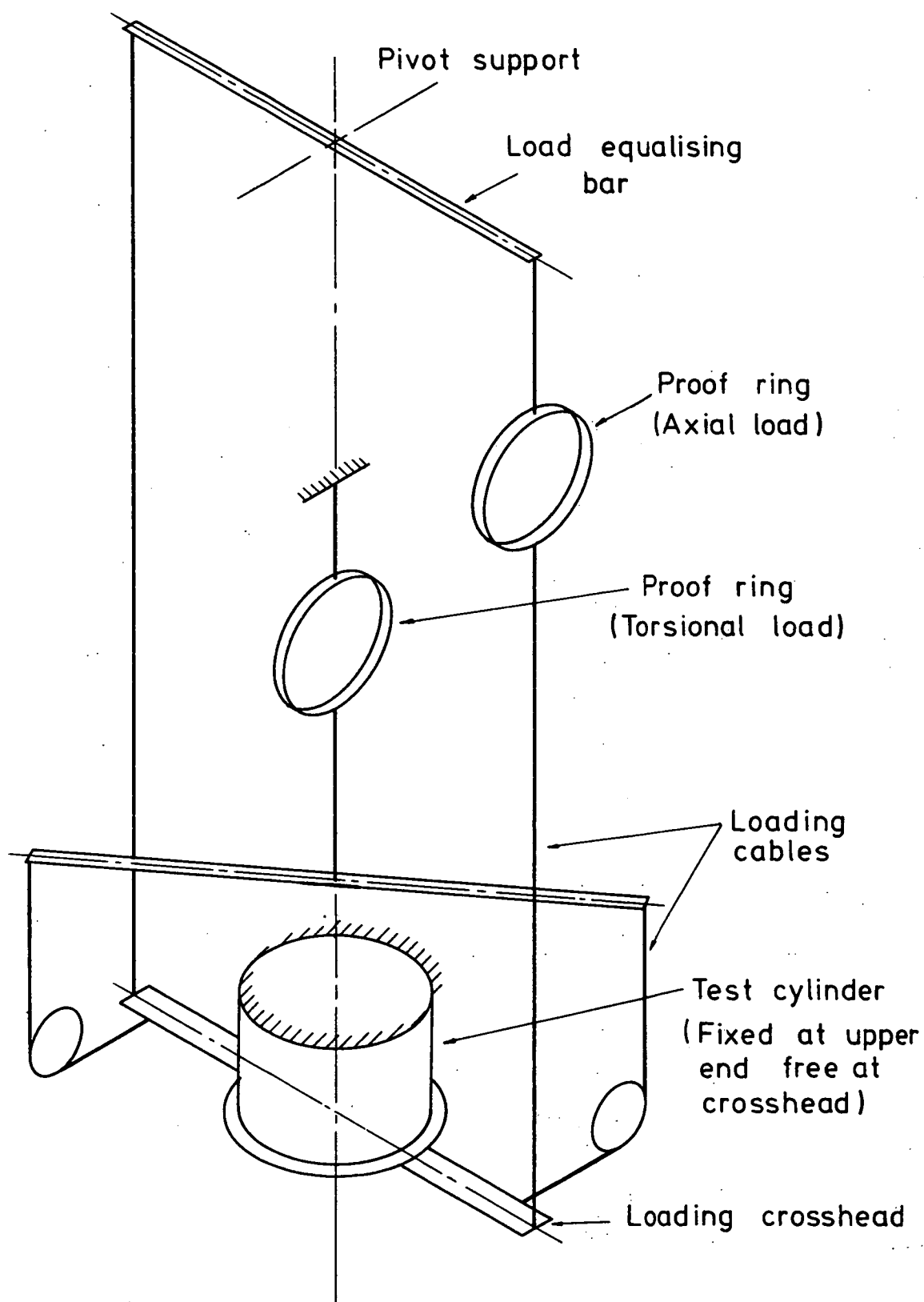


**FIGURE 7.1**  
**LOADING ARRANGEMENT**



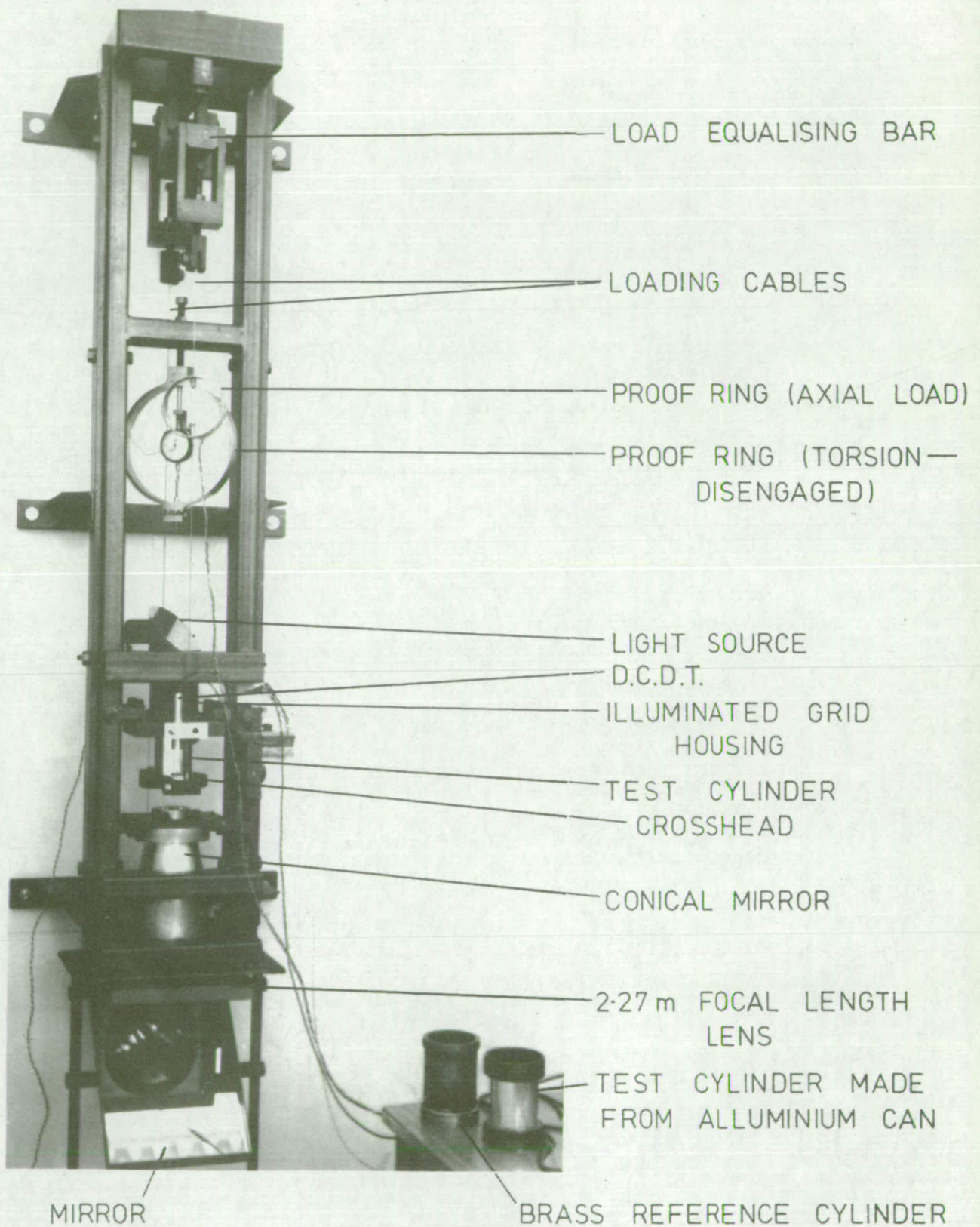


FIGURE 7.2  
TEST APPARATUS ASSEMBLED FOR AXIAL  
COMPRESSION TESTS



drawn on a Hewlett Packard X-Y plotter (type 7004B). Thus it was possible to produce a load-deformation cycle and take photographs of the deformation at several known points around the cycle permitting observation of deformation growth with load.

Since melanex had already been shown to be reloadable it was decided that the test cylinders should be made of this material. Thus a load-deformation graph could be obtained and then the load applied to any desired value which could be determined from an inspection of the form of the graph before taking photographs. The testing procedure was therefore to obtain the load-deformation graph, recycle and take photographs with one grid at the important points and then cycle again with the other grid. Thus there could be minor differences in the deformation pattern between a photograph taken with one grid and that taken with the other but in each case similar conditions of load and deformation were present.

Sometimes one grid showed information that the other did not and vice versa but in a great number of cases (particularly after collapse) they showed the same information and thus provided a check on the measurements. In general, photographs taken with the tangential grid lines (concentric circles) tended to show more information than those with axial grid lines (radial lines). The reason for this was not just due to line

orientation. The cone angle of the mirror was only  $11^{\circ}$  and this made the first grid very sensitive. Also, there were insufficient axial lines on the alternative grid. Because of the shallow cone angle there was a strong tendency for the defects and buckles to cast shadows. It seems that a cone angle of the order of  $20^{\circ}$  would have been superior but this would have imposed a further restriction on cylinder length.

Because only two thicknesses of melanex were available and the cylinder radius was limited to effectively one value only four cylinders were tested, two of each thickness. The details of these cylinders are given in table 7.1. Although only limited variability was available in the cylinders the information found from these tests shows a great deal of the behaviour of buckling cylinders and reinforces the theoretical discussions of earlier chapters.

The load-deformation chart from cylinder no.1 is shown in figure 7.3. In this chart there are two continuous lines indicating two consecutive loading cycles. The repeatability of loading was obviously very good. In fact over all the load cycles taken the greatest variation in collapse loads for any particular load condition was about 9% and usually within about 3%. Obviously, after collapse the X-Y plotter recorded the line shown as "plotter characteristic" but this was only the

TABLE 7.1DETAILS OF CYLINDERS TESTED

Cylinder	R	T	L	R/T	L/R
	mm.	mm.	mm.		
Number 1	33	0.1	67	330	2.03
Number 2	33	0.05	69	660	2.09
Number 3	33	0.1	42	330	1.27
Number 4	33	0.05	40	660	1.21

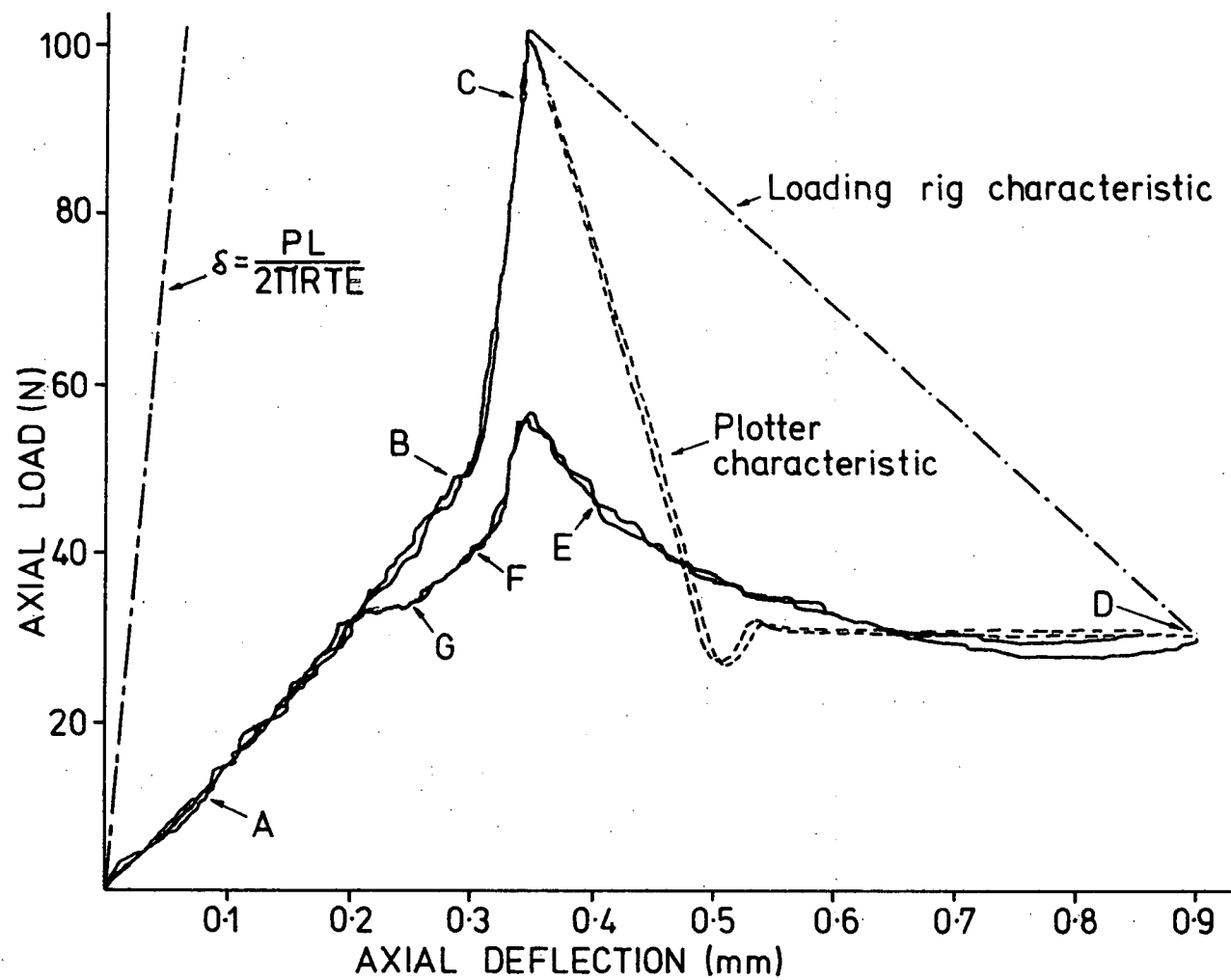
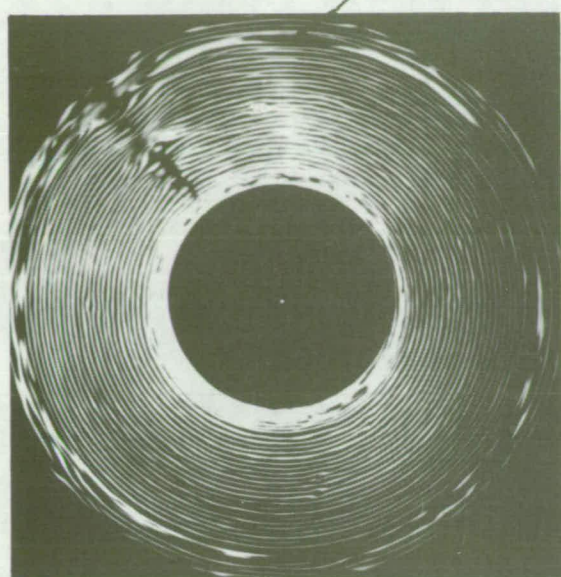


FIGURE 7.3  
LOAD DEFORMATION CHART CYLINDER No 1

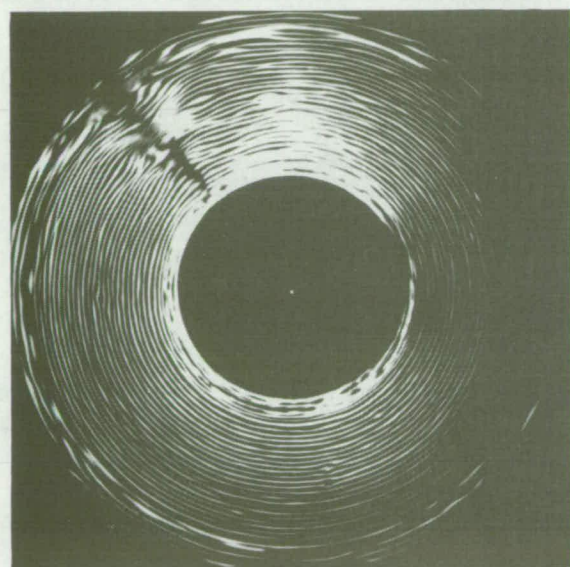
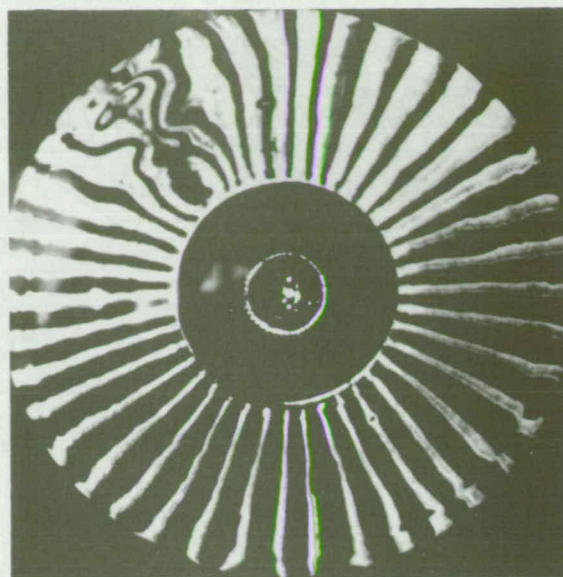
dynamic characteristic of the device. The true characteristic of the loading system is represented by the straight line.

The photographs presented in figure 7.4 are those that were taken at the various positions indicated on the plot. After collapse (position D) the facets of the Yoshimura pattern cover most of the circumference but there is considerable asymmetry, indicating bending of the shell. The photographs at D also show that small facets have formed at both ends of the cylinder of the type described in chapter 2 (left hand side of figure 2.7). The size of each facet was determined by measuring the angle that the facet subtended at the centre of the cylinder. These values are listed in table 7.2 and it is apparent that the facets become larger near the centre of the buckled section. However, two circles can be drawn on the photographs which link the ends of all the facets. Thus the axial length of the buckle pattern was constant regardless of the pattern width and aspect ratio measurements were useless on bent cylinders. This phenomenon was repeated on all cylinders indicating the need for parallel platens in the test rig. In all the test results presented the angles are measured in a clockwise direction on the photograph.

On reducing the axial deformation there was an increase in the load as the facets became smaller (condition E) until there was a sudden snap through where



A



B

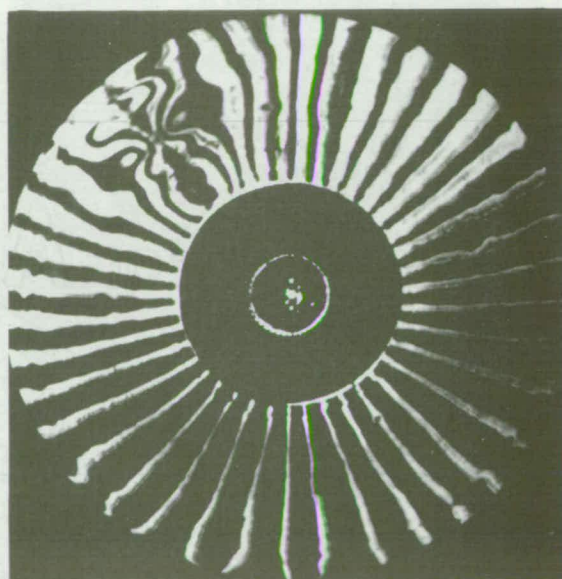
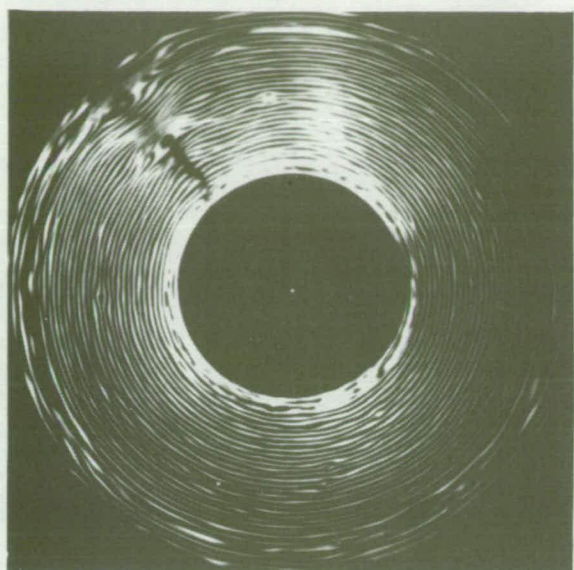
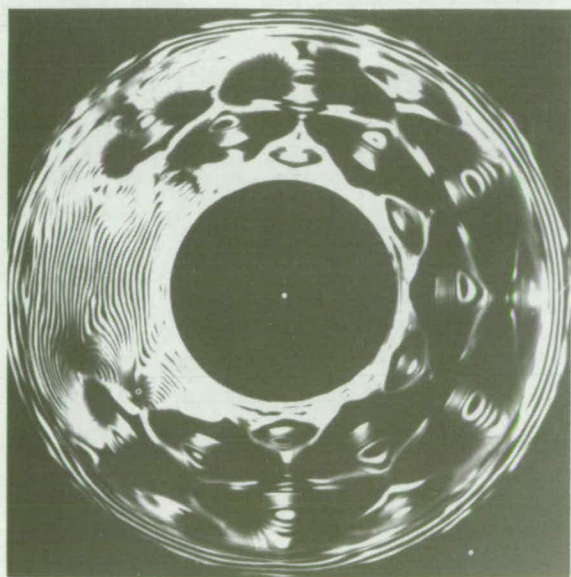
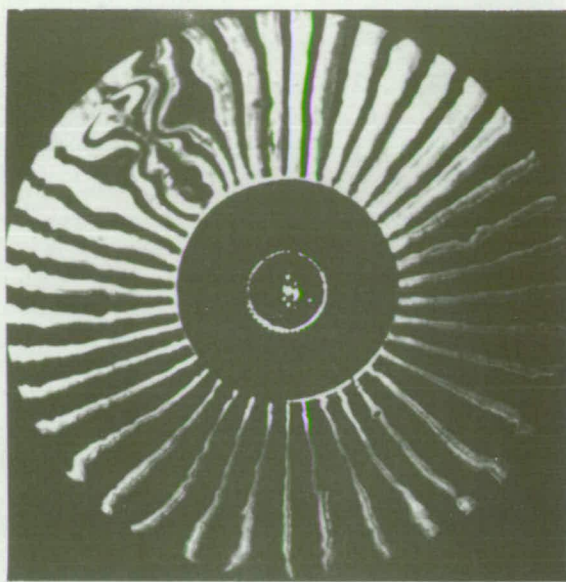


FIGURE 7.4  
GRID PATTERNS FROM CYLINDER No 1





C

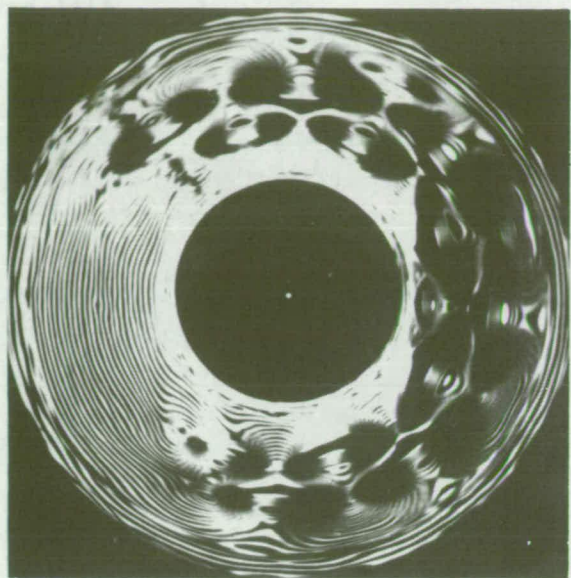


D

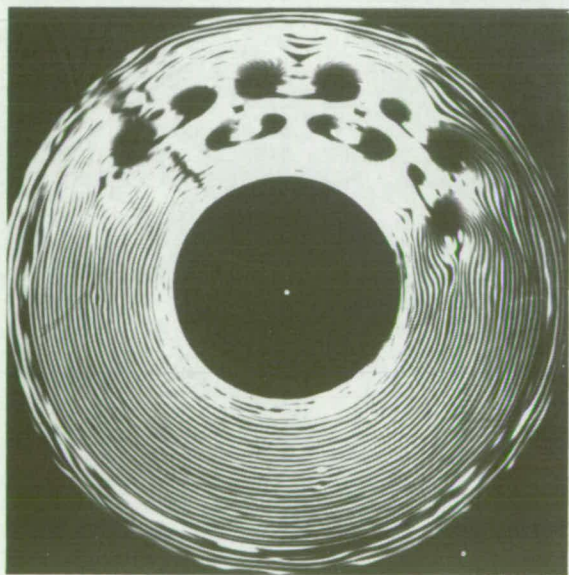


FIGURE 7.4 CONT  
GRID PATTERNS FROM CYLINDER No 1





E

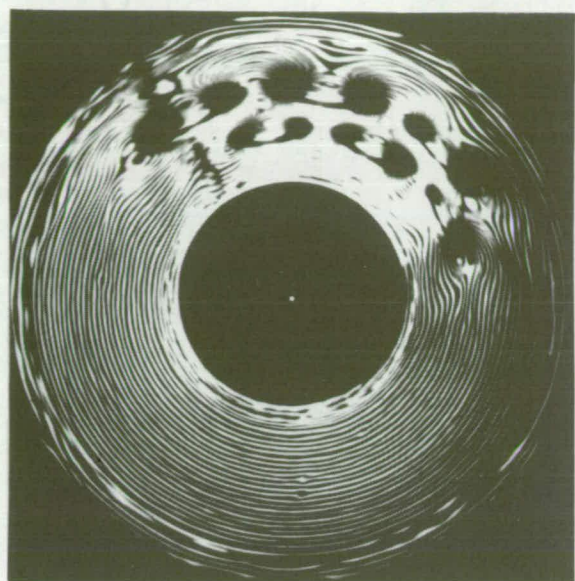


F



FIGURE 7.4 CONT  
GRID PATTERNS FROM CYLINDER No 1





G



FIGURE 7.4 CONT  
GRID PATTERNS FROM CYLINDER No 1

ANGLE SUBTENDED BY DEFECT OR FACET AT CENTRE OF CYLINDERCYLINDER No.1

Defects before collapse;-

Location of Photo.	A		B		C	
Grid Line Direction	Tgtl.	Radl.	Tgtl.	Radl.	Tgtl.	Radl.
Angle at Seam.	28	$32\frac{1}{4}$	29	33	28	33
Angle at Glue Line	35	--	35	--	38	--

Facets after collapse;-

Location of Photo.	D				E			
Grid Line Direction	Tangential		Radial		Tangential		Radial	
	Fixed End	Free End	Fixed End	Free End	Fixed End	Free End	Fixed End	Free End
Angle		$35\frac{1}{2}$	39			38		$38\frac{3}{4}$
	$48\frac{1}{2}$	$50\frac{3}{4}$	$51\frac{3}{4}$	47	$38\frac{3}{4}$	$44\frac{1}{2}$	$39\frac{1}{2}$	$41\frac{1}{2}$
	$54\frac{1}{2}$	59	$58\frac{3}{4}$	$54\frac{1}{2}$	$42\frac{3}{4}$	$46\frac{1}{2}$	$45\frac{1}{2}$	$45\frac{3}{4}$
	$59\frac{1}{4}$	$60\frac{1}{4}$	$62\frac{1}{2}$	$64\frac{1}{4}$	47	$44\frac{1}{2}$	$43\frac{1}{2}$	$46\frac{1}{4}$
	60	$54\frac{1}{2}$	54	$57\frac{1}{4}$	47	$45\frac{1}{2}$	$44\frac{1}{4}$	$41\frac{1}{4}$
	$50\frac{1}{4}$	42	39	$48\frac{1}{2}$	$42\frac{3}{4}$	$39\frac{1}{2}$	38	33
					$35\frac{1}{4}$			

TABLE 7.2 CONT.

ANGLE SUBTENDED BY DEFECT OR FACET AT CENTRE OF CYLINDER

CYLINDER No.1

Location of Photo.	F				G			
Grid Line Direction	Tangential		Radial		Tangential		Radial	
	Fixed End	Free End	Fixed End	Free End	Fixed End	Free End	Fixed End	Free End
Angle	38	38 $\frac{1}{4}$	41 $\frac{1}{2}$	41 $\frac{3}{4}$	37 $\frac{1}{4}$	37 $\frac{3}{4}$	38	37
	36	39	42	42	36	38 $\frac{1}{4}$	32 $\frac{1}{2}$	36
	33 $\frac{1}{4}$	34	40	40 $\frac{1}{4}$	32	34		30 $\frac{3}{4}$
			35	37 $\frac{1}{2}$				

N.B. All angles measured in degrees.

many facets disappeared with a marked decrease in load (conditions F and G). When all the facets had vanished the cylinder behaviour was along the same path as for increasing load.

This increasing load path was particularly interesting for cylinder no.1 in that it was in two sections each of essentially constant stiffness. The slope of the line for the second section was considerably greater than for the first. The reason for this change was that predominately two mechanisms were present in the collapse. In the lower load section the deformation appeared to be controlled by the seam while in the upper section it was controlled by the defect marked in figure 7.4. The defect was adjacent to the end of the test section of the cylinder i.e. the line where the cylinder was bonded to the end stiffening rings. Photographs A and B show that the seam defect changes substantially in this region but only slightly between B and C. There is considerable growth of the other defect over the entire loading portion. The size of the seam defect was measured at two quite different values for the two grid orientations. The reason for this difference was probably that the defect was not distinct enough with the axial grid lines. Thus the values read from the photographs with circumferential grid lines were more reliable in this case. The controlling defect appeared to grow in width between B and C while the seam defect remained constant in width.

Further evidence in support of the speculation that two distinct defects controlled the collapse is presented in figures 7.5 and 7.6. For figure 7.5 the cylinder was into the test rig so that slight changes in loading geometry occurred. The overall result was that there was a small increase in the collapse load of the cylinder. The variation between collapse loads for the two cycles shown of 10N (9%) was the maximum encountered for any of the cylinders but even this variation must be considered as adequate for buckling cylinders. More importantly, at the junction between the two sections of the loading sections of the curve there was a small dip. This dip was associated with the formation of the small buckle illustrated in figure 7.6 which was located on the seam at the position of the previously observed defect. Thus the stiffness of the cylinder in the lower load portion of the curve can be attributed to this defect.

Immediately after the small buckle appeared there was a marked stiffening of the cylinder for a short time and then a decrease in stiffness once the original load curve of figure 7.3 had been reached. At that point the small buckle disappeared again and the loading was no longer under the control of the defect at the seam. Incidentally, the stiffness in the higher load section was essentially that provided by considering a perfect cylinder and material properties only. In chapter 4 computational evidence was shown for just such a stiffening

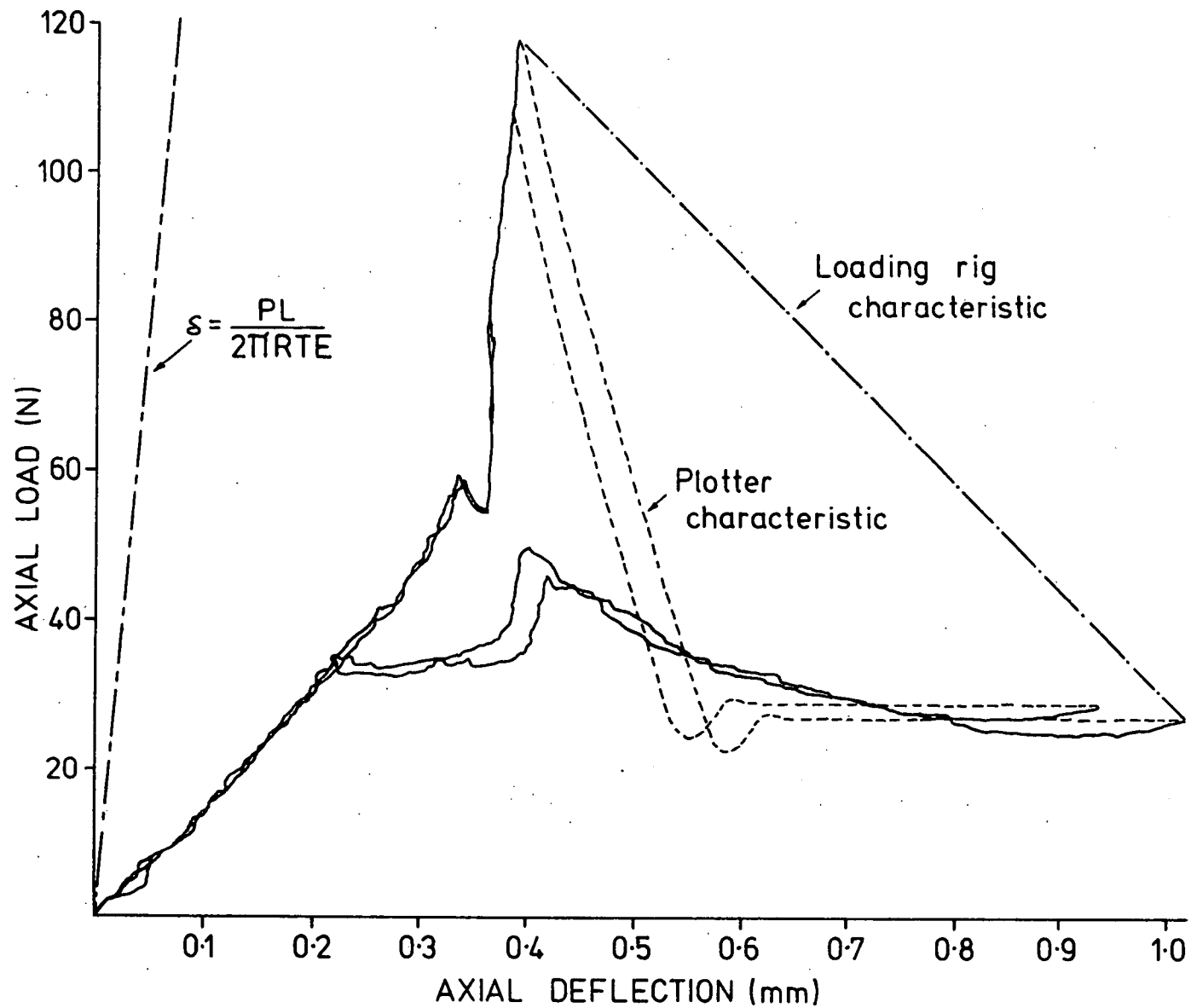


**FIGURE 7.5**  
**LOAD-DEFORMATION CHART - CYLINDER No 1 - RELOCATED**



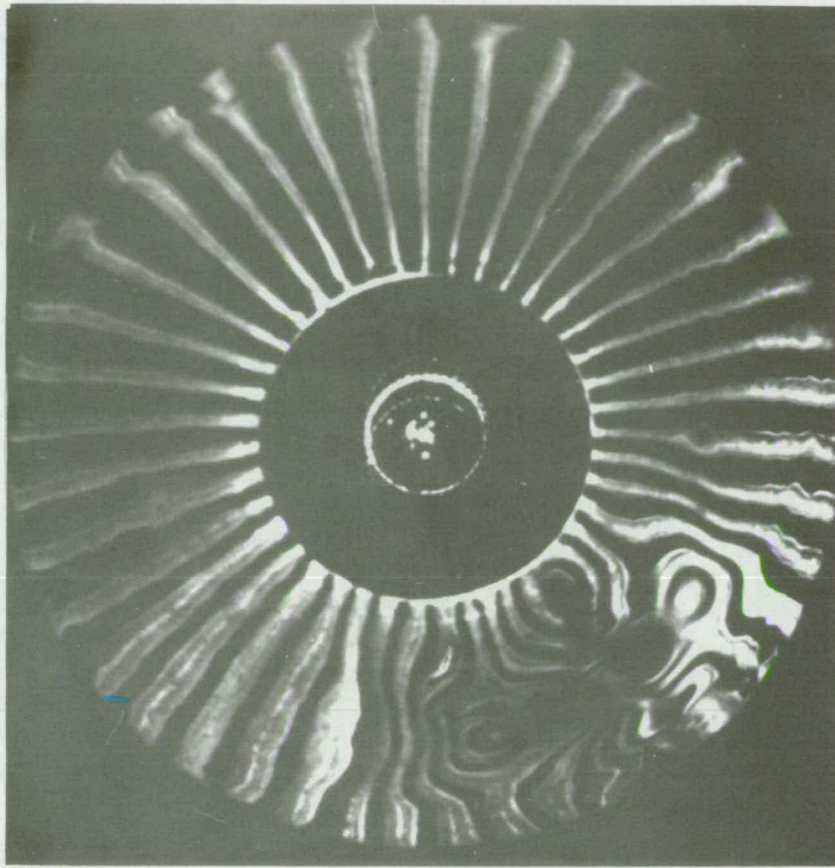


FIGURE 7-6  
DIMPLE FORMED WITH INCREASING LOAD

using the modified Timoshenko and Woinowsky-Krieger equations. This experimental result provides further support for the need to include the curvature terms in the membrane equations.

The collapse load in this cylinder was measured at 101.4N (figure 7.3). Now, in referring to the design chart based on the space frame theory (figure 5.10), a corresponding space frame with 9 lobes would buckle at this load. It is extremely encouraging to observe that the angle the defect at the seam made at the centre just before collapse was measured at  $38^\circ$  or  $\frac{1}{9.5}$  of the circumference. The accuracy of interpretation of the photograph could make this measurement vary between about  $36^\circ$  and  $40^\circ$ . Thus if one accepts the space frame theory as a reasonable explanation of the buckling behaviour of cylinders then it can be said that the defect at the glue line is the one that initiated the collapse of this cylinder.

In installing cylinder no.2 into the test apparatus it was severely damaged so that quite a lot of permanent damage was sustained. Normally, in a testing programme such a test specimen would be thrown away and ignored. However, in this case it provided an excellent opportunity to use the experimental technique to illustrate the manner in which the buckles can grow out of large initial defects. Only one load-deformation curve is plotted in figure 7.7. The reason for providing only one



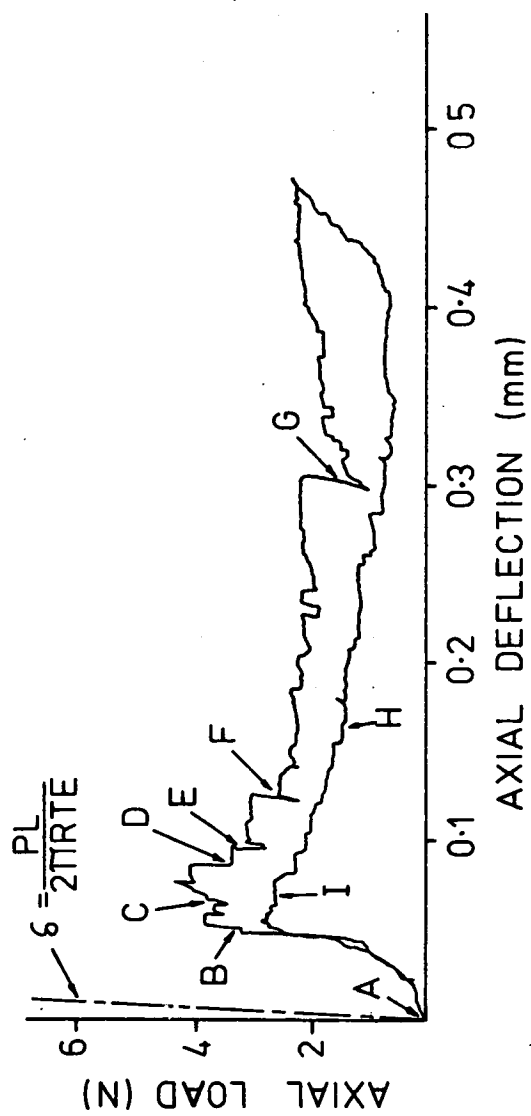


FIGURE 7.7

LOAD DEFORMATION CHART - CYLINDER No 2

curve is for clarity. In fact, there was very little difference again between all the load cycles taken. In this cylinder the photographs (figure 7.8) showed that there were several defects of substantial size which contributed to the collapse mechanism. The size of each of these defects is listed in table 7.3 to illustrate their growth as well as measurements of the angles of facets once the buckle pattern had become established.

Between A and B defect no.1 appeared to control the collapse of the cylinder. In this region this particular defect had almost doubled in size while the others had grown to a much lesser extent. This was in line with the behaviour described in chapter 2 where facets held in one position would snap through to form facets twice the size. Between B and C the defect on the seam has collapsed and in doing so has dragged defect no.3 around the circumference to join it. However, seeing that defect no.3 was effectively anchored at one end due to the initial deformation it has become a much larger facet at C. Between C and D defect no.2 has been pulled around anticlockwise on the photograph to relieve the excessive tension that must have been built up in defect no.3. However the collapse in this region was really due to defect no.4. It was difficult to suggest which defect in the earlier photographs had contributed to the formation of this defect. It could have been any one of several. Between defect no.4 and defect no.2 there was a maze of small uninterpretable defects, one of which was probably the remains of defect no.1.

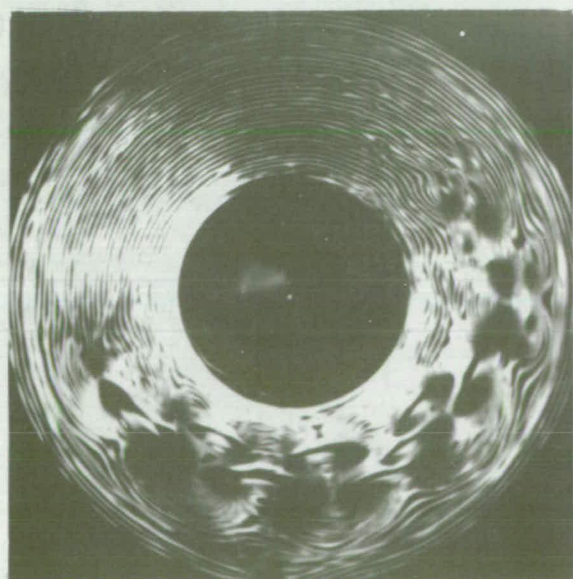
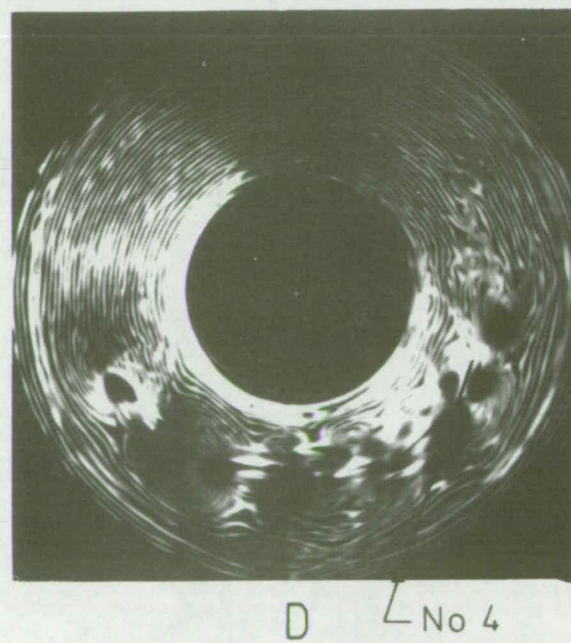
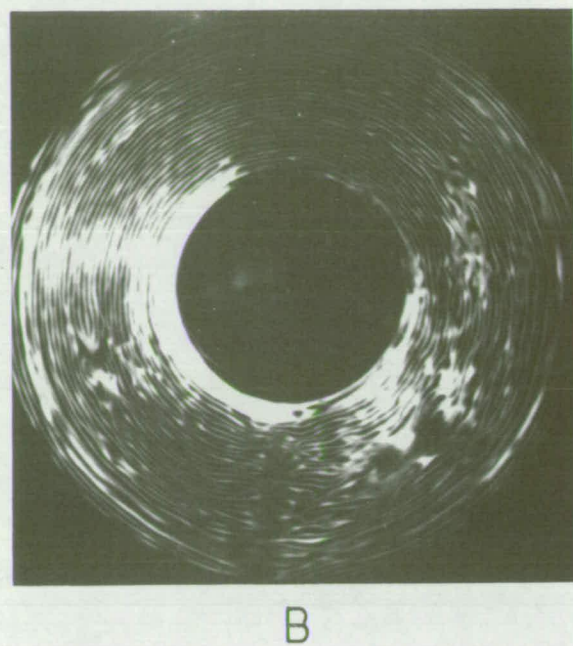
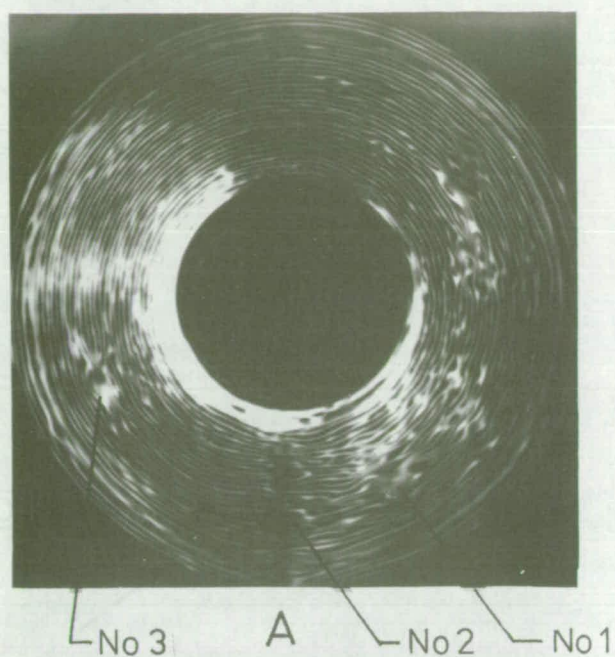
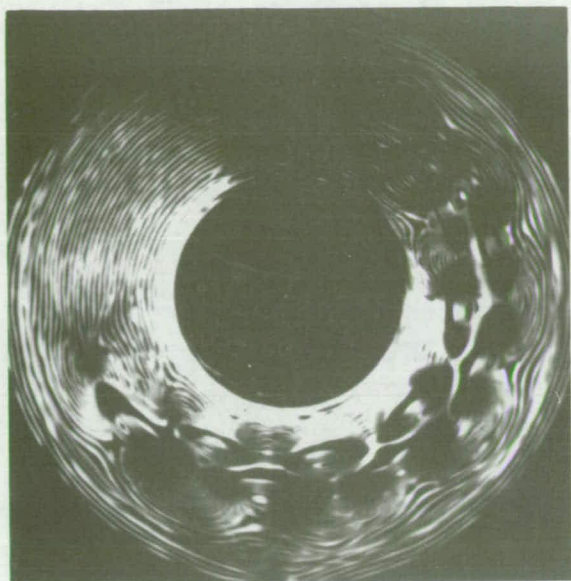
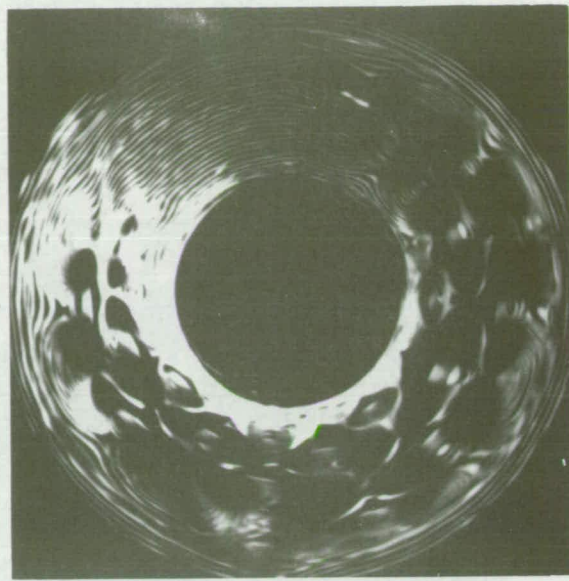


FIGURE 7.8  
GRID PATTERNS FROM  
CYLINDER No 2

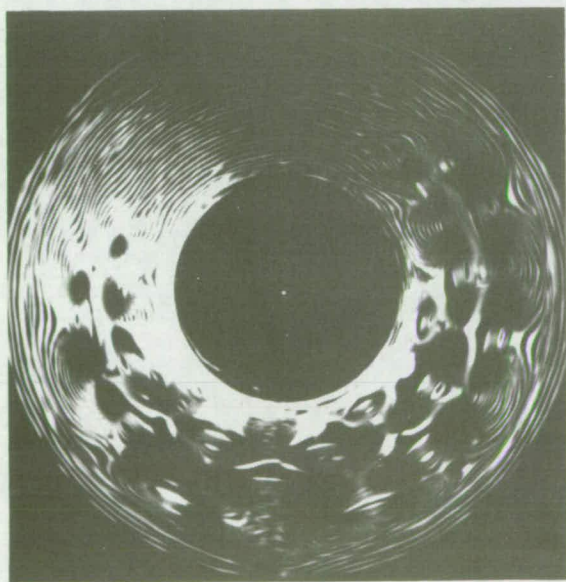




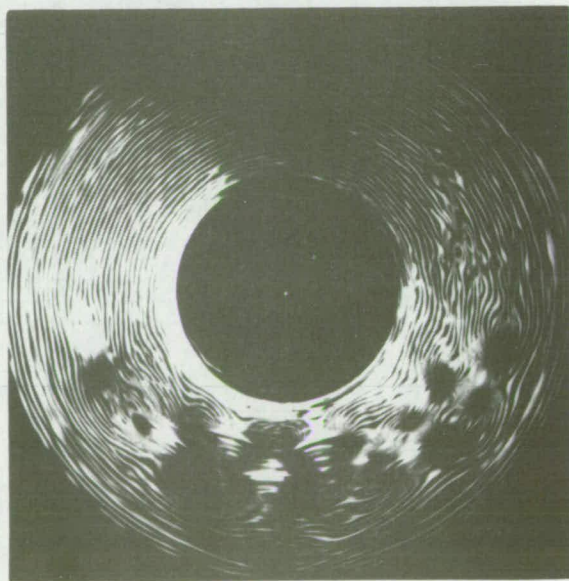
F



G



H



I

FIGURE 7-8 CONT  
GRID PATTERNS FROM CYLINDER No 2

TABLE 7.3ANGLE SUBTENDED BY DEFECT OR FACET AT CENTRE OF CYLINDERCYLINDER No.2

Defects before collapse;-

Location of Photo.	A	B	C	D
Defect No.1	17	$32\frac{1}{4}$	41	--
Defect No.2	16	$24\frac{1}{4}$	$39\frac{1}{2}$	$39\frac{3}{4}$
Defect No.3	18	$24\frac{1}{2}$	42	37
Defect No.4	--	--	--	$32\frac{1}{2}$

Facets after collapse;-

Location of Photo.	E			F			G			H	
	Fixed End	Free End		Fixed End	Free End		Fixed End	Free End		Fixed End	Free End
Angle	13	28	19	$29\frac{3}{4}$	26		$29\frac{1}{4}$	$25\frac{1}{4}$		$27\frac{1}{4}$	33
		35		35	32		42	$38\frac{1}{2}$		$35\frac{1}{4}$	$33\frac{1}{2}$
	$35\frac{1}{4}$			$38\frac{1}{2}$	36		49	$38\frac{1}{4}$		42	40
	$27\frac{1}{2}$	$35\frac{3}{4}$		39			46			$40\frac{1}{2}$	$46\frac{1}{2}$
	$38\frac{3}{4}$	$39\frac{1}{2}$		$37\frac{1}{4}$	$40\frac{3}{4}$		43	52		38	$39\frac{1}{2}$
	34			$34\frac{1}{2}$	39		44	$37\frac{1}{2}$		$38\frac{1}{2}$	
		39					$42\frac{1}{2}$				35
							$37\frac{3}{4}$			32	
							29				

N.B. All angles measured in degrees.

At D there were, therefore two separate collapsing sections of the cylinder and this was reflected in the photograph at E. Here, the two sections were joined together with facets to form a buckle pattern that was approaching the regular form. Linking the two sections was a small defect which appeared to form an additional tier on the buckle pattern. Also, adjacent to the position of defect no.2 there was an additional smaller dimple wedged in between the two main rows of dimples. This was really the remains of the unintelligible section of the photograph at D and soon vanished.

A regular buckle pattern was not reached until condition F was achieved. However, even at this point the facets did not show the same regularity in increasing and decreasing size around the photograph that occurred with cylinder no.1. At position G, the additional collapse was due to extra facets forming in the buckle pattern as well as the introduction of small facets wedged into the end of the pattern adjacent to the ends of the cylinder. The unloading behaviour was similar to that of cylinder no.1.

A different type of behaviour was observed with cylinder no.3 (figures 7.9 and 7.10 with table 7.4). In this cylinder the collapse was controlled by a defect on the seam of the cylinder but it did not form into the regular Yoshimura pattern. Instead it buckled into the shape Esslinger and Geier called the "one tier" pattern (see figure 2.10). Here it appeared that the seam was

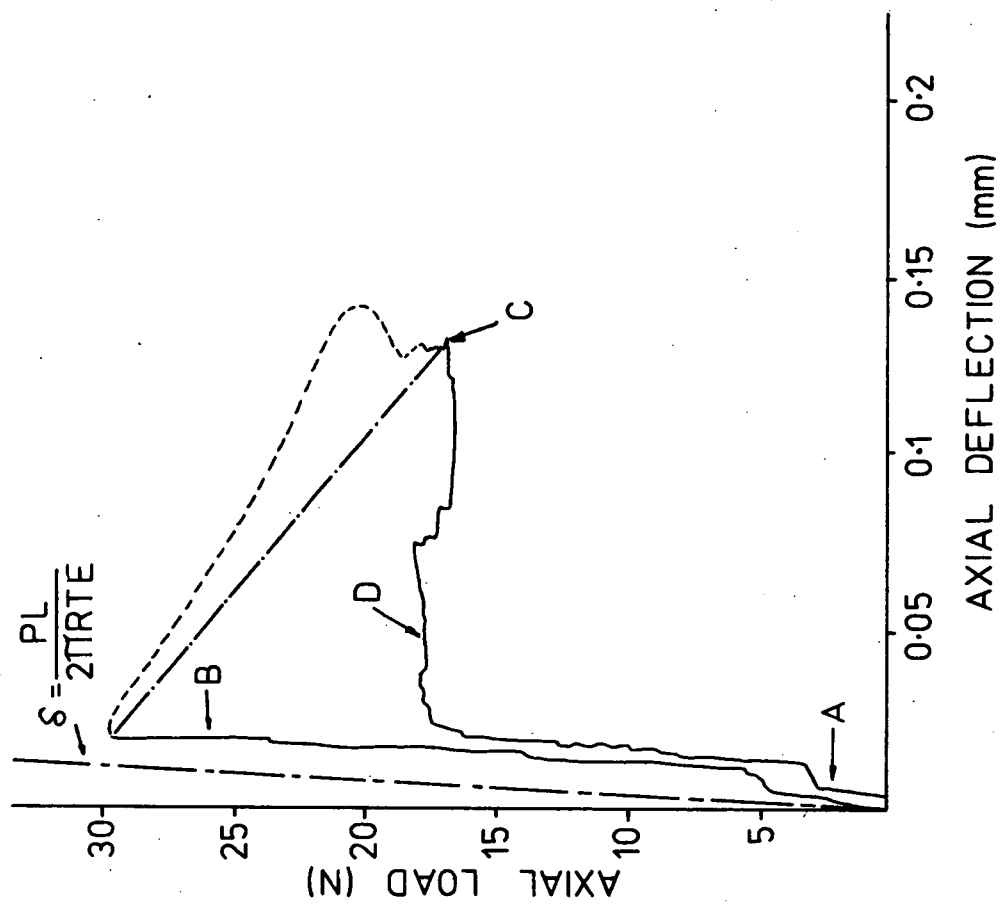
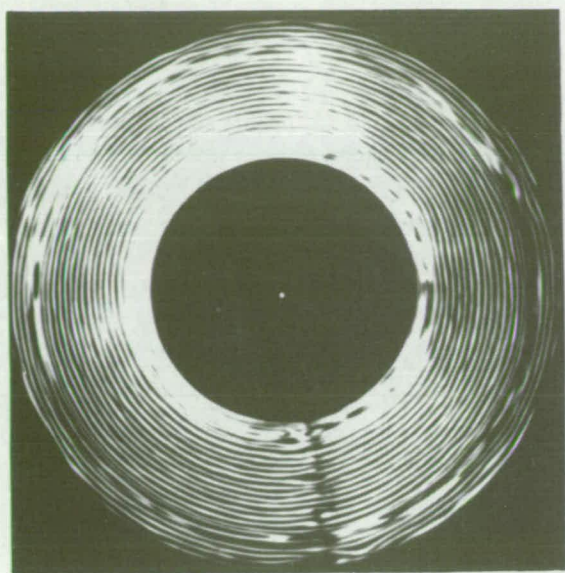


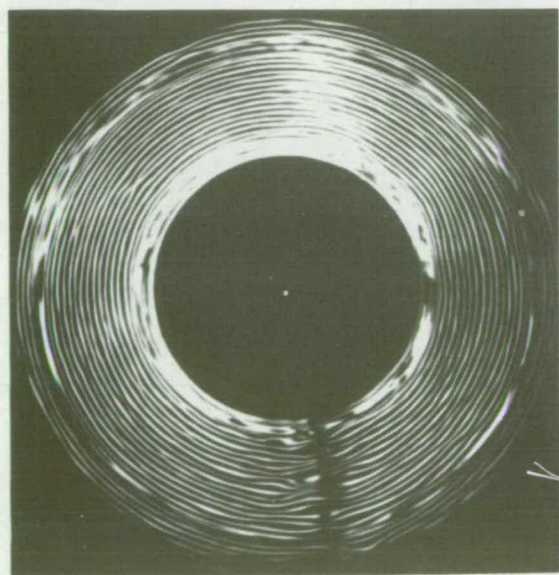
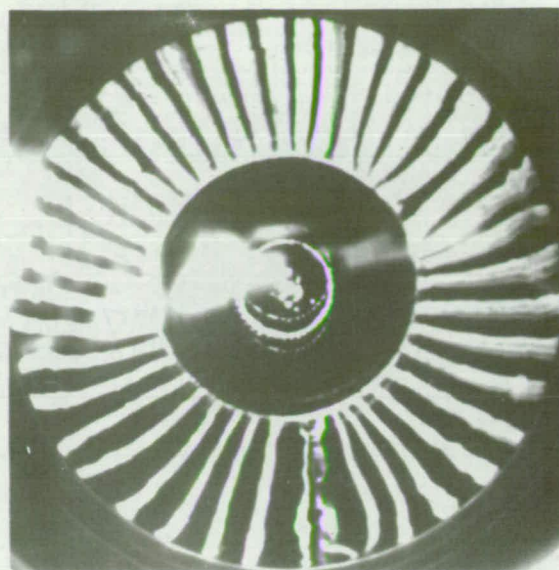
FIGURE 7.9

LOAD DEFORMATION CHART - CYLINDER No 3





A



B

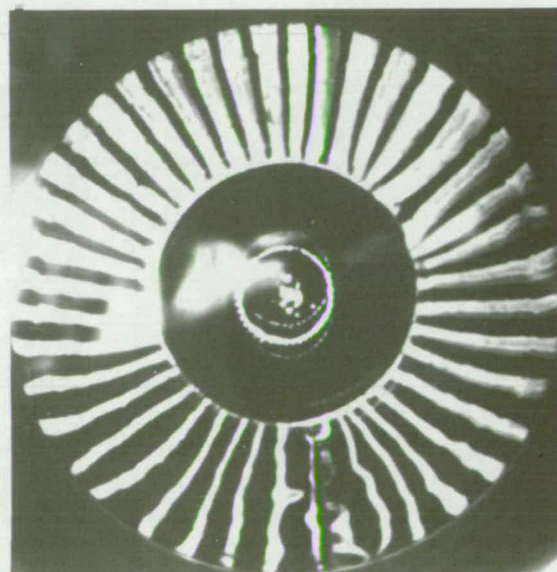
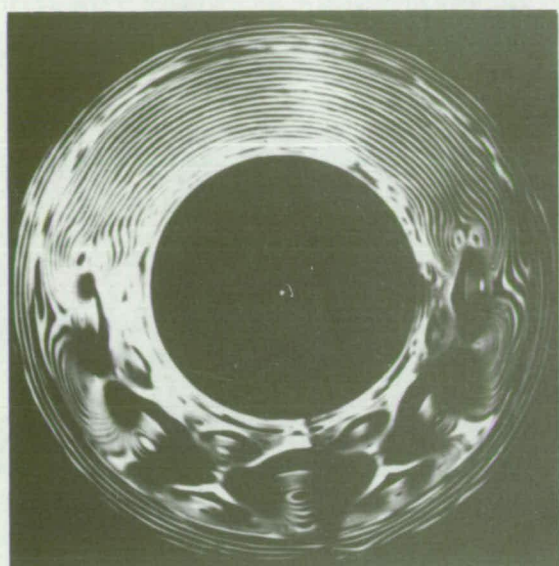
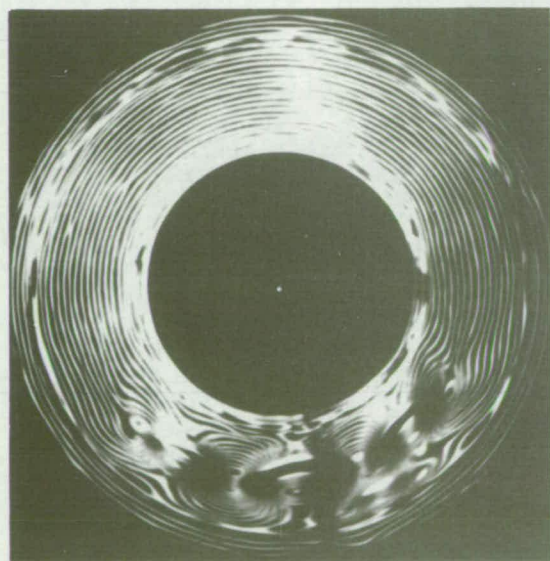


FIGURE 7-10  
GRID PATTERNS FROM CYLINDER No 3





C



D



FIGURE 7.10 CONT  
GRID PATTERNS FROM CYLINDER No 3

TABLE 7.4ANGLE SUBTENDED BY DEFECT OR FACET AT CENTRE OF CYLINDERCYLINDER No.3

Defect before collapse;-

Location of Photo.	A		B	
Grid Line Direction	Tgtl.	Radl.	Tgtl.	Radl.
Angle	16	--	22	--

Facets after collapse;-

Location of Photo.	C		D	
Grid Line Direction	Tgtl.	Radl.	Tgtl.	Radl.
Angle	31½ 45 48¼ 45 35¼	32½ 44½ 51 44½ 36	33½ 38½ 33	34½ 40 32

N.B. All angles measured in degrees.

behaving as a column almost independently of the remainder of the cylinder and once the seam had collapsed sufficiently it then promoted the collapse of the adjacent portion of the cylinder. This defect growth can be clearly seen in the photographs taken at A and B. The photographs taken at C and D show the regular "one tier" pattern at the centre of the cylinder and symmetry about the defect at the seam. This symmetry was not present in cylinder no.1. The reason for its absence in that case was that the seam effectively stopped the buckle progressing around the cylinder. Thus in cylinder no.1 the buckle pattern started at the seam. These few results show the importance of the seam in the buckling characteristics. Although useful results have been obtained at this point it is imperative that for future tests seamless cylinders are manufactured. Practical cylindrical shells would no doubt have seams and also very likely have stiffeners. Although the ultimate aim must be to understand the behaviour with both constraints, it is useless to contemplate such behaviour without first having a knowledge of basic cylinder behaviour through seamless, well made cylinders.

The behaviour of cylinder no.4 (figures 7.11 and 7.12 with table 7.5) was very similar in nature to cylinder no.1. There were again two sections of the loading curve, probably corresponding to the behaviour of the seam defect and the controlling defect marked. However, there was no appreciable difference in the size of the defect near the seam measured from the photographs taken at A and B but

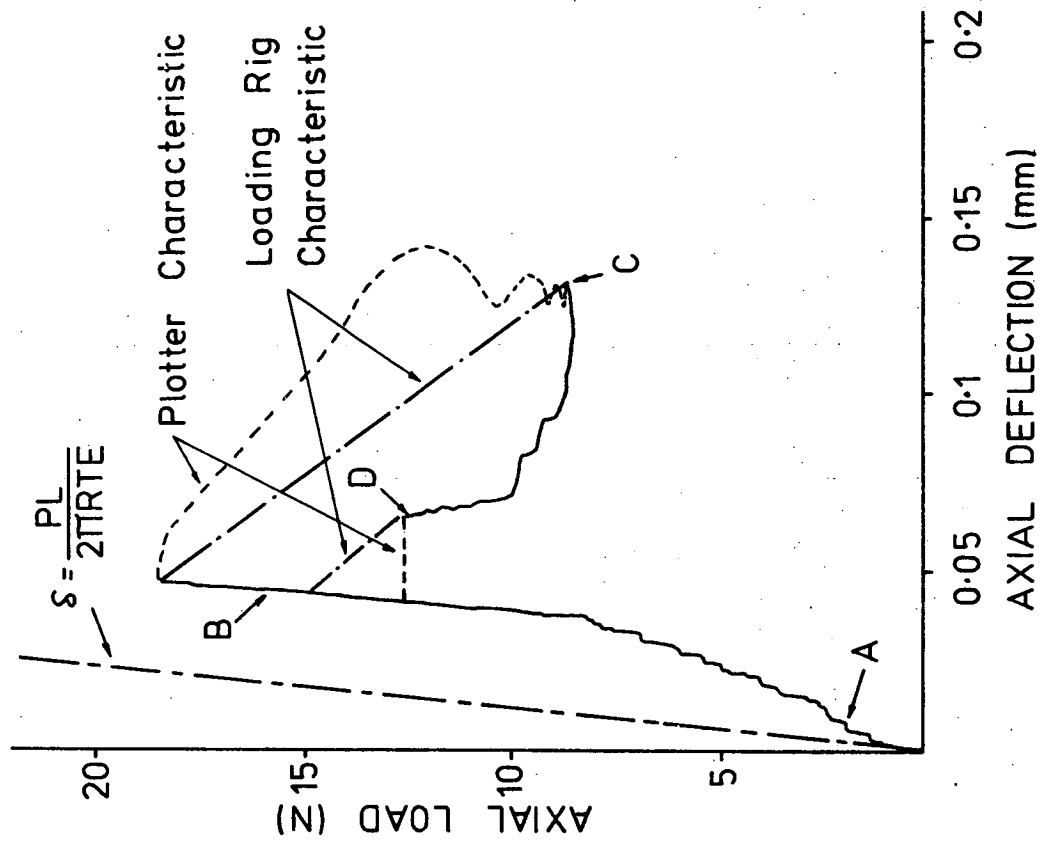
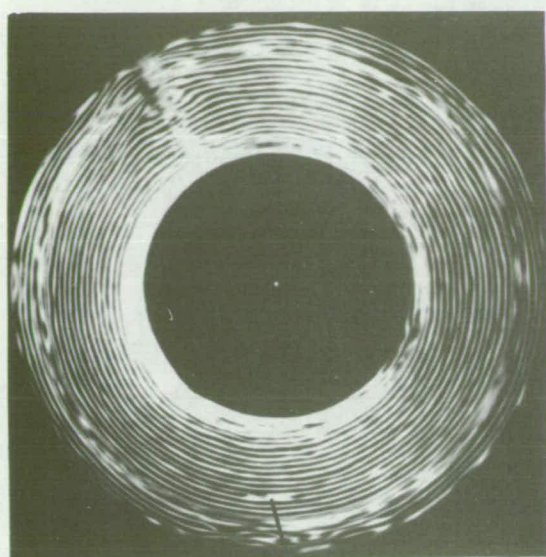


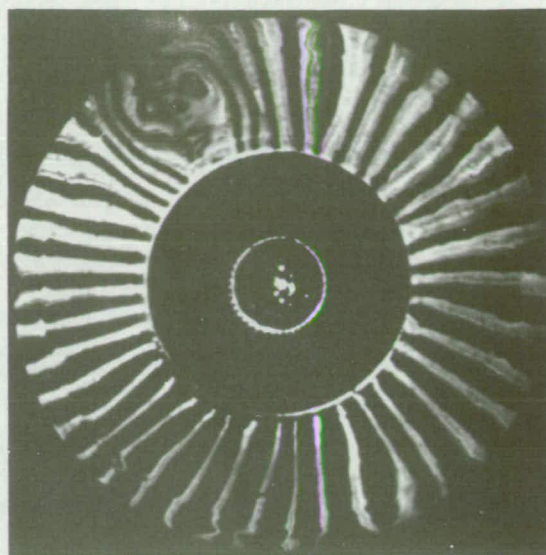
FIGURE 7.11

LOAD DEFORMATION CHART CYLINDER No 4

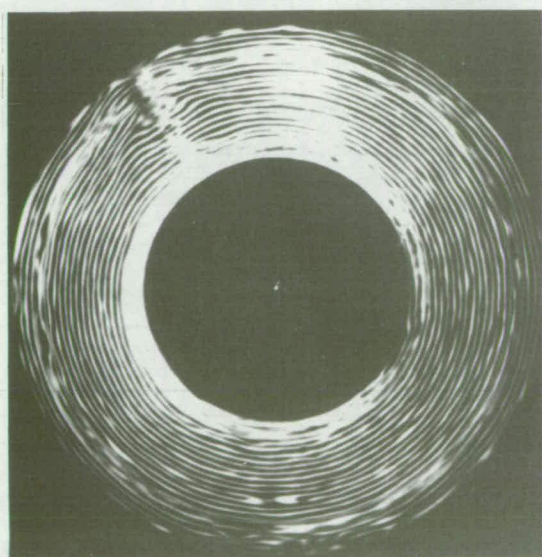




A



CONTROLLING DEFECT



B

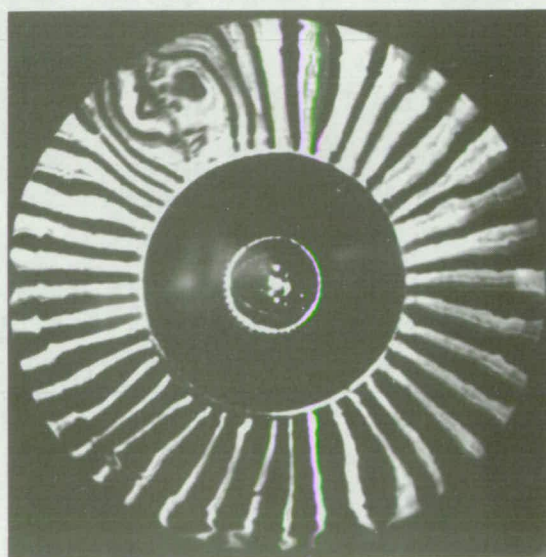
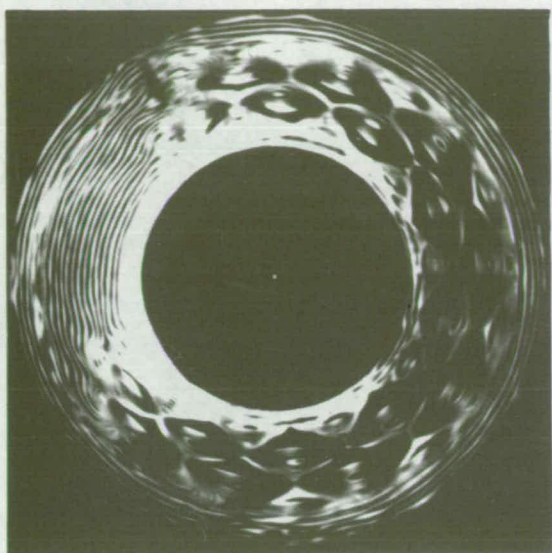
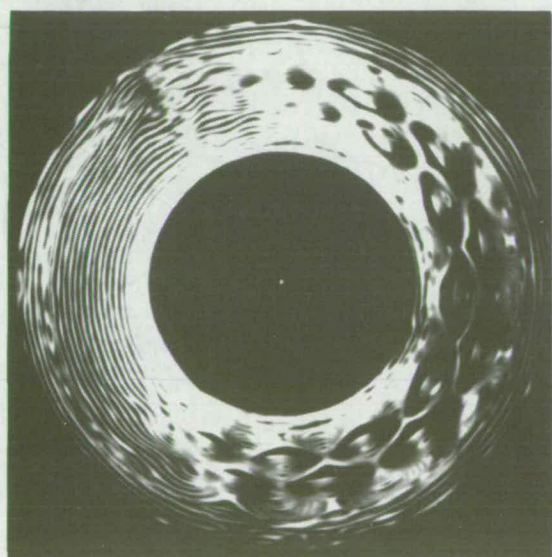
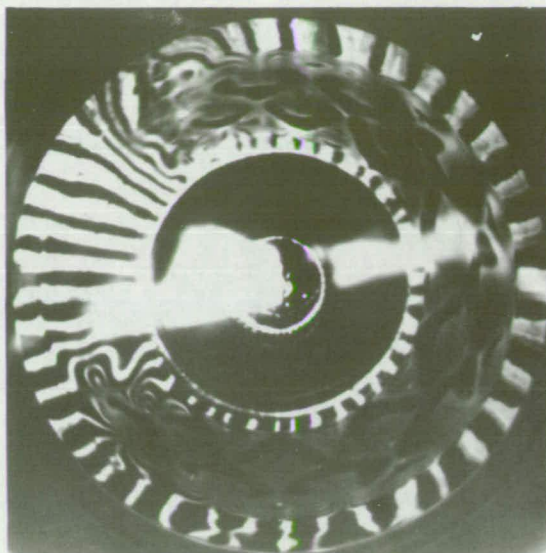


FIGURE 7.12  
GRID PATTERNS FROM CYLINDER No 4





C



D

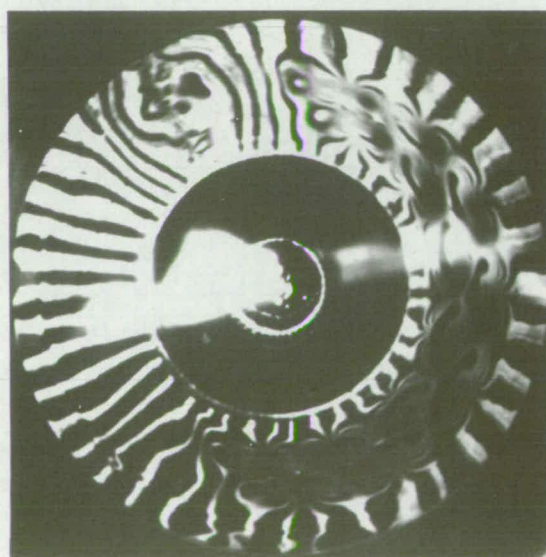


FIGURE 7-12 CONT  
GRID PATTERNS FROM CYLINDER No 4

ANGLE SUBTENDED BY DEFECT OR FACET AT CENTRE OF CYLINDERCYLINDER No.4

Defects before collapse;-

Location of Photo.	A		B	
Grid Line Direction	Tgtl.	Radl.	Tgtl.	Radl.
Angle at Seam.	$18\frac{1}{2}$	--	$19\frac{3}{4}$	--
Angle at Defect.	13	--	$14\frac{3}{4}$	--

Facets after collapse;-

Location of Photo.	C				D			
Grid Line Direction	Tangential		Radial		Tangential		Radial	
	Fixed End	Free End	Fixed End	Free End	Fixed End	Free End	Fixed End	Free End
Angle		28	$23\frac{3}{4}$			25		$13\frac{1}{4}$
	$31\frac{1}{4}$	$30\frac{1}{2}$	30	$29\frac{3}{4}$	$23\frac{3}{4}$	27	17	$22\frac{1}{2}$
	$32\frac{1}{2}$	34	$33\frac{1}{2}$	$31\frac{1}{2}$	$28\frac{1}{4}$	$27\frac{1}{2}$	$25\frac{1}{4}$	25
	34	$34\frac{1}{4}$	$35\frac{3}{4}$	$33\frac{1}{4}$	$28\frac{3}{4}$	$29\frac{1}{2}$	$26\frac{1}{4}$	$25\frac{3}{4}$
	36	$35\frac{1}{4}$	$35\frac{1}{4}$	$34\frac{3}{4}$	$30\frac{3}{4}$	$27\frac{1}{2}$	$26\frac{1}{4}$	$27\frac{1}{2}$
	35	$34\frac{1}{4}$	$34\frac{3}{4}$	$36\frac{3}{4}$	$28\frac{1}{2}$	$29\frac{1}{2}$	$27\frac{3}{4}$	$26\frac{1}{2}$
	33	32	$33\frac{3}{4}$	34	$27\frac{1}{4}$	$27\frac{1}{2}$	$23\frac{3}{4}$	$21\frac{1}{2}$
	29	$27\frac{3}{4}$	28	$31\frac{1}{4}$	$26\frac{1}{2}$	20 $\frac{1}{4}$	21	
	$24\frac{3}{4}$			26	23			

N.B. All angles measured in degrees.

the other defect had changed appreciably. Just before collapse this defect subtended an angle at the centre of the cylinder of  $14\frac{3}{4}^{\circ}$  or  $\frac{1}{24.4}$  of the circumference. Using the information of the design chart (figure 5.10) the collapse load of 18.8N would indicate that the cylinder had collapsed due to a Yoshimura pattern with 23 lobes. This further reinforces the validity of the space frame approach to the buckling problem.

At collapse this cylinder again seemed to be controlled to some extent by the seam. The buckle pattern at C stops at the seam. On unloading this particular cylinder there were several small jumps to D which involved mostly the small end facets snapping out of the cylinder. After D there was a substantial snap through where all the remaining facets suddenly disappeared and the cylinder took up a condition on the loading line at a substantially greater load.



# CHAPTER 8

# CONCLUSIONS

## CHAPTER 8

### CONCLUSIONS

Any new theory like the one presented in this thesis requires a great deal of work being performed on it before it can be accepted in its entirety. The magnitude of such work is beyond the scope of one Doctoral thesis. The results presented here, however, show a remarkable agreement with known behaviour. Perhaps the most important way in which the verification can be achieved is through experimental observation. In this regard the technique described in chapter 6 and used in chapter 7 has many advantages. Before such experiments can be conducted it is imperative that the loading device have parallelly moving plattens and that the cylinders are seamless. This author is aware that two techniques are

available for making seamless cylinders but is unfamiliar with the constructional details. Arbocz and Babcock (ref.21) used electroformed cylinders while Tennyson (ref.22) spun cast epoxy. It is this author's intention in the near future to develop a facility to make seamless cylinders. The combination of seamless cylinders and the modifications for parallel platens represents quite a substantial project in its own right.

Another substantial project that should be investigated is the establishment of the aspect ratio of the buckle pattern. Estimating the aspect ratio appears to need a better understanding of the effective width of the members. It seems unlikely that the effective width will remain constant for all buckle patterns on a particular cylinder. Although no definite procedure can be suggested for finding these values it seems likely that the approach will be through determining the stress distribution in an isosceles triangular plate loaded in tension along the two equal length sides and with compression at right angles.

Yet another project that could be suggested from this work is that a vonKarman and Tsien type analysis could be conducted with the revised equations developed in chapter 4. Such an analysis may overcome the zero load problem encountered by Hoff, Madsen and Mayers. However, this author thinks that, while such an analysis may overcome

an existing problem, it seems doubtful that the outcome would be of much practical importance.

The real value in establishing the aspect ratio and effective width more adequately is that the theory could then be expanded to embrace axial compression loading combined with some hoop compression (or tension) and/or torsion. Hoop compression has the effect of lengthening the facets and apparently it is this change in facet length that reduces the load carrying capacity. Similarly, internal pressure appears to increase the load carrying capacity substantially by making the facets shorter. Adding torsion to the axial compression has the effect of distorting the facets (figures 8.1 and 8.2). The base of the facet seems to take on an inclination corresponding to the maximum principal stress direction while the width and height remain unaltered. The ratio  $A/B$  from figure 8.1 is 0.87 which is within the range of values obtained for the similar cylinder in axial compression ( $R/T=445$ ) in figure 5.9.

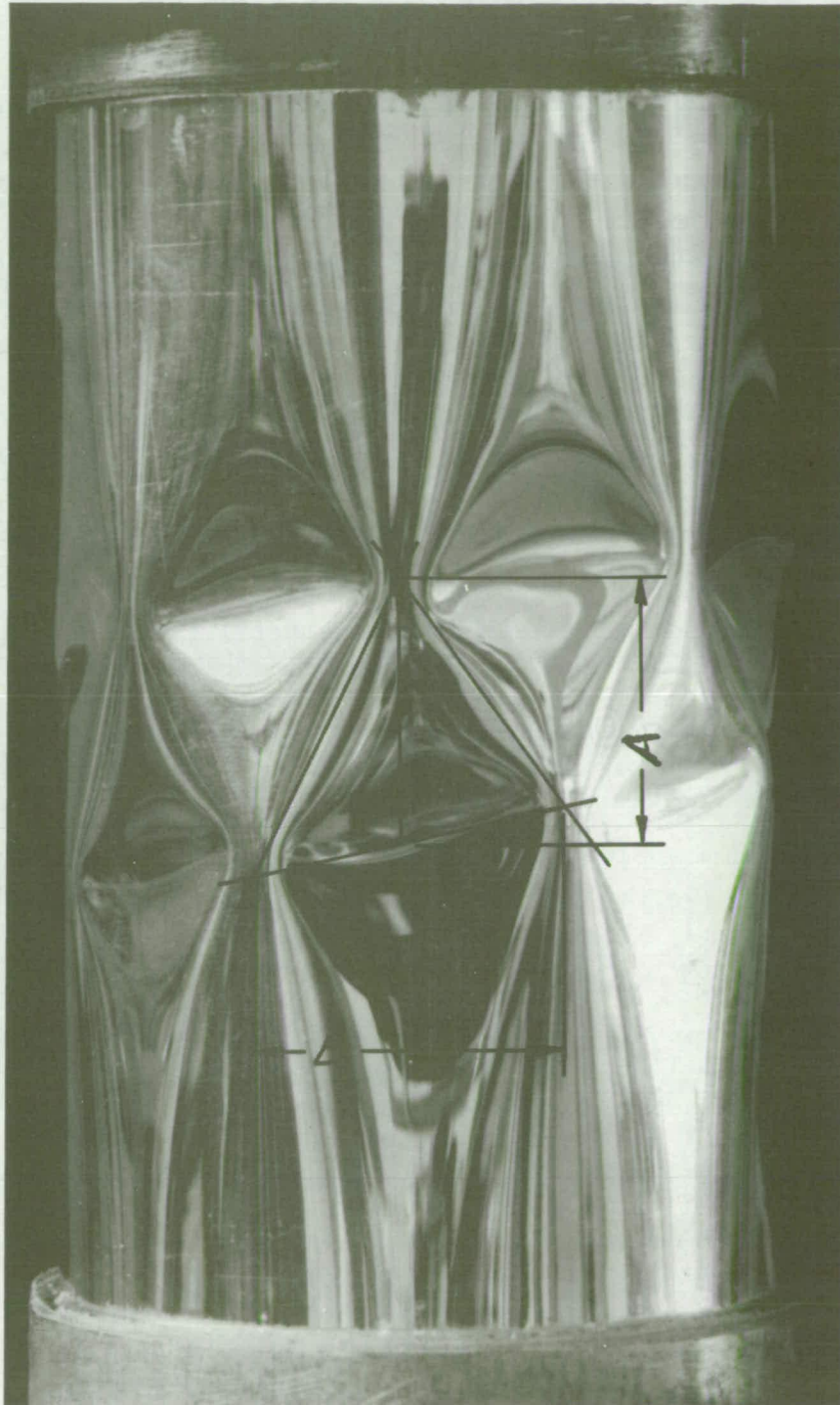


FIGURE 8.1  
EFFECT OF TORSION ON AXIAL  
COMPRESSION FAILURE





FIGURE 8.2  
PAPER MODELS OF AXIAL COMPRESSION-  
TORSION COLLAPSE

# REFERENCES

---

---



REFERENCES

1. Timoshenko.S.P. and Gere.J.M., "Theory of elastic stability". 2nd. Edn. McGraw Hill. 1961.
2. Harris.L.A., Suer.H.S., Skene.W.T. and Benjamin.R.J., "The stability of thin-walled unstiffened circular cylinders under axial compression including the effects of internal pressure". Journal of the Aeronautical Sciences. Aug.1957. pp.587-596.
3. Von Karman.T. and Hsue-Shen Tsien., "The buckling of thin cylindrical shells under axial compression". Journal of the Aeronautical Sciences. Vol.8, No.8,1941. pp.303-312.
4. Donnell.L.H. "A new theory for the buckling of thin cylinders under axial compression and bending". Trans. Am. Soc. Mech. Engrs. 56,pp795-806. 1934.
5. Flugge.W., "Stresses in shells". Springer-Verlag. 1966.
6. Yoshimura.Y., "On the mechanism of buckling of a circular cylindrical shell under axial compression". NACA., T.N. 1390 (1955).

7. Hoff.N.J.,Madsen.W.A. and Mayers.J., "Postbuckling equilibrium of axially compressed circular cylindrical Shells". A.I.A.A. Journal. Vol.4, No.1, Jan. 1966. pp.126-133.
8. Hoff.N.J., "Some recent studies of the buckling of thin shells". The Aeronautical Journal of the Royal Aeronautical Society. Vol.73, Dec.1969. pp.1057-1070.
9. Hutchinson.J.W., and Koiter.W.T., "Postbuckling theory". Applied Mechanics Reviews. Vol.12, Sept.1970. pp.1353-1366.
10. Roark.R.J., "Formulas for stress and strain". 4th. Edn. McGraw Hill. 1965.
11. Baker.E.H.,Kovalevsky.L., and Rish.F.L., "Structural analysis of shells". McGraw Hill. 1972.
12. Baker.E.H.,Cappelli.A.P.,Kovalevsky.L.,Rish.F.L. and Verette.R.H., "Shell analysis manual". NASA.CR 912. (1968).
13. Esslinger.H. and Geier.B., "Postbuckling behaviour of structures". Springer-Verlag. 1975.
14. Almroth.B.O.,Holmes.A.M.C. and Brush.D.O., "An experimental study of the buckling of cylinders under axial compression". Experimental Mechanics. 4(9),pp263-270 (Sept.1964).

15. Timoshenko.S.P., and Woinowsky Krieger.S., "Theory of plates and shells". 2nd. Edn. McGraw Hill. 1959.
16. Ligtenberg.F.K., "The moiré method-A new experimental method for the determinations of moments in small slab models". Experimental Stress Analysis, Vol.12, No.2, 1955
17. Phan Lam and Gregory.M.S., "Measurement of slope change on cylindrical shell surfaces". Civ.Engg.Trans. I.E.Aust., Vol.CE15, Nos 1 & 2, 1973. pp 94-98.
18. Gregory.M.S., "An inexpensive high quality camera for in-plane strain analysis by the moiré reflex spectrographic method". Bull.Mech.Engng.Educ., Vol.8, No.1, 1969, pp 83-84.
19. Hart-Smith.L.J., "Buckling of thin cylindrical shells under uniform axial compression". Int.J.ofMech.Sci., Vol.12, 1970, pp 299-313.
20. Kremmer.I.D., "An investigation into the behaviour of clamped square plates in shear". Univ. of Tas., Honours Thesis, Feb.1979.
21. Arbocz.J. and Babcock.C.D., "The effect of general imperfections on the buckling of cylindrical shells". J.of App.Mech., Vol.36, No.7, Mar. 1969.

22. Tennyson.R.C., "A note on the classical buckling load of circular cylindrical shells under axial compression". A.I.A.A. Journal, Vol.1., No.2., Feb.1963. pp 475-476.

# APPENDICES

APPENDIX    A

RESULTS OF COMBINED LOAD BUCKLING TESTS.

NOMINAL STRESSES AT COLLAPSE FOR CYLINDER NO.2

$\sigma_a$	$\sigma_h$	$\tau$	$A_1$	$A_2$	$A_3$	$A_4$
MPa	MPa	MPa				
-1.89	0	0	1.00	1.00	1.00	1.00
-0.05	0	1.34	1.00	1.00	1.00	1.00
-1.75	0	0.16	0.94	0.97	0.94	0.97
-1.66	0	0.32	0.93	1.00	0.93	1.00
-1.59	0	0.47	0.96	1.05	0.96	1.05
-1.19	0	0.63	0.84	0.95	0.84	0.95
-1.16	0	0.79	0.95	1.07	0.95	1.07
-0.89	0	0.95	0.96	1.07	0.96	1.07
-0.46	0	1.10	0.90	0.99	0.90	0.99
-0.18	0	1.26	0.95	1.01	0.95	1.01
-0.05	-0.314	0	1.00	1.00	1.00	1.00
-1.35	-0.270	0	1.12	1.12	1.25	1.25
-1.35	-0.262	0.16	1.11	1.14	1.24	1.27
-1.35	-0.240	0.32	1.10	1.16	1.23	1.29
-1.35	-0.196	0.47	1.07	1.16	1.18	1.27
-1.35	-0.131	0.63	1.04	1.15	1.13	1.23
-1.00	-0.283	0	1.05	1.05	1.15	1.15
-1.00	-0.262	0.16	1.00	1.03	1.11	1.14
-1.00	-0.262	0.32	1.04	1.10	1.15	1.21
-1.00	-0.218	0.47	0.99	1.08	1.09	1.18
-1.00	-0.174	0.63	0.98	1.09	1.08	1.18
-1.00	-0.131	0.79	1.01	1.13	1.09	1.20
-1.00	-0.022	0.95	1.02	1.13	1.02	1.13
-0.65	-0.283	0	0.96	0.96	1.04	1.04
-0.65	-0.262	0.16	0.92	0.94	0.99	1.02
-0.65	-0.262	0.32	0.96	1.02	1.03	1.09
-0.65	-0.231	0.47	0.93	1.02	1.00	1.09
-0.65	-0.205	0.63	0.95	1.06	1.03	1.13
-0.65	-0.174	0.79	0.99	1.10	1.06	1.17
-0.65	-0.087	0.95	0.93	1.04	0.97	1.08



NOMINAL STRESSES AT COLLAPSE FOR CYLINDER NO.2

$\sigma_a$	$\sigma_h$	$\tau$	$A_1$	$A_2$	$A_3$	$A_4$
MPa	MPa	MPa				
-0.30	-0.310	0	1.00	1.00	1.03	1.03
-0.30	-0.305	0.16	1.00	1.03	1.02	1.05
-0.30	-0.283	0.32	0.97	1.03	1.00	1.06
-0.30	-0.279	0.47	1.02	1.11	1.05	1.14
-0.30	-0.231	0.63	0.97	1.07	1.00	1.10
-0.30	-0.201	0.79	1.00	1.11	1.02	1.13
-0.30	-0.148	0.95	0.99	1.09	1.00	1.11
-0.05	-0.314	0.16	1.01	1.04	1.01	1.04
-0.05	-0.310	0.32	1.04	1.10	1.04	1.10
-0.05	-0.305	0.47	1.09	1.18	1.09	1.18
-0.05	-0.275	0.63	1.09	1.20	1.09	1.20
-0.05	-0.218	0.79	1.03	1.15	1.03	1.15
-0.05	-0.161	0.95	1.00	1.11	1.00	1.11
-0.05	-0.087	1.10	0.93	1.02	0.94	1.02
-1.46	-0.227	0	1.06	1.06	1.19	1.19
-1.46	-0.209	0.16	1.03	1.06	1.15	1.18
-1.46	-0.161	0.32	0.98	1.04	1.08	1.14
-1.46	-0.087	0.47	0.94	1.03	0.99	1.08

NOMINAL STRESSES AT COLLAPSE FOR CYLINDER NO.3

$\sigma_a$	$\sigma_h$	$\tau$	A <sub>1</sub>	A <sub>2</sub>	A <sub>3</sub>	A <sub>4</sub>
MPa	MPa	MPa				
-4.77	0	0	1.00	1.00	1.00	1.00
-0.21	0	2.38	1.00	1.00	1.00	1.00
-4.35	0	0.38	0.94	0.98	0.94	0.98
-3.58	0	0.76	0.85	0.93	0.85	0.93
-3.16	0	1.14	0.88	0.99	0.88	0.99
-2.25	0	1.52	0.86	0.98	0.86	0.98
-1.47	0	1.90	0.92	1.02	0.92	1.02
-0.63	0	2.28	1.01	1.07	1.01	1.07
-0.21	-1.132	0	1.00	1.00	1.00	1.00
-0.49	-1.115	0	0.99	0.99	1.01	1.01
-0.77	-1.097	0	0.98	0.98	1.01	1.01
-1.05	-1.045	0	0.95	0.95	0.99	0.99
-1.33	-1.028	0	0.95	0.95	1.01	1.01
-1.61	-1.028	0	0.97	0.97	1.04	1.04
-1.89	-0.923	0	0.91	0.91	0.99	0.99
-2.18	-0.889	0	0.91	0.91	1.00	1.00
-2.46	-0.906	0	0.95	0.95	1.06	1.06
-2.74	-0.871	0	0.96	0.96	1.07	1.07
-3.02	-0.767	0	0.93	0.93	1.04	1.04
-3.30	-0.679	0	0.92	0.92	1.03	1.03
-3.58	-0.627	0	0.93	0.93	1.04	1.04
-3.86	-0.610	0	0.97	0.97	1.08	1.08
-4.14	-0.523	0	0.98	0.98	1.08	1.08
-4.24	-0.331	0	0.97	0.97	1.00	1.00
-4.56	-0.279	0	0.99	0.99	1.04	1.04
-0.21	-1.063	0.38	0.96	1.00	0.97	1.01
-0.77	-0.993	0.38	0.92	0.96	0.94	0.98
-1.33	-0.906	0.38	0.87	0.91	0.93	0.97

NOMINAL STRESSES AT COLLAPSE FOR CYLINDER NO.3

$\sigma'_a$	$\sigma_h$	$\tau$	$A_1$	$A_2$	$A_3$	$A_4$
MPa	MPa	MPa				
-1.89	-0.889	0.38	0.90	0.94	0.98	1.02
-2.46	-0.732	0.38	0.85	0.89	0.95	0.99
-3.02	-0.679	0.38	0.87	0.91	1.00	1.04
-3.86	-0.279	0.38	0.87	0.91	0.92	0.96
-4.00	-0.209	0.38	0.88	0.92	0.92	0.96
-0.21	-0.993	0.76	0.98	1.06	0.98	1.06
-0.77	-0.976	0.76	0.97	1.06	1.00	1.08
-1.05	-0.784	0.76	0.82	0.91	0.87	0.95
-1.33	-0.714	0.76	0.79	0.87	0.84	0.92
-1.61	-0.697	0.76	0.80	0.88	0.87	0.95
-1.89	-0.645	0.76	0.79	0.87	0.87	0.95
-2.18	-0.575	0.76	0.78	0.86	0.86	0.94
-2.46	-0.540	0.76	0.80	0.88	0.88	0.96
-2.74	-0.436	0.76	0.79	0.87	0.86	0.94
-3.02	-0.383	0.76	0.82	0.90	0.88	0.96
-3.30	-0.209	0.76	0.81	0.90	0.85	0.93
-3.44	-0.070	0.76	0.82	0.90	0.83	0.91
-0.21	-0.749	1.14	0.88	0.99	0.88	0.99
-0.49	-0.679	1.14	0.83	0.94	0.84	0.95

NOMINAL STRESSES AT COLLAPSE FOR CYLINDER NO.5

$\sigma_a$	$\sigma_h$	$\tau$	$A_1$	$A_2$	$A_3$	$A_4$
MPa	MPa	MPa				
-4.20	0	0	1.00	1.00	1.00	1.00
-0.21	0	1.77	1.00	1.00	1.00	1.00
-3.44	0	0.59	0.92	1.01	0.92	1.01
-3.23	0	0.74	0.93	1.04	0.93	1.04
-2.60	0	0.89	0.86	0.98	0.86	0.98
-2.18	0	1.03	0.84	0.96	0.84	0.96
-1.75	0	1.18	0.84	0.96	0.84	0.96
-1.61	0	1.33	0.92	1.03	0.92	1.03
-1.05	0	1.48	0.91	1.01	0.91	1.01
-0.49	0	1.63	0.92	0.96	0.92	0.96
-0.21	-1.22	0	1.00	1.00	1.00	1.00
-0.49	-1.19	0	0.98	0.98	1.00	1.00
-1.05	-1.11	0	0.94	0.94	1.00	1.00
-1.61	-1.09	0	0.97	0.97	1.05	1.05
-2.18	-1.07	0	1.02	1.02	1.13	1.13
-2.74	-1.01	0	1.05	1.05	1.18	1.18
-3.30	-0.85	0	1.05	1.05	1.18	1.18
-3.58	-0.72	0	1.04	1.04	1.15	1.15
-3.86	-0.65	0	1.06	1.06	1.17	1.17
-4.14	-0.58	0	1.09	1.09	1.20	1.20
-0.21	-1.05	0.59	0.97	1.05	0.97	1.05
-0.49	-1.03	0.59	0.96	1.04	0.98	1.06
-1.05	-0.92	0.59	0.90	0.99	0.95	1.03
-1.61	-0.87	0.59	0.91	1.00	0.99	1.07
-2.18	-0.71	0.59	0.88	0.97	0.98	1.06
-2.46	-0.63	0.59	0.89	0.97	0.98	1.06
-2.74	-0.56	0.59	0.90	0.99	0.99	1.07
-3.02	-0.47	0.59	0.92	1.01	1.00	1.08

NOMINAL STRESSES AT COLLAPSE FOR CYLINDER NO.5

$\sigma_a$	$\sigma_h$	$\tau$	$A_1$	$A_2$	$A_3$	$A_4$
MPa	MPa	MPa				
-3.16	-0.44	0.59	0.94	1.03	1.01	1.09
-3.30	-0.35	0.59	0.94	1.03	1.00	1.08
-3.44	-0.17	0.59	0.94	1.02	0.96	1.04
-0.21	-0.84	0.89	0.93	1.05	0.93	1.05
-0.49	-0.80	0.89	0.91	1.02	0.92	1.03
-0.77	-0.75	0.89	0.88	1.00	0.90	1.02
-1.05	-0.71	0.89	0.87	0.99	0.91	1.03
-1.33	-0.70	0.89	0.89	1.01	0.94	1.06
-1.61	-0.65	0.89	0.90	1.01	0.95	1.07
-1.89	-0.61	0.89	0.91	1.03	0.97	1.09
-2.18	-0.49	0.89	0.90	1.01	0.95	1.07
-2.32	-0.42	0.89	0.89	1.01	0.94	1.06
-2.46	-0.35	0.89	0.89	1.01	0.93	1.05
-2.60	-0.17	0.89	0.87	0.99	0.88	1.00
-0.21	-0.66	1.18	0.96	1.09	0.96	1.09
-0.49	-0.66	1.18	0.97	1.10	0.97	1.10
-0.77	-0.63	1.18	0.97	1.09	0.98	1.10
-1.05	-0.52	1.18	0.91	1.04	0.94	1.06
-1.33	-0.47	1.18	0.92	1.04	0.96	1.08
-1.47	-0.44	1.18	0.92	1.05	0.96	1.08
-1.61	-0.30	1.18	0.88	1.00	0.90	1.02
-1.75	-0.21	1.18	0.87	1.00	0.89	1.01

### NOMINAL STRESSES AT COLLAPSE FOR CYLINDER NO.6

[illegible]

NOMINAL STRESSES AT COLLAPSE FOR CYLINDER NO.7

$\sigma_a$	$\sigma_h$	$\tau$	$A_1$	$A_2$	$A_3$	$A_4$
MPa	MPa	MPa				
-1.63	0	0	1.00	1.00	1.00	1.00
-0.09	0	0.687	1.00	1.00	1.00	1.00
-1.63	0	0.172	1.06	1.12	1.06	1.12
-1.49	0	0.240	1.03	1.11	1.03	1.11
-1.29	0	0.344	1.03	1.13	1.03	1.13
-1.16	0	0.412	1.05	1.15	1.05	1.15
-0.96	0	0.515	1.12	1.20	1.12	1.20
-0.76	0	0.584	1.15	1.21	1.15	1.21
-0.09	-0.179	0	1.00	1.00	1.00	1.00
-0.36	-0.174	0	1.00	1.00	1.04	1.04
-0.63	-0.165	0	1.00	1.00	1.08	1.08
-0.89	-0.133	0	0.92	0.92	1.03	1.03
-1.16	-0.115	0	0.96	0.96	1.08	1.08
-1.43	-0.037	0	0.90	0.90	0.94	0.94
-1.29	-0.092	0	0.94	0.94	1.05	1.05
-1.56	-0.023	0	0.97	0.97	0.99	0.99
-0.09	-0.151	0.344	1.08	1.18	1.09	1.19
-0.36	-0.142	0.344	1.06	1.16	1.10	1.20
-0.63	-0.128	0.344	1.05	1.15	1.13	1.23
-0.89	-0.092	0.344	0.99	1.08	1.08	1.18
-1.16	-0.041	0.344	0.98	1.08	1.03	1.13
-0.09	-0.124	0.515	1.22	1.31	1.24	1.32
-0.36	-0.101	0.515	1.14	1.22	1.19	1.27
-0.63	-0.073	0.515	1.09	1.17	1.16	1.24
-0.76	-0.050	0.515	1.07	1.16	1.13	1.21
-0.49	-0.092	0.515	1.13	1.21	1.19	1.27

NOMINAL STRESSES AT COLLAPSE FOR CYLINDER NO.7

$\sigma_a$	$\sigma_h$	$\tau$	$A_1$	$A_2$	$A_3$	$A_4$
MPa	MPa	MPa				
-0.09	-0.165	0.172	0.98	1.04	0.99	1.05
-0.36	-0.151	0.172	0.93	0.99	0.98	1.04
-0.63	-0.128	0.172	0.87	0.93	0.95	1.01
-0.89	-0.115	0.172	0.90	0.96	1.00	1.06
-1.16	-0.060	0.172	0.85	0.90	0.92	0.98
-1.43	-0.046	0.172	0.97	1.03	1.03	1.09



NOMINAL STRESSES AT COLLAPSE FOR CYLINDER NO.8

$\sigma_a$	$\sigma_h$	$\tau$	$A_1$	$A_2$	$A_3$	$A_4$
MPa	MPa	MPa				
-1.07	0	0	1.00	1.00	1.00	1.00
-0.12	0	0.378	1.00	1.00	1.00	1.00
-0.96	0	0.090	0.95	1.00	0.95	1.00
-0.96	0	0.126	1.00	1.07	1.00	1.07
-0.86	0	0.180	1.01	1.10	1.01	1.10
-0.75	0	0.216	0.99	1.08	0.99	1.08
-0.61	0	0.270	1.02	1.11	1.02	1.11
-0.51	0	0.307	1.06	1.13	1.06	1.13
-0.12	-0.218	0	1.00	1.00	1.00	1.00
-0.26	-0.209	0	0.99	0.99	1.04	1.04
-0.40	-0.192	0	0.96	0.96	1.04	1.04
-0.54	-0.183	0	0.98	0.98	1.08	1.08
-0.68	-0.140	0	0.90	0.90	1.01	1.01
-0.82	-0.131	0	0.97	0.97	1.09	1.09
-0.89	-0.070	0	0.89	0.89	0.96	0.96
-0.12	-0.209	0.090	1.02	1.07	1.04	1.09
-0.26	-0.174	0.090	0.88	0.94	0.94	0.99
-0.40	-0.166	0.090	0.90	0.95	0.98	1.03
-0.54	-0.157	0.090	0.93	0.98	1.03	1.08
-0.68	-0.122	0.090	0.90	0.95	1.00	1.05
-0.75	-0.105	0.090	0.90	0.95	1.00	1.05
-0.82	-0.070	0.090	0.88	0.93	0.95	1.00
-0.12	-0.166	0.180	0.97	1.06	0.99	1.08
-0.26	-0.148	0.180	0.92	1.01	0.97	1.06
-0.40	-0.131	0.180	0.91	1.00	0.99	1.08
-0.54	-0.113	0.180	0.93	1.02	1.01	1.10
-0.68	-0.078	0.180	0.93	1.02	1.01	1.10

NOMINAL STRESSES AT COLLAPSE FOR CYLINDER NO.8

$\sigma_a$	$\sigma_h$	$\tau$	$A_1$	$A_2$	$A_3$	$A_4$
MPa	MPa	MPa				
-0.12	-0.148	0.270	1.14	1.22	1.17	1.25
-0.26	-0.140	0.270	1.14	1.22	1.19	1.27
-0.40	-0.105	0.270	1.07	1.15	1.14	1.22
-0.54	-0.078	0.270	1.08	1.16	1.15	1.23
-0.12	-0.183	0.126	0.95	1.02	0.97	1.04
-0.26	-0.174	0.126	0.94	1.01	0.99	1.06
-0.40	-0.148	0.126	0.88	0.95	0.95	1.02
-0.54	-0.131	0.126	0.89	0.96	0.98	1.05
-0.68	-0.105	0.126	0.90	0.97	0.99	1.06
-0.75	-0.078	0.126	0.89	0.96	0.96	1.03
-0.12	-0.157	0.216	1.02	1.11	1.04	1.13
-0.26	-0.140	0.216	0.98	1.07	1.03	1.12
-0.40	-0.131	0.216	1.00	1.09	1.08	1.17
-0.54	-0.087	0.216	0.94	1.03	1.01	1.10
-0.61	-0.078	0.216	0.97	1.06	1.04	1.13

NOMINAL STRESSES AT COLLAPSE FOR CYLINDER NO.9

$\sigma_a$	$\sigma_h$	$\tau$	$A_1$	$A_2$	$A_3$	$A_4$
MPa	MPa	MPa				
-1.10	0	0	1.00	1.00	1.00	1.00
-0.96	0	0.075	0.90	0.93	0.90	0.93
-0.96	0	0.105	0.92	0.97	0.92	0.97
-0.96	0	0.150	0.97	1.04	0.97	1.04
-0.93	0	0.180	0.98	1.06	0.98	1.06
-0.79	0	0.224	0.93	1.02	0.93	1.02
-0.75	0	0.254	0.95	1.04	0.95	1.04
-0.61	0	0.299	0.92	1.02	0.92	1.02
-0.12	0	0.464	1.00	1.00	1.00	1.00
-0.40	0	0.374	0.94	1.01	0.94	1.01
-0.44	0	0.329	0.85	0.93	0.85	0.93
-0.12	-0.201	0	1.00	1.00	1.00	1.00
-0.26	-0.192	0	0.98	0.98	1.03	1.03
-0.40	-0.183	0	0.98	0.98	1.06	1.06
-0.54	-0.157	0	0.92	0.92	1.02	1.02
-0.68	-0.122	0	0.87	0.87	0.97	0.97
-0.82	-0.105	0	0.91	0.91	1.01	1.01
-0.89	-0.087	0	0.92	0.92	1.01	1.01
-0.96	-0.070	0	0.94	0.94	1.01	1.01
-0.12	-0.192	0.150	1.06	1.13	1.07	1.14
-0.26	-0.174	0.150	0.99	1.06	1.04	1.11
-0.40	-0.166	0.150	1.00	1.07	1.07	1.14
-0.54	-0.148	0.150	0.98	1.05	1.08	1.15
-0.68	-0.140	0.150	1.03	1.10	1.14	1.21
-0.82	-0.096	0.150	0.98	1.05	1.08	1.15
-0.89	-0.078	0.150	0.99	1.06	1.07	1.14

NOMINAL STRESSES AT COLLAPSE FOR CYLINDER NO.9

$\sigma_a$	$\sigma_h$	$\tau$	$A_1$	$A_2$	$A_3$	$A_4$
MPa	MPa	MPa				
-0.12	-0.166	0.224	1.04	1.13	1.06	1.15
-0.26	-0.157	0.224	1.03	1.12	1.07	1.16
-0.40	-0.131	0.224	0.96	1.05	1.03	1.12
-0.54	-0.113	0.224	0.96	1.05	1.05	1.14
-0.61	-0.096	0.224	0.94	1.03	1.03	1.12
-0.68	-0.087	0.224	0.96	1.05	1.05	1.14
-0.12	-0.148	0.299	1.12	1.21	1.14	1.23
-0.26	-0.131	0.299	1.06	1.15	1.11	1.20
-0.40	-0.113	0.299	1.04	1.13	1.11	1.20
-0.54	-0.078	0.299	1.00	1.09	1.07	1.16

NOMINAL STRESSES AT COLLAPSE FOR CYLINDER NO.11

$\sigma_a$	$\sigma_h$	$\tau$	$A_1$	$A_2$	$A_3$	$A_4$
MPa	MPa	MPa				
-1.33	0	0	1.00	1.00	1.00	1.00
-0.18	0	0.474	1.00	1.00	1.00	1.00
-1.23	0	0.068	0.94	0.97	0.94	0.97
-1.09	0	0.135	0.89	0.95	0.89	0.95
-0.95	0	0.203	0.87	0.96	0.87	0.96
-0.81	0	0.237	0.82	0.91	0.82	0.91
-0.77	0	0.271	0.86	0.95	0.86	0.95
-0.70	0	0.305	0.88	0.97	0.88	0.97
-0.60	0	0.339	0.89	0.97	0.89	0.97
-0.49	0	0.406	1.00	1.05	1.00	1.05
		CYLINDER DAMAGED				

NOMINAL STRESSES AT COLLAPSE FOR CYLINDER NO.12

$\sigma_a$	$\sigma_h$	$\tau$	$A_1$	$A_2$	$A_3$	$A_4$
MPa	MPa	MPa				
-1.09	0	0	1.00	1.00	1.00	1.00
-0.18	0	0.684	1.00	1.00	1.00	1.00
-1.02	0	0.098	0.95	0.98	0.95	0.98
-0.95	0	0.195	0.94	1.00	0.94	1.00
-0.84	0	0.293	0.92	1.00	0.92	1.00
-0.81	0	0.391	1.02	1.10	1.02	1.10
-0.67	0	0.488	1.04	1.12	1.04	1.12
-0.32	0	0.586	0.91	0.96	0.91	0.96
-0.18	-0.270	0	1.00	1.00	1.00	1.00
-0.32	-0.270	0	1.04	1.04	1.10	1.10
-0.46	-0.244	0	1.00	1.00	1.09	1.09
-0.60	-0.227	0	1.00	1.00	1.12	1.12
-0.74	-0.209	0	1.03	1.03	1.15	1.15
-0.88	-0.183	0	1.05	1.05	1.18	1.18
-0.95	-0.157	0	1.05	1.05	1.16	1.16
-1.02	-0.096	0	1.00	1.00	1.08	1.08
-0.18	-0.270	0.098	1.03	1.06	1.06	1.09
-0.32	-0.262	0.098	1.03	1.06	1.09	1.12
-0.46	-0.244	0.098	1.01	1.04	1.10	1.13
-0.60	-0.227	0.098	1.02	1.05	1.13	1.16
-0.74	-0.209	0.098	1.05	1.08	1.17	1.20
-0.88	-0.174	0.098	1.05	1.08	1.17	1.20
-0.95	-0.044	0.098	0.90	0.93	0.93	0.96
-0.18	-0.262	0.195	1.05	1.11	1.08	1.14
-0.32	-0.235	0.195	0.99	1.05	1.05	1.11
-0.46	-0.209	0.195	0.95	1.01	1.04	1.10
-0.60	-0.209	0.195	1.02	1.08	1.13	1.19

NOMINAL STRESSES AT COLLAPSE FOR CYLINDER NO.12

$\sigma_a$	$\sigma_h$	$\tau$	$A_1$	$A_2$	$A_3$	$A_4$
MPa	MPa	MPa				
-0.74	-0.174	0.195	1.00	1.06	1.12	1.18
-0.81	-0.140	0.195	0.97	1.03	1.08	1.14
-0.88	-0.035	0.195	0.89	0.94	0.91	0.97
-0.18	-0.227	0.293	1.01	1.09	1.04	1.12
-0.32	-0.218	0.293	1.01	1.09	1.08	1.16
-0.46	-0.192	0.293	0.98	1.06	1.07	1.15
-0.60	-0.174	0.293	1.00	1.08	1.10	1.18
-0.67	-0.157	0.293	1.00	1.08	1.10	1.18
-0.74	-0.113	0.293	0.95	1.03	1.04	1.12
-0.18	-0.218	0.391	1.10	1.18	1.14	1.22
-0.32	-0.201	0.391	1.07	1.16	1.14	1.22
-0.46	-0.174	0.391	1.04	1.13	1.14	1.22
-0.60	-0.131	0.391	1.01	1.09	1.10	1.18
-0.67	-0.061	0.391	0.93	1.02	0.98	1.06
-0.18	-0.174	0.488	1.09	1.17	1.12	1.20
-0.32	-0.157	0.488	1.08	1.16	1.14	1.22
-0.46	-0.131	0.488	1.07	1.15	1.14	1.22
-0.53	-0.113	0.488	1.07	1.15	1.14	1.22
-0.60	-0.061	0.488	1.02	1.10	1.07	1.15

NOMINAL STRESSES AT COLLAPSE FOR CYLINDER NO.13

$\sigma_a$	$\sigma_h$	$\tau$	$A_1$	$A_2$	$A_3$	$A_4$
MPa	MPa	MPa				
-1.19	0	0	1.00	1.00	1.00	1.00
-0.18	0	0.681	1.00	1.00	1.00	1.00
-1.12	0	0.076	0.95	0.97	0.95	0.97
-1.09	0	0.151	0.96	1.00	0.96	1.00
-1.05	0	0.227	0.98	1.04	0.98	1.04
-0.98	0	0.302	0.99	1.07	0.99	1.07
-0.88	0	0.378	1.00	1.09	1.00	1.09
-0.77	0	0.454	1.02	1.11	1.02	1.11
-0.67	0	0.529	1.07	1.14	1.07	1.14
-0.42	0	0.605	1.02	1.06	1.02	1.06
-0.18	-0.262	0	1.00	1.00	1.00	1.00
-0.32	-0.262	0	1.04	1.04	1.09	1.09
-0.46	-0.244	0	1.01	1.01	1.09	1.09
-0.60	-0.227	0	1.00	1.00	1.10	1.10
-0.74	-0.218	0	1.04	1.04	1.16	1.16
-0.88	-0.183	0	1.02	1.02	1.14	1.14
-1.02	-0.131	0	0.99	0.99	1.10	1.10
-1.09	-0.078	0	0.96	0.96	1.03	1.03
-0.18	-0.262	0.151	1.05	1.10	1.08	1.13
-0.32	-0.253	0.151	1.04	1.09	1.10	1.15
-0.46	-0.235	0.151	1.01	1.06	1.10	1.15
-0.60	-0.218	0.151	1.01	1.06	1.11	1.16
-0.74	-0.183	0.151	0.97	1.02	1.09	1.14
-0.88	-0.157	0.151	0.99	1.04	1.10	1.15
-1.02	-0.113	0.151	1.00	1.05	1.09	1.14
-0.18	-0.244	0.302	1.11	1.19	1.14	1.22
-0.32	-0.227	0.302	1.08	1.16	1.13	1.21
-0.46	-0.218	0.302	1.09	1.17	1.17	1.25
-0.60	-0.192	0.302	1.06	1.14	1.16	1.24



NOMINAL STRESSES AT COLLAPSE FOR CYLINDER NO.13

$\sigma_a$	$\sigma_h$	$\tau$	$A_1$	$A_2$	$A_3$	$A_4$
MPa	MPa	MPa				
-0.74	-0.174	0.302	1.08	1.16	1.19	1.27
-0.88	-0.131	0.302	1.06	1.14	1.16	1.24
-0.95	-0.087	0.302	1.03	1.11	1.10	1.18
-0.18	-0.218	0.454	1.22	1.31	1.24	1.33
-0.32	-0.201	0.454	1.18	1.27	1.24	1.33
-0.46	-0.174	0.454	1.14	1.23	1.22	1.31
-0.60	-0.148	0.454	1.13	1.22	1.22	1.31
-0.67	-0.113	0.454	1.08	1.17	1.16	1.25

NOMINAL STRESSES AT COLLAPSE FOR CYLINDER NO.14

$\sigma_a$	$\sigma_h$	$\tau$	$A_1$	$A_2$	$A_3$	$A_4$
MPa	MPa	MPa				
-3.17	0	0	1.00	1.00	1.00	1.00
-0.09	0	1.795	1.00	1.00	1.00	1.00
-2.96	0	0.271	0.96	0.99	0.96	0.99
-2.82	0	0.474	0.96	1.02	0.96	1.02
-2.61	0	0.610	0.94	1.02	0.94	1.02
-2.47	0	0.813	0.98	1.08	0.98	1.08
-2.26	0	0.948	0.98	1.09	0.98	1.09
-1.91	0	1.152	1.00	1.10	1.00	1.10
-1.28	0	1.287	0.90	0.99	0.90	0.99
-1.00	0	1.490	0.98	1.05	0.98	1.05
-0.51	0	1.626	0.96	1.00	0.96	1.00
-0.16	0	1.761	0.98	0.99	0.98	0.99
-0.09	-0.602	0	1.00	1.00	1.00	1.00
-0.33	-0.580	0	0.97	0.97	0.99	0.99
-0.54	-0.567	0	0.96	0.96	0.99	0.99
-0.71	-0.558	0	0.95	0.95	1.00	1.00
-0.90	-0.541	0	0.94	0.94	1.00	1.00
-1.09	-0.536	0	0.96	0.96	1.03	1.03
-1.27	-0.510	0	0.94	0.94	1.02	1.02
-1.46	-0.462	0	0.90	0.90	0.99	0.99
-1.63	-0.458	0	0.92	0.92	1.02	1.02
-1.82	-0.423	0	0.91	0.91	1.02	1.02
-2.00	-0.401	0	0.92	0.92	1.03	1.03
-2.19	-0.401	0	0.96	0.96	1.08	1.08
-2.37	-0.314	0	0.91	0.91	1.02	1.02
-2.56	-0.279	0	0.93	0.93	1.03	1.03
-2.73	-0.214	0	0.93	0.93	1.01	1.01
-2.92	-0.140	0	0.95	0.95	1.00	1.00
-3.10	-0.026	0	0.98	0.98	0.98	0.98

NOMINAL STRESSES AT COLLAPSE FOR CYLINDER NO.14

$\sigma_a$	$\sigma_h$	$\tau$	$A_1$	$A_2$	$A_3$	$A_4$
MPa	MPa	MPa				
-0.09	-0.593	0.474	1.05	1.12	1.05	1.12
-0.33	-0.576	0.474	1.02	1.09	1.04	1.11
-0.51	-0.520	0.474	0.94	1.01	0.97	1.04
-0.68	-0.506	0.474	0.93	1.00	0.97	1.04
-0.86	-0.480	0.474	0.90	0.97	0.96	1.03
-1.04	-0.467	0.474	0.90	0.97	0.97	1.04
-1.21	-0.436	0.474	0.88	0.95	0.96	1.03
-1.39	-0.410	0.474	0.87	0.94	0.96	1.03
-1.56	-0.406	0.474	0.90	0.97	0.99	1.06
-1.74	-0.375	0.474	0.89	0.96	0.99	1.06
-1.91	-0.336	0.474	0.88	0.95	0.98	1.05
-2.09	-0.288	0.474	0.88	0.95	0.97	1.04
-2.26	-0.253	0.474	0.89	0.96	0.98	1.05
-2.44	-0.227	0.474	0.92	0.99	1.00	1.07
-2.61	-0.122	0.474	0.91	0.98	0.95	1.02
-0.09	-0.523	0.813	1.07	1.16	1.08	1.17
-0.33	-0.506	0.813	1.05	1.14	1.07	1.16
-0.51	-0.484	0.813	1.03	1.12	1.06	1.15
-0.68	-0.475	0.813	1.02	1.11	1.07	1.16
-0.86	-0.432	0.813	0.97	1.06	1.03	1.12
-1.04	-0.392	0.813	0.94	1.03	1.00	1.09
-1.21	-0.336	0.813	0.88	0.97	0.96	1.05
-1.39	-0.301	0.813	0.87	0.96	0.95	1.04
-1.56	-0.266	0.813	0.87	0.96	0.95	1.04
-1.74	-0.222	0.813	0.87	0.96	0.94	1.03
-1.91	-0.183	0.813	0.88	0.97	0.95	1.04
-2.09	-0.144	0.813	0.91	1.00	0.96	1.05
-2.26	-0.092	0.813	0.94	1.03	0.97	1.06
-2.33	-0.074	0.813	0.95	1.04	0.97	1.06

NOMINAL STRESSES AT COLLAPSE FOR CYLINDER NO.14

$\sigma_a$	$\sigma_h$	$\tau$	$A_1$	$A_2$	$A_3$	$A_4$
MPa	MPa	MPa				
-0.09	-0.292	1.490	1.16	1.22	1.16	1.22
-0.33	-0.262	1.490	1.12	1.18	1.14	1.20
-0.51	-0.222	1.490	1.08	1.14	1.11	1.17
-0.68	-0.205	1.490	1.08	1.14	1.12	1.18
-0.75	-0.174	1.490	1.05	1.11	1.09	1.15
-0.86	-0.174	1.490	1.07	1.13	1.12	1.18
-0.93	-0.057	1.490	0.98	1.04	1.00	1.06

NOMINAL STRESSES AT COLLAPSE FOR CYLINDER NO.15

$\sigma_a$	$\sigma_h$	$\tau$	$A_1$	$A_2$	$A_3$	$A_4$
MPa	MPa	MPa				
-2.59	0	0	1.00	1.00	1.00	1.00
-0.13	0	0.957	1.00	1.00	1.00	1.00
-2.59	0	0.080	1.01	1.02	1.01	1.02
-2.46	0	0.160	0.98	1.01	0.98	1.01
-2.19	0	0.239	0.90	0.96	0.90	0.96
-2.06	0	0.319	0.90	0.98	0.90	0.98
-1.86	0	0.399	0.88	0.97	0.88	0.97
-1.79	0	0.479	0.93	1.03	0.93	1.03
-1.53	0	0.558	0.91	1.01	0.91	1.01
-1.39	0	0.638	0.96	1.05	0.96	1.05
-1.13	0	0.718	0.97	1.05	0.97	1.05
-1.06	0	0.798	1.07	1.13	1.07	1.13
-0.53	0	0.877	1.00	1.04	1.00	1.04
-0.13	-0.147	0	1.00	1.00	1.00	1.00
-0.39	-0.147	0	1.01	1.01	1.04	1.04
-0.66	-0.142	0	1.00	1.00	1.05	1.05
-0.93	-0.138	0	1.01	1.01	1.08	1.08
-1.19	-0.133	0	1.01	1.01	1.11	1.11
-1.46	-0.119	0	0.99	0.99	1.10	1.10
-1.73	-0.115	0	1.03	1.03	1.15	1.15
-1.99	-0.110	0	1.07	1.07	1.20	1.20
-2.26	-0.092	0	1.07	1.07	1.20	1.20
-2.39	-0.073	0	1.05	1.05	1.15	1.15
-2.46	-0.046	0	1.00	1.00	1.07	1.07
-0.13	-0.142	0.160	0.99	1.03	1.00	1.04
-0.39	-0.133	0.160	0.94	0.98	0.97	1.01
-0.66	-0.133	0.160	0.96	1.00	1.02	1.06
-0.93	-0.128	0.160	0.97	1.01	1.04	1.08
-1.19	-0.124	0.160	0.99	1.03	1.08	1.12

NOMINAL STRESSES AT COLLAPSE FOR CYLINDER NO.15

$\sigma_a$	$\sigma_h$	$\tau$	$A_1$	$A_2$	$A_3$	$A_4$
MPa	MPa	MPa				
-1.46	-0.119	0.160	1.01	1.05	1.12	1.16
-1.73	-0.105	0.160	1.00	1.04	1.12	1.16
-1.99	-0.101	0.160	1.06	1.10	1.18	1.22
-2.26	-0.078	0.160	1.05	1.09	1.16	1.20
-2.39	-0.055	0.160	1.02	1.06	1.10	1.14
-0.13	-0.128	0.319	0.98	1.06	0.98	1.06
-0.39	-0.124	0.319	0.96	1.04	0.99	1.07
-0.66	-0.110	0.319	0.89	0.97	0.95	1.03
-0.93	-0.105	0.319	0.90	0.98	0.98	1.06
-1.19	-0.096	0.319	0.90	0.98	0.99	1.07
-1.46	-0.083	0.319	0.90	0.98	1.00	1.08
-1.73	-0.073	0.319	0.94	1.02	1.03	1.11
-1.86	-0.060	0.319	0.93	1.01	1.01	1.09
-1.93	-0.037	0.319	0.89	0.97	0.94	1.02
-1.99	-0.009	0.319	0.87	0.95	0.88	0.96
-0.13	-0.119	0.479	1.05	1.15	1.05	1.15
-0.39	-0.115	0.479	1.03	1.13	1.06	1.16
-0.66	-0.105	0.479	0.99	1.09	1.05	1.15
-0.93	-0.096	0.479	0.98	1.08	1.06	1.16
-1.19	-0.092	0.479	1.01	1.11	1.10	1.20
-1.46	-0.078	0.479	1.01	1.11	1.11	1.21
-1.59	-0.064	0.479	0.99	1.09	1.08	1.18
-1.66	-0.050	0.479	0.96	1.06	1.03	1.13
-1.73	-0.041	0.479	0.96	1.06	1.02	1.12

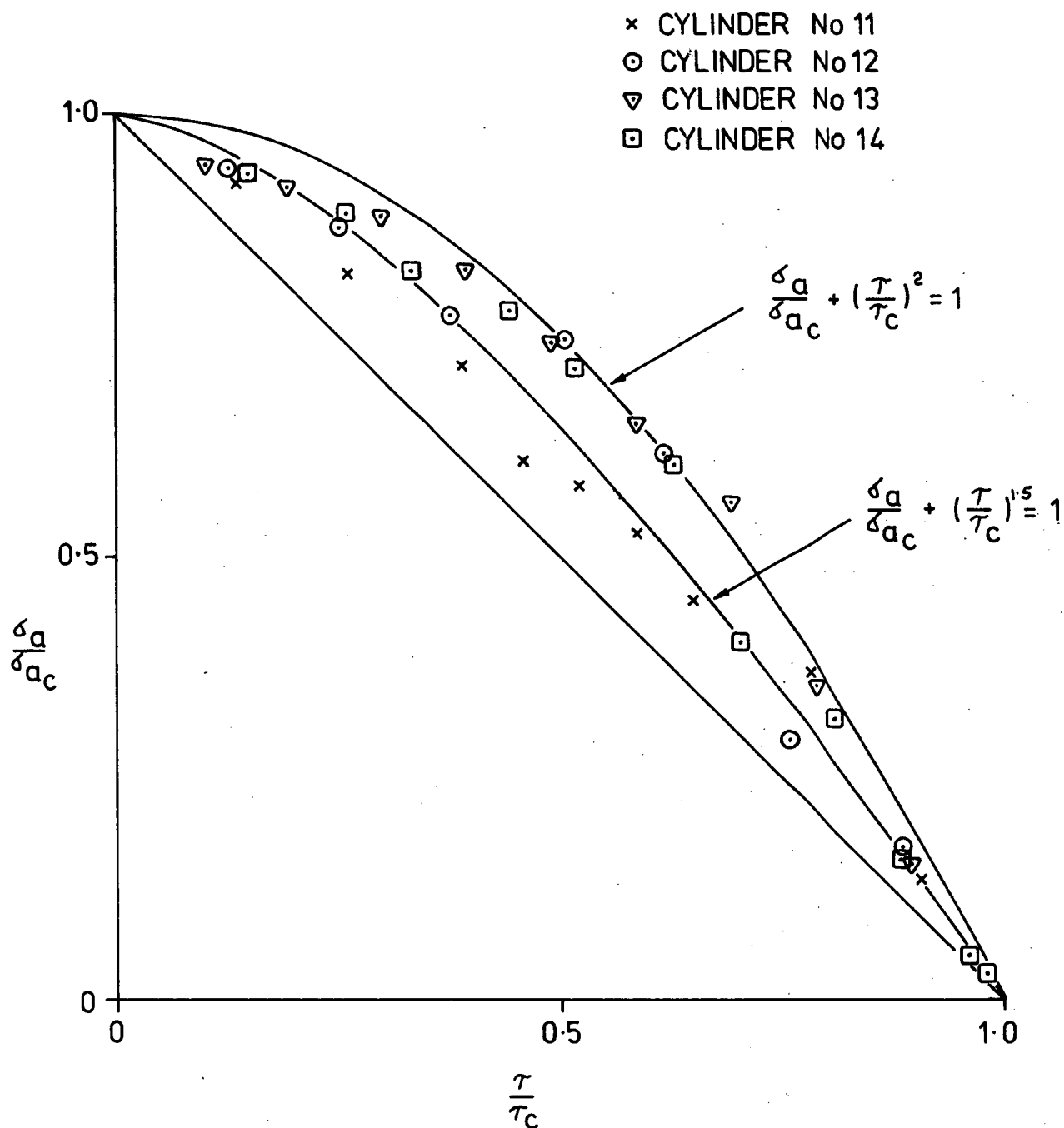
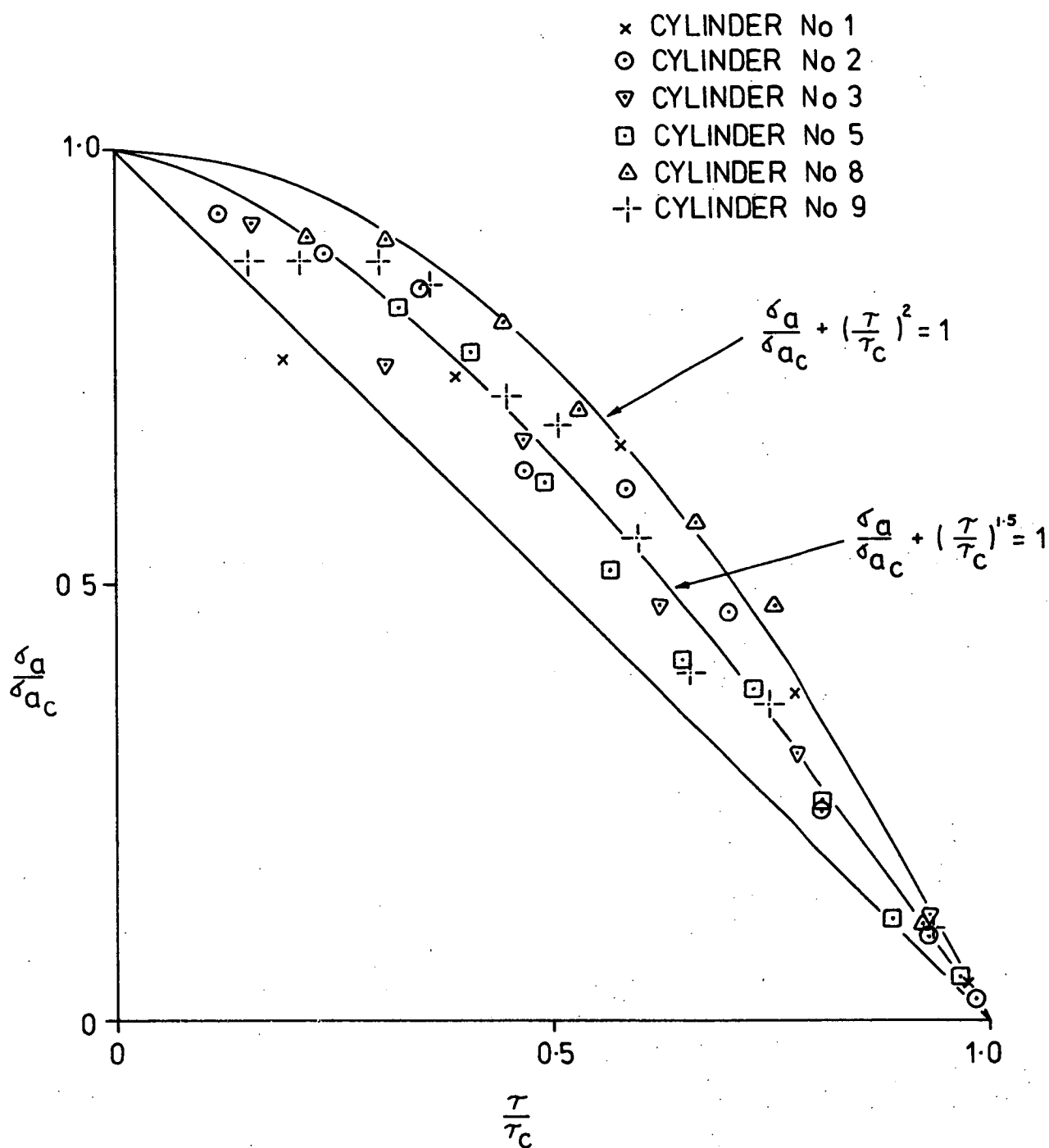


FIGURE A1

BUCKLING STRESS STATE DIAGRAM FOR AXIAL  
COMPRESSION - TORSION INTERACTION IN SHORTER  
CYLINDERS ( $L/R=1.21$ )



**FIGURE A2**

BUCKLING STRESS STATE DIAGRAM FOR AXIAL  
COMPRESSION - TORSION INTERACTION IN MEDIUM  
LENGTH CYLINDERS ( $L/R=2.81$  TO  $2.85$ )



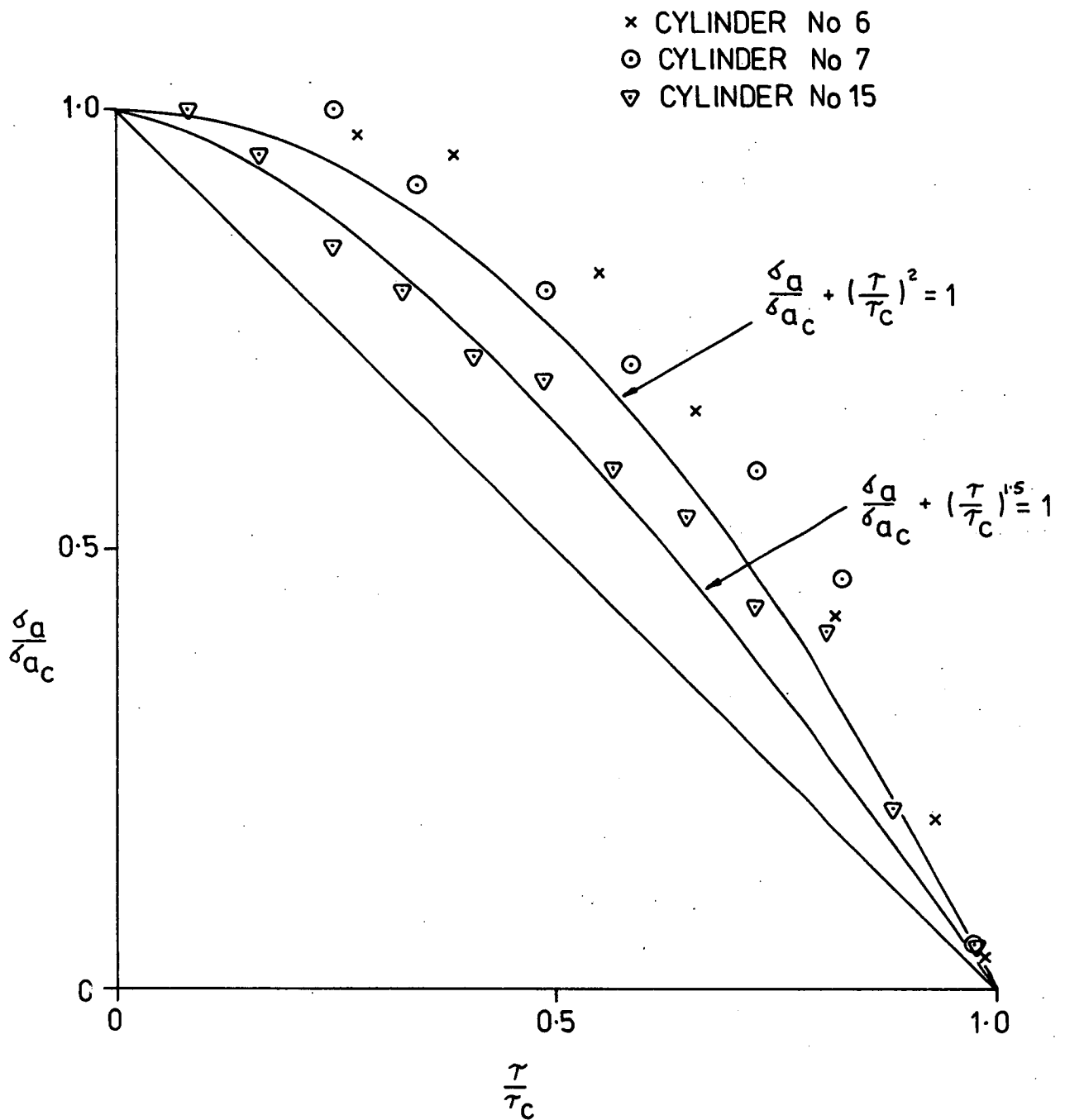


FIGURE A 3

BUCKLING STRESS STATE DIAGRAM FOR AXIAL  
COMPRESSION - TORSION INTERACTION IN LONGER  
CYLINDERS ( $L/R=5.68$ )

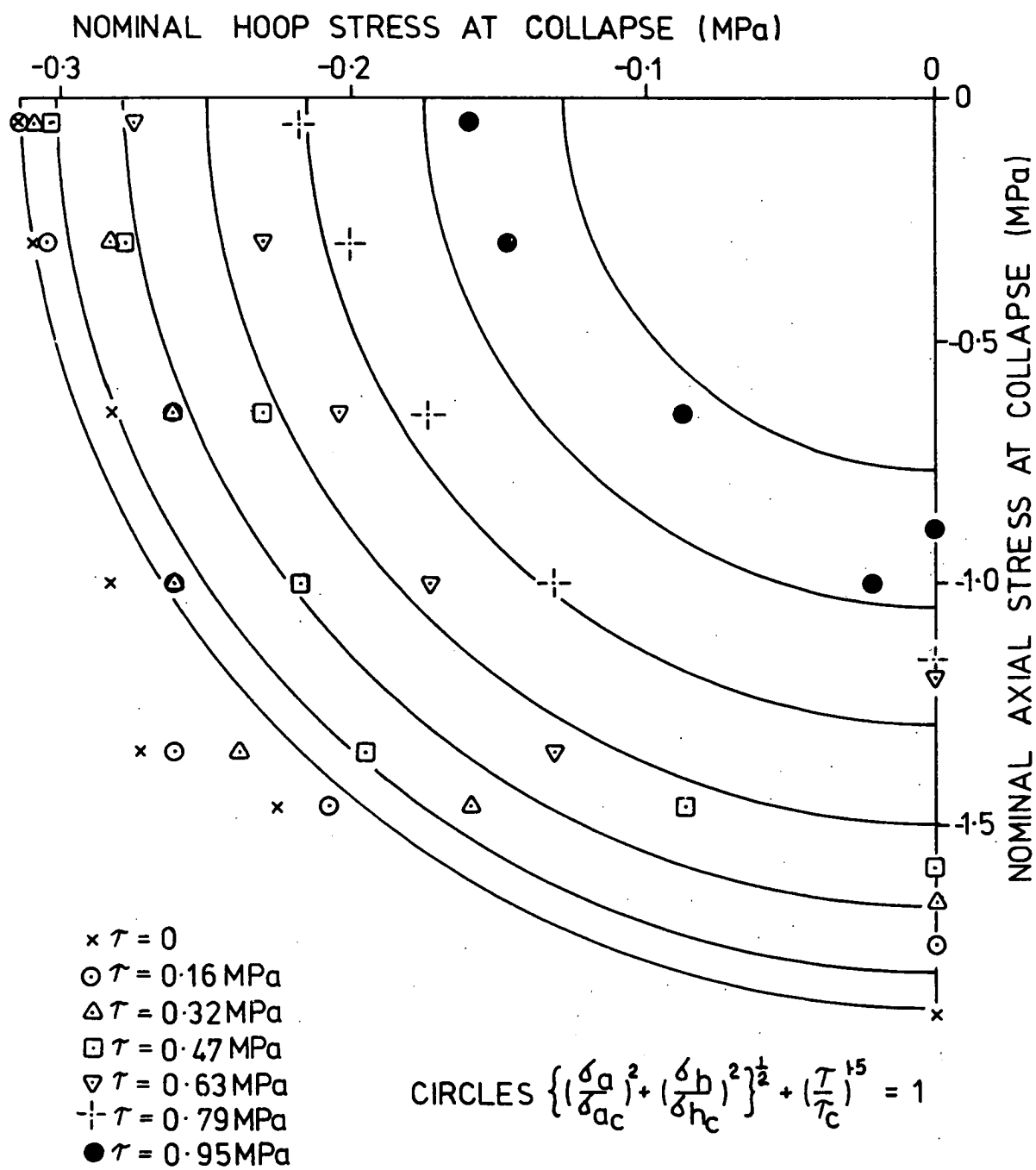


FIGURE A4

BUCKLING STRESS STATE DIAGRAM

INTERACTION OF BUCKLING MODES-CYLINDER No 2

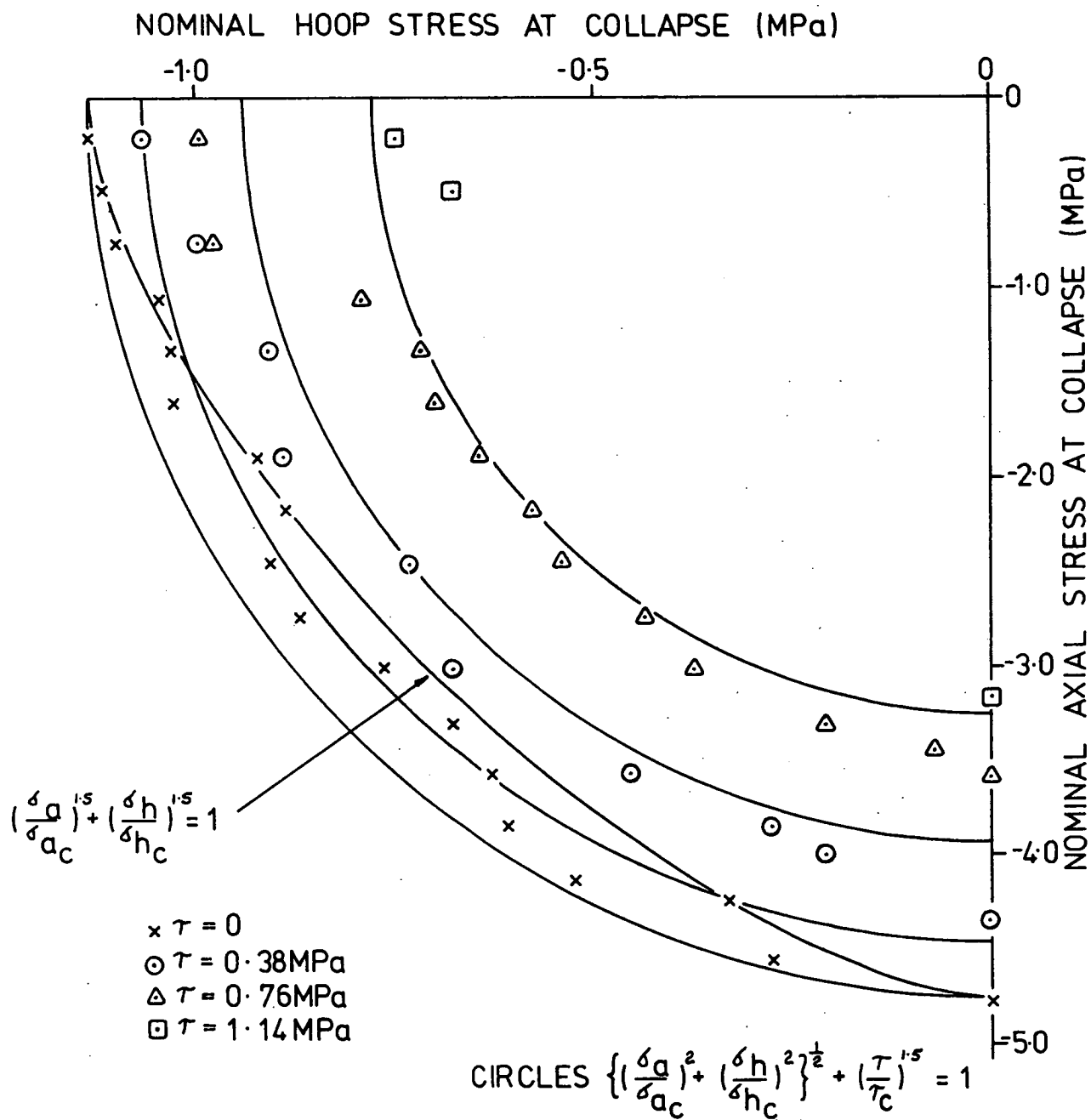
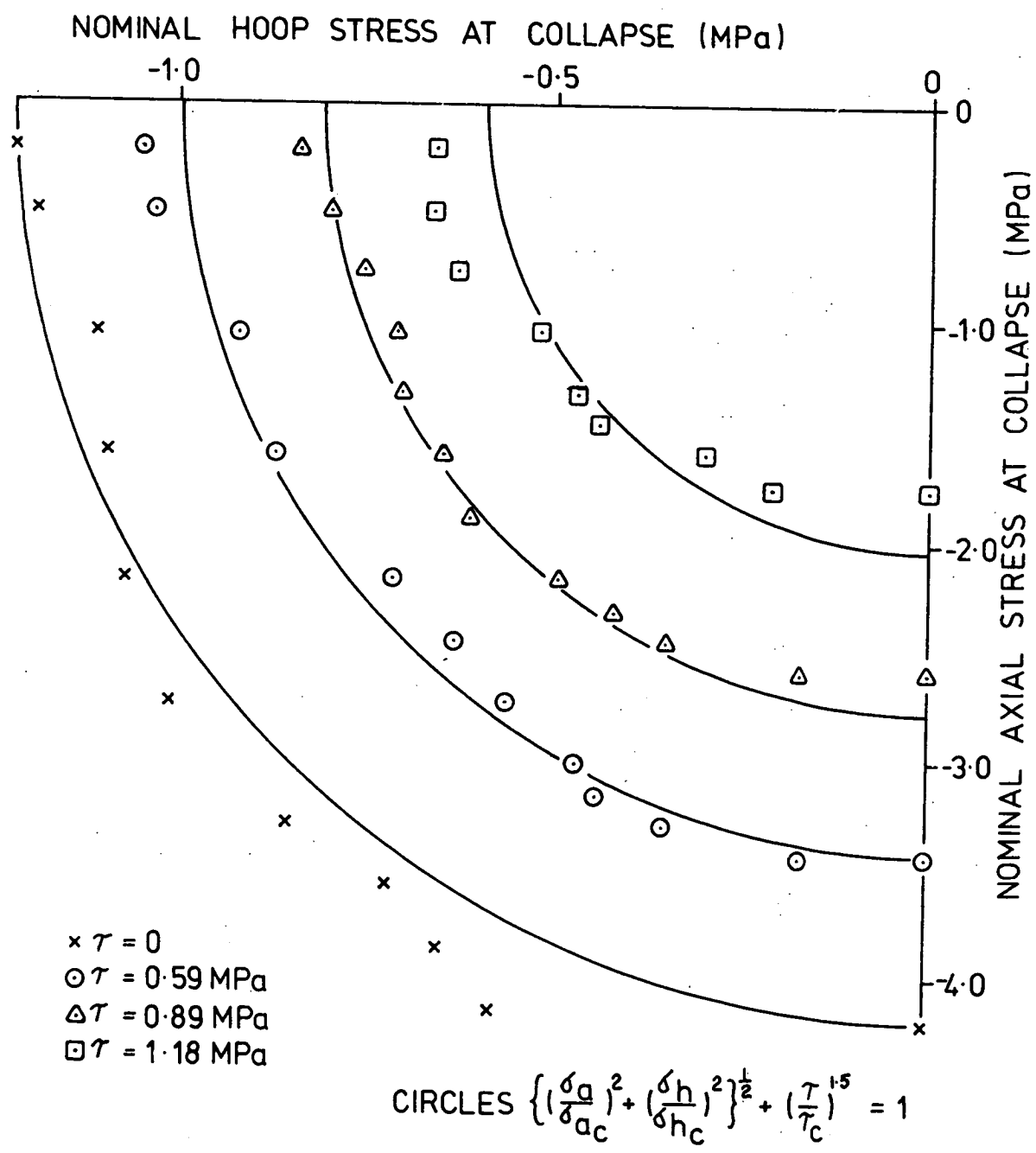
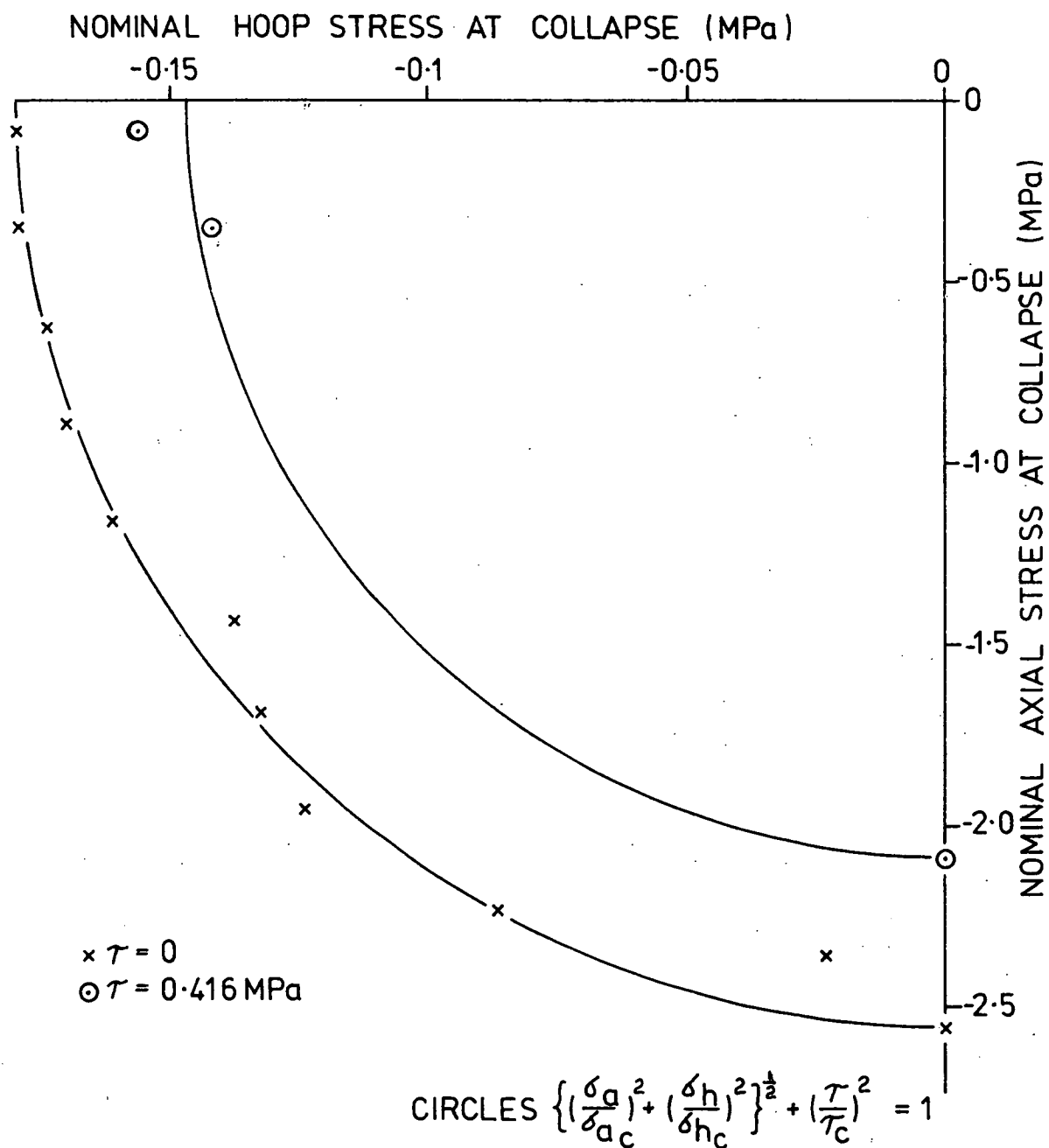


FIGURE A 5

BUCKLING STRESS STATE DIAGRAM  
INTERACTION OF BUCKLING MODES-CYLINDER No 3



**FIGURE A6**  
**BUCKLING STRESS STATE DIAGRAM**  
**INTERACTION OF BUCKLING MODES - CYLINDER No 5**



**FIGURE A7**  
**BUCKLING STRESS STATE DIAGRAM**  
**INTERACTION OF BUCKLING MODES-CYLINDER No 6**

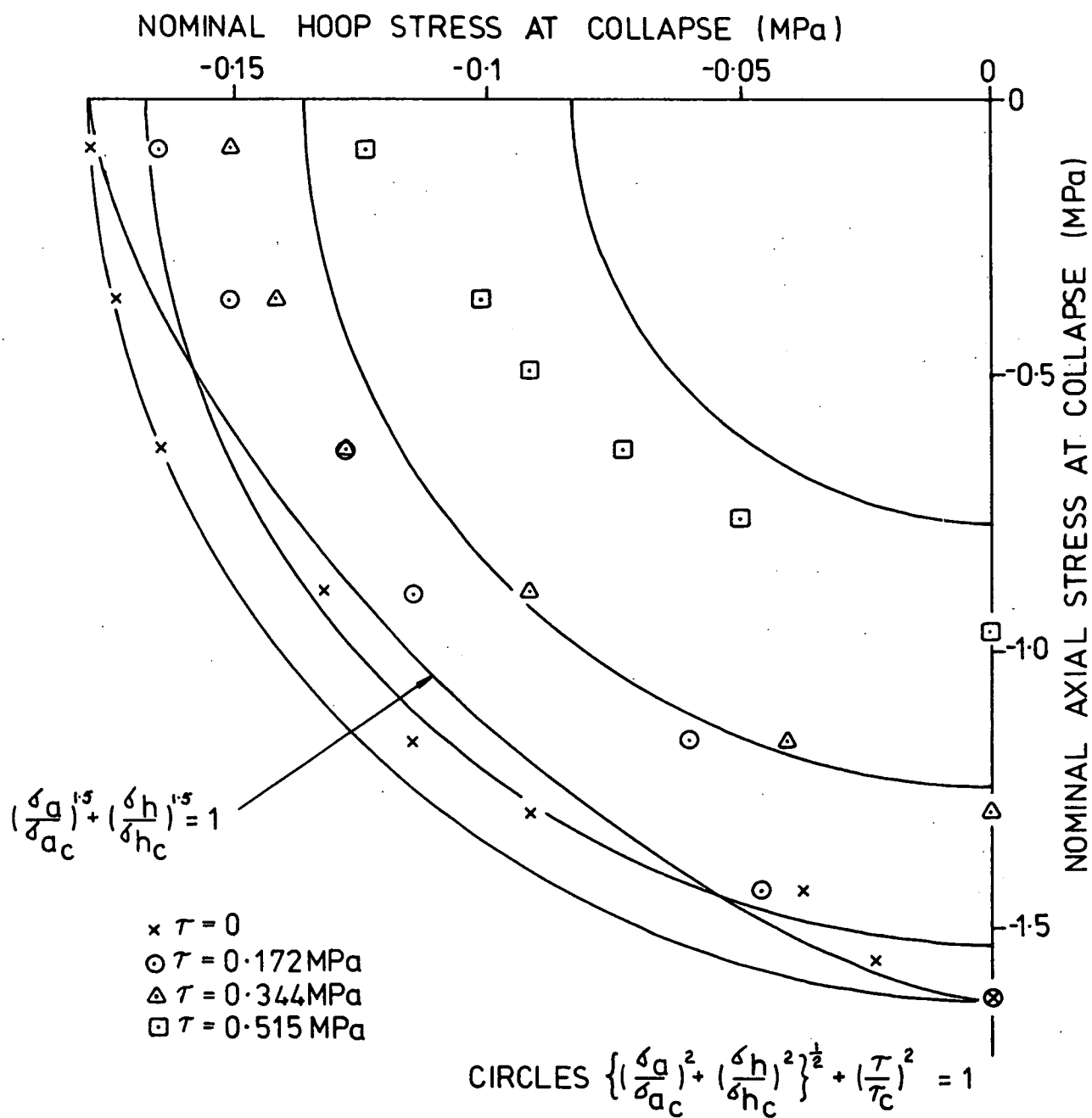
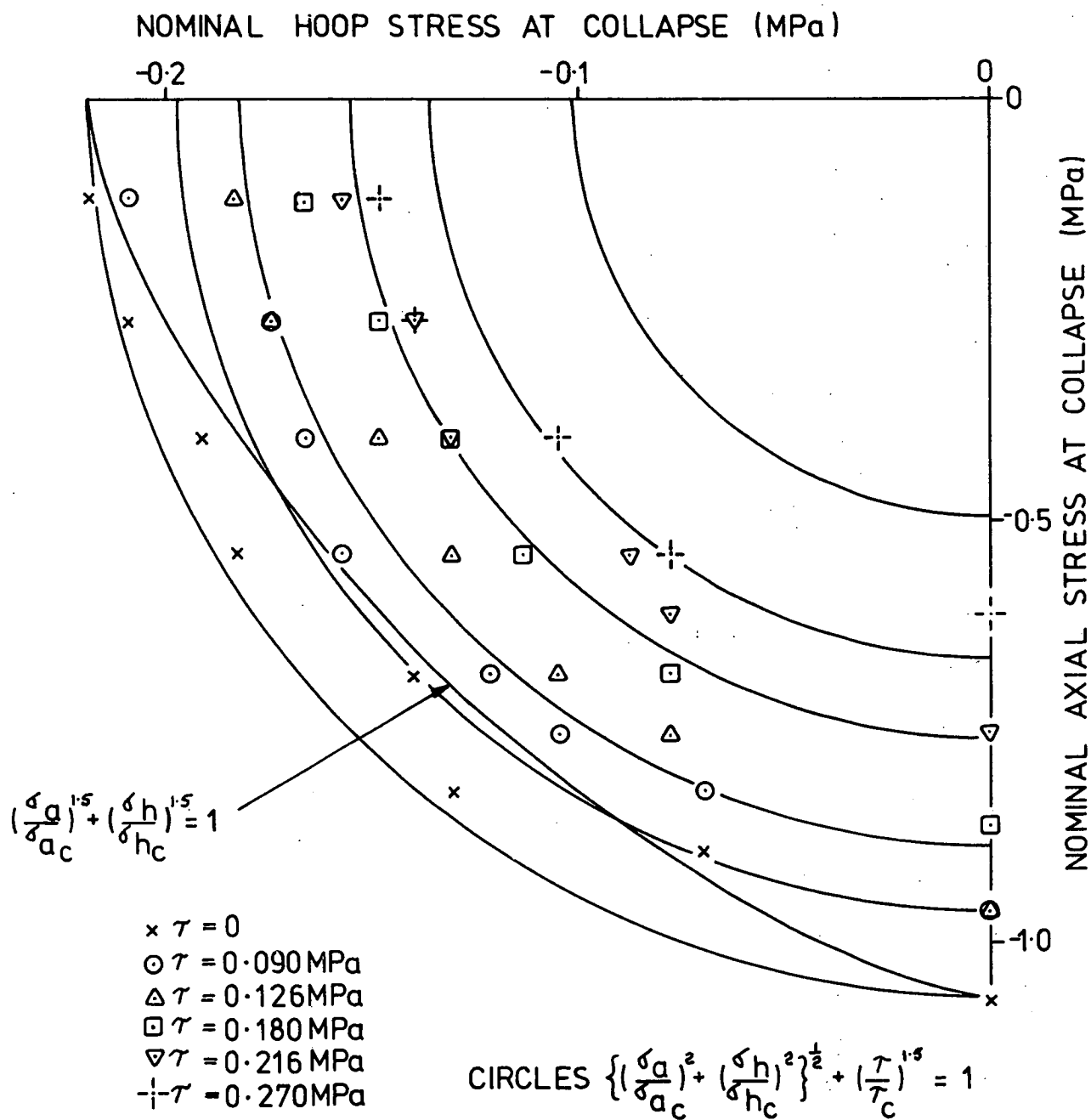


FIGURE A8

BUCKLING STRESS STATE DIAGRAM  
INTERACTION OF BUCKLING MODES-CYLINDER No 7



**FIGURE A9**  
**BUCKLING STRESS STATE DIAGRAM**  
**INTERACTION OF BUCKLING MODES - CYLINDER No 8**

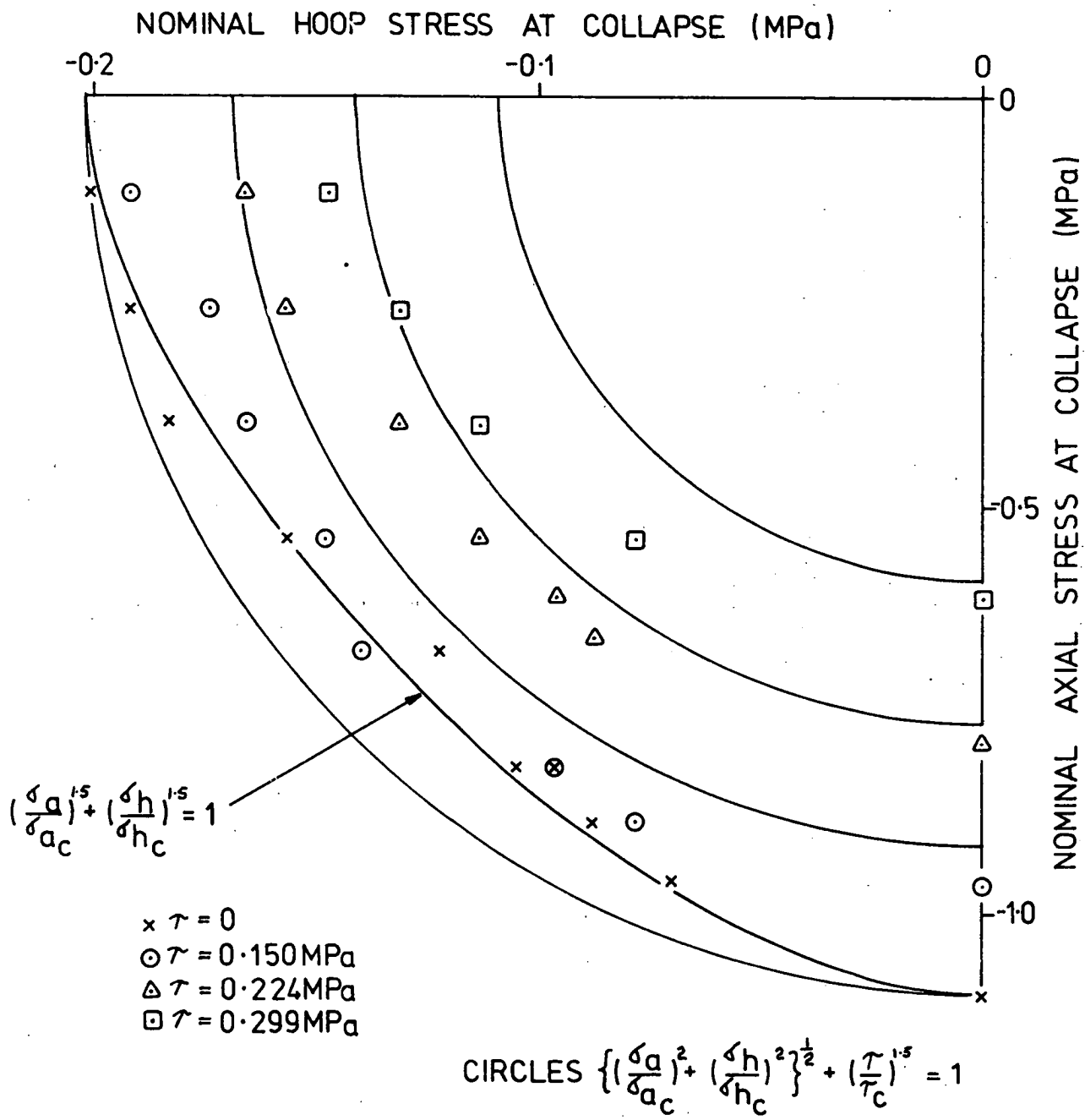


FIGURE A10

BUCKLING STRESS STATE DIAGRAM

INTERACTION OF BUCKLING MODES-CYLINDER No9



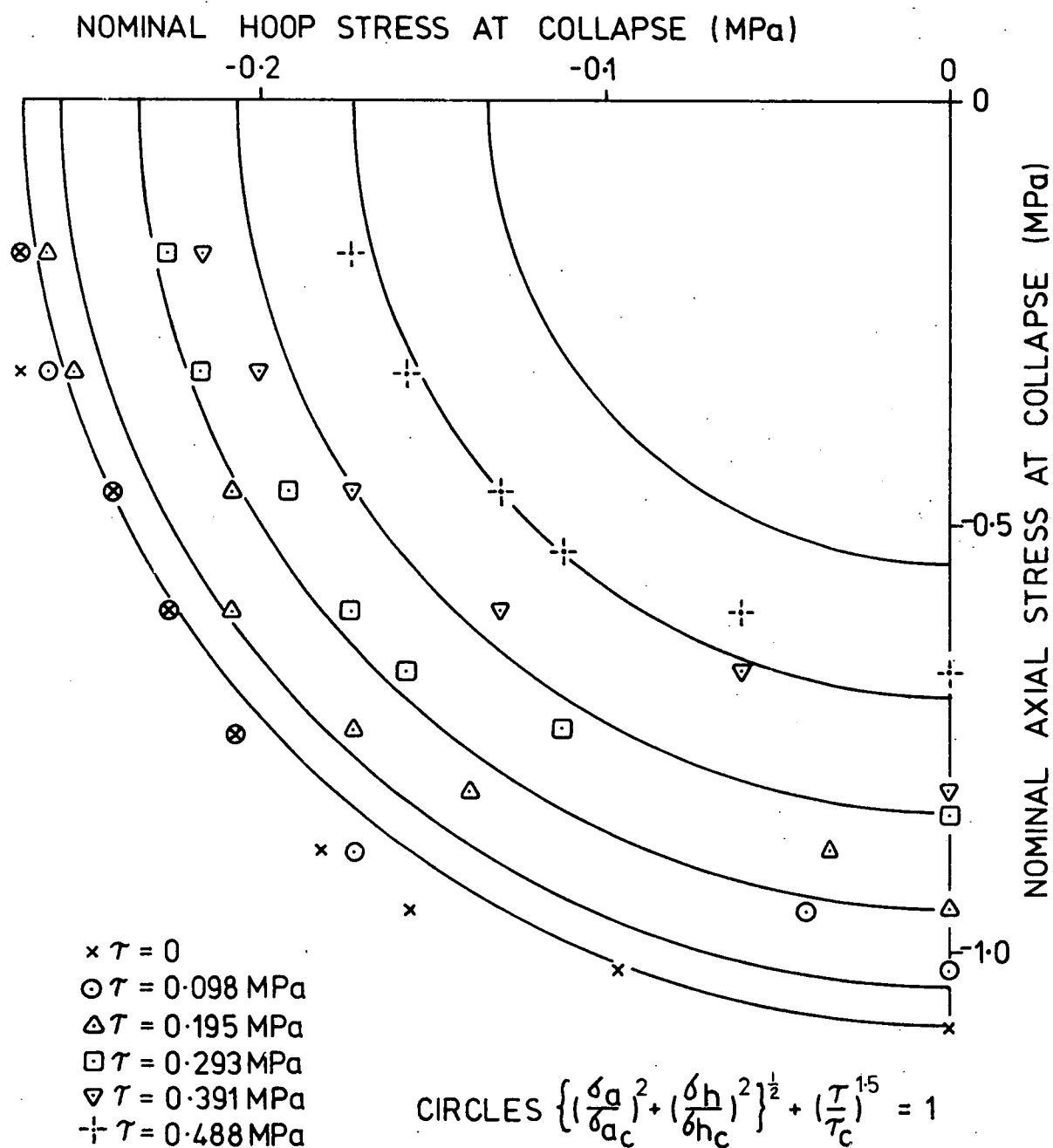


FIGURE A11

BUCKLING STRESS STATE DIAGRAM  
INTERACTION OF BUCKLING MODES-CYLINDER No 12

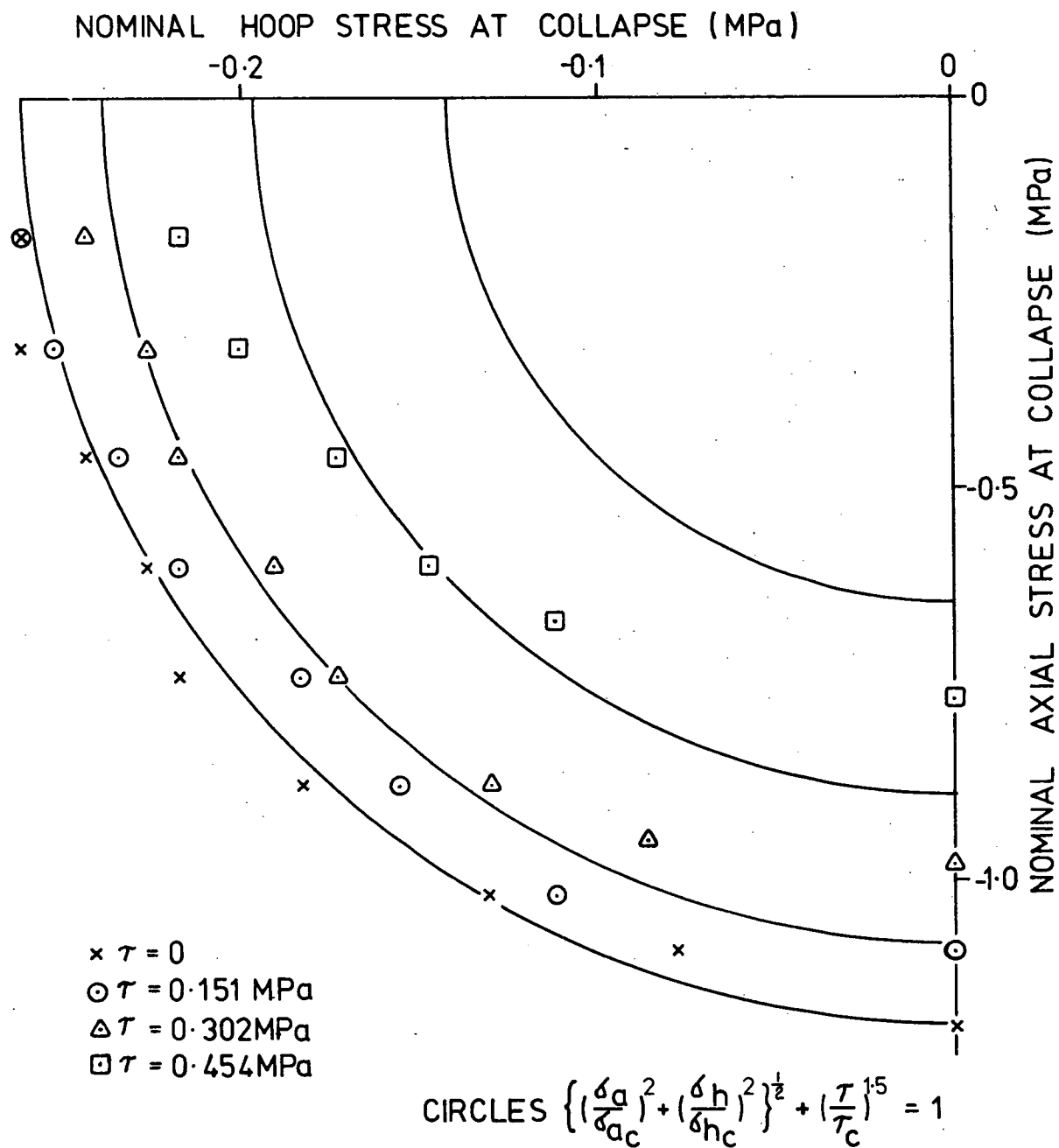


FIGURE A12

BUCKLING STRESS STATE DIAGRAMINTERACTION OF BUCKLING MODES CYLINDER No 13

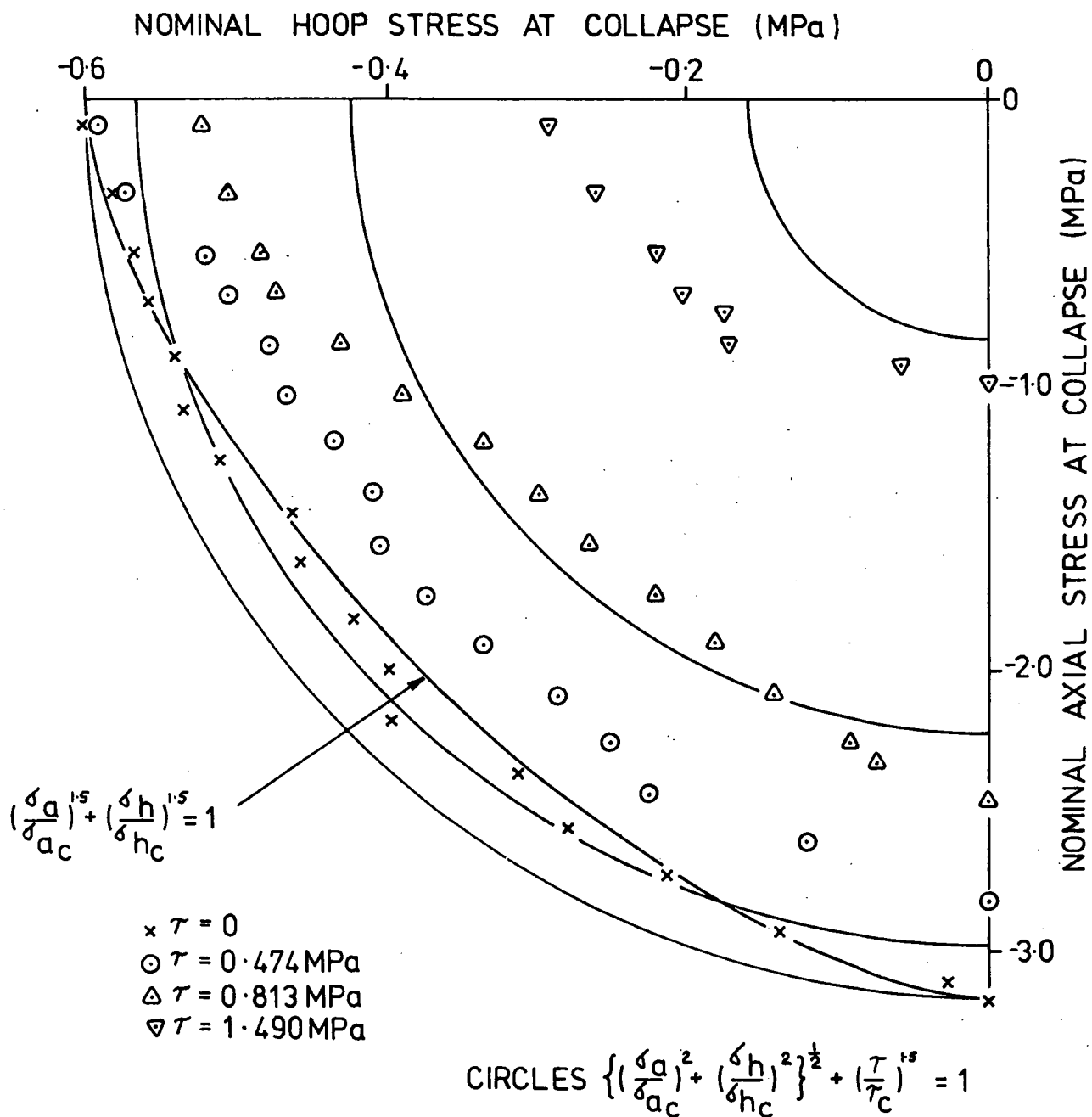


FIGURE A13

BUCKLING STRESS STATE DIAGRAM  
INTERACTION OF BUCKLING MODES-CYLINDER No 14

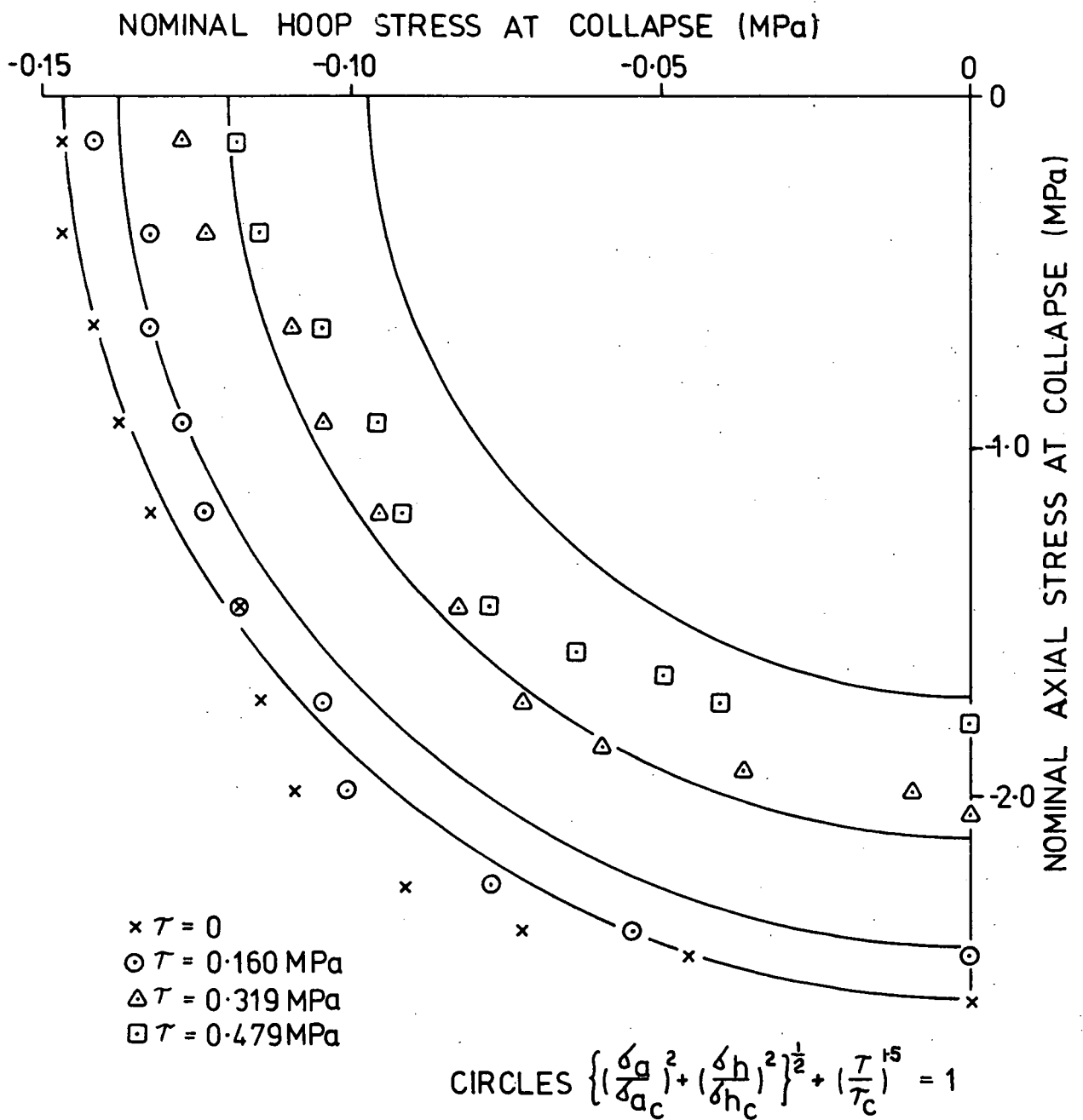
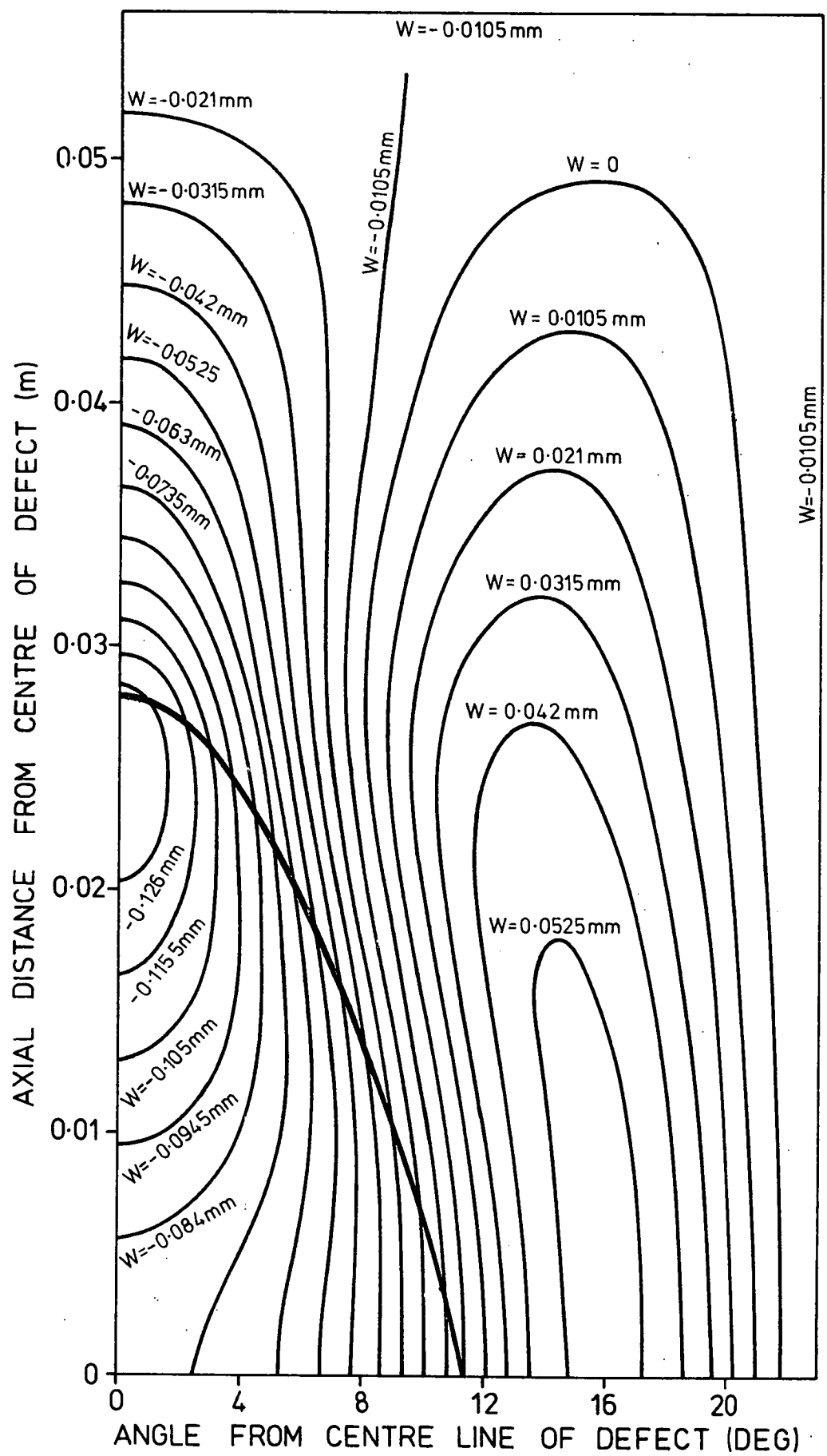


FIGURE A14

BUCKLING STRESS STATE DIAGRAM  
INTERACTION OF BUCKLING MODES-CYLINDER No 15

APPENDIX    B

RESULTS OF FINITE DIFFERENCE SOLUTION OF THE PARTIAL  
DIFFERENTIAL EQUATIONS.



**FIGURE B1**

**CONTOURS OF CONSTANT RADIAL DISPLACEMENT**  
**SOLUTION OF DONNELL'S EQUATIONS**

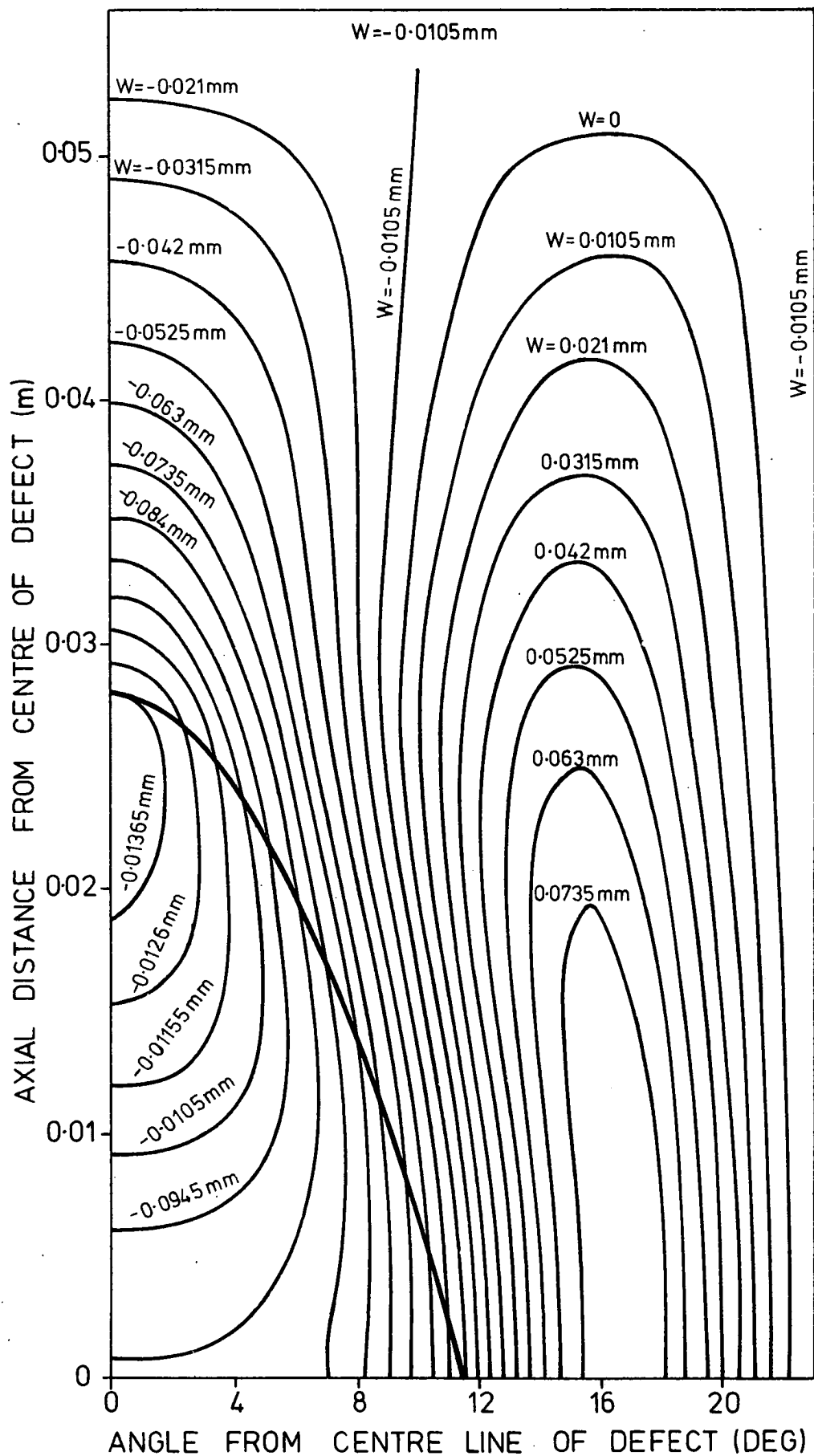


FIGURE B2

CONTOURS OF CONSTANT RADIAL DISPLACEMENT

TIMOSHENKO'S EQUATIONS WITH DONNELL'S RESULTANTS

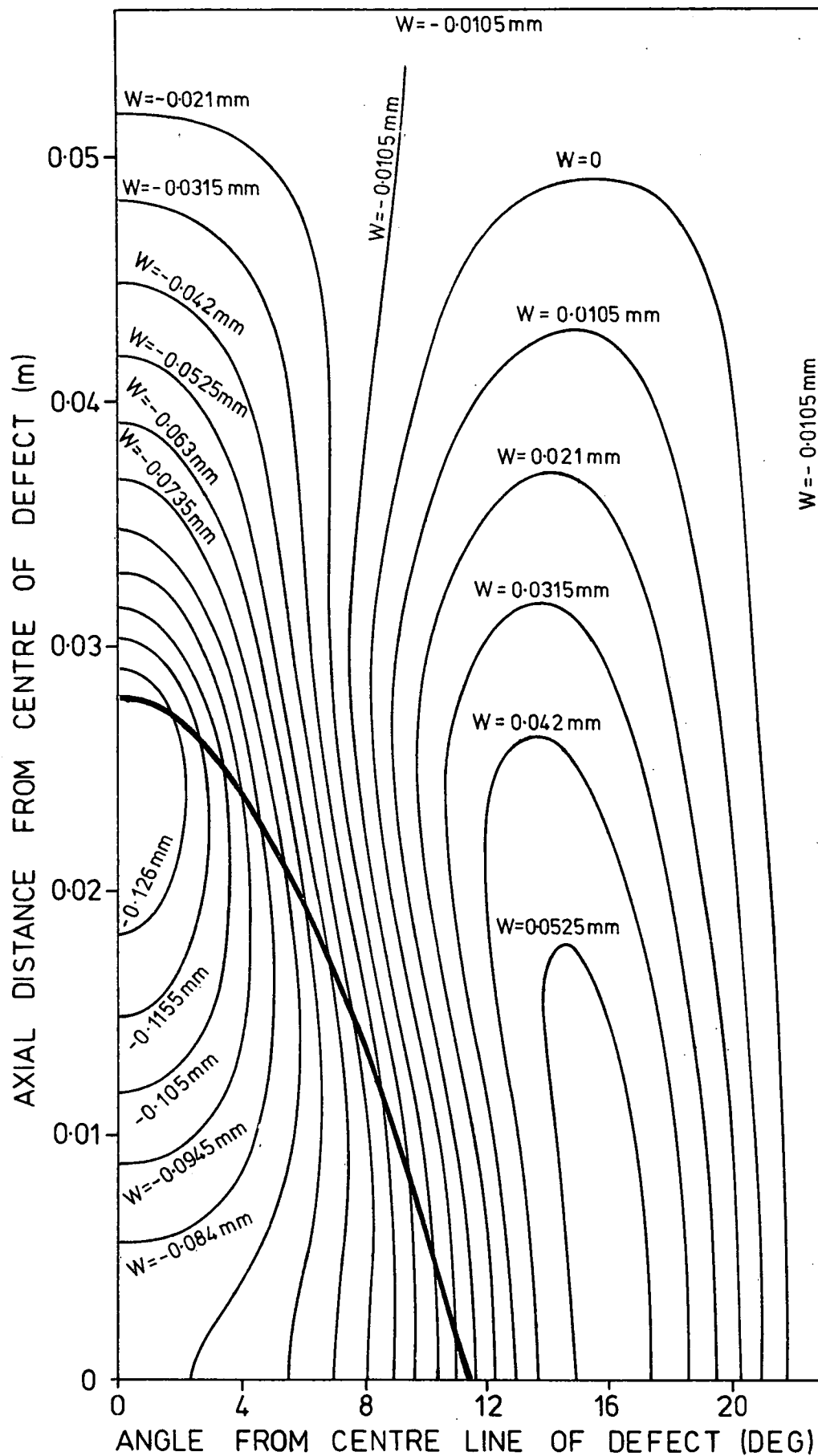
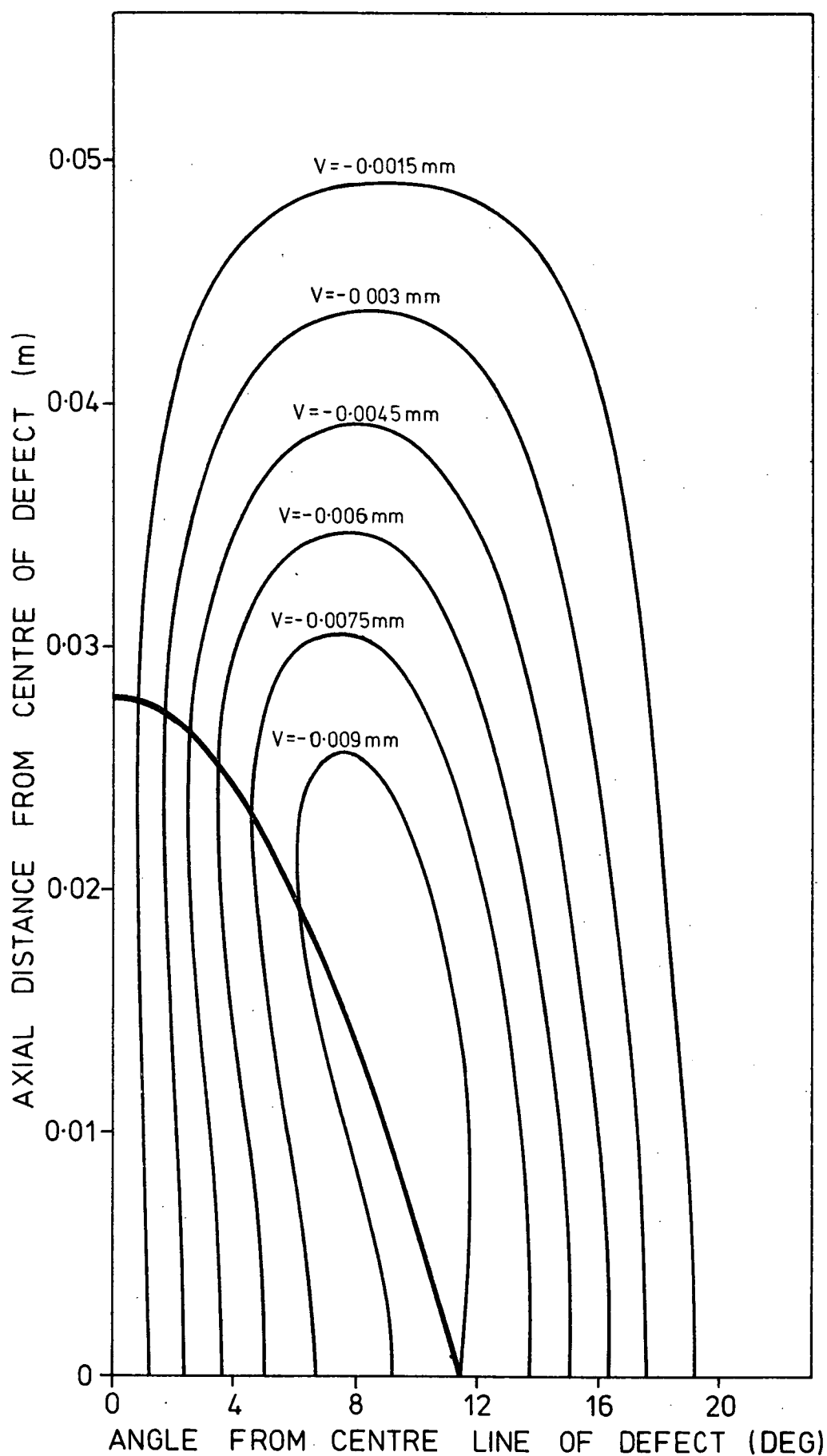


FIGURE B3

CONTOURS OF CONSTANT RADIAL DISPLACEMENT

TIMOSHENKO'S EQUATIONS - RESULTANTS WITHOUT PRODUCTS OF SLOPES





**FIGURE B4**

**CONTOURS OF CONSTANT TANGENTIAL DISPLACEMENT**

SOLUTION OF DONNELL'S EQUATIONS

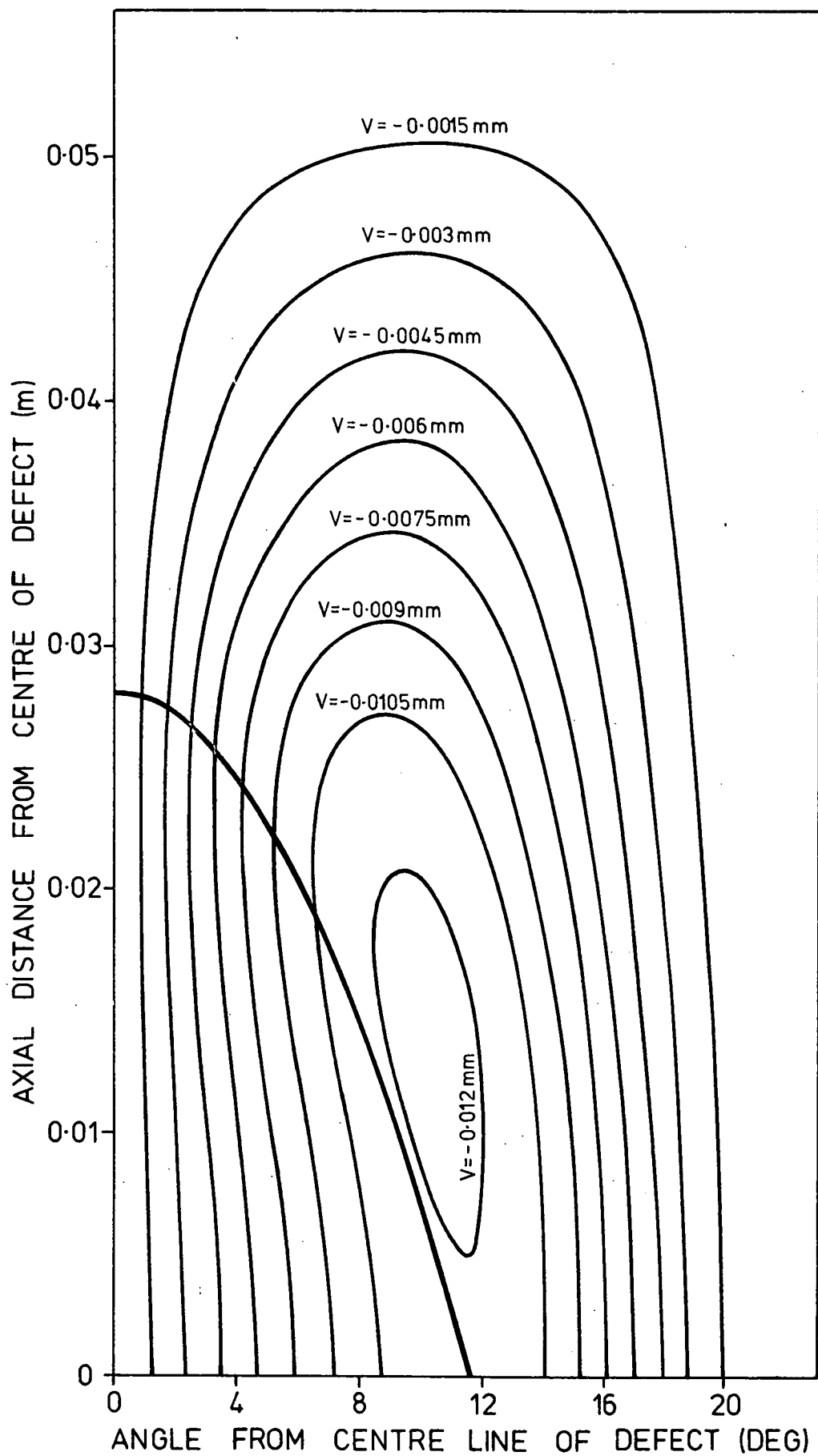


**FIGURE B5**

**CONTOURS OF CONSTANT TANGENTIAL DISPLACEMENT**

TIMOSHENKO'S EQUATIONS WITH DONNELL'S RESULTANTS

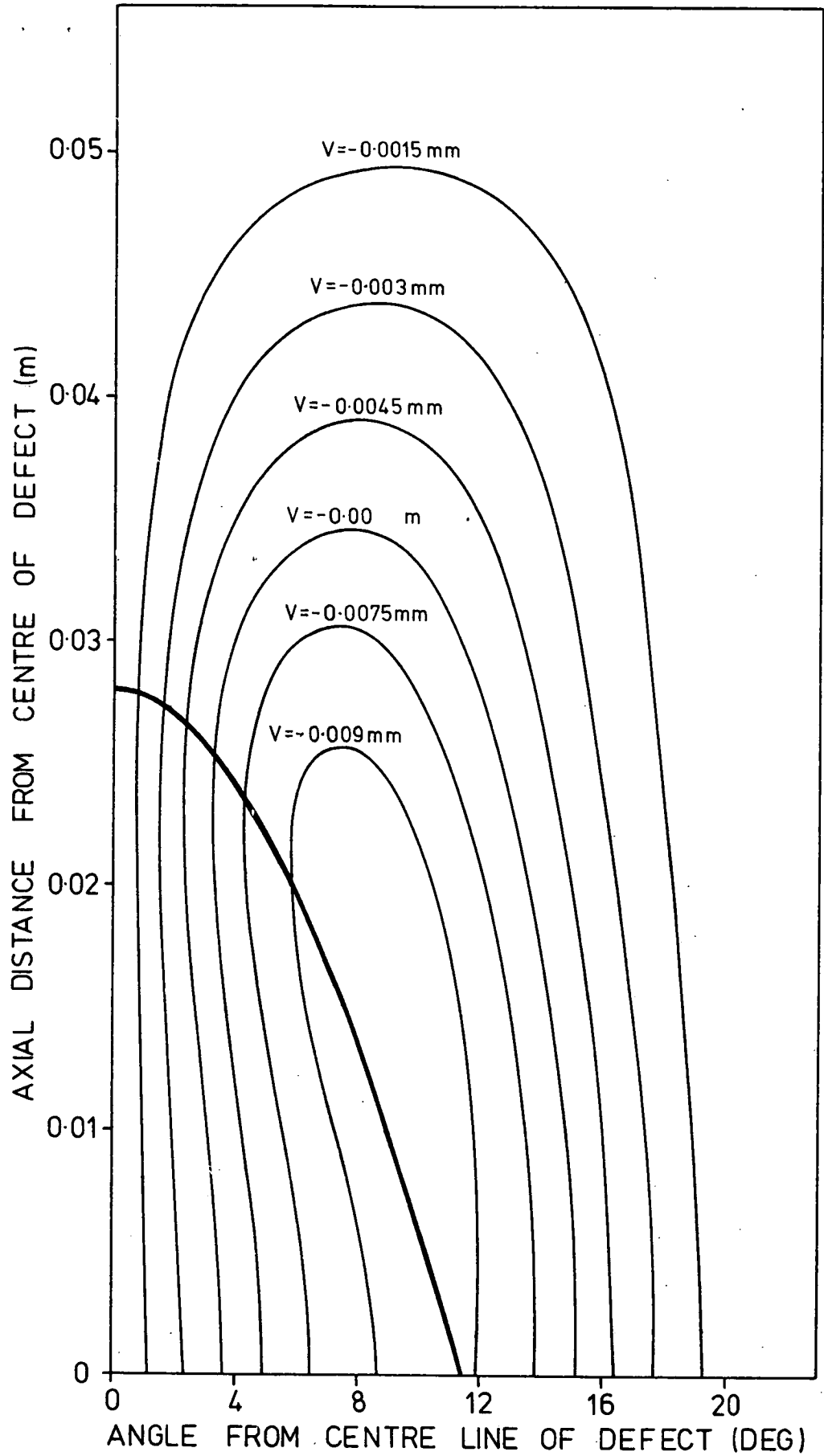


**FIGURE B6**

**CONTOURS OF CONSTANT TANGENTIAL DISPLACEMENT**

TIMOSHENKO'S EQUATIONS - RESULTANTS WITHOUT PRODUCTS OF SLOPES

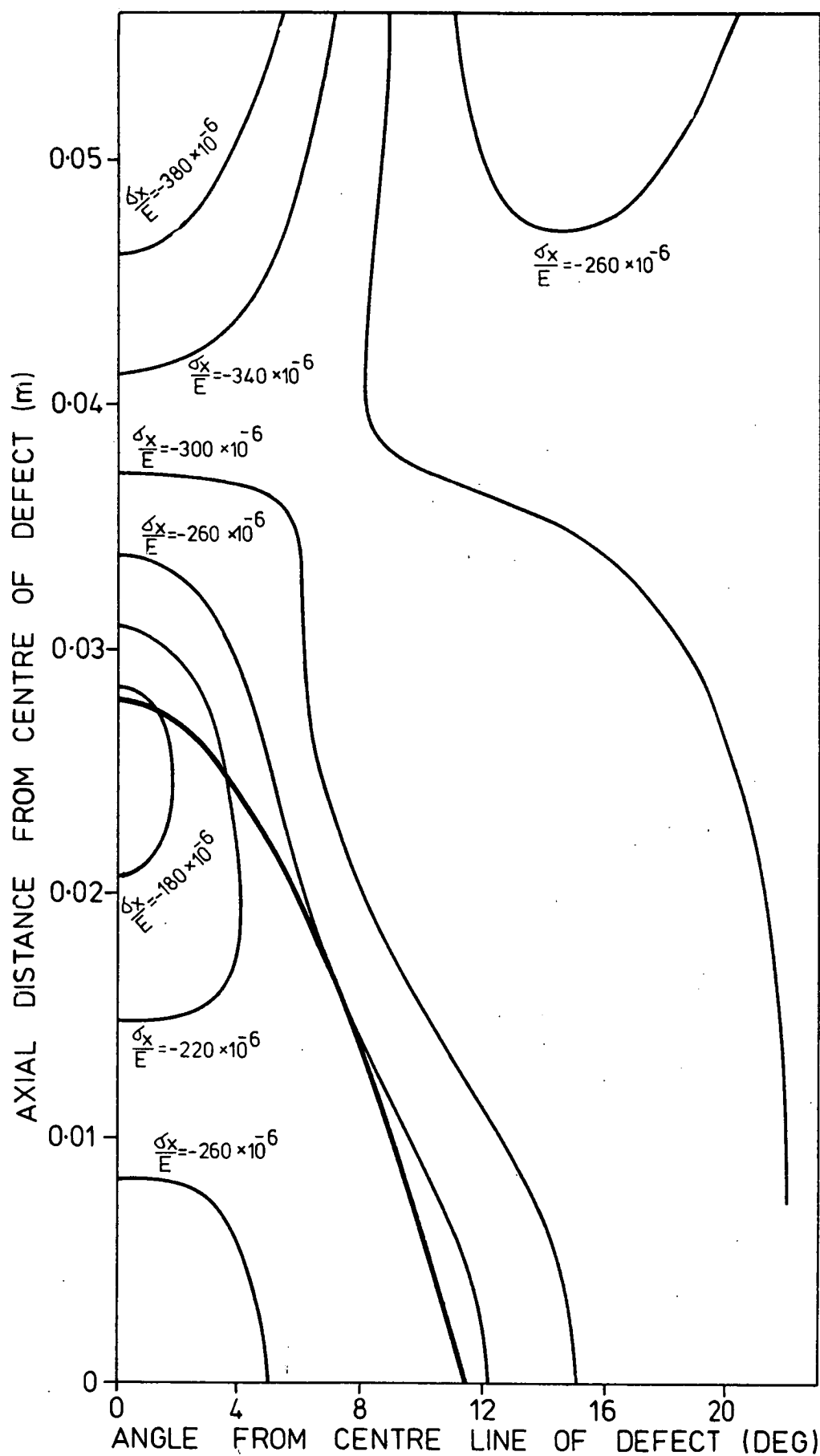


FIGURE B7

CONTOURS OF CONSTANT AXIAL STRESS

SOLUTION OF DONNELL'S EQUATIONS

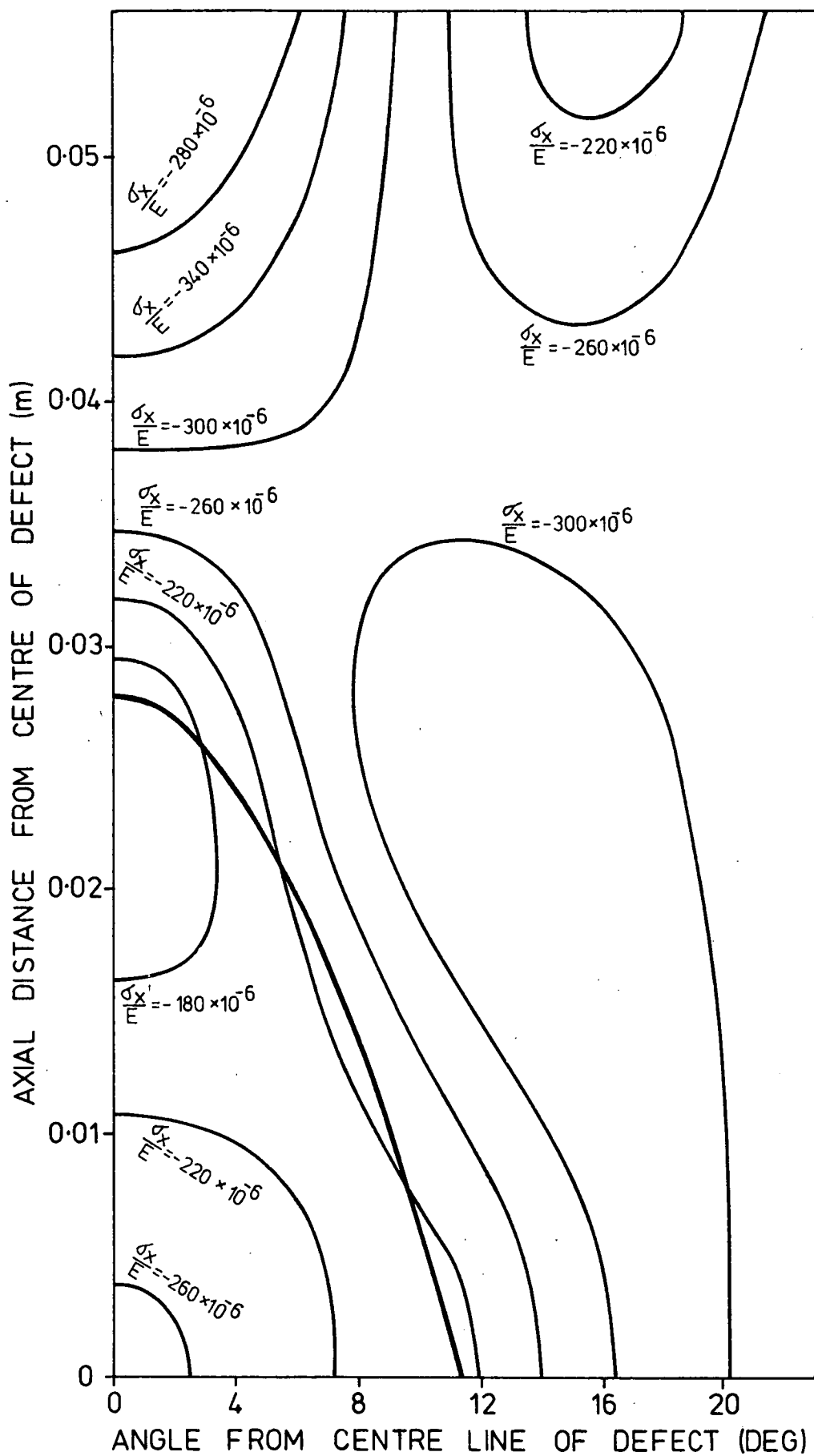


FIGURE B8

CONTOURS OF CONSTANT AXIAL STRESS

TIMOSHENKO'S EQUATIONS WITH DONNELL'S RESULTANTS

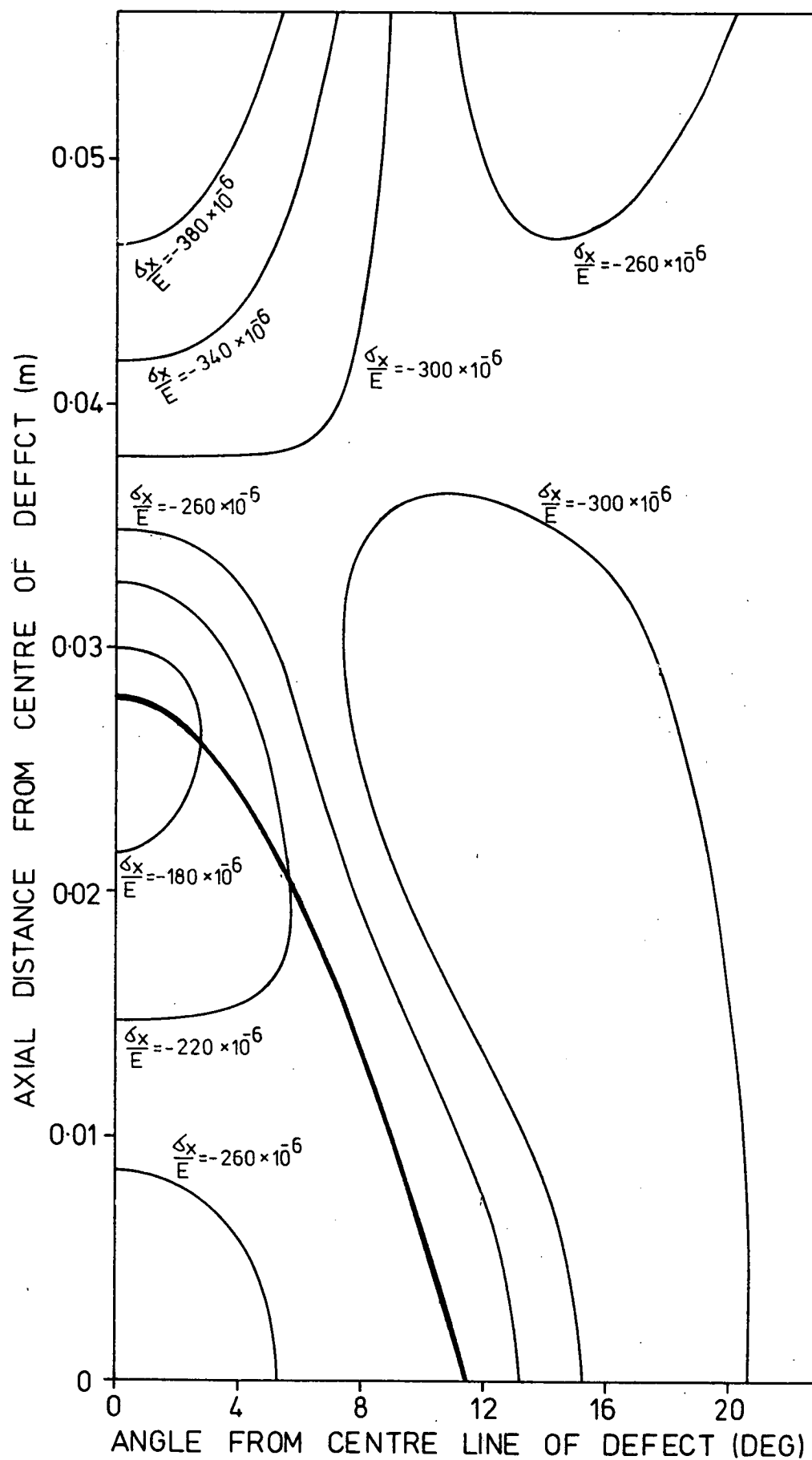
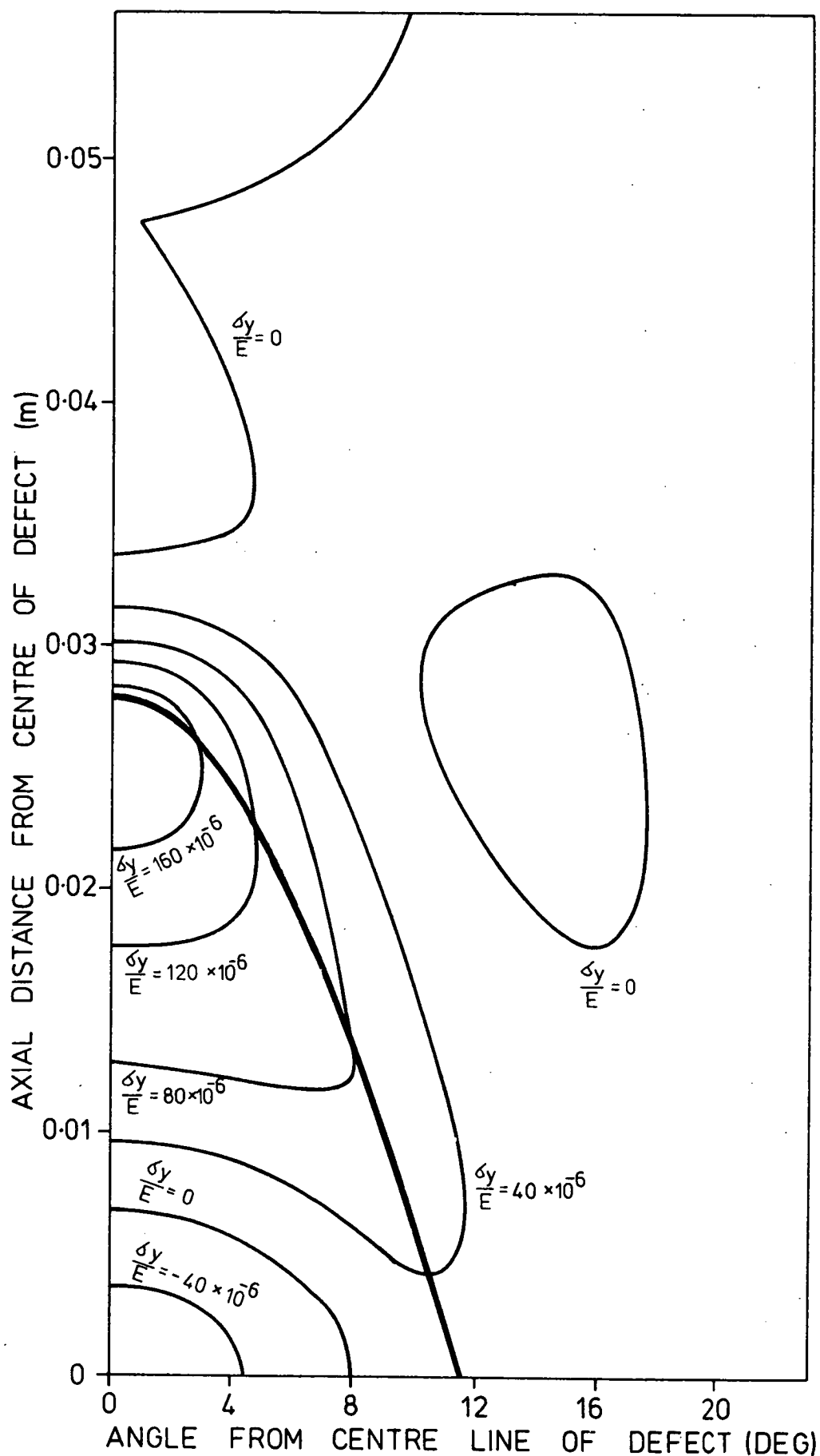


FIGURE B9

CONTOURS OF CONSTANT AXIAL STRESS

TIMOSHENKO'S EQUATIONS-RESULTANTS WITHOUT PRODUCTS OF SLOPES



**FIGURE B10**

**CONTOURS OF CONSTANT TANGENTIAL STRESS**

SOLUTION OF DONNELL'S EQUATIONS

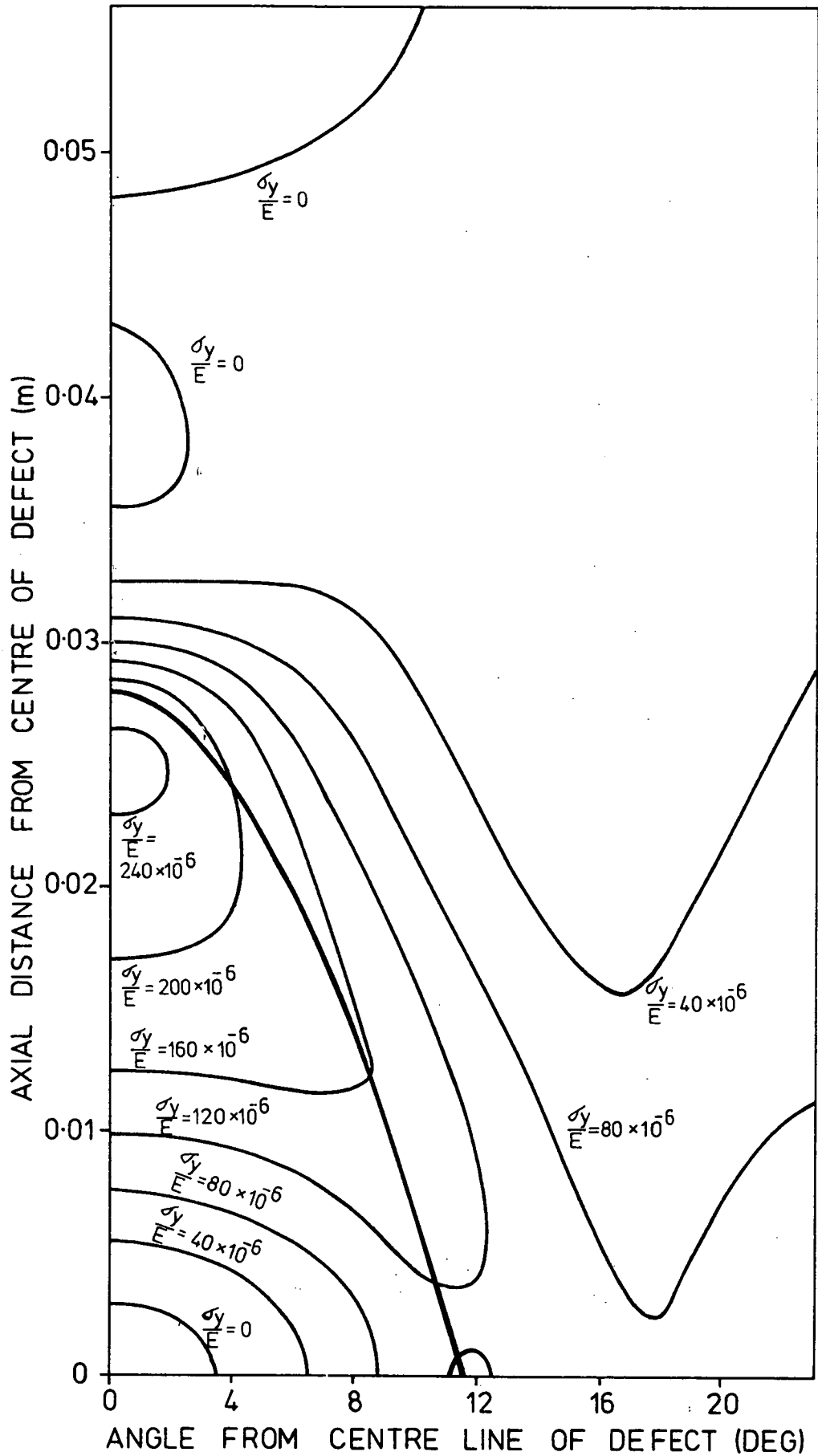


**FIGURE B11**

**CONTOURS OF CONSTANT TANGENTIAL STRESS**  
TIMOSHENKO'S EQUATIONS WITH DONNELL'S RESULTANTS



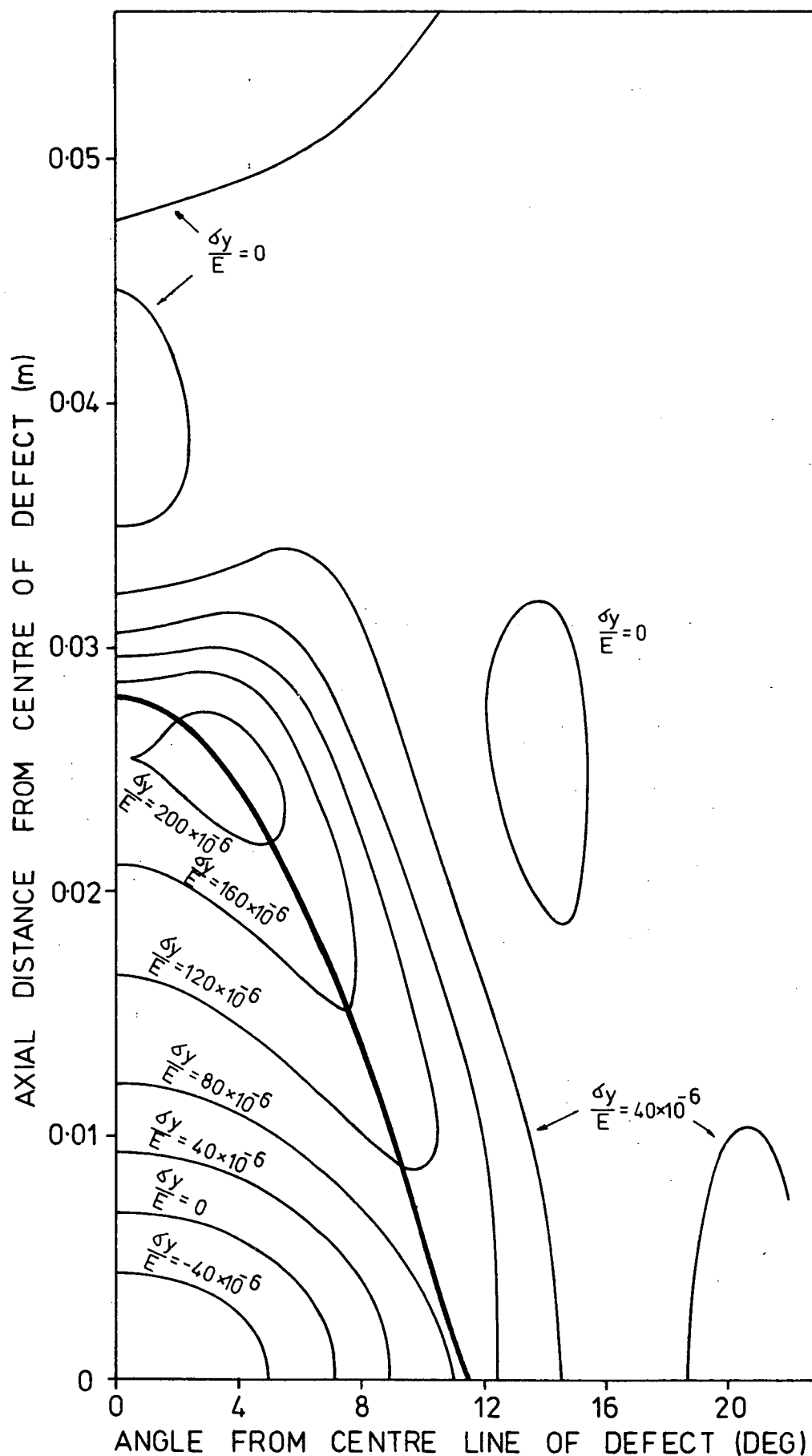
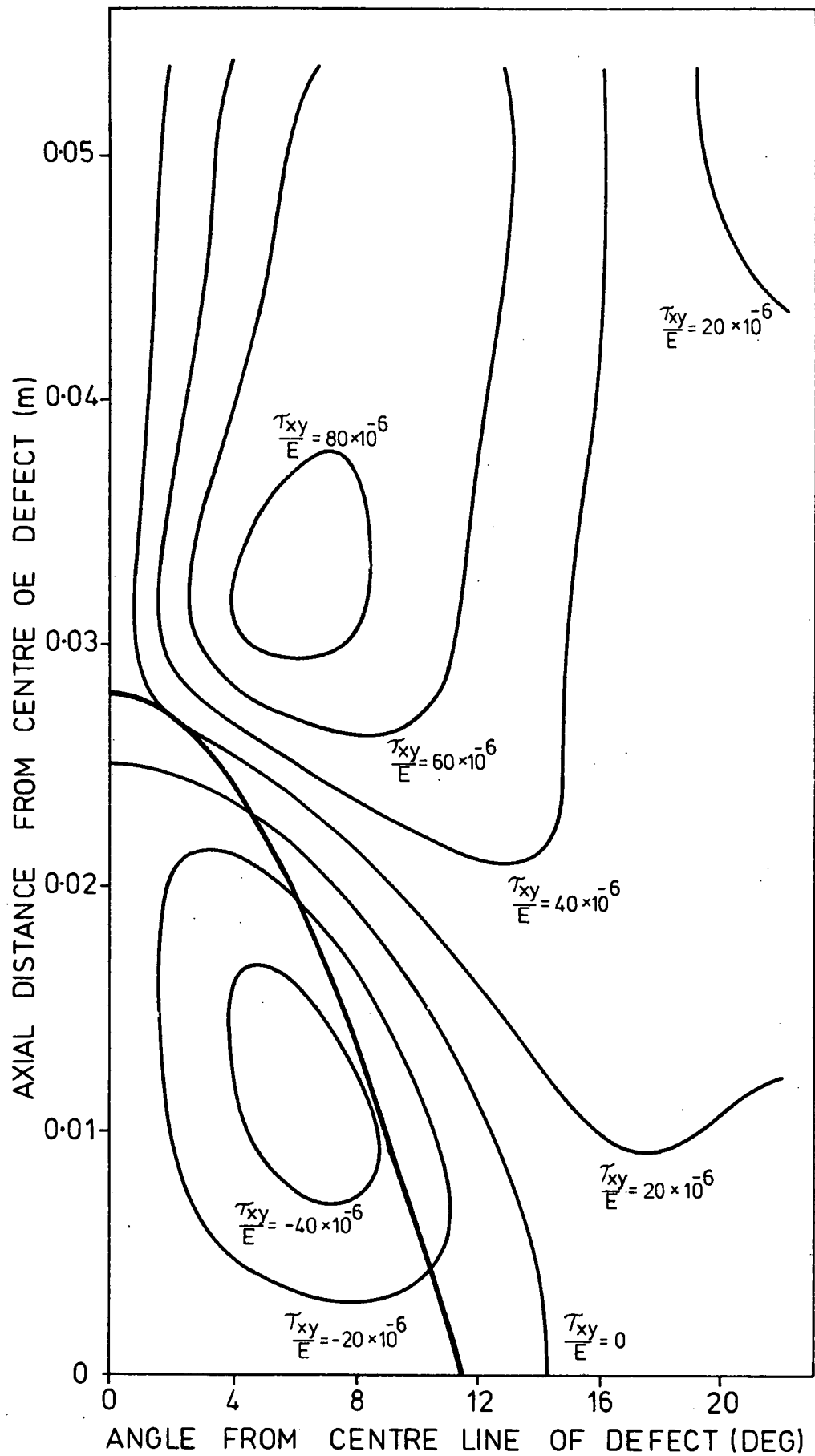


FIGURE B12

# CONTOURS OF CONSTANT TANGENTIAL STRESS

TIMOSHENKO'S EQUATIONS-RESULTANTS WITHOUT PRODUCTS OF SLOPES



**FIGURE B13**

**CONTOURS OF CONSTANT SHEAR STRESS**

SOLUTION OF DONNELL'S EQUATIONS

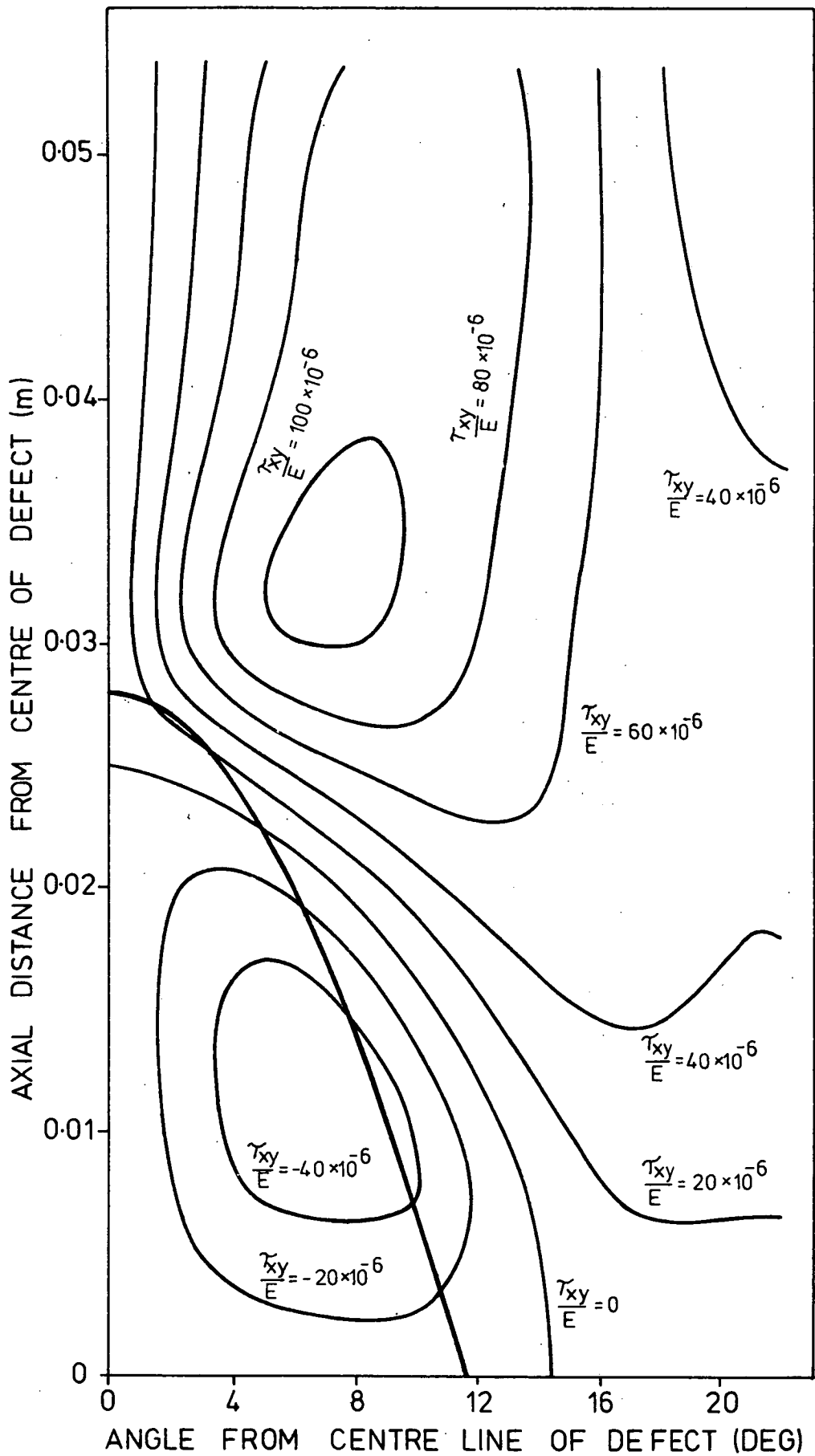


FIGURE B14

CONTOURS OF CONSTANT SHEAR STRESS  
TIMOSHENKO'S EQUATIONS WITH DONNELL'S RESULTANTS

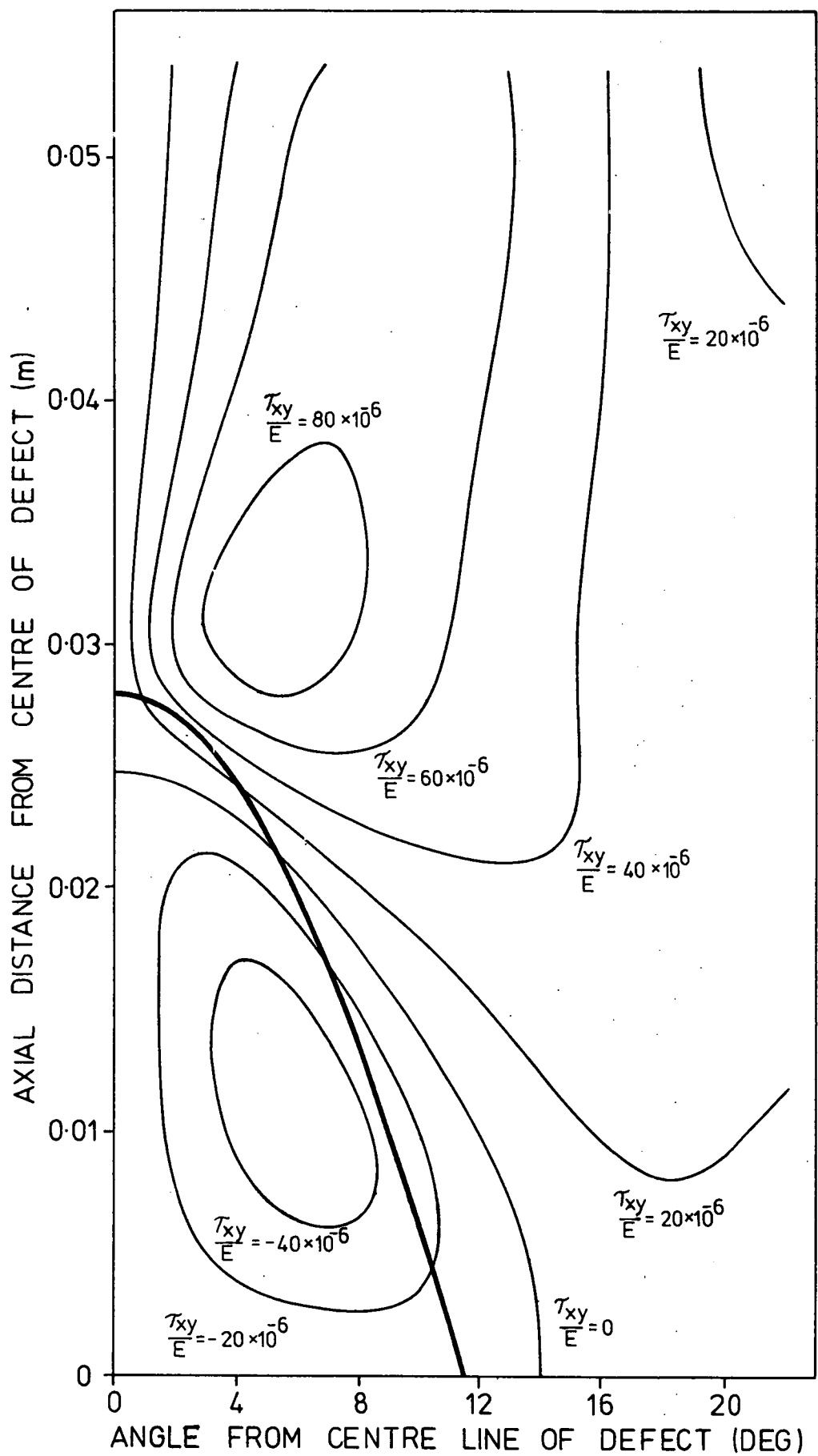


FIGURE B15

CONTOURS OF CONSTANT SHEAR STRESS

TIMOSHENKO'S EQUATIONS-RESULTANTS WITHOUT PRODUCTS OF SLOPES

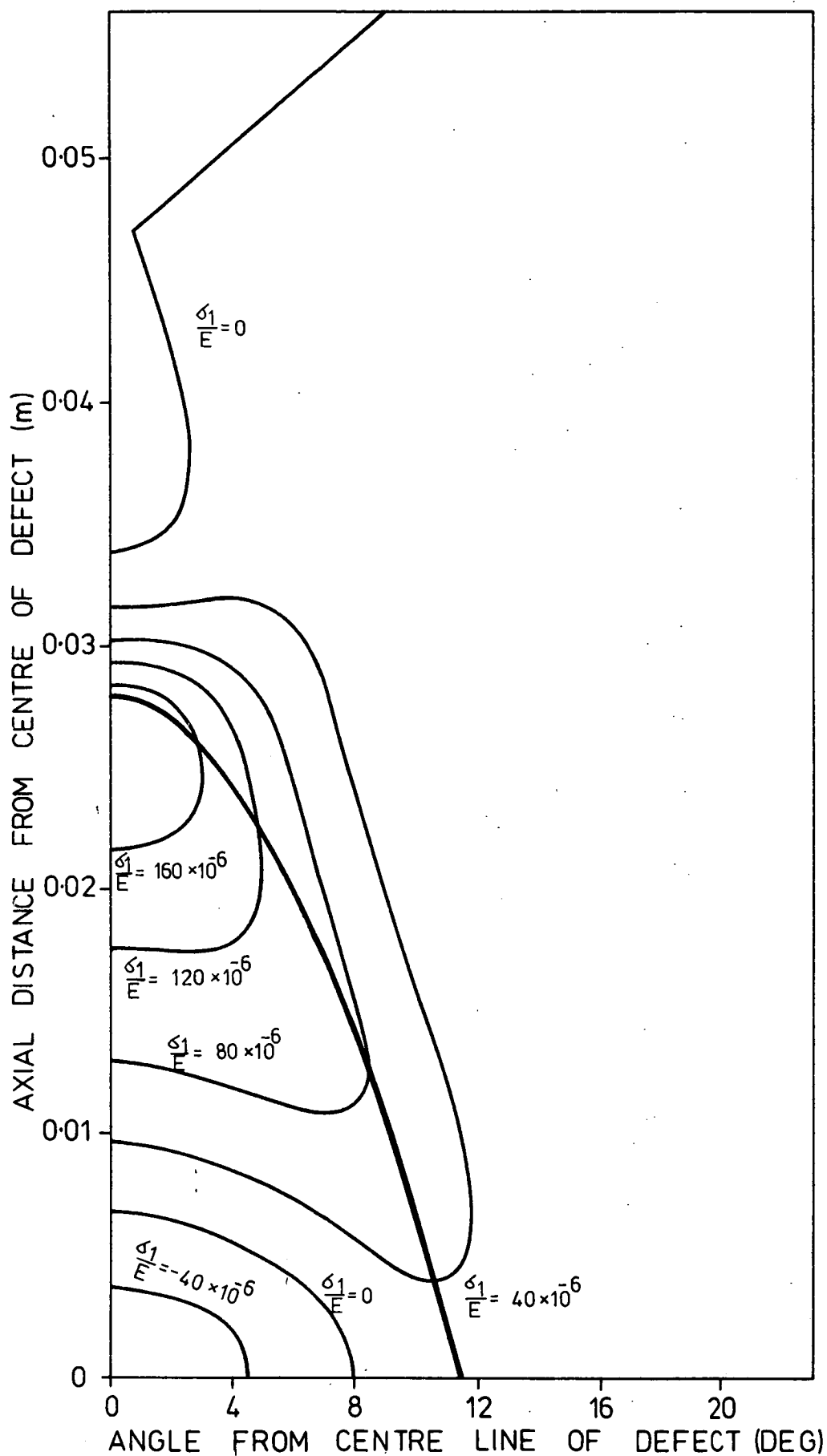


FIGURE B16

CONTOURS OF CONSTANT PRINCIPAL STRESS

SOLUTION OF DONNELL'S EQUATIONS

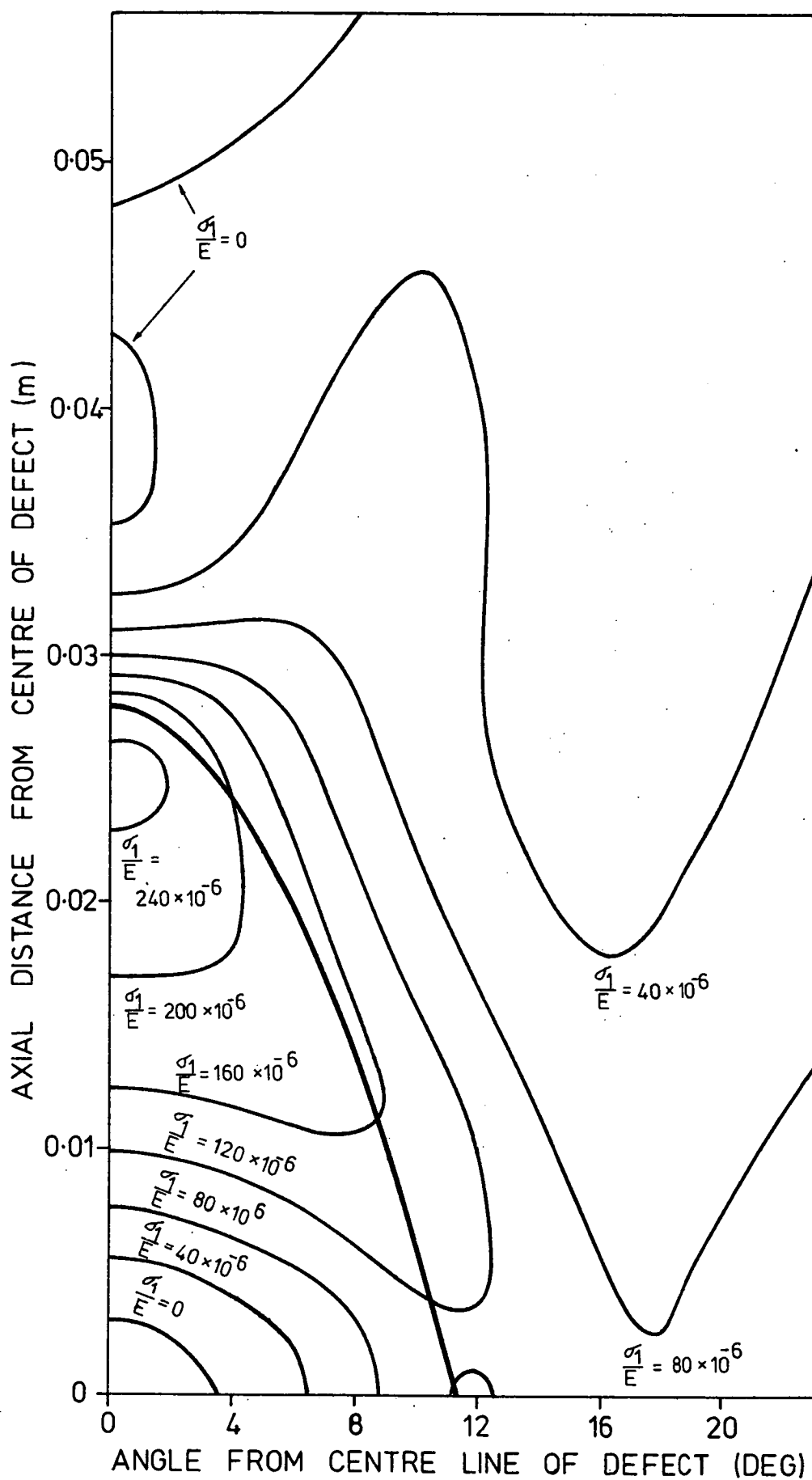


FIGURE B17

CONTOURS OF CONSTANT PRINCIPAL STRESS

TIMOSHENKO'S EQUATIONS WITH DONNELL'S RESULTANTS

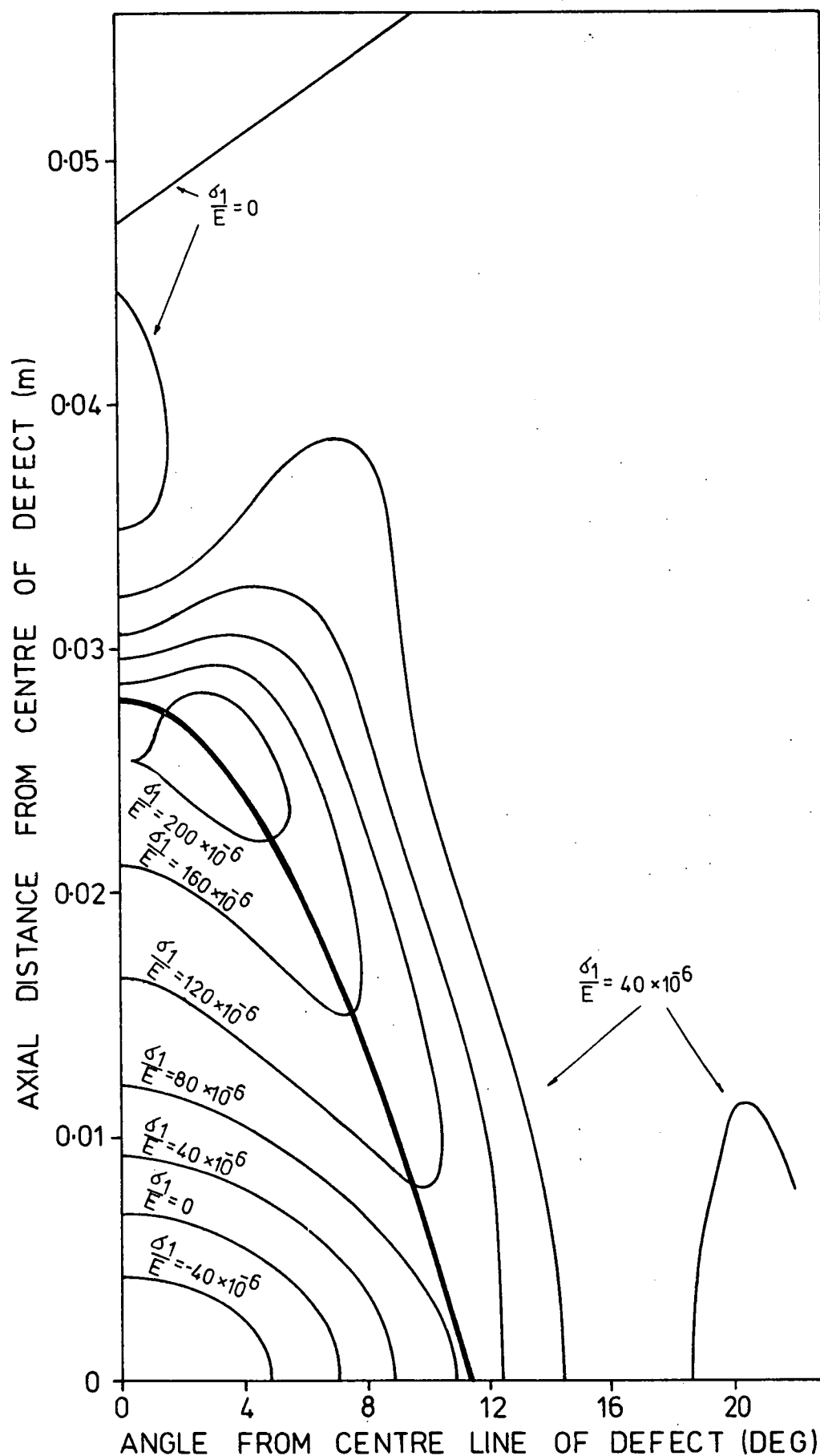


FIGURE B18

CONTOURS OF CONSTANT PRINCIPAL STRESS

TIMOSHENKO'S EQUATIONS-RESULTANTS WITHOUT PRODUCTS OF SLOPES

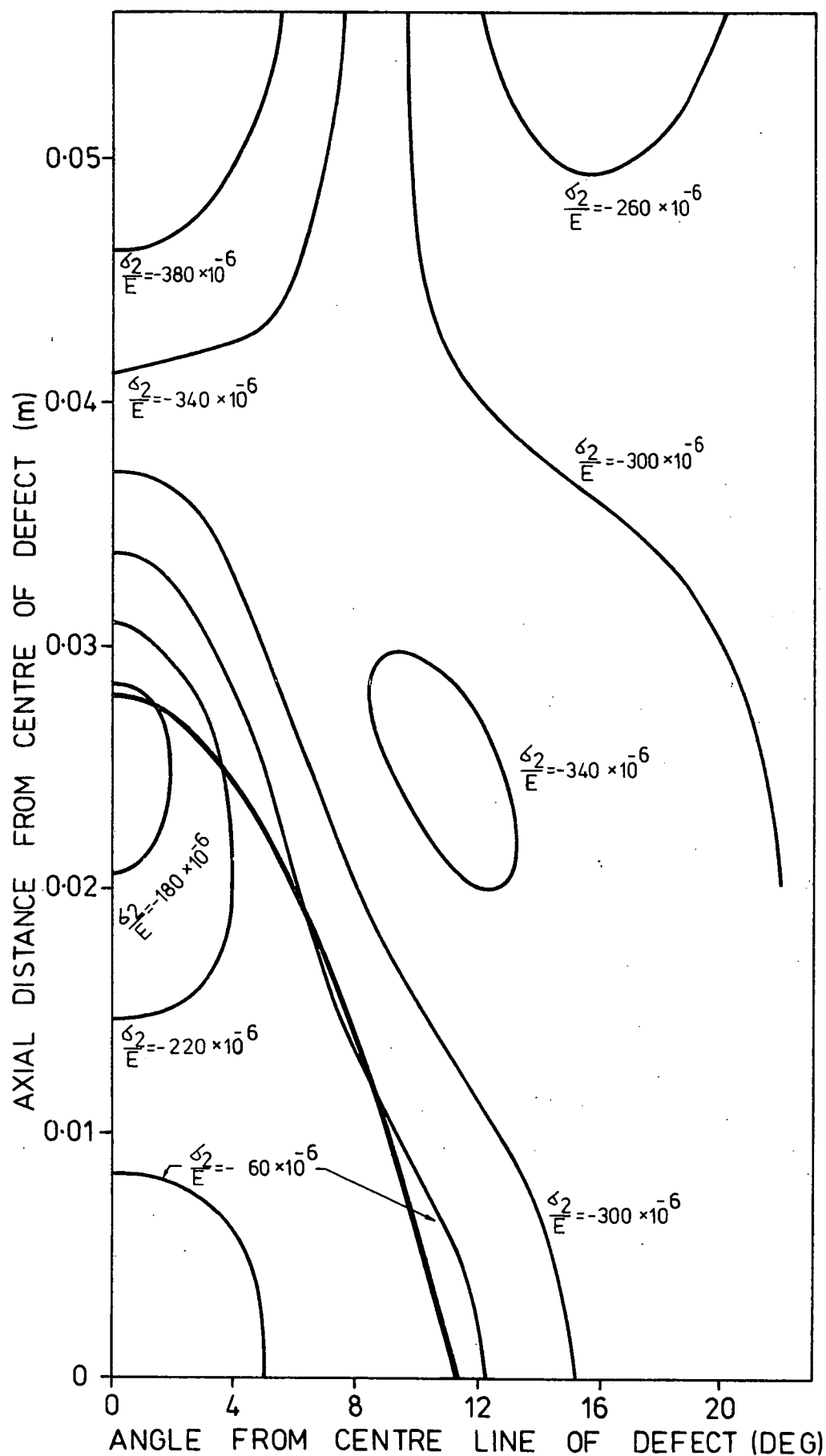
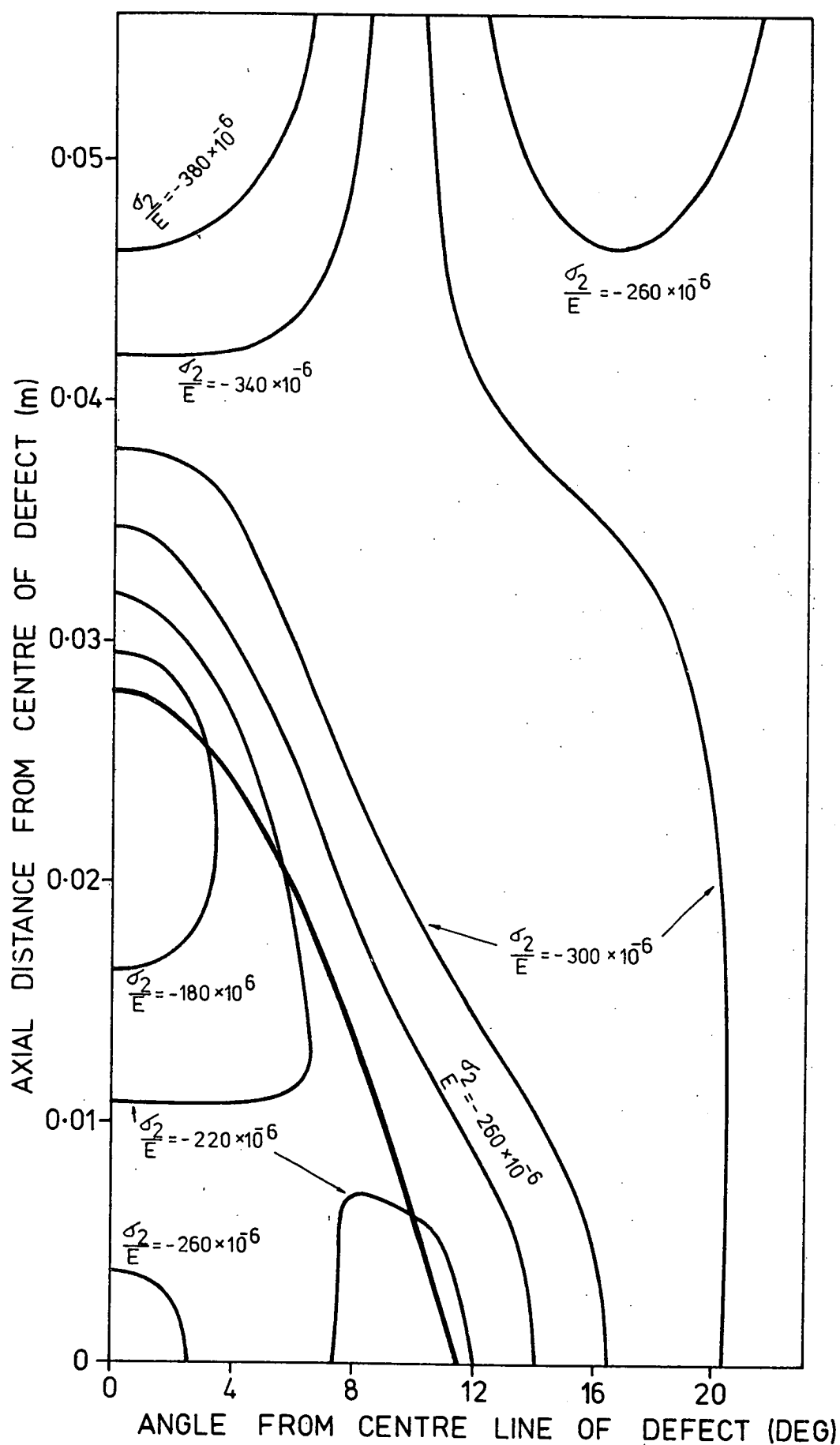


FIGURE B19

CONTOURS OF CONSTANT PRINCIPAL STRESS

SOLUTION OF DONNELL'S EQUATIONS





**FIGURE B20**

**CONTOURS OF CONSTANT PRINCIPAL STRESS**

TIMOSHENKO'S EQUATIONS WITH DONNELL'S RESULTANTS

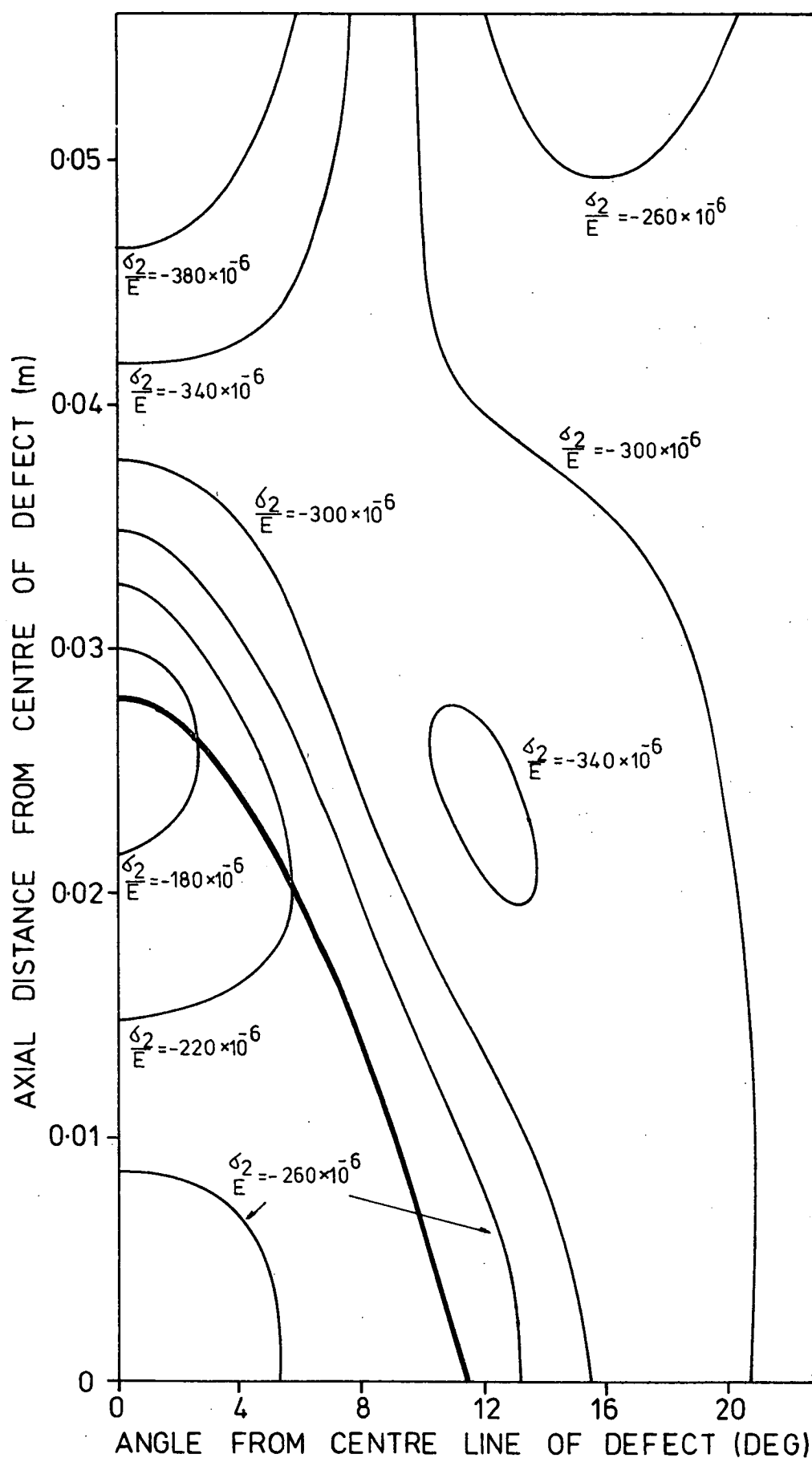


FIGURE B 21

CONTOURS OF CONSTANT PRINCIPAL STRESS

TIMOSHENKO'S EQUATIONS-RESULTANTS WITHOUT PRODUCTS OF SLOPES

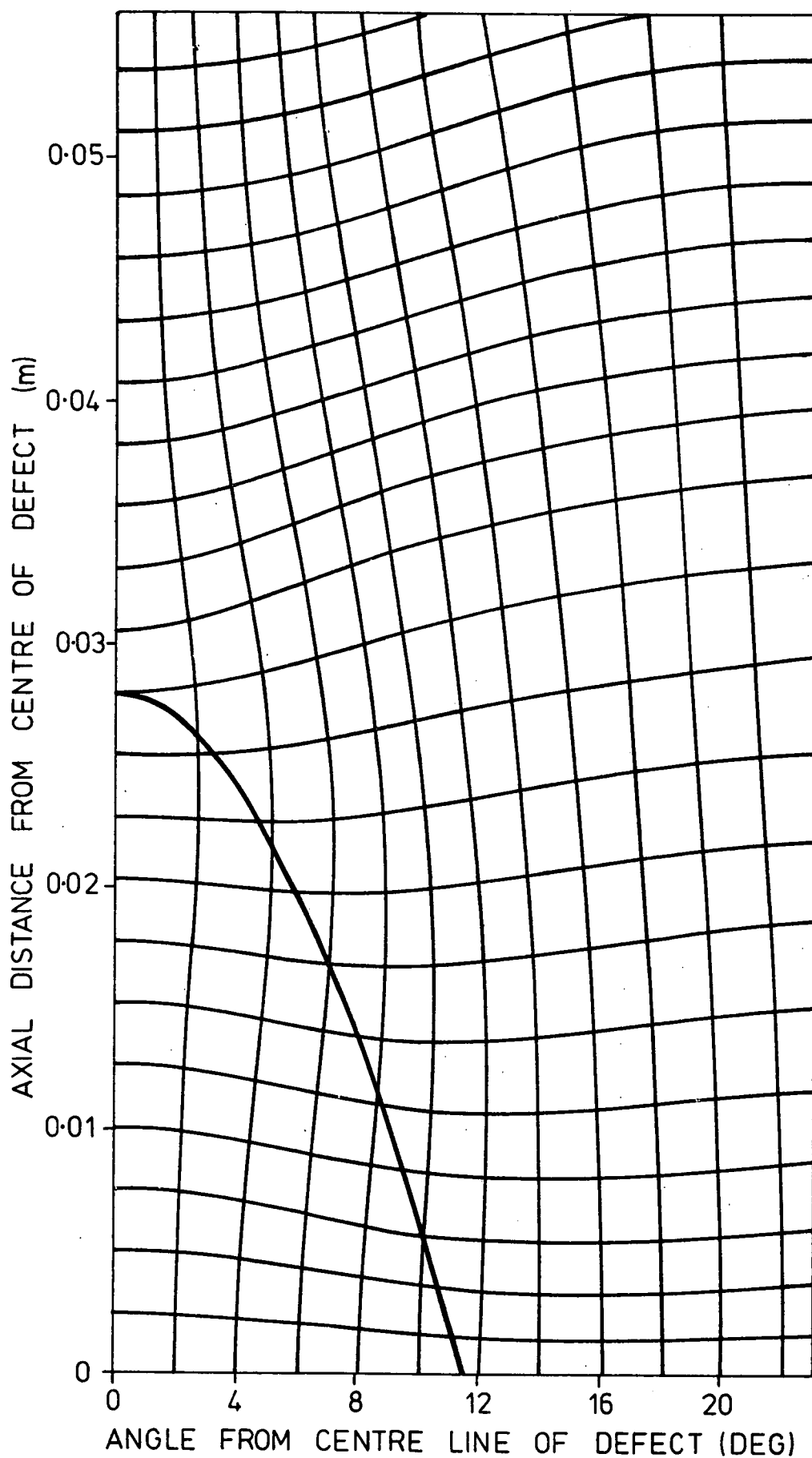
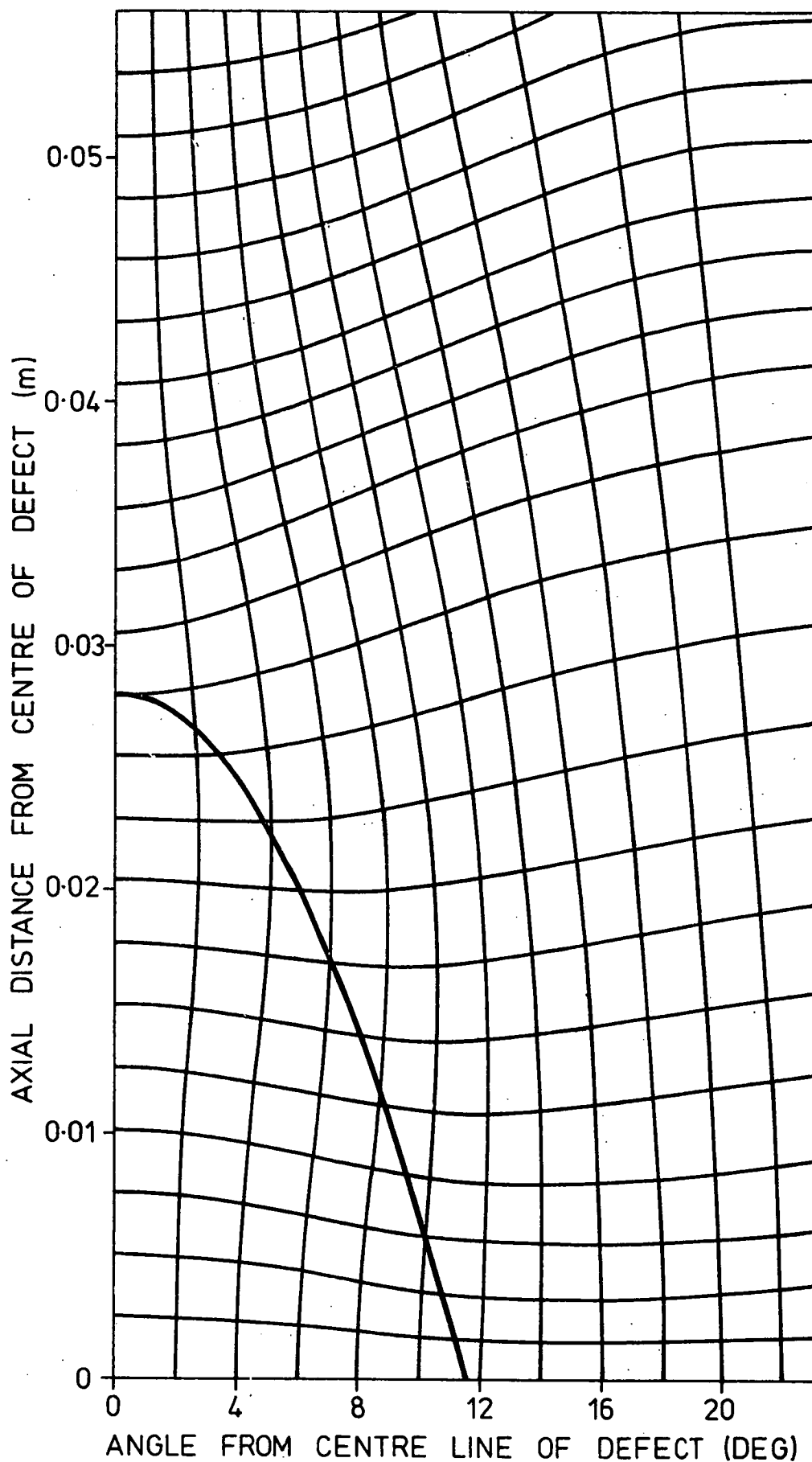


FIGURE B22

STRESS TRAJECTORIES

SOLUTION OF DONNELL'S EQUATIONS



**FIGURE B23**  
**STRESS TRAJECTORIES**

TIMOSHENKO'S EQUATIONS WITH DONNELL'S RESULTANTS

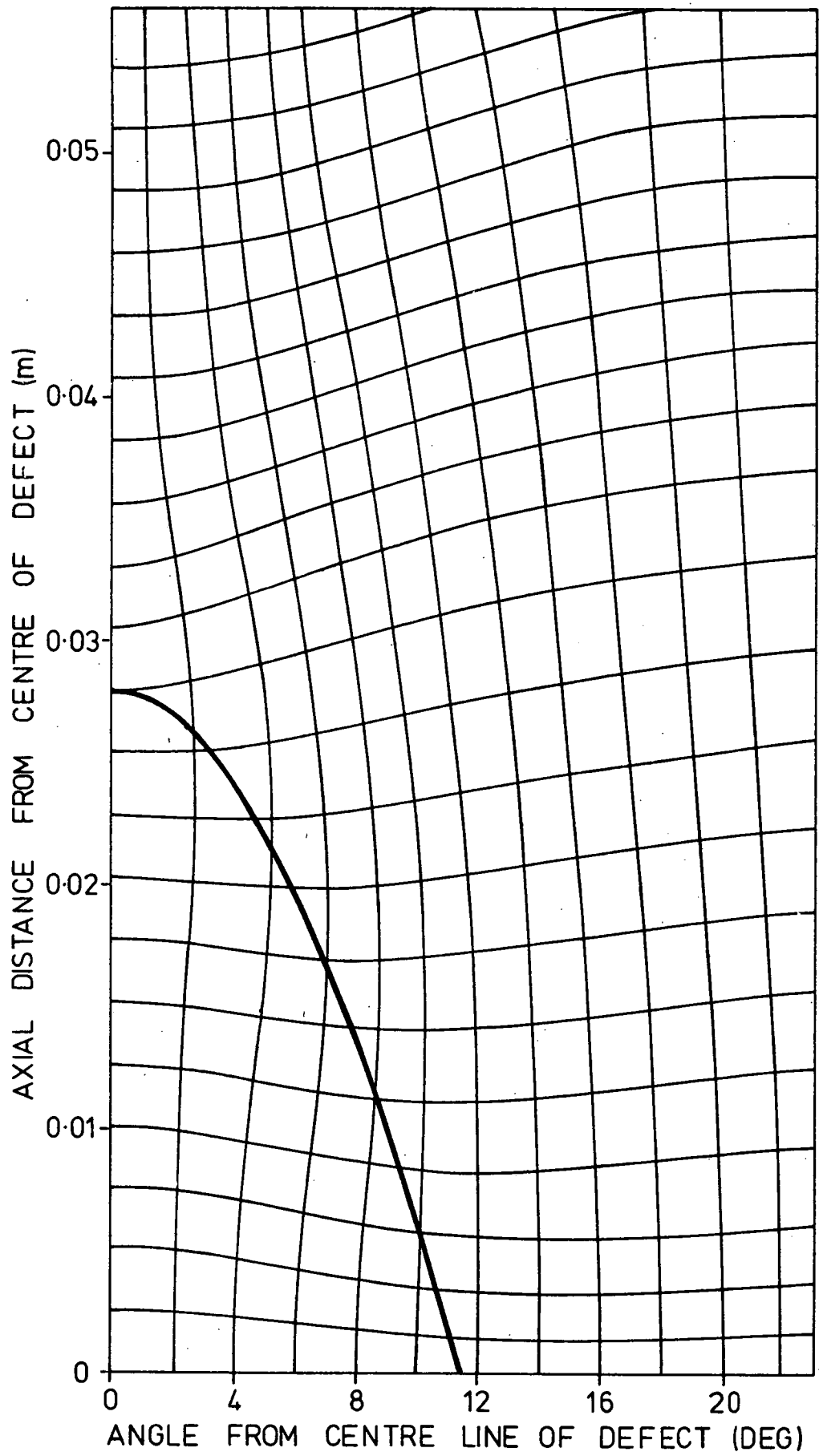


FIGURE B24  
STRESS TRAJECTORIES

TIMOSHENKO'S EQUATIONS - RESULTANTS WITHOUT PRODUCTS OF SLOPES

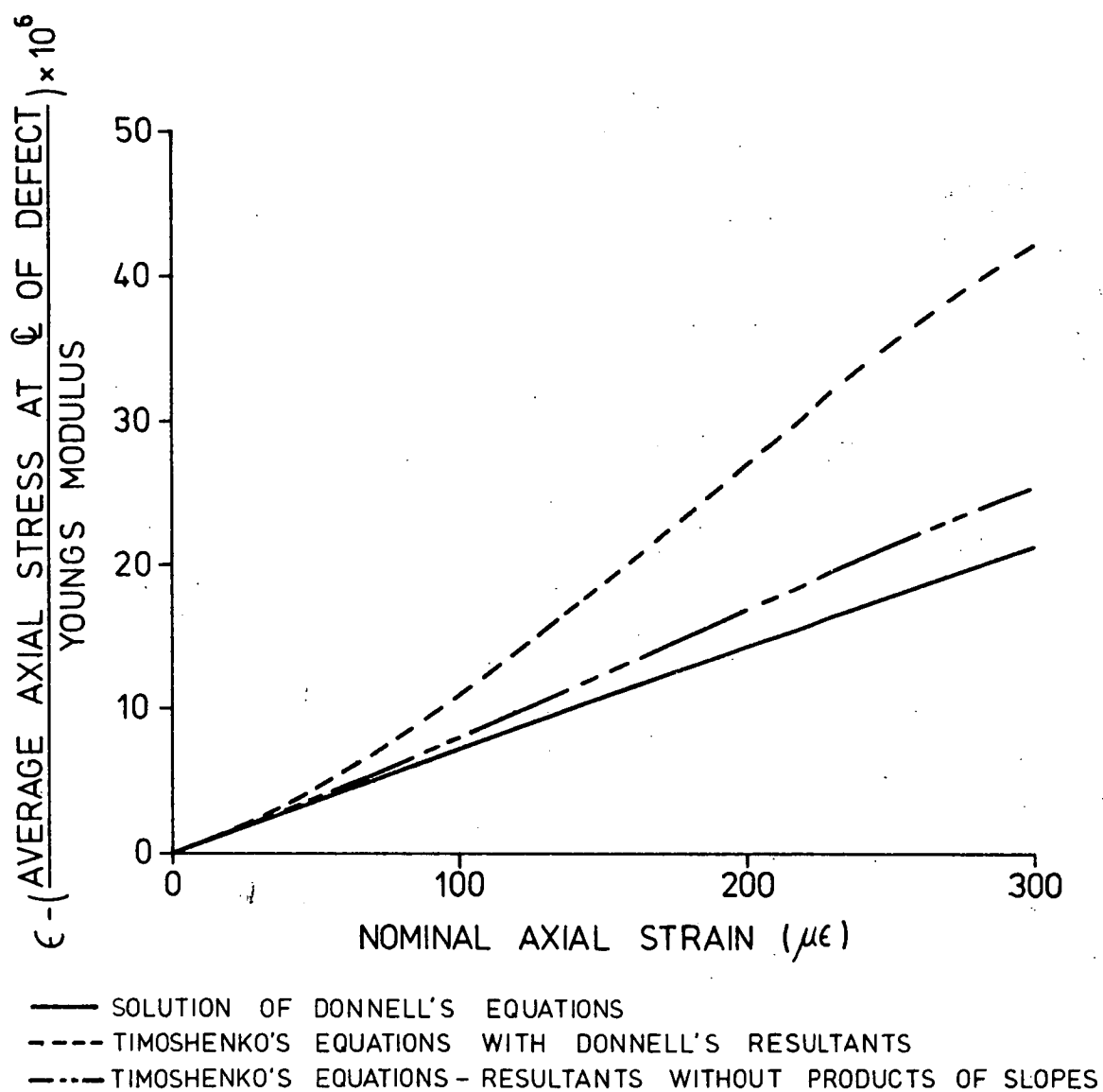


FIGURE B25

LOAD DEFORMATION CURVES FOR THE  
THREE THEORETICAL RELATIONS

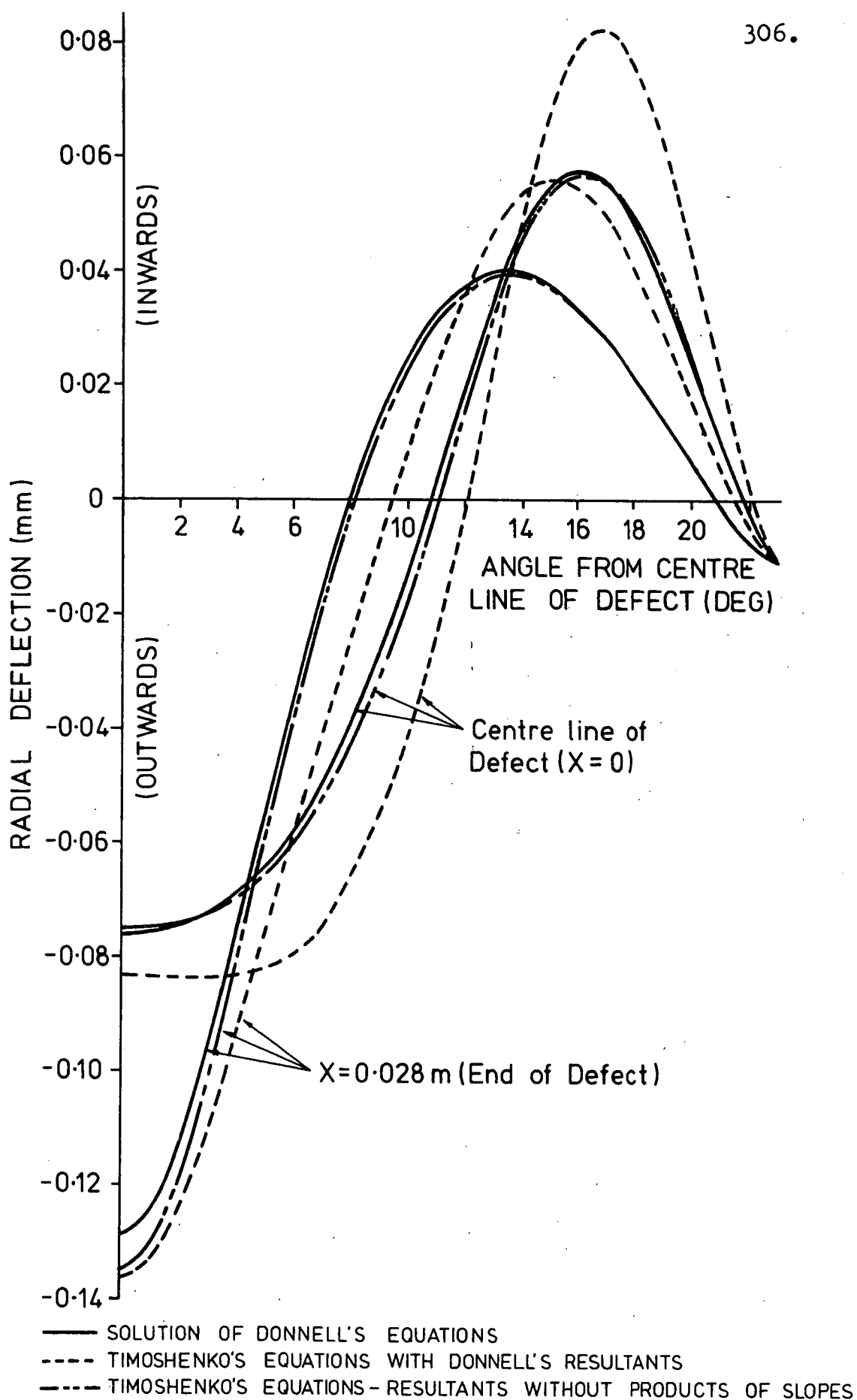


FIGURE B26

COMPARISON OF CALCULATED RADIAL DEFLECTIONS

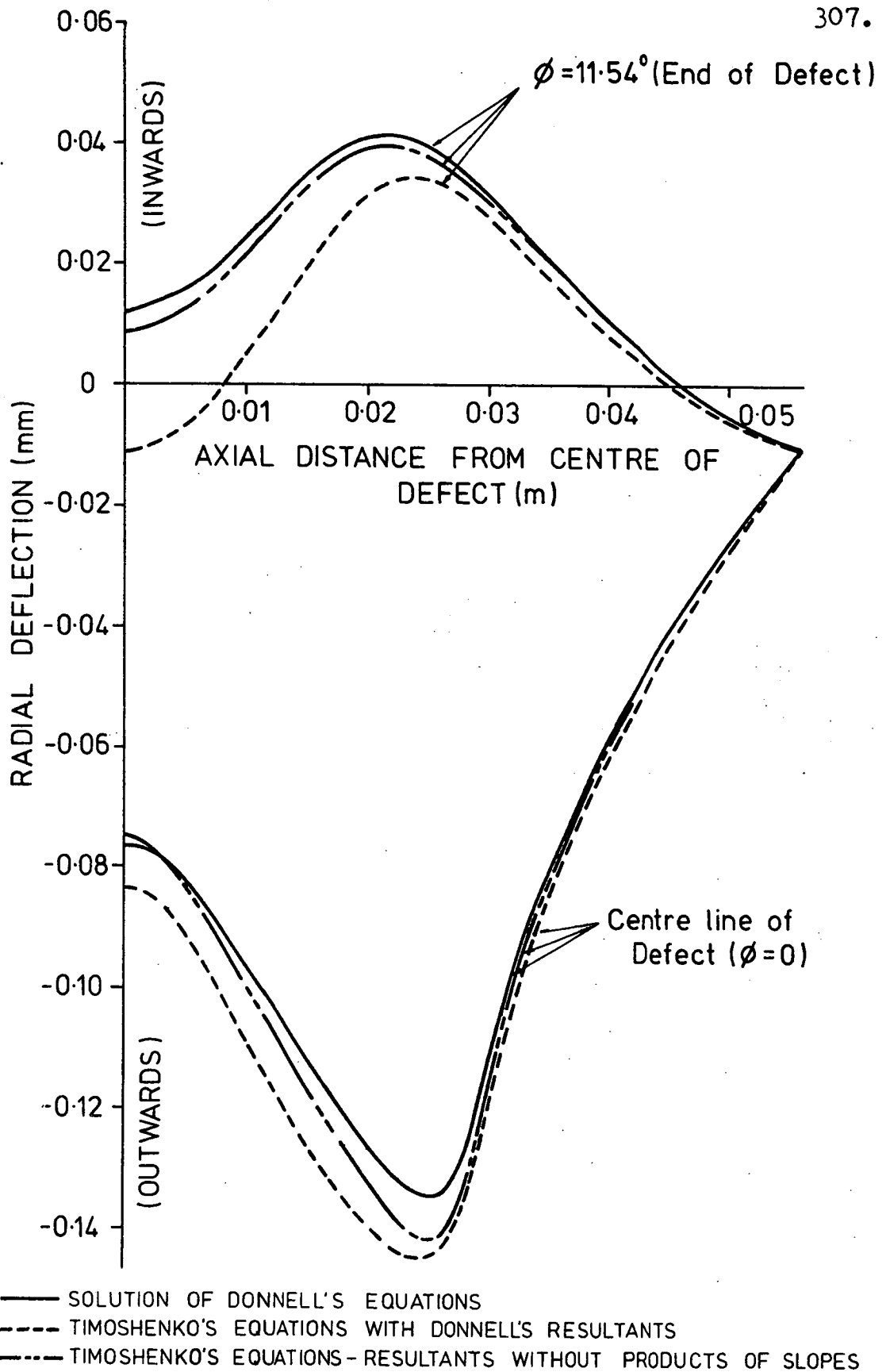
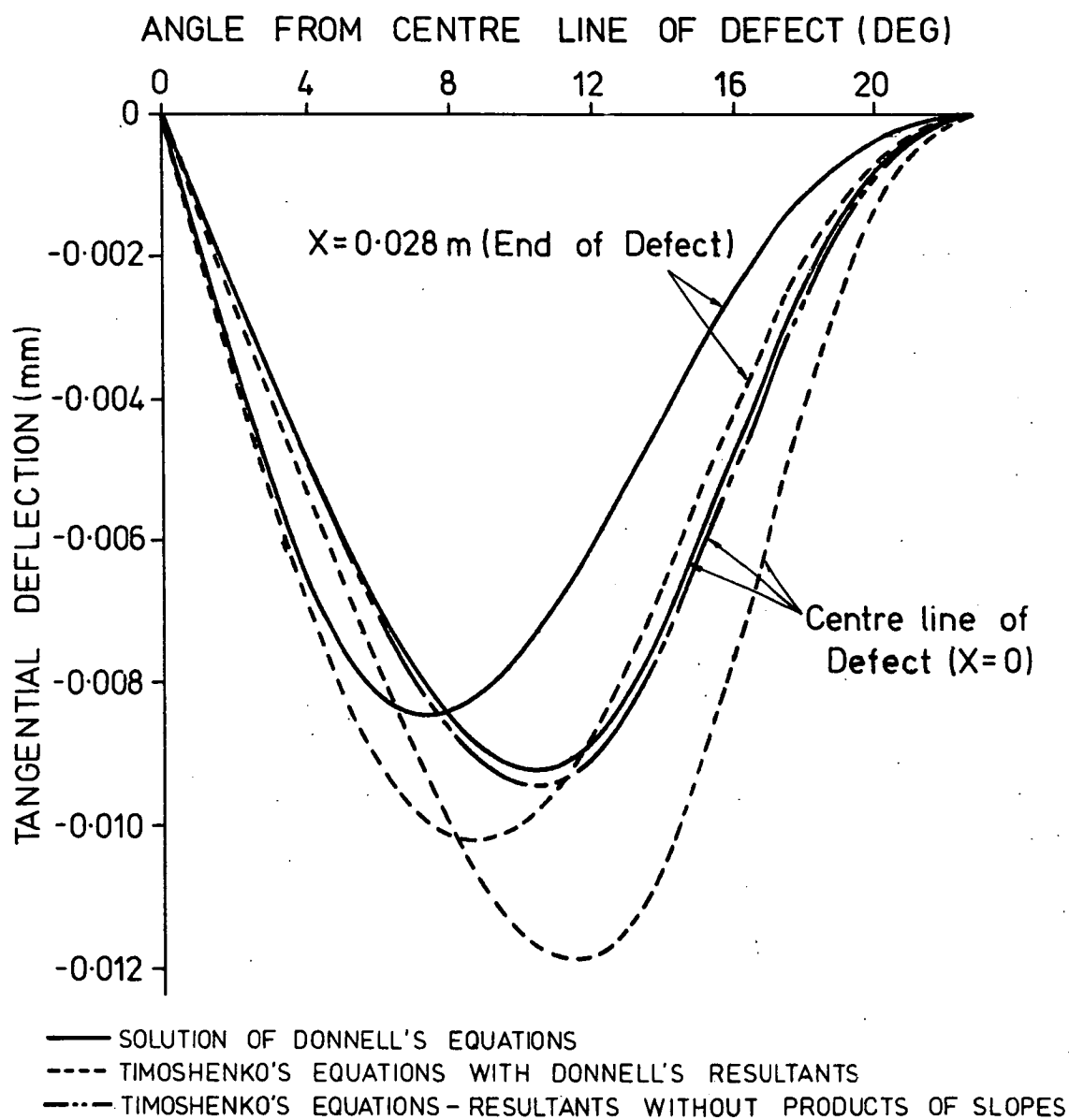


FIGURE B27

COMPARISON OF CALCULATED RADIAL DEFLECTIONS





**FIGURE B28**

**COMPARISON OF CALCULATED TANGENTIAL DEFLECTIONS**

Note: The third solution at the end of the defect coincides with the Donnell Solution

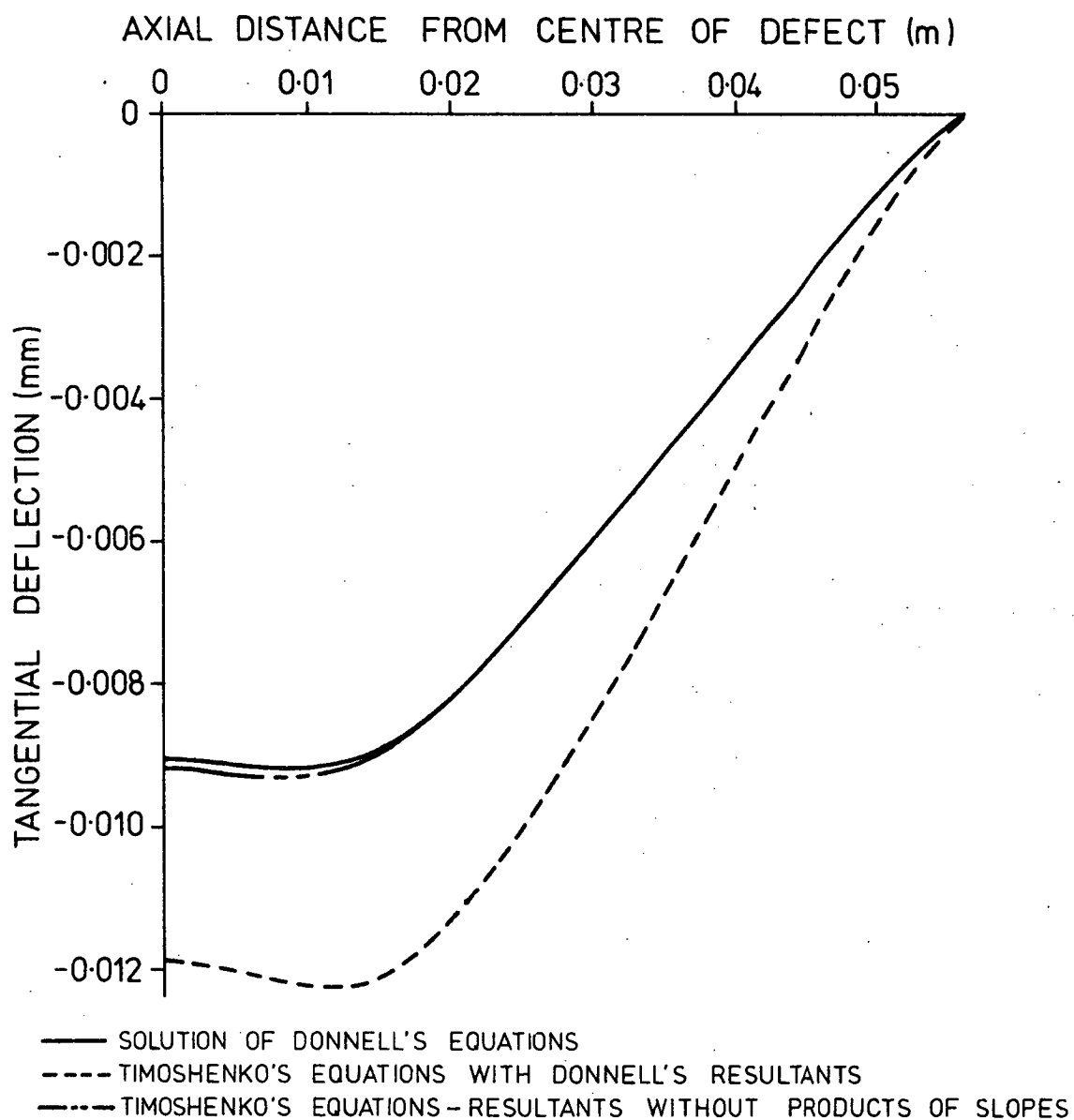


FIGURE B29

COMPARISON OF CALCULATED TANGENTIAL  
 DEFLECTIONS

( $\phi = 11.54^\circ$  - END OF DEFECT)

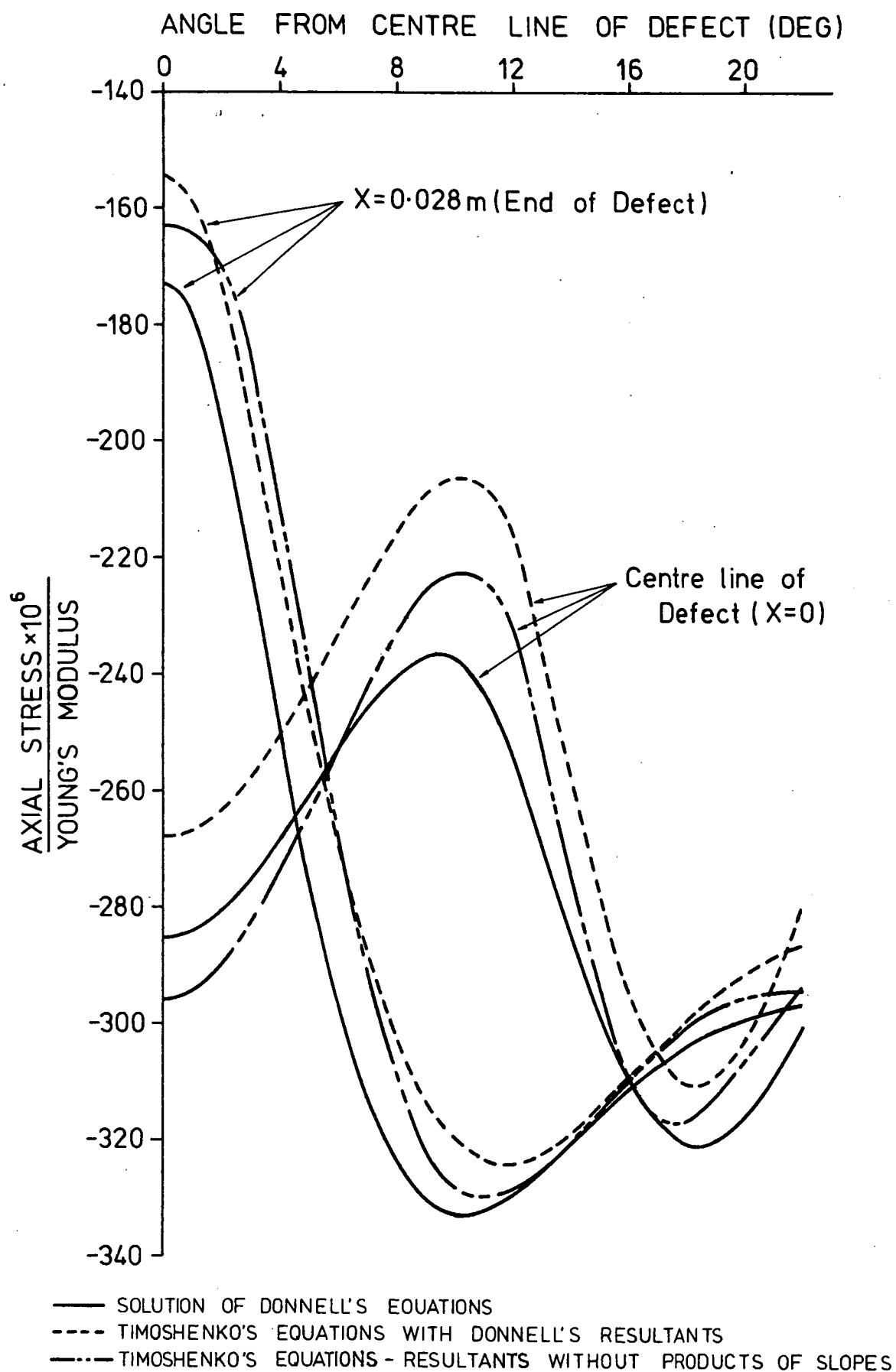
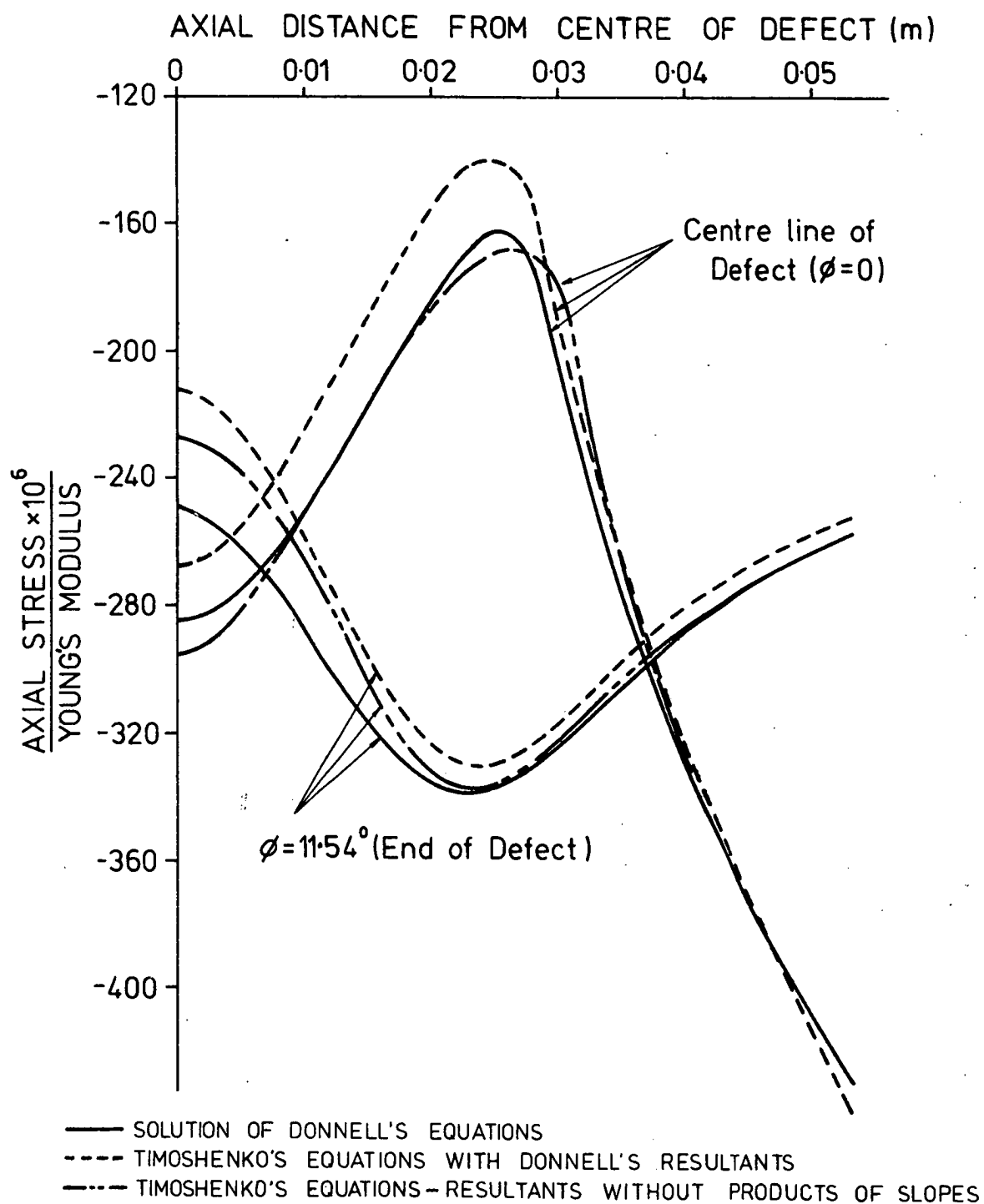


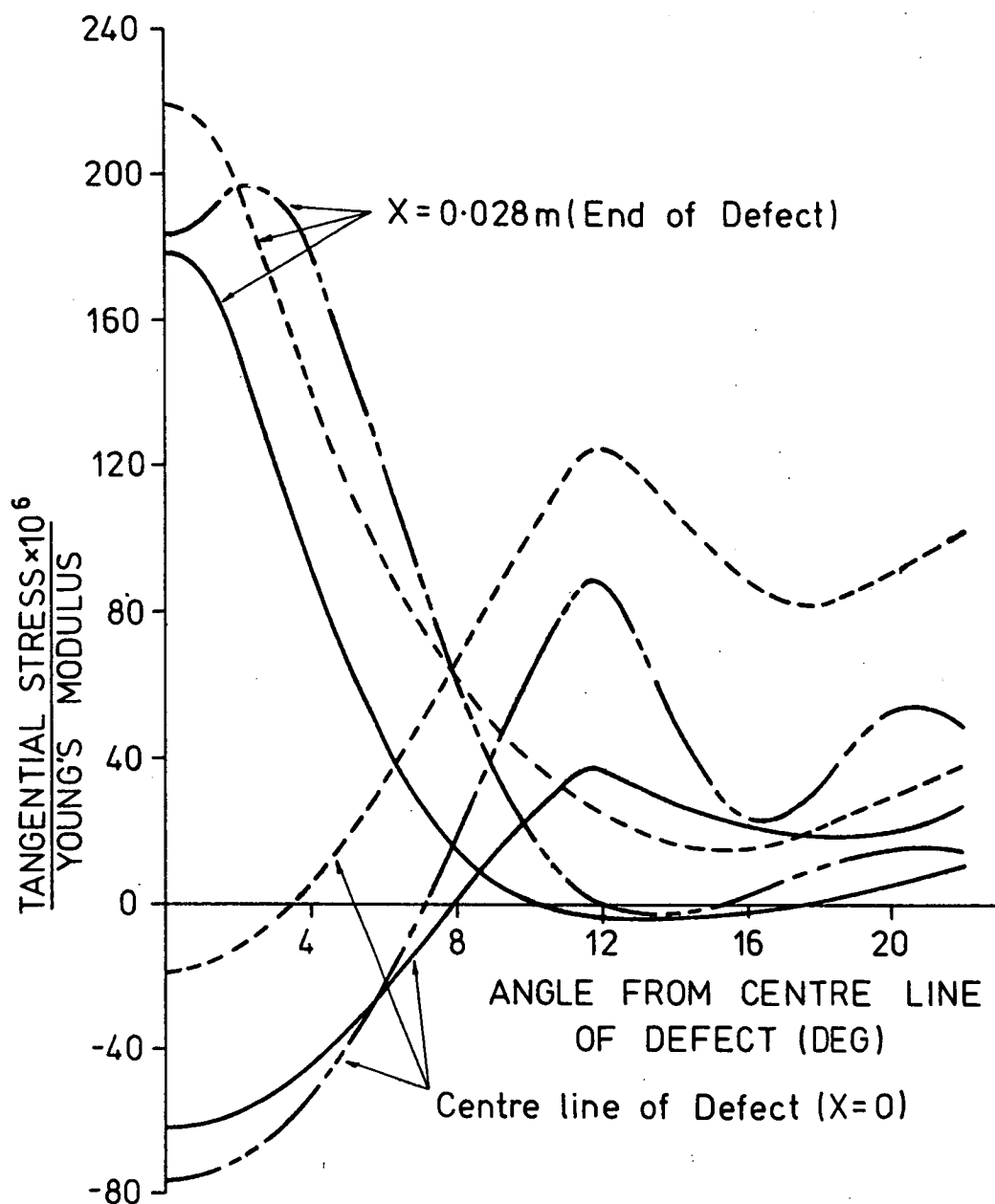
FIGURE B30

COMPARISON OF CALCULATED AXIAL STRESSES



**FIGURE B31**

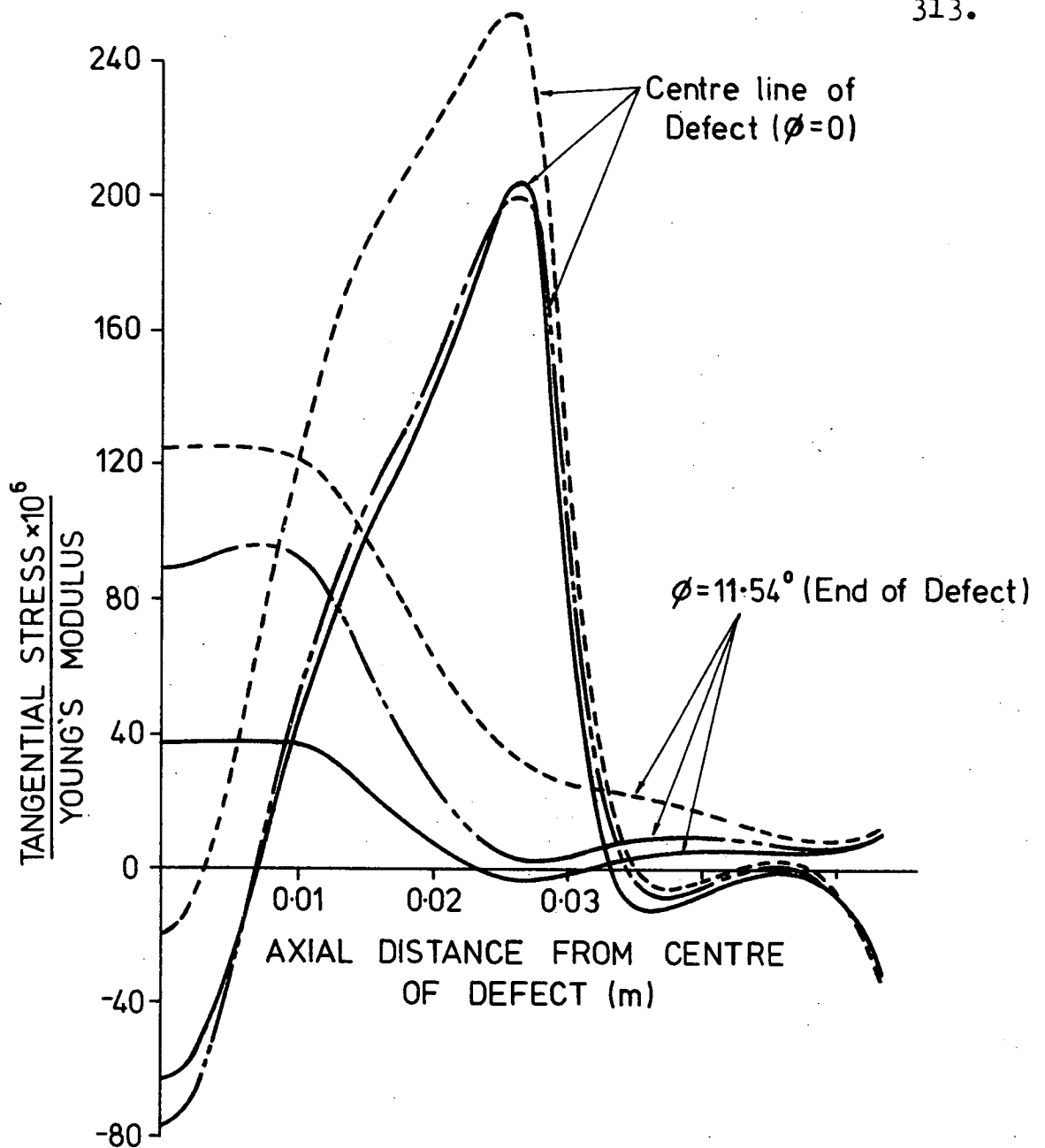
COMPARISON OF CALCULATED AXIAL STRESSES



- SOLUTION OF DONNELL'S EQUATIONS
- - - TIMOSHENKO'S EQUATIONS WITH DONNELL'S RESULTANTS
- · - TIMOSHENKO'S EQUATIONS - RESULTANTS WITHOUT PRODUCTS OF SLOPES

FIGURE B 32

COMPARISON OF CALCULATED TANGENTIAL STRESSES



- SOLUTION OF DONNELL'S EQUATIONS  
 ---- TIMOSHENKO'S EQUATIONS WITH DONNELL'S RESULTANTS  
 -.- TIMOSHENKO'S EQUATIONS - RESULTANTS WITHOUT PRODUCTS OF SLOPES

FIGURE B33

COMPARISON OF CALCULATED TANGENTIAL STRESSES

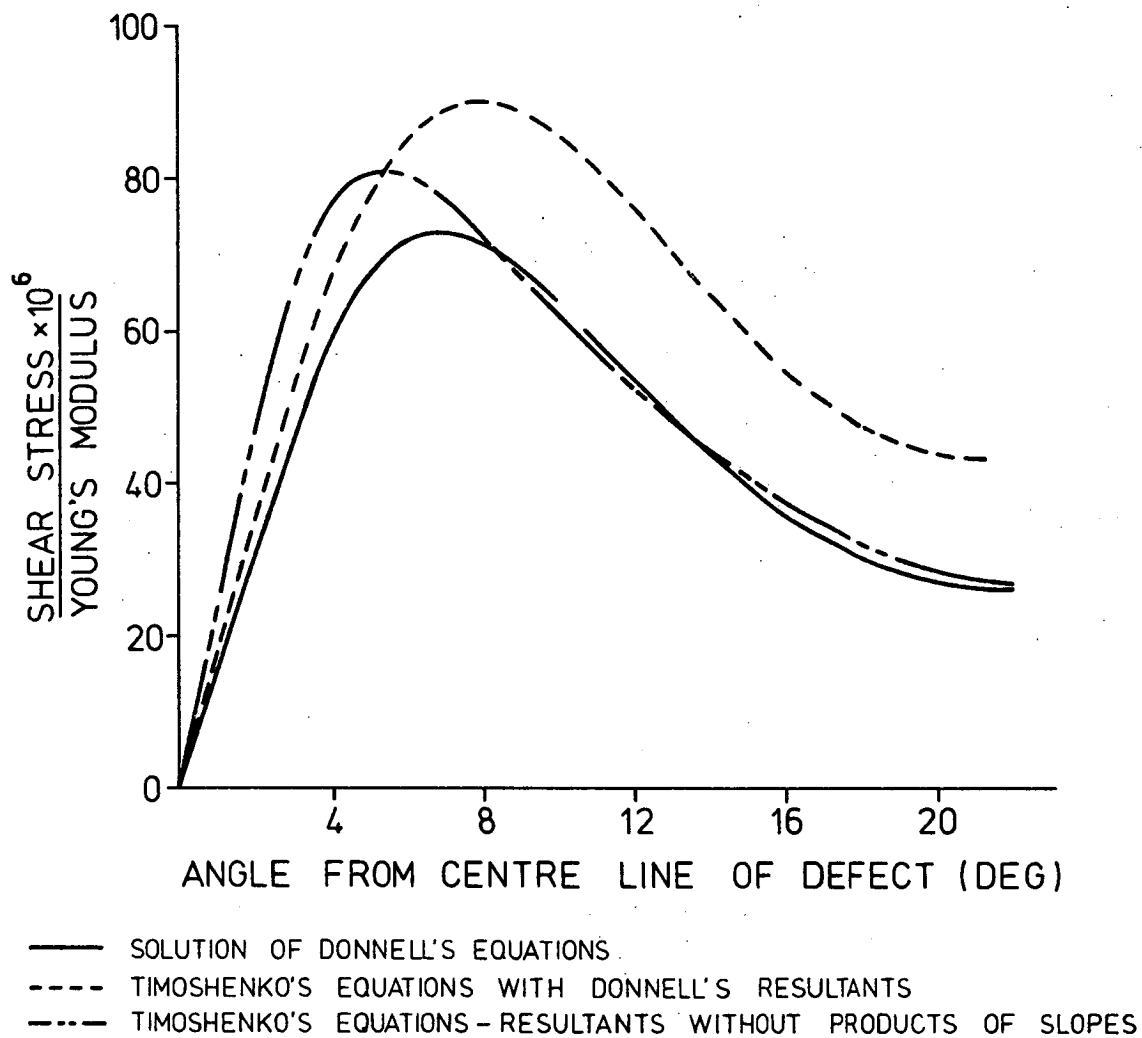


**FIGURE B 34**

COMPARISON OF CALCULATED SHEAR STRESSES  
 (x = 0.028 m - END OF DEFECT)

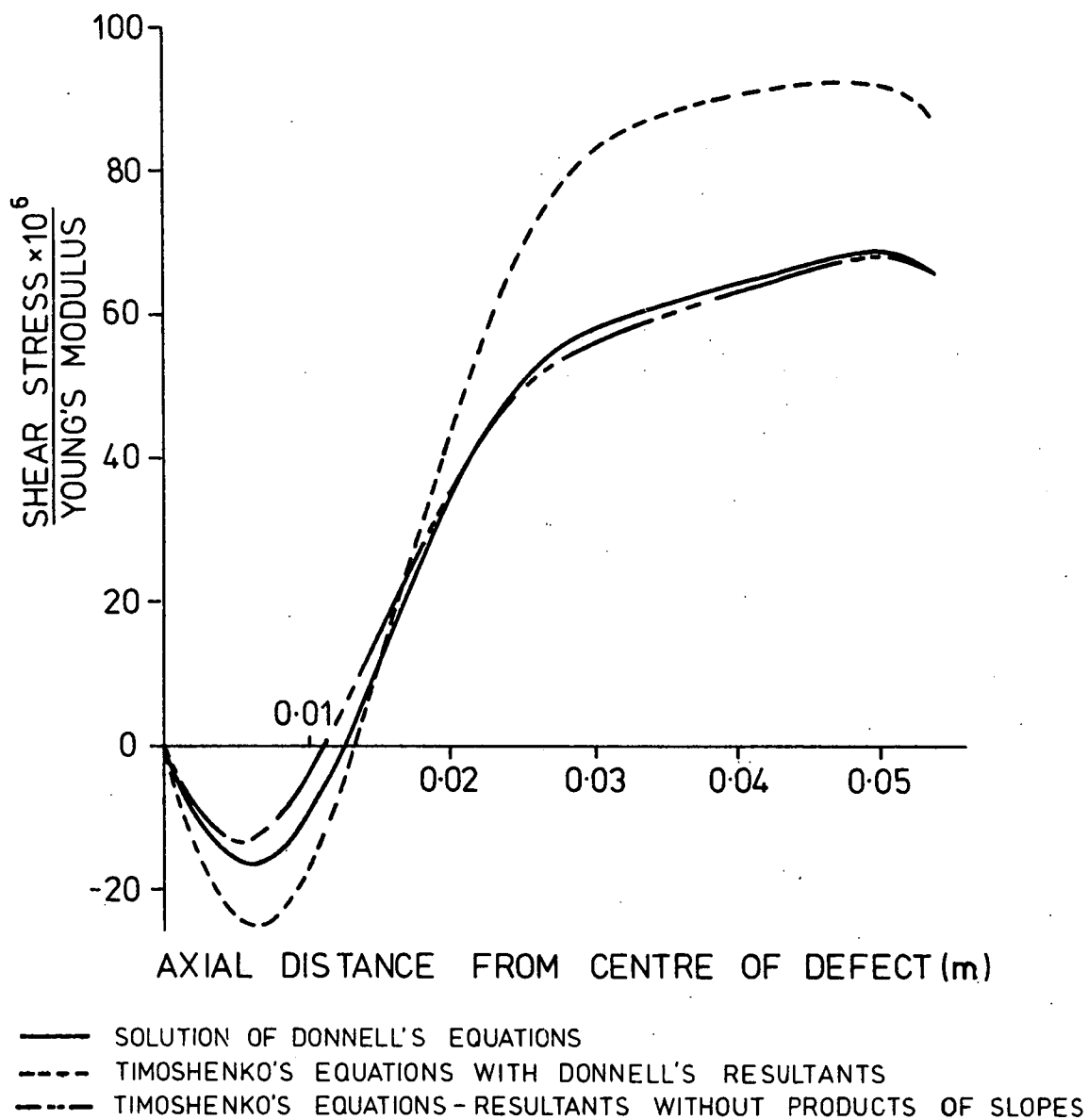


FIGURE B 35

COMPARISON OF CALCULATED SHEAR STRESSES  
 ( $\phi = 11.54^\circ$  - END OF DEFECT)



APPENDIX    C

PROGRAM LISTING FOR BUCKLING ANALYSIS OF CYLINDER AS A  
SPACE FRAME

AND

TYPICAL OUTPUT

```

01.10 T I, "CYLINDER BUCKLING-SPACE FRAME ANALYSIS",!!
01.20 A "WIDTH OF FACET=",L1,"M. HALF DEVELOPED LENGTH OF FACET=",L2,"M.":T !
01.25 A "EFFECTIVE WIDTH OF FLANGE=",W,"M. THICKNESS=",T,"M.":T !
01.27 A "NUMBER OF FACETS=",N," YOUNG'S MODULUS=",E,"GPA":T !!!
01.28 S E=E*109
01.30 S K=FSQT(L2*L2+L1*L1/4)
01.40 S PH=6.283185308/N
01.50 S H=L2*FSQT(1-L1*L1*(1-FCOS(PH/2))/(1+FCOS(PH/2))/L2/L2/4)
01.60 S S=(L2-H)*100/L2
01.70 T "FIRST BUCKLING MODE",!!
01.80 T Z 8.06, "AXIAL LENGTH OF HALF FACET=",H,"M. SHORTENING=",S,"%":!
01.90 S CT=FSIN(PH/2)*FSQT(1+L1*L1/L2/L2/4)/2/FCOS(PH/4)

02.10 S A=FATN(FSQT(1-CT*CT)/CT)
02.20 S S=A*180/3.1415927
02.30 T Z 7.04, "ANGLE BETWEEN FACETS=",2*S,"DEG":!
02.40 S S=1-L1*L1*(1-FCOS(PH/2))/(1+FCOS(PH/2))/4/L2/L2
02.50 S S=(1+L1*L1/4/L2/L2)/S
02.60 S AC=FSQT(S)/2/N
02.70 T Z 7.06, "FORCE IN DIAGONAL MEMBER/AXIAL LOAD=",AC,!
02.80 S CF=-2*AC/FSQT(L2*L2/L1/L1+0.25)
02.90 T Z 7.06, "FORCE IN TANGENTIAL MEMBER/AXIAL LOAD=",CF:!!

04.20 S RE=PH/2:C CALCULATION OF BETA BY NEWTON RAPHSON
04.30 S GR=2*FSIN(RE/2)-FSIN(PH-RE)
04.40 S G1=FCOS(RE/2)+FCOS(PH-RE)
04.50 I (FABS(GR)-0.0000001)10.03-4.40-4.40:C CHECK FOR CONVERGENCE
04.60 S RE=RE-0.7*GR/G1:C CONVERGENCE FACTOR
04.70 S 4.30
04.74 T I, "SECOND BUCKLING MODE",!!
04.80 T Z 7.04, "BETA=",RE*180/3.1415927,"DEG.":!

```

```

05.10 T Z 6.04, "RADIUS OF CORNERS OF FACETS=", R, "M.", !
05.20 S H=FSQT(L2*L2+L1*L1/4-4*R*R*FSIN(BE/2)^2)
05.30 S S=(L2-H)*100/L2
05.40 T Z 8.06, "AXIAL LENGTH OF HALF FACET=", 2*H, "M. SHORTENING=", S, "%", !
05.50 S L=FSIN(BE/2)^2-FSIN(PH-BE/2)^2
05.55 D 7
05.60 S AG=2*FSIN(BE/2)^2*FSQT(L2*L2+9*L1*L1/4)/N/H/L
05.70 S AC=2*FSIN(BE/2)^2*FSIN(2*PH-BE)/FSIN(2*PH-2*BE)-FSIN(PH-BE/2)^2
05.80 S AC=AC*K/N/H/L/(0.5+FSIN(BE)/FSIN(2*PH-2*BE))

06.10 T Z 7.06, "FORCE IN COMPRESSION MEMBERS/AXIAL LOAD=", AC, !
06.30 T Z 7.06, "FORCE IN TENSION MEMBER/AXIAL LOAD=", AG, ! ! ! !
06.40 D

07.10 C ANGLES BETWEEN FACETS IN SECOND BUCKLING MODE
07.20 S S=L2*L2/2+L1*L1/8+4*L2*L2*R*R*FSIN(BE/2)^2/L1/L1+R*R*FSIN(BE/2)^2
07.30 S S=S/(2*R*FCOS(BE/2)*L2*K/L1)
07.40 S B=FATN(FSQT(1-S*S)/S)
07.50 T Z 7.04, "ANGLE BETWEEN FACETS=", B*360/3.1415927, "DEG", !

10.03 T "COLLAPSE OF DIAGONAL MEMBER ----"
10.09 S R=FSQT(L1*L1/2/(FSIN(PH-BE/2)^2-FSIN(BE/2)^2))
10.15 S P1=5.0; C CALCULATION OF COLLAPSE LOAD BY NEWTON RAPHSON
10.20 S J=FSQT(P1*6/E/W^3/T/FSIN(PH/4)^2/(1+(L1/2/L2)^2))
10.25 S RE=16*L1*L1*E*W*T*FSIN(PH/4)^2*(K-2*FSIN(J*K/2)/J/FCOS(J*K/2))
10.30 S RE=2*FSQT((L2*L2+2.25*L1*L1)^3)*P1-RE
10.35 S DR=16*L1*L1*E*W*T*FSIN(PH/4)*(K/2/FCOS(J*K/2)^2-FSIN(J*K/2)/J/FCOS(J*K/2))/P1
10.40 S DR=DR+2*FSQT((L2*L2+2.25*L1*L1)^3)
10.42 S P1=P1-0.5*RE/DR; C CONVERGENCE FACTOR
10.45 I (FABS(RE)-0.000000001)10.60,10.20,10.20
10.60 T Z 7.04, "CRITICAL LOAD =", P1/AC, " N", !
10.75 S AF=K*(1-P1/2/E/W/T)
10.80 S AB=L1*(1+P1*L1/K/E/W/T)
10.85 S DE=FSQT(AF*AF-AB*AB/2/(1+FCOS(PH/2)))
10.90 T "AXIAL DEFLECTION OF SPACE FRAME", !
10.92 T " COMPLETE YOSHIMURA PATTERN--DEFL'N=", Z 9.07, H-DE, "M. ----"
10.95 T Z 6.04, (L2-DE)*100/L2, " % OF ORIGINAL LENGTH", !
10.96 S AB=L1*(1+P1*L1/K/E/W/T/2); D 10.85
10.97 T " ACTUAL BUCKLE PATTERN-----DEFL'N=", Z 9.07, H-DE, "M. ----"
10.98 D 10.95; T 1; G 4.74

```

CYLINDER BUCKLING-SPACE FRAME ANALYSIS

WIDTH OF FACET=.0419979 M. HALF DEVELOPED LENGTH OF FACET=.0293215 M.  
EFFECTIVE WIDTH OF FLANGE=.00399 M. THICKNESS=.00019 M.  
NUMBER OF FACETS=15 YOUNG'S MODULUS=5.5 GPa

FIRST BUCKLING MODE

AXIAL LENGTH OF HALF FACET= 0.029239M. SHORTENING= 0.282207%  
ANGLE BETWEEN FACETS= 165.2393DEG  
FORCE IN DIAGONAL MEMBER/AXIAL LOAD= 0.041079  
FORCE IN TANGENTIAL MEMBER/AXIAL LOAD=-0.095508

COLLAPSE OF DIAGONAL MEMBER ---- CRITICAL LOAD = 271.1973 N

AXIAL DEFLECTION OF SPACE FRAME

COMPLETE YOSHIMURA PATTERN--DEFL'N= 0.0001067M.---- 0.6460 % OF ORIGINAL LENGTH  
ACTUAL BUCKLE PATTERN-----DEFL'N= 0.0000830M.---- 0.5652 % OF ORIGINAL LENGTH

SECOND BUCKLING MODE

BETA= 11.9667DEG  
RADIUS OF CORNERS OF FACETS= 0.1017M.  
AXIAL LENGTH OF HALF FACET= 0.058266M. SHORTENING= 0.643227%  
ANGLE BETWEEN FACETS= 157.8120DEG  
FORCE IN COMPRESSION MEMBERS/AXIAL LOAD= 0.062016  
FORCE IN TENSION MEMBER/AXIAL LOAD=-0.040664

APPENDIX    D

PROGRAM LISTING AND TYPICAL OUTPUT OF PROGRAMMES USED IN  
THE FINITE DIFFERENCE SOLUTION OF THE DEFLECTIONS IN A  
CYLINDRICAL SHELL WITH A GEOMETRICAL DEFECT

```

C      DEFORMATIONS IN A CYLINDRICAL SHELL WITH INITIAL IMPERFECTIONS
C      PART ONE----OPEN FILES AND CALCULATE INITIAL GUESSES
0001  DIMENSION U(26,26),V(26,26),W(26,26),B(26,26)
C      READ CONSTANTS
0002  WRITE(7,1)
0003  1 FORMAT(25H$CYLINDER RADIUS(METRES)=)
0004  READ(5,2)R
0005  2 FORMAT(F6.3)
0006  WRITE(7,5)
0007  5 FORMAT(17H$POISSON'S RATIO=)
0008  READ(5,2)ANU
0009  WRITE(7,6)
0010  6 FORMAT(21H$FACET WIDTH(METRES)=)
0011  READ(5,7)A
0012  7 FORMAT(F8.5)
0013  WRITE(7,8)
0014  8 FORMAT(27H$FACET HALF LENGTH(METRES)=)
0015  READ(5,7)C
0016  WRITE(7,12)
0017  12 FORMAT(22H$WALL THICKNESS(M.M.)=)
0018  READ(5,2)T
0019  T=T/1000.
0020  WRITE(7,13)
0021  13 FORMAT(27H$AXIAL STRAIN(MICROSTRAIN)=)
0022  READ(5,14)STR
0023  14 FORMAT(F8.2)
0024  STR=STR/10.**6

```

```

0025      CALL ASSIGN (1,'DX0:DATA1')
0026      DEFINE FILE 1 (1,16,U,IZ)
C      CALCULATE DERIVED CONSTANTS AND STORE ON DISK
0027      PH=ATAN(A/2./SQRT(R*R-A*A/4.))
0028      DF=PH/11.
0029      DX=C/11.
0030      WRITE(1'1)R,ANU,A,C,T,STR,DX,DF
0031      DO 200 J=1,26
0032      DO 200 I=1,26
0033      U(I,J)=-STR*(J-3)*DX
0034      V(I,J)=0.0
0035      W(I,J)=-ANU*STR*R
0036      IF (J-2)300,400,500
0037      300 K=5
0038      GO TO 600
0039      400 K=4
0040      GO TO 600
0041      500 K=J
0042      600 B(I,J)=R-(SQRT(R*R-A*A/4.)+(J-3)*(R-SQRT(R*R-A*A/4.))/11.)/COS((
      1I-3)*DF)
0043      IF (B(I,J))700,200,200
0044      700 B(I,J)=0.0
0045      200 CONTINUE
0046      CALL ASSIGN (2,'DX0:DATA2')
0047      DEFINE FILE 2 (1,5408,U,IZ)
0048      WRITE (2'1)((((U(I,J),V(I,J),W(I,J),B(I,J)),I=1,26),J=1,26)
0049      END

```

TYPICAL OUTPUT TO OPENING PROGRAMME

CYLINDER RADIUS(METRES)=.1

POISSON'S RATIO=.35

FACET WIDTH(METRES)=.04

FACET HALF LENGTH(METRES)=.028

WALL THICKNESS(M.M.)=.19

AXIAL STRAIN(MICROSTRAIN)=50.

STOP --



PROGRAMME USED IN THE SUCCESSIVE APPROXIMATION PROCEDURE  
USING DONNELL'S EQUATIONS

```

C      DEFORMATION OF A CYLINDRICAL SHELL WITH AN INITIAL IMPERFECTION
C      PART TWO-----SUCCESSIVE APPROXIMATION PROCEDURE
C      SOLUTION OF DONNELL'S EQUATIONS
0001      DIMENSION U(26,26),V(26,26),W(26,26),B(26,26)
0002      CALL ASSIGN (1,'DX0:DATA1')
0003      DEFINE FILE 1 (1,16,U,IZ)
C      READ CONSTANTS AND OUTPUT VALUES
0004      READ (1,1)R,ANU,A,C,T,STR,DX,DP
0005      WRITE(7,1)R,T*1000.
0006      1 FORMAT(17H CYLINDER RADIUS=,F6.3,25H METRES---WALL THICKNESS=,F6.3
        1,5H M.M.)
0007      WRITE(7,2)ANU,STR*10.**6
0008      2 FORMAT(17H POISSON'S RATIO=,F6.3,16H---AXIAL STRAIN=,F8.2,12H MICR
        10STRAIN)
0009      WRITE(7,3)A,C,C/A
0010      3 FORMAT(20H IMPERFECTION WIDTH=,F8.5,22H METRES---HALF LENGTH=,F8.5
        1,23H METRES---ASPECT RATIO=,F5.3)
0011      IT1=0
0012      ITNS=0
0013      WRITE(7,6)
0014      6 FORMAT(39H$U,V,AND W RELAXATION CONSTANTS ARE:- )
0015      READ(5,7)C1,C2,C3
0016      7 FORMAT(3F4.2)
0017      WRITE(7,8)
0018      8 FORMAT(30H$MAXIMUM NUMBER OF ITERATIONS=)
0019      READ(5,9)MAX
0020      9 FORMAT(I5)

```

```

0021      CALL ASSIGN (2,'DX0:DATA2')
0022      DEFINE FILE 2 (1,5408,U,IZ)
0023      READ (2,1)((U(I,J),V(I,J),W(I,J),B(I,J)),I=1,26),J=1,26)
      C
0024      1600 UMAX=0.0
0025           VMAX=0.0
0026           WMAX=0.0
0027      DO 100 J=3,24
      C
0028      DO 300 I=3,24
0029          DWX=(W(I,J+1)-W(I,J-1))/2./DX
0030          DUX=(U(I,J+1)-U(I,J-1))/2./DX
0031          DVX=(V(I,J+1)-V(I,J-1))/2./DX
0032          DWF=(W(I+1,J)-W(I-1,J))/2./DF
0033          DUF=(U(I+1,J)-U(I-1,J))/2./DF
0034          DVF=(V(I+1,J)-V(I-1,J))/2./DF
0035          D2WX2=(W(I,J+1)-2.*W(I,J)+W(I,J-1))/DX/DX
0036          D2BX2=(B(I,J+1)-2.*B(I,J)+B(I,J-1))/DX/DX
0037          D2WF2=(W(I+1,J)-2.*W(I,J)+W(I-1,J))/DF/DF
0038          D2BF2=(B(I+1,J)-2.*B(I,J)+B(I-1,J))/DF/DF
0039          D2WXP=(W(I+1,J+1)-W(I+1,J-1)-W(I-1,J+1)+W(I-1,J-1))/4./DX/DF
0040          D2UXP=(U(I+1,J+1)-U(I+1,J-1)-U(I-1,J+1)+U(I-1,J-1))/4./DX/DF
0041          D2VXP=(V(I+1,J+1)-V(I+1,J-1)-V(I-1,J+1)+V(I-1,J-1))/4./DX/DF
0042          D2BXP=(B(I+1,J+1)-B(I+1,J-1)-B(I-1,J+1)+B(I-1,J-1))/4./DX/DF
0043          UNEW=(-DWX*D2WX2-(1.+ANU)*D2VXP/2./R-(1.+ANU)*DWF*D2WXP/2./R/R+ANU
1          *DWX/R-(1.-ANU)*DWX*D2WF2/2./R/R-(U(I,J+1)+U(I,J-1))/DX/DX-(1.-ANU
2          *2)*(U(I+1,J)+U(I-1,J))/DF/DF/2./R/R)/(-2./DX/DX-(1.-ANU)/DF/DF/R/R)

```

```

0044      VNEW=(-(1.+ANU)*D2UXP/2./R-(1.+ANU)*DWX*D2WXP/2./R+DWF/R/R-(1.-ANU
1)*DWP*D2WX2/2./R-DWP*D2WF2/R/R/R-(V(I+1,J)+V(I-1,J))/DF/DF/R/R-(1.
2-ANU)*(V(I,J+1)+V(I,J-1))/2./DX/DX)/(-2./DF/DF/R/R-(1.-ANU)/DX/DX)
0045      ANP=12.*(DVP/R+DWP**2/2./R/R-W(I,J)/R+ANU*(DUX+DWX**2/2.))/T/T
0046      ANX=12.*(DUX+DWX**2/2.+ANU*(DVP/R+DWP**2/2./R/R-W(I,J)/R))/T/T
0047      ANXP=6.*(1.-ANU)*(DUP/R+DVX+DWX*DWP/R)/T/T
0048      WNEW=(ANP/R+ANX*D2WX2+ANX*D2BX2+2.*ANXP*D2WXP/R+2.*ANXP*D2BXP/R+
1ANP*D2WF2/R/R+ANP*D2BF2/R/R-(W(I,J+2)-4.*W(I,J+1)-4.*W(I,J-1)+W(I,
2J-2))/DX**4-2.*(W(I+1,J+1)-2.*W(I,J+1)+W(I-1,J+1)-2.*W(I+1,J)-2.*W
3(I-1,J)+W(I+1,J-1)-2.*W(I,J-1)+W(I-1,J-1))/DX/DX/DF/DF/R/R-(W(I+2,
4J)-4.*W(I+1,J)-4.*W(I-1,J)+W(I-2,J))/DF**4/R**4)/(6./DX**4+8./DX/D
5X/DF/DF/R/R+6./DF**4/R**4)
0049      IF(ABS(U(I,J)-UNEW)-UMAX)500,500,400
C      CHECK FOR MAXIMUM CHANGES
0050      400 UMAX=ABS(U(I,J)-UNEW)
0051      K1=I-2
0052      L1=J-2
0053      500 IF(ABS(V(I,J)-VNEW)-VMAX)700,700,600
0054      600 VMAX=ABS(V(I,J)-VNEW)
0055      K2=I-2
0056      L2=J-2
0057      700 IF(ABS(W(I,J)-WNEW)-WMAX)900,900,800
0058      800 WMAX=ABS(W(I,J)-WNEW)
0059      K3=I-2
0060      L3=J-2
0061      900 U(I,J)=U(I,J)+C1*(UNEW-U(I,J))
C      MODIFY DEFLECTION VALUES
0062      V(I,J)=V(I,J)+C2*(VNEW-V(I,J))
0063      W(I,J)=W(I,J)+C3*(WNEW-W(I,J))
0064      IF(J-3)300,1000,300
0065      1000 U(I,J)=0.0

```

```

0066      300 CONTINUE
C      CORRECT BOUNDARY VALUES ON AXIAL BOUNDARIES
0067      U(2,J)=U(4,J)
0068      V(2,J)=-V(4,J)
0069      W(1,J)=W(5,J)
0070      W(2,J)=W(4,J)
0071      V(3,J)=0.0
0072      100 CONTINUE
C      CORRECT BOUNDARY VALUES ON CIRCUMFERENTIAL BOUNDARY
0073      DO 1100 I=1,26
0074      U(I,2)=-U(I,4)
0075      V(I,2)=V(I,4)
0076      W(I,2)=W(I,4)
0077      W(I,1)=W(I,5)
0078      1100 CONTINUE
0079      ITNS=ITNS+1
0080      IT1=IT1+1
0081      IF (IT1-10)1700,200,1700
0082      200 WRITE(7,5)ITNS,UMAX,K1,L1,UMAX,K2,L2,WMAX,K3,L3
0083      5  FORMAT(3H IN,I4,11H ITNS,UMAX=,E10.3,3H AT,I3,1H,,I2,6H,UMAX=,E10.
13,3H AT,I3,1H,,I2,6H,WMAX=,E10.3,3H AT,I3,1H,,I2)
0084      IT1=0
0085      WRITE (2,1)((U(I,J),V(I,J),W(I,J),E(I,J)),I=1,26),J=1,26)
C      CHECK FOR CONVERGENCE
0086      1700 IF(UMAX-0.00000000000001)1200,1400,1400
0087      1200 IF(UMAX-0.00000000000001)1300,1400,1400
0088      1300 IF(WMAX-0.00000000000001)1500,1400,1400
0089      1400 IF(ITNS-MAX)1600,1500,1500
0090      1500 END

```

PROGRAMME USED IN THE SUCCESSIVE APPROXIMATION PROCEDURE  
USING TIMOSHENKO'S EQUILIBRIUM EQUATIONS WITH THE  
SHORTENED FORM OF STRESS RESULTANTS

```

C      DEFORMATION OF A CYLINDRICAL SHELL WITH AN INITIAL IMPERFECTION
C      PART TWO-----SUCCESSIVE APPROXIMATION PROCEDURE
C      SOLUTION OF TIMOSHENKO'S EQUATIONS WITH TIMOSHENKO'S STRESS
C      RESULTANTS
0001      DIMENSION U(26,26),V(26,26),W(26,26),B(26,26)
0002      CALL ASSIGN (1,'DX0:DATA1')
0003      DEFINE FILE 1 (1,16,U,IZ)
C      READ CONSTANTS AND OUTPUT VALUES
0004      READ (1,1)R,ANU,A,C,T,STR,DX,DP
0005      WRITE(7,1)R,T*1000.
0006      1 FORMAT(17H CYLINDER RADIUS=,F6.3,25H METRES---WALL THICKNESS=,F6.3
        1,5H M.M.)
0007      WRITE(7,2)ANU,STR*10.**6
0008      2 FORMAT(17H POISSON'S RATIO=,F6.3,16H---AXIAL STRAIN=,F8.2,12H MICR
        10STRAIN)
0009      WRITE(7,3)A,C,C/A
0010      3 FORMAT(20H IMPERFECTION WIDTH=,F8.5,22H METRES---HALF LENGTH=,F8.5
        1,23H METRES---ASPECT RATIO=,F5.3)
0011      IT1=0
0012      ITNS=0
0013      WRITE(7,6)
0014      6 FORMAT(39H$U,V,AND W RELAXATION CONSTANTS ARE:- )
0015      READ(5,7)C1,C2,C3
0016      7 FORMAT(3F4.2)
0017      WRITE(7,8)
0018      8 FORMAT(30H$MAXIMUM NUMBER OF ITERATIONS=)
0019      READ(5,9)MAX
0020      9 FORMAT(I5)
0021      CALL ASSIGN (2,'DX0:DATA2')
0022      DEFINE FILE 2 (1,5408,U,IZ)
0023      READ (2,1)(((U(I,J),V(I,J),W(I,J),B(I,J)),I=1,26),J=1,26)
C      START ITERATION FOR WHOLE SHELL
0024      1600 UMAX=0.0
0025      VMAX=0.0
0026      WMAX=0.0

```

```

0027      DO 100 J=3,24
C      START ITERATION FOR ROW
0028      DO 300 I=3,24
0029      DWX=(W(I,J+1)-W(I,J-1))/2./DX
0030      DUX=(U(I,J+1)-U(I,J-1))/2./DX
0031      DVX=(V(I,J+1)-V(I,J-1))/2./DX
0032      DBX=(B(I,J+1)-B(I,J-1))/2./DX
0033      DWP=(W(I+1,J)-W(I-1,J))/2./DP
0034      DUP=(U(I+1,J)-U(I-1,J))/2./DP
0035      DVP=(V(I+1,J)-V(I-1,J))/2./DP
0036      DBP=(B(I+1,J)-B(I-1,J))/2./DP
0037      D2WX2=(W(I,J+1)-2.*W(I,J)+W(I,J-1))/DX/DX
0038      D2BX2=(B(I,J+1)-2.*B(I,J)+B(I,J-1))/DX/DX
0039      D2WP2=(W(I+1,J)-2.*W(I,J)+W(I-1,J))/DP/DP
0040      D2BP2=(B(I+1,J)-2.*B(I,J)+B(I-1,J))/DP/DP
0041      D2WXP=(W(I+1,J+1)-W(I+1,J-1)-W(I-1,J+1)+W(I-1,J-1))/4./DX/DP
0042      D2UXP=(U(I+1,J+1)-U(I+1,J-1)-U(I-1,J+1)+U(I-1,J-1))/4./DX/DP
0043      D2VXP=(V(I+1,J+1)-V(I+1,J-1)-V(I-1,J+1)+V(I-1,J-1))/4./DX/DP
0044      D2BXP=(B(I+1,J+1)-B(I+1,J-1)-B(I-1,J+1)+B(I-1,J-1))/4./DX/DP
0045      D3WX3=(W(I,J+2)-2.*W(I,J+1)+2.*W(I,J-1)-W(I,J-2))/2./DX/DX/DX
0046      D3WP3=(W(I+2,J)-2.*W(I+1,J)+2.*W(I-1,J)-W(I-2,J))/2./DP/DP/DP
0047      D3WX2P=(W(I+1,J+1)-2.*W(I+1,J)+W(I+1,J-1)-W(I-1,J+1)+2.*W(I-1,J)-W
1(I-1,J-1))/2./DX/DX/DP
0048      D3WXP2=(W(I+1,J+1)-2.*W(I,J+1)+W(I-1,J+1)-W(I+1,J-1)+2.*W(I,J-1)-W
1(I-1,J-1))/2./DX/DP/DP
0049      ANP=DVP/R-W(I,J)/R+ANU*DUX
0050      ANX=DUX+ANU*(DVP-W(I,J))/R
0051      ANXP=(1.-ANU)*(DUP/R+DVX)/2.
0052      AMP=-(D2WP2/R/R+ANU*D2WX2)
0053      AMXP=(1.-ANU)*D2WXP/R
0054      DMXDX=-(D3WX3+ANU*D3WXP2/R/R)
0055      DMPDP=-(D3WP3/R/R+ANU*D3WX2P)
0056      DMPDX=-(D3WXP2/R/R+ANU*D3WX3)
0057      DMPXDP=-(1.-ANU)*D3WXP2/R
0058      DMXPDX=(1.-ANU)*D3WX2P/R

```

```

0059      UNEW=(-ANP*(DWX+DBX)/R+AMP*(D2WX2+D2BX2)*(DWX+DBX)*T*T/12./R+AMXP*
1(D2WXP+D2BXP)*(DWX+DBX)*T*T/12./R/R+DMXDX*(D2WX2+D2BX2)*T*T/12.+DM
2PDF*(D2WXP+D2BXP)*T*T/12./R/R+DMPXDP*(D2WX2+D2BX2)*T*T/12./R-DMXPD
3X*(D2WXP+D2BXP)*T*T/12./R+ANU*DWX/R-(1.+ANU)*D2VXP/2./R-(U(I,J+1)+
4U(I,J-1))/DX/DX-(1.-ANU)*(U(I+1,J)+U(I-1,J))/2./R/R/DF/DF/(-2./DX
5/DX-(1.-ANU)/DF/DF/R/R)
0060      VNEW=(ANXP*(DWX+DBX)/R+AMP*(DWX+DBX)*(D2WXP+D2BXP)*T*T/12./R/R+
1AMXP*(DWX+DBX)*(1.+D2WP2/R+D2BP2/R)*T*T/12./R/R+DMXDX*(D2WXP+
2D2BXP)*T*T/12./R+DMPDP*(1.+D2WP2/R+D2BP2/R)*T*T/12./R/R+DMPXDP
3*(D2WXP+D2BXP)*T*T/12./R/R-DMXPD*(1.+D2WP2/R+D2BP2/R)*T*T/12./R+
4DWP/R/R-(1.+ANU)*D2UXP/2./R-(U(I+1,J)+U(I-1,J))/R/R/DF/DF-(1.-ANU)
5*(U(I,J+1)+U(I,J-1))/2./DX/DX/(-2./R/R/DF/DF-(1.-ANU)/DX/DX)
0061      WNEW=(ANXP*(D2WXP+D2BXP)*24./T/T/R+ANX*(D2WX2+D2BX2)*12./T/T+
1ANP*(1.+D2WP2/R+D2BP2/R)*12./T/T/R+AMP*(DWX*DBX/R+DBX*DBX/R+D2WX2+
2D2BX2)/R+DMPDX*(DWX+DBX)/R+DMPDP*DBP/R/R+AMXF*(D2WXP+D2BXP+
3DBP*DWX/R+DBP*DBX/R)/R/R-DMPXDP*(DWX+2.*DBX)/R/R-(W(I,J+2)-4.*
4W(I,J+1)-4.*W(I,J-1)+W(I,J-2))/DX**4-(W(I+2,J)-4.*W(I+1,J)-4.*W(I-
51,J)+W(I-2,J))/R**4/DF**4-2.*(W(I+1,J+1)-2.*W(I+1,J)+W(I+1,J-1)-2.
6*W(I,J+1)-2.*W(I,J-1)+W(I-1,J+1)-2.*W(I-1,J)+W(I-1,J-1))/DX/DX/DF/
7DF/R/R)/(6./DX**4+6./DF**4/R**4+8./R/R/DX/DX/DF/DF)
0062      IF(ABS(U(I,J)-UNEW)-UMAX)500,500,400
C
0063      400 UMAX=ABS(U(I,J)-UNEW)
0064      K1=I-2
0065      L1=J-2
0066      500 IF(ABS(V(I,J)-VNEW)-VMAX)700,700,600
0067      600 VMAX=ABS(V(I,J)-VNEW)
0068      K2=I-2
0069      L2=J-2
0070      700 IF(ABS(W(I,J)-WNEW)-WMAX)900,900,800
0071      800 WMAX=ABS(W(I,J)-WNEW)
0072      K3=I-2
0073      L3=J-2
0074      900 U(I,J)=U(I,J)+C1*(UNEW-U(I,J))
C
0075      MODIFY DEFLECTION VALUES
0076      V(I,J)=V(I,J)+C2*(VNEW-V(I,J))
0077      W(I,J)=W(I,J)+C3*(WNEW-W(I,J))
      IF(J-3)300,1000,300

```

```

0078 1000 U(I,J)=0.0
0079 300 CONTINUE
C    CORRECT BOUNDARY VALUES ON AXIAL BOUNDARIES
0080      U(2,J)=U(4,J)
0081      V(2,J)=-V(4,J)
0082      W(1,J)=W(5,J)
0083      W(2,J)=W(4,J)
0084      V(3,J)=0.0
0085 100 CONTINUE
C    CORRECT BOUNDARY VALUES ON CIRCUMFERENTIAL BOUNDARY
0086      DO 1100 I=1,26
0087        U(I,2)=-U(I,4)
0088        V(I,2)=V(I,4)
0089        W(I,2)=W(I,4)
0090        W(I,1)=W(I,5)
0091 1100 CONTINUE
0092      ITNS=ITNS+1
0093      IT1=IT1+1
0094      IF (IT1-10)1700,200,1700
0095 200 WRITE(7,5)ITNS,UMAX,K1,L1,UMAX,K2,L2,WMAX,K3,L3
0096      5 FORMAT(3H IN,I4,11H ITNS,UMAX=,E10.3,3H AT,I3,1H,,I2,6H,UMAX=,E10.
13,3H AT,I3,1H,,I2,6H,WMAX=,E10.3,3H AT,I3,1H,,I2)
0097      IT1=0
0098      WRITE (2,1)((U(I,J),V(I,J),W(I,J),B(I,J)),I=1,26),J=1,26)
C    CHECK FOR CONVERGENCE
0099 1700 IF(UMAX-0.0000000000001)1200,1400,1400
0100 1200 IF(UMAX-0.0000000000001)1300,1400,1400
0101 1300 IF(WMAX-0.0000000000001)1500,1400,1400
0102 1400 IF(ITNS-MAX)1600,1500,1500
0103 1500 END

```



PROGRAMME USED IN THE SUCCESSIVE APPROXIMATION PROCEDURE  
USING TIMOSHENKO'S EQUILIBRIUM EQUATIONS WITH DONNELL'S  
STRESS RESULTANTS

```

C      DEFORMATION OF A CYLINDRICAL SHELL WITH AN INITIAL IMPERFECTION
C      PART TWO-----SUCCESSIVE APPROXIMATION PROCEDURE
C      SOLUTION OF TIMOSHENKO'S EQUATIONS WITH DONNELL'S STRESS
C      RESULTANTS
0001      DIMENSION U(26,26),V(26,26),W(26,26),B(26,26)
0002      CALL ASSIGN (1,'DX0:DATA1')
0003      DEFINE FILE 1 (1,16,U,IZ)
C      READ CONSTANTS AND OUTPUT VALUES
0004      READ (1,1)R,ANU,A,C,T,STR,DX,DP
0005      WRITE(7,1)R,T*1000.
0006      1 FORMAT(17H CYLINDER RADIUS=,F6.3,25H METRES---WALL THICKNESS=,F6.3
1,5H M.M.)
0007      WRITE(7,2)ANU,STR*10.**6
0008      2 FORMAT(17H POISSON'S RATIO=,F6.3,16H---AXIAL STRAIN=,F8.2,12H MICR
10STRAIN)
0009      WRITE(7,3)A,C,C/A
0010      3 FORMAT(20H IMPERFECTION WIDTH=,F8.5,22H METRES---HALF LENGTH=,F8.5
1,23H METRES---ASPECT RATIO=,F5.3)
0011      IT1=0
0012      ITNS=0
0013      WRITE(7,6)
0014      6 FORMAT(39H$U,V,AND W RELAXATION CONSTANTS ARE:- )
0015      READ(5,7)C1,C2,C3
0016      7 FORMAT(3F4.2)
0017      WRITE(7,8)
0018      8 FORMAT(30H$MAXIMUM NUMBER OF ITERATIONS=)
0019      READ(5,9)MAX
0020      9 FORMAT(I5)
0021      CALL ASSIGN (2,'DX0:DATA2')
0022      DEFINE FILE 2 (1,5408,U,IZ)
0023      READ (2,1) (((U(I,J),V(I,J),W(I,J),B(I,J)),I=1,26),J=1,26)
C      START ITERATION FOR WHOLE SHELL
0024      1600 UMAX=0.0
0025      VMAX=0.0
0026      WMAX=0.0
0027      DO 100 J=3,24

```

```

C      START ITERATION FOR ROW
0028      DO 300 I=3,24
0029      DWX=(W(I,J+1)-W(I,J-1))/2./DX
0030      DUX=(U(I,J+1)-U(I,J-1))/2./DX
0031      DVX=(V(I,J+1)-V(I,J-1))/2./DX
0032      DBX=(B(I,J+1)-B(I,J-1))/2./DX
0033      DWP=(W(I+1,J)-W(I-1,J))/2./DP
0034      DUP=(U(I+1,J)-U(I-1,J))/2./DP
0035      DVP=(V(I+1,J)-V(I-1,J))/2./DP
0036      DBP=(B(I+1,J)-B(I-1,J))/2./DP
0037      D2WX2=(W(I,J+1)-2.*W(I,J)+W(I,J-1))/DX/DX
0038      D2BX2=(B(I,J+1)-2.*B(I,J)+B(I,J-1))/DX/DX
0039      D2WP2=(W(I+1,J)-2.*W(I,J)+W(I-1,J))/DP/DP
0040      D2BP2=(B(I+1,J)-2.*B(I,J)+B(I-1,J))/DP/DP
0041      D2WXP=(W(I+1,J+1)-W(I+1,J-1)-W(I-1,J+1)+W(I-1,J-1))/4./DX/DP
0042      D2UXP=(U(I+1,J+1)-U(I+1,J-1)-U(I-1,J+1)+U(I-1,J-1))/4./DX/DP
0043      D2VXP=(V(I+1,J+1)-V(I+1,J-1)-V(I-1,J+1)+V(I-1,J-1))/4./DX/DP
0044      D2BXP=(B(I+1,J+1)-B(I+1,J-1)-B(I-1,J+1)+B(I-1,J-1))/4./DX/DP
0045      D3WX3=(W(I,J+2)-2.*W(I,J+1)+2.*W(I,J-1)-W(I,J-2))/2./DX/DX/DX
0046      D3WP3=(W(I+2,J)-2.*W(I+1,J)+2.*W(I-1,J)-W(I-2,J))/2./DP/DP/DP
0047      D3WX2F=(W(I+1,J+1)-2.*W(I+1,J)+W(I+1,J-1)-W(I-1,J+1)+2.*W(I-1,J)-W(
1(I-1,J-1))/2./DX/DX/DP
0048      D3WXP2=(W(I+1,J+1)-2.*W(I,J+1)+W(I-1,J+1)-W(I+1,J-1)+2.*W(I,J-1)-W(
1(I-1,J-1))/2./DX/DP/DP
0049      ANP=DVP/R-W(I,J)/R+ANU*DUX
0050      ANX=DUX+ANU*(DVP-W(I,J))/R
0051      ANXP=(1.-ANU)*(DUP/R+DVX)/2.
0052      AMP=- (D2WP2/R/R+ANU*D2WX2)
0053      AMXP=(1.-ANU)*D2WXP/R
0054      DMXDX=- (D3WX3+ANU*D3WXP2/R/R)
0055      DMPDP=- (D3WP3/R/R+ANU*D3WX2F)
0056      DMPDX=- (D3WXP2/R/R+ANU*D3WX3)
0057      DMPXDP=- (1.-ANU)*D3WXP2/R
0058      DMXPDX=(1.-ANU)*D3WX2F/R

```

```

0059      UNEW=(-ANF*(DWX+DBX)/R+AMP*(D2WX2+D2BX2)*(DWX+DBX)*T*T/12./R+AMXP*
1(D2WXP+D2BXP)*(DWX+DBX)*T*T/12./R/R+DMXDX*(D2WX2+D2BX2)*T*T/12.+DM
2PDP*(D2WXP+D2BXP)*T*T/12./R/R+DMPXDF*(D2WX2+D2BX2)*T*T/12./R-DMXPD
3X*(D2WXP+D2BXP)*T*T/12./R+ANU*DWX/R-(1.+ANU)*D2VXP/2./R
4-DWX*D2WX2-(1.+ANU)*DWP*D2WXP/2./R/R-(1.-ANU)*DWX*D2WPF/2./R/R
5-(U(I,J+1)+U(I,J-1))/DX/DX-(1.-ANU)*(U(I+1,J)+U(I-1,J))/2./R/R/DF/
6DP)/(-2./DX/DX-(1.-ANU)/DF/DF/R/R)
0060      UNEW=(ANXP*(DWX+DBX)/R+AMP*(DWX+DBX)*(D2WXP+D2BXP)*T*T/12./R/R+
1AMXP*(DWX+DBX)*(1.+D2WPF/2./R+D2BPF/2./R)*T*T/12./R/R+DMXDX*(D2WXP+
2D2BXP)*T*T/12./R+DMPDP*(1.+D2WPF/2./R+D2BPF/2./R)*T*T/12./R/R+DMPXDF
3*(D2WXP+D2BXP)*T*T/12./R/R-DMXPD*(1.+D2WPF/2./R+D2BPF/2./R)*T*T/12./R-
4(1.+ANU)*DWX*D2WXP/2./R-(1.-ANU)*DWP*D2WX2/2./R-DWP*D2WPF/2./R/R+
5DWP/R/R-(1.+ANU)*D2UXF/2./R-(V(I+1,J)+V(I-1,J))/R/R/DF/DF-(1.-ANU)
6*(V(I,J+1)+V(I,J-1))/2./DX/DX)/(-2./R/R/DF/DF-(1.-ANU)/DX/DX)
0061      UNEW=(ANXP*(D2WXP+D2BXP)*24./T/T/R+ANX*(D2WX2+D2BX2)*12./T/T+
1ANF*(1.+D2WPF/2./R+D2BPF/2./R)*12./T/T/R+AMP*(DWX*DBX/R+DBX*DEX/R+D2WX2+
2D2BX2)/R+DMFDX*(DWX+DBX)/R+DMPDP*DBF/R/R/R+AMXP*(D2WXP+D2BXP+
3DBF*DWX/R+DBF*DBX/R)/R/R-DMPXDF*(DWX+2.*DBX)/R/R-(W(I,J+2)-4.*
4W(I,J+1)-4.*W(I,J-1)+W(I,J-2))/DX**4-(W(I+2,J)-4.*W(I+1,J)-4.*W(I-
51,J)+W(I-2,J))/R**4/DF**4-2.*(W(I+1,J+1)-2.*W(I+1,J)+W(I+1,J-1)-2.
6*W(I,J+1)-2.*W(I,J-1)+W(I-1,J+1)-2.*W(I-1,J)+W(I-1,J-1))/DX/DX/DF/
7DF/R/R)/(6./DX**4+6./DF**4/R**4+8./R/R/DX/DX/DF/DF)
0062      IF(ABS(U(I,J)-UNEW)-UMAX)500,500,400
C      CHECK FOR MAXIMUM CHANGES
0063      400 UMAX=ABS(U(I,J)-UNEW)
0064      K1=I-2
0065      L1=J-2
0066      500 IF(ABS(V(I,J)-VNEW)-VMAX)700,700,600
0067      600 VMAX=ABS(V(I,J)-VNEW)
0068      K2=I-2
0069      L2=J-2
0070      700 IF(ABS(W(I,J)-WNEW)-WMAX)900,900,800
0071      800 WMAX=ABS(W(I,J)-WNEW)
0072      K3=I-2
0073      L3=J-2
0074      900 U(I,J)=U(I,J)+C1*(UNEW-U(I,J))
C      MODIFY DEFLECTION VALUES
0075      V(I,J)=V(I,J)+C2*(VNEW-V(I,J))

```

```

0076      W(I,J)=W(I,J)+C3*(WNEW-W(I,J))
0077      IF(J-3)300,1000,300
0078 1000 U(I,J)=0.0
0079 300 CONTINUE
C      CORRECT BOUNDARY VALUES ON AXIAL BOUNDARIES
0080      U(2,J)=U(4,J)
0081      V(2,J)=-V(4,J)
0082      W(1,J)=W(5,J)
0083      W(2,J)=W(4,J)
0084      V(3,J)=0.0
0085 100 CONTINUE
C      CORRECT BOUNDARY VALUES ON CIRCUMFERENTIAL BOUNDARY
0086      DO 1100 I=1,26
0087      U(I,2)=-U(I,4)
0088      V(I,2)=V(I,4)
0089      W(I,2)=W(I,4)
0090      W(I,1)=W(I,5)
0091 1100 CONTINUE
0092      ITNS=ITNS+1
0093      IT1=IT1+1
0094      IF (IT1-10)1700,200,1700
0095 200 WRITE(7,5)ITNS,UMAX,K1,L1,UMAX,K2,L2,WMAX,K3,L3
0096 5  FORMAT(3H 1N,14,11H ITNS,UMAX=,E10.3,3H AT,13,1H,,12,6H,UMAX=,E10.
13,3H AT,13,1H,,12,6H,WMAX=,E10.3,3H AT,13,1H,,12)
0097      IT1=0
0098      WRITE (2,1)((U(I,J),V(I,J),W(I,J),B(I,J)),I=1,26),J=1,26)
C      CHECK FOR CONVERGENCE
0099 1700 IF(UMAX-0.000000000000001)1200,1400,1400
0100 1200 IF(VMAX-0.000000000000001)1300,1400,1400
0101 1300 IF(WMAX-0.000000000000001)1500,1400,1400
0102 1400 IF(ITNS-MAX)1600,1500,1500
0103 1500 END

```

CYLINDER RADIUS= 0.100 METRES---WALL THICKNESS= 0.190 M.M.  
 POISSON'S RATIO= 0.350---AXIAL STRAIN= 50.00 MICROSTRAIN  
 IMPERFECTION WIDTH= 0.04000 METRES---HALF LENGTH= 0.02800 METRES---ASPECT RATIO=0.700  
 U,V,AND W RELAXATION CONSTANTS ARE:- 1.0,1.0,1.0

MAXIMUM NUMBER OF ITERATIONS=2000

TYPICAL OUTPUT TO ALL THREE SUCCESSIVE APPROXIMATION PROCEDURES

IN 10	ITNS.UMAX=	0.572E-09	AT	1,11,UMAX=	0.290E-08	AT	6,11,WMAX=	0.834E-07	AT	1,10
IN 20	ITNS.UMAX=	0.571E-09	AT	1,10,UMAX=	0.276E-08	AT	6,11,WMAX=	0.721E-07	AT	1,10
IN 30	ITNS.UMAX=	0.546E-09	AT	1, 9,UMAX=	0.262E-08	AT	6,10,WMAX=	0.627E-07	AT	1,10
IN 40	ITNS.UMAX=	0.538E-09	AT	1, 9,UMAX=	0.251E-08	AT	6,10,WMAX=	0.551E-07	AT	1,10
IN 50	ITNS.UMAX=	0.510E-09	AT	1, 9,UMAX=	0.239E-08	AT	6,10,WMAX=	0.489E-07	AT	1,10
IN 60	ITNS.UMAX=	0.486E-09	AT	1, 8,UMAX=	0.228E-08	AT	6,10,WMAX=	0.447E-07	AT	1, 9
IN 70	ITNS.UMAX=	0.460E-09	AT	1, 8,UMAX=	0.217E-08	AT	7,10,WMAX=	0.413E-07	AT	1, 9
IN 80	ITNS.UMAX=	0.428E-09	AT	1, 8,UMAX=	0.208E-08	AT	7,10,WMAX=	0.384E-07	AT	1, 9
IN 90	ITNS.UMAX=	0.395E-09	AT	1, 8,UMAX=	0.200E-08	AT	7,10,WMAX=	0.357E-07	AT	1, 9
IN 100	ITNS.UMAX=	0.366E-09	AT	1, 7,UMAX=	0.192E-08	AT	7,10,WMAX=	0.334E-07	AT	1, 9
IN 110	ITNS.UMAX=	0.339E-09	AT	1, 7,UMAX=	0.185E-08	AT	7, 9,WMAX=	0.313E-07	AT	1, 9
IN 120	ITNS.UMAX=	0.312E-09	AT	1, 7,UMAX=	0.179E-08	AT	7, 9,WMAX=	0.295E-07	AT	1, 9
IN 130	ITNS.UMAX=	0.286E-09	AT	1, 7,UMAX=	0.173E-08	AT	7, 9,WMAX=	0.278E-07	AT	1, 9
IN 140	ITNS.UMAX=	0.262E-09	AT	1, 7,UMAX=	0.168E-08	AT	7, 9,WMAX=	0.264E-07	AT	1, 9
IN 150	ITNS.UMAX=	0.239E-09	AT	1, 7,UMAX=	0.163E-08	AT	7, 9,WMAX=	0.253E-07	AT	1, 8
IN 160	ITNS.UMAX=	0.219E-09	AT	1,16,UMAX=	0.158E-08	AT	7, 9,WMAX=	0.243E-07	AT	1, 8
IN 170	ITNS.UMAX=	0.216E-09	AT	1,16,UMAX=	0.154E-08	AT	7, 9,WMAX=	0.234E-07	AT	1, 8
IN 180	ITNS.UMAX=	0.213E-09	AT	1,16,UMAX=	0.150E-08	AT	8, 9,WMAX=	0.225E-07	AT	1, 8
IN 190	ITNS.UMAX=	0.211E-09	AT	1,16,UMAX=	0.146E-08	AT	8, 9,WMAX=	0.217E-07	AT	1, 8
IN 200	ITNS.UMAX=	0.208E-09	AT	1,16,UMAX=	0.143E-08	AT	8, 9,WMAX=	0.210E-07	AT	1, 8
IN 210	ITNS.UMAX=	0.206E-09	AT	1,16,UMAX=	0.140E-08	AT	8, 9,WMAX=	0.203E-07	AT	1, 8
IN 220	ITNS.UMAX=	0.203E-09	AT	1,16,UMAX=	0.137E-08	AT	8, 8,WMAX=	0.197E-07	AT	1, 8
IN 230	ITNS.UMAX=	0.201E-09	AT	1,16,UMAX=	0.135E-08	AT	8, 8,WMAX=	0.191E-07	AT	1, 8
IN 240	ITNS.UMAX=	0.199E-09	AT	1,16,UMAX=	0.132E-08	AT	8, 8,WMAX=	0.185E-07	AT	1, 8
IN 250	ITNS.UMAX=	0.197E-09	AT	1,16,UMAX=	0.130E-08	AT	8, 8,WMAX=	0.180E-07	AT	1, 8
IN 260	ITNS.UMAX=	0.195E-09	AT	1,16,UMAX=	0.128E-08	AT	8, 8,WMAX=	0.175E-07	AT	1, 8
IN 270	ITNS.UMAX=	0.193E-09	AT	1,16,UMAX=	0.126E-08	AT	8, 8,WMAX=	0.170E-07	AT	1, 8
IN 280	ITNS.UMAX=	0.191E-09	AT	1,16,UMAX=	0.124E-08	AT	8, 8,WMAX=	0.165E-07	AT	1, 8
IN 290	ITNS.UMAX=	0.189E-09	AT	1,16,UMAX=	0.122E-08	AT	8, 8,WMAX=	0.161E-07	AT	1, 8
IN 300	ITNS.UMAX=	0.187E-09	AT	1,16,UMAX=	0.120E-08	AT	8, 8,WMAX=	0.157E-07	AT	1, 8

```

C      DEFORMATIONS IN A CYLINDRICAL SHELL WITH AN INITIAL IMPERFECTION
C      PART THREE---PRINT DEFLECTION VALUES
0001      DIMENSION U(26,26),V(26,26),W(26,26),B(26,26)
0002      CALL ASSIGN (1,'DX0:DATA1')
0003      DEFINE FILE 1 (1,16,U,IZ)
0004      READ (1,1)R,ANU,A,C,T,STR,DX,DP
0005      WRITE (7,1)R,T*1000.
0006      1 FORMAT (17H CYLINDER RADIUS=,F6.3,25H METRES---WALL THICKNESS=,F6.
13,5H M.M.)
0007      WRITE (7,2)ANU,STR*10.**6
0008      2 FORMAT(17H POISSON'S RATIO=,F6.3,16H---AXIAL STRAIN=,F8.2,12H MICR
10STRAIN)
0009      WRITE (7,3)A,C,C/A
0010      3 FORMAT(20H IMPERFECTION WIDTH=,F8.5,22H METRES---HALF LENGTH=,F8.5
1,23H METRES---ASPECT RATIO=,F5.3//)
0011      CALL ASSIGN (2,'DX0:DATA2')
0012      DEFINE FILE 2 (1,5408,U,IZ)
0013      READ (2,1)((U(I,J),V(I,J),W(I,J),B(I,J)),I=1,26),J=1,26)
0014      WRITE (7,4)
0015      4 FORMAT(54H0      PHI.      U-AXIAL      V-TGTL.      W-RAD.      B)
0016      WRITE (7,7)
0017      7 FORMAT(12H      DEG.      ,4(12H      M.      ))
0018      DO 100 J=3,25
0019      WRITE (7,5)(J-3)*DX
0020      5 FORMAT(18H0DEFLECTIONS AT X=,E11.4,7H METRES)
0021      DO 100 I=3,25
0022      WRITE(7,6)(I-3)*DP*180./3.1415927,U(I,J),V(I,J),W(I,J),B(I,J)
0023      6 FORMAT(5E12.4)
0024      100 CONTINUE
0025      END

```

CYLINDER RADIUS= 0.100 METRES---WALL THICKNESS= 0.190 M.M.  
 POISSON'S RATIO= 0.350---AXIAL STRAIN= 300.00 MICROSTRAIN  
 IMPERFECTION WIDTH= 0.04000 METRES---HALF LENGTH= 0.02800 METRES---ASPECT RATIO=0.700

PHI. DEG.	U-AXIAL M.	V-TGTL. M.	W-RAD. M.	B M.
DEFLECTIONS AT X= 0.0000E+00 METRES				
0.0000E+00	0.0000E+00	0.0000E+00	-0.7618E-04	0.2020E-02
0.1049E+01	0.0000E+00	-0.1326E-05	-0.7575E-04	0.2004E-02
0.2098E+01	0.0000E+00	-0.2633E-05	-0.7439E-04	0.1955E-02
0.3146E+01	0.0000E+00	-0.3902E-05	-0.7195E-04	0.1872E-02
0.4195E+01	0.0000E+00	-0.5107E-05	-0.6820E-04	0.1757E-02
0.5244E+01	0.0000E+00	-0.6223E-05	-0.6285E-04	0.1609E-02
0.6293E+01	0.0000E+00	-0.7217E-05	-0.5563E-04	0.1426E-02
0.7342E+01	0.0000E+00	-0.8052E-05	-0.4628E-04	0.1211E-02
0.8391E+01	0.0000E+00	-0.8689E-05	-0.3465E-04	0.9603E-03
0.9439E+01	0.0000E+00	-0.9087E-05	-0.2080E-04	0.6755E-03
0.1049E+02	0.0000E+00	-0.9203E-05	-0.5087E-05	0.3556E-03
0.1154E+02	0.0000E+00	-0.9006E-05	0.1163E-04	0.7451E-08
0.1259E+02	0.0000E+00	-0.8481E-05	0.2902E-04	0.0000E+00
0.1363E+02	0.0000E+00	-0.7625E-05	0.4338E-04	0.0000E+00
0.1468E+02	0.0000E+00	-0.6508E-05	0.5305E-04	0.0000E+00
0.1573E+02	0.0000E+00	-0.5238E-05	0.5732E-04	0.0000E+00
0.1678E+02	0.0000E+00	-0.3935E-05	0.5611E-04	0.0000E+00
0.1783E+02	0.0000E+00	-0.2714E-05	0.4980E-04	0.0000E+00
0.1888E+02	0.0000E+00	-0.1672E-05	0.3929E-04	0.0000E+00
0.1993E+02	0.0000E+00	-0.8756E-06	0.2588E-04	0.0000E+00
0.2098E+02	0.0000E+00	-0.3526E-06	0.1138E-04	0.0000E+00
0.2203E+02	0.0000E+00	-0.8374E-07	-0.1796E-05	0.0000E+00
0.2307E+02	0.0000E+00	0.0000E+00	-0.1050E-04	0.0000E+00
DEFLECTIONS AT X= 0.2545E-02 METRES				
0.0000E+00	-0.6704E-06	0.0000E+00	-0.7783E-04	0.1837E-02
0.1049E+01	-0.6683E-06	-0.1339E-05	-0.7737E-04	0.1820E-02
0.2098E+01	-0.6622E-06	-0.2659E-05	-0.7595E-04	0.1771E-02

TYPICAL OUTPUT TO PROGRAMME TO PRINT DEFLECTION VALUES

```

C      DEFORMATIONS IN A CYLINDRICAL SHELL WITH AN INITIAL IMPERFECTION
C      PART FOUR---CALCULATE MEMBRANE STRESSES AND PRINT VALUES
0001  DIMENSION U(26,26),V(26,26),W(26,26),B(26,26)
0002  CALL ASSIGN (1,'DX0:DATA1')
0003  DEFINE FILE 1 (1,16,U,IZ)
0004  READ (1,1)R,ANU,A,C,T,STR,DX,DP
0005  WRITE (7,1)R,TK*1000.
0006  1 FORMAT (17H CYLINDER RADIUS=,F6.3,25H METRES---WALL THICKNESS=,F6.
    13,5H M.M.)
0007  WRITE (7,2)ANU,STR*10.**6
0008  2 FORMAT(17H POISSON'S RATIO=,F6.3,16H---AXIAL STRAIN=,F8.2,12H MICR
    10STRAIN)
0009  WRITE (7,3)A,C,C/A
0010  3 FORMAT(20H IMPERFECTION WIDTH=,F8.5,22H METRES---HALF LENGTH=,F8.5
    1,23H METRES---ASPECT RATIO=,F5.3//)
0011  CALL ASSIGN (2,'DX0:DATA2')
0012  DEFINE FILE 2 (1,5408,U,IZ)
0013  READ (2,1)((U(I,J),V(I,J),W(I,J),B(I,J)),I=1,26),J=1,26)
0014  WRITE (7,4)
0015  4 FORMAT (43HOMEMBRANE STRESSES IN SHELL/YOUNG'S MODULUS)
0016  WRITE (7,5)
0017  5 FORMAT (55H0 PHI.      AXIAL    TGTL.    SHEAR      PRINCIPAL    DIRN.
    1)
0018  WRITE (7,6)
0019  6 FORMAT (7H DEG. ,5(8H X10**6),7H DEG.)

```



```

0020      DO 100 J=3,24
0021      WRITE (7,7)(J-3)*DX
0022      7 FORMAT (15H0STRESSES AT X=,E11.4,7H METRES)
0023      DO 100 I=3,24
0024      DUP=(U(I+1,J)-U(I-1,J))/2./DP
0025      DUX=(U(I,J+1)-U(I,J-1))/2./DX
0026      DVP=(V(I+1,J)-V(I-1,J))/2./DP
0027      DVX=(V(I,J+1)-V(I,J-1))/2./DX
0028      DWX=(W(I,J+1)-W(I,J-1))/2./DX
0029      DWP=(W(I+1,J)-W(I-1,J))/2./DP
0030      SX=(DUX+DWX*DWX/2.+ANU*DVP/R-ANU*W(I,J)/R+ANU*DWP*DWP/2./R/R)/(1.-
1ANU*ANU)
0031      SP=(DVP/R+DWP*DWP/2./R/R-W(I,J)/R+ANU*DUX+ANU*DWX*DWX/2.)/(1.-ANU*
1ANU)
0032      SXP=(DUP/R+DVX+DWX*DWP/R)/2./(1.+ANU)
0033      S1=(SX+SP)/2.+SQRT((SX-SP)**2/4.+SXP**2)
0034      S2=(SX+SP)/2.-SQRT((SX-SP)**2/4.+SXP**2)
0035      TH=ATAN(SXP*2./(SX-SP))*90./3.1415927
0036      WRITE (7,8)(I-3)*DP*180./3.1415927,SX*1000000.,SP*1000000.,SXP*100
10000.,S1*1000000.,S2*1000000.,TH
0037      8 FORMAT (7F8.2)
0038      100 CONTINUE
0039      END

```

CYLINDER RADIUS= 0.100 METRES---WALL THICKNESS= 0.190 M.M.  
 POISSON'S RATIO= 0.350---AXIAL STRAIN= 300.00 MICROSTRAIN  
 IMPERFECTION WIDTH= 0.04000 METRES---HALF LENGTH= 0.02800 METRES---ASPECT RATIO=0.700

# MEMBRANE STRESSES IN SHELL/YOUNG'S MODULUS

PHI.	AXIAL	TGTL.	SHEAR	PRINCIPAL	DIRN.
DEG.	X10**6	X10**6	X10**6	X10**6	DEG.

## STRESSES AT X= 0.0000E+00 METRES

0.00	-285.20	-62.37	0.00	-62.37	-285.20	0.00
1.05	-283.92	-61.06	0.00	-61.06	-283.92	0.00
2.10	-280.18	-57.18	0.00	-57.18	-280.18	0.00
3.15	-274.33	-50.90	0.00	-50.90	-274.33	0.00
4.20	-266.89	-42.49	0.00	-42.49	-266.89	0.00
5.24	-258.63	-32.29	0.00	-32.29	-258.63	0.00
6.29	-250.45	-20.70	0.00	-20.70	-250.45	0.00
7.34	-243.41	-8.19	0.00	-8.19	-243.41	0.00
8.39	-238.63	4.70	0.00	4.70	-238.63	0.00
9.44	-237.27	17.14	0.00	17.14	-237.27	0.00
10.49	-240.52	27.87	0.00	27.87	-240.52	0.00
11.54	-248.75	37.26	0.00	37.26	-248.75	0.00
12.59	-264.20	32.19	0.00	32.19	-264.20	0.00
13.63	-280.02	28.75	0.00	28.75	-280.02	0.00
14.68	-294.68	25.56	0.00	25.56	-294.68	0.00
15.73	-306.74	22.63	0.00	22.63	-306.74	0.00
16.78	-315.25	20.24	0.00	20.24	-315.25	0.00
17.83	-319.77	18.75	0.00	18.75	-319.77	0.00
18.88	-320.19	18.50	0.00	18.50	-320.19	0.00
19.93	-316.73	19.72	0.00	19.72	-316.73	0.00
20.98	-309.84	22.58	0.00	22.58	-309.84	0.00
22.03	-300.16	27.09	0.00	27.09	-300.16	0.00

## STRESSES AT X= 0.2545E-02 METRES

0.00	-282.65	-52.11	0.00	-52.11	-282.65	0.00
1.05	-281.40	-50.83	-3.16	-50.78	-281.45	0.79
2.10	-277.77	-47.03	-6.23	-46.86	-277.94	1.54

TYPICAL OUTPUT TO PROGRAMME TO CALCULATE AND PRINT STRESSES

PROGRAMME USED TO CHANGE VALUE OF AXIAL STRAIN AND MODIFY  
 DEFLECTION VALUES TO PROVIDE INITIAL GUESSES TO SUBSEQUENT  
 CALCULATIONS

```

C   DEFORMATIONS IN A CYLINDRICAL SHELL WITH AN INITIAL IMPERFECTION
C   PROGRAMME TO MODIFY AXIAL STRAIN
0001  DIMENSION U(26,26),V(26,26),W(26,26),B(26,26)
0002  CALL ASSIGN (1,'DX0:DATA1')
0003  DEFINE FILE 1 (1,16,U,IZ)
0004  READ (1,1)R,ANU,A,C,T,STR,DX,DP
0005  WRITE (7,1)R,T*1000.
0006  1 FORMAT (17H CYLINDER RADIUS=,F6.3,25H METRES---WALL THICKNESS=,F6.
    13,5H M.M.)
0007  WRITE (7,2)ANU,STR*10.**6
0008  2 FORMAT(17H POISSON'S RATIO=,F6.3,16H---AXIAL STRAIN=,F8.2,12H MICR
    10STRAIN)
0009  WRITE (7,3)A,C,C/A
0010  3 FORMAT(20H IMPERFECTION WIDTH=,F8.5,22H METRES---HALF LENGTH=,F8.5
    1,23H METRES---ASPECT RATIO=,F5.3//)
0011  CALL ASSIGN (2,'DX0:DATA2')
0012  DEFINE FILE 2 (1,5408,U,IZ)
0013  READ (2,1)((U(I,J),V(I,J),W(I,J),B(I,J)),I=1,26),J=1,26)
0014  WRITE (7,4)
0015  4 FORMAT (31H$NEW AXIAL STRAIN(MICROSTRAIN)=)
0016  READ (5,5) STR1
0017  5 FORMAT (F8.2)
0018  STR1=STR1/10.**6
0019  DO 100 J=1,26
0020  DO 100 I=1,26
0021  U(I,J)=U(I,J)*STR1/STR
0022  V(I,J)=V(I,J)*STR1/STR
0023  W(I,J)=W(I,J)*STR1/STR
0024  100 CONTINUE
0025  WRITE (1,1)R,ANU,A,C,T,STR1,DX,DP
0026  WRITE (2,1)((U(I,J),V(I,J),W(I,J),B(I,J)),I=1,26),J=1,26)
0027  END

```

TYPICAL OUTPUT TO PROGRAMME TO MODIFY AXIAL STRAIN

CYLINDER RADIUS= 0.100 METRES---WALL THICKNESS= 0.190 M.M.  
POISSON'S RATIO= 0.350---AXIAL STRAIN= 250.00 MICROSTRAIN  
IMPERFECTION WIDTH= 0.04000 METRES---HALF LENGTH= 0.02800 METRES---ASPECT RATIO=0.700

NEW AXIAL STRAIN(MICROSTRAIN)=300.0

APPENDIX    E

PROGRAM LISTING AND TYPICAL OUTPUT OF PROGRAMS USED IN  
CALCULATING THE FOLD SHAPE BASED ON THE BI-HARMONIC EQUATION

```

C      PROGRAMME TO CALCULATE THE SHAPE OF THE FOLD IN A YOSHIMURA BUCKLE
C      PATTERN FOR THIN WALLED CYLINDRICAL SHELLS
C      PART 1---OPEN FILES AND ESTIMAT INITIAL VALUES
0001      DIMENSION W(54,54)
C      READ IN DATA
0002      WRITE(7,1)
0003      1 FORMAT(48H$LENGTH OF DIAGONAL COMPRESSION MEMBER(METRES) =)
0004      READ(5,2)X
0005      2 FORMAT(F8.5)
0006      WRITE(7,3)
0007      3 FORMAT(49H$WIDTH OF FACET PERP.TO DIAGONAL MEMBER(METRES) =)
0008      READ(5,4)Y
0009      4 FORMAT(F8.5)
0010      WRITE(7,5)
0011      5 FORMAT(32H$ANGLE BETWEEN FACETS(DEGREES) =)
0012      READ(5,6)AL
0013      6 FORMAT(F6.2)
0014      WRITE(7,7)
0015      7 FORMAT(45H$NO.OF POINTS IN HALF MEMBER LENGTH(MAX.50) =)
0016      READ(5,8)N
0017      8 FORMAT(I2)
0018      WRITE(7,9)
0019      9 FORMAT(43H$NO.OF POINTS ACROSS FACET WIDTH(MAX.100) =)
0020      READ(5,10)M
0021      10 FORMAT(I3)
0022      AL=(90.0-AL/2.)*3.1415927/180.0
0023      DX=X/N/2.
0024      DY=Y/M
0025      CALL ASSIGN (1,'DX0:DATA3')
0026      DEFINE FILE 1 (1,12,U,IZ)
0027      WRITE(1'1)X,Y,AL,N,M,DX,DY
0028      CALL ASSIGN (2,'DX0:DATA4')
0029      DEFINE FILE 2 (1,5832,U,IZ)
0030      DO 100 I=1,N+4
0031      W(I,1)=2.*DY*SIN(AL)
0032      100 W(I,2)=DY*SIN(AL)
0033      DO 200 J=3,M+4
0034      DO 200 I=1,N+4
0035      200 W(I,J)=(J-3)*DY*SIN(AL)
0036      WRITE (2'1)((W(I,J),I=1,N+4),J=1,M+4)
0037      END

```

TYPICAL OUTPUT TO OPENING PROGRAMME

LENGTH OF DIAGONAL COMPRESSION MEMBER(METRES) =.15  
WIDTH OF FACET PERP.TO DIAGONAL MEMBER(METRES) =.045  
ANGLE BETWEEN FACETS(DEGREES) =175.  
NO.OF POINTS IN HALF MEMBER LENGTH(MAX.50) =15  
NO.OF POINTS ACROSS FACET WIDTH(MAX.100) =9  
STOP ---

```

C      PROGRAMME TO CALCULATE THE SHAPE OF THE FOLD IN A YOSHIMURA BUCKLE
C      PATTERN FOR THIN WALLED CYLINDRICAL SHELLS
C      PART 2 --- SUCCESSIVE APPROXIMATION PROCEDURE TO CALCULATE BETTER
C      GUESSES
0001      DIMENSION W(54,54)
0002      CALL ASSIGN (1,'DX0:DATA3')
0003      DEFINE FILE 1 (1,12,U,IZ)
0004      READ (1,1)X,Y,AL,N,M,DX,DY
0005      WRITE (7,1)X,Y
0006      1 FORMAT(32H LENGTH OF DIAGONAL COMP.MEMBER=,F8.5,32H M.  FACET WIDT
1H PERP.TO MEMBER=,F8.5,3H M.)
0007      WRITE (7,2)180.0-AL*360.0/3.1415927
0008      2 FORMAT(22H ANGLE BETWEEN FACETS=,F6.2,5H DEG.)
0009      WRITE (7,3)N,DX
0010      3 FORMAT(36H NO.OF POINTS IN HALF MEMBER LENGTH=,I4,21H -- INCREMENT
1 LENGTH=,F10.7,3H M.)
0011      WRITE (7,4)M,DY
0012      4 FORMAT(33H NO.OF POINTS ACROSS FACET WIDTH=,I4,21H -- INCREMENT LE
1NGTH=,F10.7,3H M.)
0013      IT1=0
0014      ITNS=0
0015      WRITE (7,7)
0016      7 FORMAT(27H$RELAXATION CONSTANT IS:- )
0017      READ (5,8)C
0018      8 FORMAT(F4.2)
0019      WRITE (7,9)
0020      9 FORMAT(30H$MAXIMUM NUMBER OF ITERATIONS=)
0021      READ (5,10)MAX
0022      10 FORMAT(I5)

```



```

0023      CALL ASSIGN (2,'DX0:DATA4')
0024      DEFINE FILE 2 (1,5832,U,IZ)
0025      READ (2'1)((W(I,J),I=1,N+4),J=1,M+4)
0026      500 WMAX=0.0
0027      DO 200 J=3,M+2
0028      DO 100 I=3,N+2
0029      WNEW=(-(W(I+2,J)-4.*W(I+1,J)-4.*W(I-1,J)+W(I-2,J))/DX**4
1-(W(I,J+2)-4.*W(I,J+1)-4.*W(I,J-1)+W(I,J-2))/DY**4
2-2.*(W(I+1,J+1)-2.*W(I+1,J)+W(I+1,J-1)-2.*W(I,J+1)-2.*W(I,J-1)
3+W(I-1,J+1)-2.*W(I-1,J)+W(I-1,J-1))/DX/DX/DY/DY)/(6./DX**4
4+6./DY**4+8./DX/DX/DY/DY)
0030      IF (ABS(W(I,J)-WNEW)-WMAX)100,100,300
0031      300 WMAX=ABS(W(I,J)-WNEW)
0032      K=I-2
0033      L=J-3
0034      100 W(I,J)=W(I,J)+C*(WNEW-W(I,J))
0035      W(1,J)=W(3,J)
0036      W(N+3,J)=W(N+1,J)
0037      200 W(N+4,J)=W(N,J)
0038      DO 400 I=3,N+4
0039      W(I,1)=W(I,5)
0040      400 W(I,2)=W(I,4)
0041      ITNS=ITNS+1
0042      IT1=IT1+1
0043      IF(IT1-50)1000,900,1000
0044      900 WRITE (7,6)ITNS,WMAX,K,L
0045      6 FORMAT (3H IN,I4,18H ITERATIONS, WMAX=,E10.3,6H AT I=,I3,7H AND J=
1,I3)
0046      IT1=0
0047      WRITE (2'1)((W(I,J),I=1,N+4),J=1,M+4)
0048      1000 IF(WMAX-0.000000001)800,700,700
0049      700 IF(ITNS-MAX)500,800,800
0050      800 END

```

LENGTH OF DIAGONAL COMP.MEMBER= 0.15000 M. FACET WIDTH PERP.TO MEMBER= 0.04500 M.  
ANGLE BETWEEN FACETS=175.00 DEG.  
NO.OF POINTS IN HALF MEMBER LENGTH= 15 -- INCREMENT LENGTH= 0.0050000 M.  
NO.OF POINTS ACROSS FACET WIDTH= 9 -- INCREMENT LENGTH= 0.0050000 M.  
RELAXATION CONSTANT IS:- 1.0

MAXIMUM NUMBER OF ITERATIONS=20000

IN 50 ITERATIONS, WMAX= 0.204E-08 AT I= 14 AND J= 0  
IN 100 ITERATIONS, WMAX= 0.198E-08 AT I= 14 AND J= 0  
IN 150 ITERATIONS, WMAX= 0.204E-08 AT I= 14 AND J= 0  
IN 200 ITERATIONS, WMAX= 0.180E-08 AT I= 12 AND J= 0  
IN 250 ITERATIONS, WMAX= 0.180E-08 AT I= 15 AND J= 1  
IN 300 ITERATIONS, WMAX= 0.175E-08 AT I= 14 AND J= 0  
IN 350 ITERATIONS, WMAX= 0.175E-08 AT I= 15 AND J= 0  
IN 400 ITERATIONS, WMAX= 0.163E-08 AT I= 15 AND J= 0  
IN 450 ITERATIONS, WMAX= 0.157E-08 AT I= 13 AND J= 0  
IN 500 ITERATIONS, WMAX= 0.157E-08 AT I= 13 AND J= 0  
IN 550 ITERATIONS, WMAX= 0.151E-08 AT I= 15 AND J= 0  
IN 600 ITERATIONS, WMAX= 0.146E-08 AT I= 13 AND J= 1  
IN 650 ITERATIONS, WMAX= 0.151E-08 AT I= 15 AND J= 1  
IN 700 ITERATIONS, WMAX= 0.151E-08 AT I= 14 AND J= 0  
IN 750 ITERATIONS, WMAX= 0.140E-08 AT I= 14 AND J= 0  
IN 800 ITERATIONS, WMAX= 0.146E-08 AT I= 15 AND J= 0  
IN 850 ITERATIONS, WMAX= 0.134E-08 AT I= 15 AND J= 0  
IN 900 ITERATIONS, WMAX= 0.128E-08 AT I= 14 AND J= 1  
IN 950 ITERATIONS, WMAX= 0.134E-08 AT I= 14 AND J= 1  
IN1000 ITERATIONS, WMAX= 0.128E-08 AT I= 13 AND J= 0  
IN1050 ITERATIONS, WMAX= 0.122E-08 AT I= 14 AND J= 0  
IN1100 ITERATIONS, WMAX= 0.116E-08 AT I= 13 AND J= 0  
IN1150 ITERATIONS, WMAX= 0.116E-08 AT I= 15 AND J= 0  
IN1200 ITERATIONS, WMAX= 0.116E-08 AT I= 14 AND J= 0  
IN1250 ITERATIONS, WMAX= 0.105E-08 AT I= 13 AND J= 0  
STOP --

TYPICAL OUTPUT TO SUCCESSIVE APPROXIMATION PROCEDURE

PROGRAMME USED TO PRINT DEFLECTION VALUES AND CALCULATE  
THE APPLIED MOMENT

```

C      PROGRAMME TO CALCULATE THE SHAPE OF THE FOLD IN A YOSHIMURA BUCKLE
C      PATTERN FOR THIN WALLED CYLINDRICAL SHELLS
C      PRINT DEFLECTIONS AND CALCULATE MOMENT
0001      DIMENSION W(54,54)
0002      CALL ASSIGN (1,'DX0:DATA3')
0003      DEFINE FILE 1 (1,12,U,IZ)
0004      READ (1'1)X,Y,AL,N,M,DX,DY
0005      WRITE (7,1)X,Y
0006      1 FORMAT(32H LENGTH OF DIAGONAL COMP.MEMBER=,F8.5,32H M.  FACET WIDT
1H PERP.TO MEMBER=,F8.5,3H M.)
0007      WRITE (7,3)N,DX
0008      3 FORMAT(36H NO.OF POINTS IN HALF MEMBER LENGTH=,I4,21H -- INCREMENT
1 LENGTH=,F10.7,3H M.)
0009      WRITE (7,4)M,DY
0010      4 FORMAT(33H NO.OF POINTS ACROSS FACET WIDTH=,I4,21H -- INCREMENT LE
1NGTH=,F10.7,3H M.)
0011      WRITE (7,2)180.0-AL*360.0/3.1415927
0012      2 FORMAT(22H ANGLE BETWEEN FACETS=,F6.2,5H DEG.)
0013      WRITE (7,5)
0014      5 FORMAT (17H$POISSON'S RATIO=)
0015      READ (5,6)ANU
0016      6 FORMAT (F6.4)
0017      CALL ASSIGN (2,'DX0:DATA4')
0018      DEFINE FILE 2 (1,5832,U,IZ)
0019      READ (2'1)((W(I,J),I=1,N+4),J=1,M+4)
0020      WRITE (7,11)
0021      11 FORMAT (28HOCURVATURES ALONG FOLD (1/M))

```

```

0022      WRITE (7,12)
0023 12  FORMAT (3H I,4X,6HTRANS.,4X,5HAXIAL)
0024      TOTM=0.0
0025      DO 200 I=3,N+1
0026      WRITE (7,13) I-2,2.*(W(I,4)-W(I,3))/DY/DY,(W(I+1,3)-2.*W(I,3)
1+W(I-1,3))/DX/DX
0027 13  FORMAT (I3,2E11.4)
0028      TOTM=TOTM-(2.*(W(I,4)-W(I,3))/DY/DY+ANU*(W(I+3,3)-2.*W(I,3)
1+W(I-1,3))/DX/DX)
0029 200 CONTINUE
0030      WRITE (7,13) N,2*(W(N+2,4)-W(N+2,3))/DY/DY,(W(N+3,3)-2.*W(N+2,3)
1+W(N+1,3))/DX/DX
0031      TOTM=TOTM-(2.*(W(2,4)-W(2,3))/DY/DY+ANU*(W(3,3)-2.*W(2,3)
1+W(1,3))/DX/DX)/2.
0032      TOTM=TOTM-((W(N+2,4)-W(N+2,3))/DY/DY+ANU*(W(N+1,3)-W(N+2,3))
1/DX/DX)/2.
0033      WRITE (7,10) TOTM*DX*2.
0034 10  FORMAT(34H0APPLIED MOMENT/FLEXURAL RIGIDITY=,E11.4)
0035      WRITE (7,14)
0036 14  FORMAT (22H0DEFLECTIONS IN METRES)
0037      DO 100 J=3,M+3
0038      WRITE (7,8) J-3
0039      8  FORMAT (3H0J=,I4)
0040      WRITE (7,9)((I-2,W(I,J))*1000.),I=2,N+2)
0041      9  FORMAT(3(3H I=,I3,3H W=,E11.4,2X))
0042 100 CONTINUE
0043      END

```

LENGTH OF DIAGONAL COMP.MEMBER= 0.15000 M. FACET WIDTH PERP.TO MEMBER= 0.04500 M.  
NO.OF POINTS IN HALF MEMBER LENGTH= 15 -- INCREMENT LENGTH= 0.0050000 M.  
NO.OF POINTS ACROSS FACET WIDTH= 9 -- INCREMENT LENGTH= 0.0050000 M.  
ANGLE BETWEEN FACETS=175.00 DEG.  
POISSON'S RATIO=.35

## CURVATURES ALONG FOLD (1/M)

I	TRANS.	AXIAL
1	0.1008E+02	0.2886E+00
2	0.5880E+01	-0.5511E+00
3	0.3902E+01	-0.5111E+00
4	0.2906E+01	-0.4505E+00
5	0.2341E+01	-0.4185E+00
6	0.1984E+01	-0.3990E+00
7	0.1739E+01	-0.3824E+00
8	0.1563E+01	-0.3652E+00
9	0.1432E+01	-0.3471E+00
10	0.1333E+01	-0.3287E+00
11	0.1259E+01	-0.3113E+00
12	0.1205E+01	-0.2962E+00
13	0.1168E+01	-0.2844E+00
14	0.1147E+01	-0.2770E+00
15	0.1140E+01	-0.2745E+00

APPLIED MOMENT/FLEXURAL RIGIDITY=-0.6435E+00

## DEFLECTIONS IN METRES

J= 0

I= 0 W= 0.0000E+00	I= 1 W= 0.1193E+00	I= 2 W= 0.2458E+00
I= 3 W= 0.3585E+00	I= 4 W= 0.4584E+00	I= 5 W= 0.5471E+00
I= 6 W= 0.6253E+00	I= 7 W= 0.6936E+00	I= 8 W= 0.7522E+00
I= 9 W= 0.8018E+00	I= 10 W= 0.8427E+00	I= 11 W= 0.8753E+00
I= 12 W= 0.9002E+00	I= 13 W= 0.9176E+00	I= 14 W= 0.9280E+00
I= 15 W= 0.9314E+00	I=	

J= 1

I= 0 W= 0.2181E+00	I= 1 W= 0.2453E+00	I= 2 W= 0.3193E+00
I= 3 W= 0.4073E+00	I= 4 W= 0.4948E+00	I= 5 W= 0.5764E+00
I= 6 W= 0.6501E+00	I= 7 W= 0.7153E+00	I= 8 W= 0.7718E+00
I= 9 W= 0.8197E+00	I= 10 W= 0.8593E+00	I= 11 W= 0.8910E+00
I= 12 W= 0.9152E+00	I= 13 W= 0.9323E+00	I= 14 W= 0.9423E+00
I= 15 W= 0.9457E+00	I=	

J= 2

I= 0 W= 0.4362E+00	I= 1 W= 0.4389E+00	I= 2 W= 0.4732E+00
I= 3 W= 0.5287E+00	I= 4 W= 0.5933E+00	I= 5 W= 0.6591E+00
I= 6 W= 0.7217E+00	I= 7 W= 0.7788E+00	I= 8 W= 0.8292E+00
I= 9 W= 0.8726E+00	I= 10 W= 0.9087E+00	I= 11 W= 0.9378E+00
I= 12 W= 0.9601E+00	I= 13 W= 0.9757E+00	I= 14 W= 0.9850E+00
I= 15 W= 0.9881E+00	I=	

J= 3

I= 0 W= 0.6543E+00	I= 1 W= 0.6508E+00	I= 2 W= 0.6637E+00
I= 3 W= 0.6945E+00	I= 4 W= 0.7370E+00	I= 5 W= 0.7849E+00
I= 6 W= 0.8335E+00	I= 7 W= 0.8796E+00	I= 8 W= 0.9215E+00
I= 9 W= 0.9582E+00	I= 10 W= 0.9891E+00	I= 11 W= 0.1014E+01
I= 12 W= 0.1033E+01	I= 13 W= 0.1047E+01	I= 14 W= 0.1055E+01
I= 15 W= 0.1058E+01	I=	

J= 4

I= 0 W= 0.8724E+00	I= 1 W= 0.8678E+00	I= 2 W= 0.8704E+00
I= 3 W= 0.8852E+00	I= 4 W= 0.9107E+00	I= 5 W= 0.9427E+00
I= 6 W= 0.9775E+00	I= 7 W= 0.1012E+01	I= 8 W= 0.1044E+01
I= 9 W= 0.1073E+01	I= 10 W= 0.1098E+01	I= 11 W= 0.1118E+01
I= 12 W= 0.1134E+01	I= 13 W= 0.1145E+01	I= 14 W= 0.1151E+01
I= 15 W= 0.1154E+01	I=	

J= 5

I= 0 W= 0.1090E+01	I= 1 W= 0.1086E+01	I= 2 W= 0.1084E+01
I= 3 W= 0.1090E+01	I= 4 W= 0.1104E+01	I= 5 W= 0.1123E+01
I= 6 W= 0.1146E+01	I= 7 W= 0.1170E+01	I= 8 W= 0.1193E+01
I= 9 W= 0.1214E+01	I= 10 W= 0.1232E+01	I= 11 W= 0.1247E+01
I= 12 W= 0.1259E+01	I= 13 W= 0.1267E+01	I= 14 W= 0.1272E+01
I= 15 W= 0.1274E+01	I=	

J= 6

I= 0 W= 0.1309E+01	I= 1 W= 0.1305E+01	I= 2 W= 0.1302E+01
I= 3 W= 0.1303E+01	I= 4 W= 0.1310E+01	I= 5 W= 0.1320E+01
I= 6 W= 0.1334E+01	I= 7 W= 0.1349E+01	I= 8 W= 0.1363E+01
I= 9 W= 0.1377E+01	I= 10 W= 0.1389E+01	I= 11 W= 0.1399E+01
I= 12 W= 0.1407E+01	I= 13 W= 0.1412E+01	I= 14 W= 0.1415E+01
I= 15 W= 0.1416E+01	I=	

J= 7

I= 0 W= 0.1527E+01	I= 1 W= 0.1525E+01	I= 2 W= 0.1522E+01
--------------------	--------------------	--------------------

APPENDIX    F

PROGRAM LISTING AND TYPICAL OUTPUT OF PROGRAMS USED IN  
CALCULATING THE FOLD SHAPE ALLOWING FOR MEMBRANE STRESSES

```

C      PROGRAMME TO CALCULATE THE SHAPE OF THE FOLD IN A YOSHIMURA BUCKLE
C      PATTERN FOR THIN WALLED CYLINDRICAL SHELLS
C      PART 1---OPEN FILES AND ESTIMATE INITIAL VALUES
0001  DIMENSION U(19,13),V(19,13),W(19,13)
C      READ IN DATA .
0002  WRITE(7,1)
0003  1 FORMAT(48H$LENGTH OF DIAGONAL COMPRESSION MEMBER(METRES) =)
0004  READ(5,2)X
0005  2 FORMAT(F8.5)
0006  D=X/30.
0007  Y=D*9.
0008  WRITE (7,3)D,Y
0009  3 FORMAT (18H LENGTH INCREMENT=,F10.7,15HM.,FACET WIDTH=,F8.5,2HM.)
0010  WRITE(7,5)
0011  5 FORMAT(32H$ANGLE BETWEEN FACETS(DEGREES) =)
0012  READ(5,6)AL
0013  6 FORMAT(F6.2)
0014  WRITE(7,7)
0015  7 FORMAT (16H$THICKNESS(MM.)=)
0016  READ (5,8)T
0017  8 FORMAT (F8.5)
0018  T=T/1000.
0019  WRITE (7,9)
0020  9 FORMAT (17H$POISSON'S RATIO=)
0021  READ (5,8)ANU
0022  AL=(90.0-AL/2.)*3.1415927/180.0
0023  CALL ASSIGN (1,'DX0:DATA5')
0024  DEFINE FILE 1 (1,12,U,IZ)
0025  WRITE(1,1)X,Y,AL,D,T,ANU
0026  CALL ASSIGN (2,'DX0:DATA6')
0027  DEFINE FILE 2 (1,1482,U,IZ)
0028  DO 100 I=1,19
0029  W(I,1)=2.*D*SIN(AL)
0030  U(I,1)=0.0
0031  V(I,1)=0.0
0032  U(I,2)=0.0
0033  V(I,2)=0.0
0034  100 W(I,2)=D*SIN(AL)

```



```

0035      DO 200 J=3,13
0036      DO 200 I=1,19
0037      U(I,J)=0.0
0038      V(I,J)=0.0
0039      200 W(I,J)=(J-3)*D*SIN(AL)
0040      WRITE (2,1)((U(I,J),V(I,J),W(I,J)),I=1,19),J=1,13)
0041      END

```

#### TYPICAL OUTPUT TO OPENING PROGRAMME

```

LENGTH OF DIAGONAL COMPRESSION MEMBER(METRES) =.15
LENGTH INCREMENT= 0.0050000M.,FACET WIDTH= 0.04500M.
ANGLE BETWEEN FACETS(DEGREES) =173.9

THICKNESS(MM.)=.1

POISSON'S RATIO=.35

STOP ---

```

```

C      PROGRAMME TO CALCULATE THE SHAPE OF THE FOLD IN A YOSHIMURA BUCKLE
C      PATTERN FOR THIN WALLED CYLINDRICAL SHELLS
C      PART 2 --- SUCCESSIVE APPROXIMATION PROCEDURE TO CALCULATE BETTER
C      GUESSES
0001      DIMENSION U(19,13),V(19,13),W(19,13)
0002      CALL ASSIGN (1,'DX0:DATA5')
0003      DEFINE FILE 1 (1,12,U,IZ)
0004      READ (1,1)X,Y,AL,D,T,ANU
0005      WRITE (7,1)X,Y
0006      1 FORMAT(32H LENGTH OF DIAGONAL COMP.MEMBER=,F8.5,32H M.  FACET WIDT
1H PERP.TO MEMBER=,F8.5,3H M.)
0007      WRITE (7,2)180.0-AL*360.0/3.1415927
0008      2 FORMAT(22H ANGLE BETWEEN FACETS=,F6.2,5H DEG.)
0009      WRITE (7,3)D
0010      3 FORMAT (18H INCREMENT LENGTH=,F10.7,3H M.)
0011      WRITE (7,4)T*1000.,ANU
0012      4 FORMAT (11H THICKNESS=,F8.5,21HMM.--POISSON'S RATIO=,F8.5)
0013      IT1=0
0014      ITNS=0
0015      WRITE (7,7)
0016      7 FORMAT(39H$U,V,AND W RELAXATION CONSTANTS ARE:- .)
0017      READ (5,8)C1,C2,C3
0018      8 FORMAT(3F4.2)
0019      WRITE (7,9)
0020      9 FORMAT(30H$MAXIMUM NUMBER OF ITERATIONS=)
0021      READ (5,10)MAX
0022      10 FORMAT(I5)
0023      CALL ASSIGN (2,'DX0:DATA6')
0024      DEFINE FILE 2 (1,1482,U,IZ)
0025      READ (2,1)((U(I,J),V(I,J),W(I,J)),I=1,19),J=1,13)
0026      500 WMAX=0.0
0027      UMAX=0.0
0028      VMAX=0.0

```

```

0029      DO 200 J=3,11
0030      DO 100 I=3,17
0031          DUX=(U(I+1,J)-U(I-1,J))/2.
0032          DUY=(U(I,J+1)-U(I,J-1))/2.
0033          DVX=(V(I+1,J)-V(I-1,J))/2.
0034          DUY=(V(I,J+1)-V(I,J-1))/2.
0035          D2UXY=(U(I+1,J+1)-U(I+1,J-1)-U(I-1,J+1)+U(I-1,J-1))/4.
0036          D2VXY=(V(I+1,J+1)-V(I+1,J-1)-V(I-1,J+1)+V(I-1,J-1))/4.
0037          D2WXY=(W(I+1,J+1)-W(I+1,J-1)-W(I-1,J+1)+W(I-1,J-1))/4.
0038          D2WX2=(W(I+1,J)-2.*W(I,J)+W(I-1,J))
0039          D2WY2=(W(I,J+1)-2.*W(I,J)+W(I,J-1))
0040          D3WY3=(W(I,J+2)-2.*W(I,J+1)+2.*W(I,J-1)+W(I,J-2))/2.
0041          D3WX3=(W(I+2,J)-2.*W(I+1,J)+2.*W(I-1,J)-W(I-2,J))/2.
0042          D3WX2Y=(W(I+1,J+1)-2.*W(I,J+1)+W(I-1,J+1)-W(I+1,J-1)+2.*W(I,J-1)-W
1(I-1,J-1))/2.
0043          D3WXY2=(W(I+1,J+1)-2.*W(I+1,J)+W(I+1,J-1)-W(I-1,J+1)+2.*W(I-1,J)-W
1(I-1,J-1))/2.
0044          UNEW=((1.+ANU)*D2VXY/2.+U(I+1,J)+U(I-1,J)+(1.-ANU)*(U(I,J+1)+U(I,J
1-1))/2.+T*T*(D2WXY*(D3WY3+D3WX2Y)+D2WX2*(D3WX3+D3WXY2))/12./D/D/D
2)/(3.-ANU)
0045          VNEW=((1.+ANU)*D2UXY/2.+V(I,J+1)+V(I,J-1)+(1.-ANU)*(V(I+1,J)+V(I-1
1,J))/2.+T*T*(D2WXY*(D3WX3+D3WXY2)+D2WY2*(D3WY3+D3WX2Y))/12./D/D/D
2)/(3.-ANU)
0046          ANX=DUX+ANU*DUY
0047          ANY=DUY+ANU*DUX
0048          ANXY=DUY+DVX
0049          WNEW=(12.*D*(D2WX2*ANX+(1.-ANU)*D2WXY*ANXY+D2WY2*ANY)/T/T
1=W(I+2,J)+8.*W(I+1,J)+8.*W(I-1,J)-W(I-2,J)-W(I,J+2
2)+8.*W(I,J+1)+8.*W(I,J-1)-W(I,J-2)-2.*W(I+1,J+1)-2.*W(I+1,J-1)-2.*
3W(I-1,J+1)-2.*W(I-1,J-1))/20.
0050      IF (ABS(U(I,J)-UNEW)-UMAX)400,400,300
0051      300 UMAX=ABS(U(I,J)-UNEW)
0052      K1=I-2
0053      L1=J-3
0054      400 IF (ABS(V(I,J)-VNEW)-VMAX)700,700,600
0055      600 VMAX=ABS(V(I,J)-VNEW)

```

```

0056      K2=I-2
0057      L2=J-3
0058      700 IF (ABS(W(I,J)-WNEW)-WMAX)900,900,800
0059      800 WMAX=ABS(W(I,J)-WNEW)
0060      K3=I-2
0061      L3=J-3
0062      900 U(I,J)=U(I,J)+C1*(UNEW-U(I,J))
0063      V(I,J)=V(I,J)+C2*(VNEW-V(I,J))
0064      100 W(I,J)=W(I,J)+C3*(WNEW-W(I,J))
0065      U(17,J)=0.0
0066      U(18,J)=-U(16,J)
0067      V(18,J)=V(16,J)
0068      W(18,J)=W(16,J)
0069      200 W(19,J)=W(15,J)
0070      DO 1000 I=3,19
0071      W(I,1)=W(I,5)
0072      U(I,2)=U(I,4)
0073      V(I,2)=-V(I,4)
0074      W(I,2)=W(I,4)
0075      1000 V(I,3)=0.0
0076      ITNS=ITNS+1
0077      IT1=IT1+1
0078      IF (IT1-50)1200,1100,1200
0079      1100 WRITE (7,6)ITNS,UMAX,K1,L1,UMAX,K2,L2,WMAX,K3,L3
0080      6 FORMAT (3H IN,I4,11H ITNS UMAX=,E10.3,3H AT,I3,1H,,I2,6H,UMAX=,E10
1.3,3H AT,I3,1H,,I2,6H,WMAX=,E10.3,3H AT,I3,1H,,I2)
0081      IT1=0
0082      WRITE (2,1)((U(I,J),V(I,J),W(I,J)),I=1,19),J=1,13)
0083      1200 IF (UMAX-0.000000001)1300,1500,1500
0084      1300 IF (UMAX-0.000000001)1400,1500,1500
0085      1400 IF (WMAX-0.000000001)1600,1500,1500
0086      1500 IF (ITNS-MAX)500,1600,1600
0087      1600 END

```

LENGTH OF DIAGONAL COMP.MEMBER= 0.15000 M. FACET WIDTH PERP.TO MEMBER= 0.04500 M.  
 ANGLE BETWEEN FACETS=173.90 DEG.

INCREMENT LENGTH= 0.0050000 M.

THICKNESS= 0.10000MM.--POISSON'S RATIO= 0.35000

U,V,AND W RELAXATION CONSTANTS ARE:- 1.0,1.0,1.0

MAXIMUM NUMBER OF ITERATIONS=20000

IN 50 ITNS	UMAX= 0.365E-12 AT	6, 6, VMAX= 0.392E-09 AT	1, 0, WMAX= 0.251E-06 AT	15, 0
IN 100 ITNS	UMAX= 0.358E-12 AT	6, 6, VMAX= 0.392E-09 AT	1, 0, WMAX= 0.245E-06 AT	15, 0
IN 150 ITNS	UMAX= 0.351E-12 AT	6, 6, VMAX= 0.392E-09 AT	1, 0, WMAX= 0.240E-06 AT	15, 0
IN 200 ITNS	UMAX= 0.345E-12 AT	6, 6, VMAX= 0.393E-09 AT	1, 0, WMAX= 0.234E-06 AT	15, 0
IN 250 ITNS	UMAX= 0.339E-12 AT	6, 6, VMAX= 0.393E-09 AT	1, 0, WMAX= 0.229E-06 AT	15, 0
IN 300 ITNS	UMAX= 0.334E-12 AT	7, 5, VMAX= 0.393E-09 AT	1, 0, WMAX= 0.224E-06 AT	15, 0
IN 350 ITNS	UMAX= 0.329E-12 AT	7, 5, VMAX= 0.394E-09 AT	1, 0, WMAX= 0.218E-06 AT	15, 0
IN 400 ITNS	UMAX= 0.324E-12 AT	7, 5, VMAX= 0.394E-09 AT	1, 0, WMAX= 0.213E-06 AT	15, 0
IN 450 ITNS	UMAX= 0.318E-12 AT	7, 5, VMAX= 0.394E-09 AT	1, 0, WMAX= 0.208E-06 AT	15, 0
IN 500 ITNS	UMAX= 0.313E-12 AT	7, 5, VMAX= 0.394E-09 AT	1, 0, WMAX= 0.203E-06 AT	15, 0
IN 550 ITNS	UMAX= 0.308E-12 AT	7, 5, VMAX= 0.395E-09 AT	1, 0, WMAX= 0.198E-06 AT	15, 0
IN 600 ITNS	UMAX= 0.302E-12 AT	7, 5, VMAX= 0.395E-09 AT	1, 0, WMAX= 0.193E-06 AT	15, 0
IN 650 ITNS	UMAX= 0.297E-12 AT	7, 5, VMAX= 0.395E-09 AT	1, 0, WMAX= 0.189E-06 AT	15, 0
IN 700 ITNS	UMAX= 0.291E-12 AT	7, 5, VMAX= 0.395E-09 AT	1, 0, WMAX= 0.184E-06 AT	15, 0
IN 750 ITNS	UMAX= 0.286E-12 AT	7, 5, VMAX= 0.395E-09 AT	1, 0, WMAX= 0.179E-06 AT	15, 0
IN 800 ITNS	UMAX= 0.281E-12 AT	7, 5, VMAX= 0.396E-09 AT	1, 0, WMAX= 0.175E-06 AT	15, 0
IN 850 ITNS	UMAX= 0.276E-12 AT	7, 5, VMAX= 0.396E-09 AT	1, 0, WMAX= 0.171E-06 AT	15, 0
IN 900 ITNS	UMAX= 0.270E-12 AT	7, 5, VMAX= 0.396E-09 AT	1, 0, WMAX= 0.167E-06 AT	15, 0
IN 950 ITNS	UMAX= 0.265E-12 AT	7, 5, VMAX= 0.396E-09 AT	1, 0, WMAX= 0.162E-06 AT	15, 0
IN1000 ITNS	UMAX= 0.259E-12 AT	7, 5, VMAX= 0.396E-09 AT	1, 0, WMAX= 0.159E-06 AT	15, 0
IN1050 ITNS	UMAX= 0.254E-12 AT	7, 5, VMAX= 0.397E-09 AT	1, 0, WMAX= 0.154E-06 AT	15, 0
IN1100 ITNS	UMAX= 0.249E-12 AT	7, 5, VMAX= 0.397E-09 AT	1, 0, WMAX= 0.151E-06 AT	15, 0
IN1150 ITNS	UMAX= 0.244E-12 AT	7, 5, VMAX= 0.397E-09 AT	1, 0, WMAX= 0.147E-06 AT	15, 0
IN1200 ITNS	UMAX= 0.239E-12 AT	7, 5, VMAX= 0.397E-09 AT	1, 0, WMAX= 0.143E-06 AT	15, 0

TYPICAL OUTPUT TO THE SUCCESSIVE APPROXIMATION PROCEDURE

```

C      PROGRAMME TO CALCULATE THE SHAPE OF THE FOLD IN A YOSHIMURA BUCKLE
C      PATTERN FOR THIN WALLED CYLINDRICAL SHELLS
C      PRINT DEFLECTIONS AND CALCULATE MOMENT
0001      DIMENSION U(19,13),V(19,13),W(19,13)
0002      CALL ASSIGN (1,'DX0:DATA5')
0003      DEFINE FILE 1 (1,12,U,IZ)
0004      READ (1,1)X,Y,AL,D,T,ANU
0005      WRITE (7,1)X,Y
0006      1 FORMAT(32H LENGTH OF DIAGONAL COMP.MEMBER=,F8.5,32H M.  FACET WIDT
1H PERP.TO MEMBER=,F8.5,3H M.)
0007      WRITE (7,3)D
0008      3 FORMAT (18H INCREMENT LENGTH=,F10.7,3H M.)
0009      WRITE (7,4)T*1000.,ANU
0010      4 FORMAT (11H THICKNESS=,F8.5,21HMM.--POISSON'S RATIO=,F8.5)
0011      WRITE (7,2)180.0-AL*360.0/3.1415927
0012      2 FORMAT(22H ANGLE BETWEEN FACETS=,F6.2,5H DEG.)
0013      CALL ASSIGN (2,'DX0:DATA6')
0014      DEFINE FILE 2 (1,1482,U,IZ)
0015      READ (2,1)((U(I,J),V(I,J),W(I,J)),I=1,19),J=1,13)
0016      WRITE (7,11)
0017      11 FORMAT (28HOCURVATURES ALONG FOLD (1/M))
0018      WRITE (7,12)
0019      12 FORMAT (3H  I,4X,6HTRANS.,4X,5HAXIAL)
0020      TOTM=0.0
  
```

```

0021      DO 200 I=3,16
0022      WRITE (7,13) I-2, 2.*(W(I,4)-W(I,3))/D/D, (W(I+1,3)-2.*W(I,3)
      1+W(I-1,3))/D/D
0023      13 FORMAT (I3,2E11.4)
0024      TOTM=TOTM-(2.*(W(I,4)-W(I,3))/D/D+ANU*(W(I+3,3)-2.*W(I,3)
      1+W(I-1,3))/D/D)
0025      200 CONTINUE
0026      WRITE (7,13) 15, 2*(W(17,4)-W(17,3))/D/D, (W(18,3)-2.*W(17,3)
      1+W(16,3))/D/D
0027      TOTM=TOTM-(2.*(W(2,4)-W(2,3))/D/D+ANU*(W(3,3)-2.*W(2,3)
      1+W(1,3))/D/D)/2.
0028      TOTM=TOTM-((W(17,4)-W(17,3))/D/D+ANU*(W(16,3)-W(17,3))
      1/D/D)/2.
0029      WRITE (7,10) TOTM*D*2.
0030      10 FORMAT(34H0APPLIED MOMENT/FLEXURAL RIGIDITY=,E11.4)
0031      WRITE (7,5)
0032      5 FORMAT (38H0 I J U(I,J) V(I,J) W(I,J))
0033      WRITE (7,6)
0034      6 FORMAT (1H0,10X,3(2HM.,9X))
0035      DO 100 J=3,12
0036      WRITE (7,7)
0037      7 FORMAT (1H0)
0038      DO 100 I=2,17
0039      100 WRITE (7,8) I-2, J-3, U(I,J), V(I,J), W(I,J)
0040      8 FORMAT (2I3,3E11.4)
0041      END

```

LENGTH OF DIAGONAL COMP.MEMBER= 0.15000 M. FACET WIDTH PERP.TO MEMBER= 0.04500 M.  
INCREMENT LENGTH= 0.0050000 M.  
THICKNESS= 0.10000MM.--POISSON'S RATIO= 0.35000  
ANGLE BETWEEN FACETS=173.90 DEG.

## CURVATURES ALONG FOLD (1/M)

I	TRANS.	AXIAL
1	0.1164E+02	-0.6044E+00
2	0.6697E+01	-0.9433E+00
3	0.4444E+01	-0.7310E+00
4	0.3323E+01	-0.6042E+00
5	0.2688E+01	-0.5415E+00
6	0.2286E+01	-0.5037E+00
7	0.2010E+01	-0.4735E+00
8	0.1810E+01	-0.4449E+00
9	0.1662E+01	-0.4166E+00
10	0.1550E+01	-0.3892E+00
11	0.1466E+01	-0.3641E+00
12	0.1404E+01	-0.3427E+00
13	0.1362E+01	-0.3264E+00
14	0.1338E+01	-0.3163E+00
15	0.1330E+01	-0.3128E+00

APPLIED MOMENT/FLEXURAL RIGIDITY=-0.7412E+00



I	J	U(I,J)	V(I,J)	W(I,J)
		M.	M.	M.

364.

0	0	0.0000E+00	0.0000E+00	0.0000E+00
1	0	0.5724E-10	0.0000E+00	0.1790E-03
2	0	-0.1309E-10	0.0000E+00	0.3428E-03
3	0	-0.1182E-09	0.0000E+00	0.4831E-03
4	0	-0.2232E-09	0.0000E+00	0.6051E-03
5	0	-0.3165E-09	0.0000E+00	0.7119E-03
6	0	-0.3912E-09	0.0000E+00	0.8053E-03
7	0	-0.4424E-09	0.0000E+00	0.8860E-03
8	0	-0.4672E-09	0.0000E+00	0.9549E-03
9	0	-0.4644E-09	0.0000E+00	0.1013E-02
10	0	-0.4348E-09	0.0000E+00	0.1060E-02
11	0	-0.3804E-09	0.0000E+00	0.1098E-02
12	0	-0.3050E-09	0.0000E+00	0.1126E-02
13	0	-0.2129E-09	0.0000E+00	0.1146E-02
14	0	-0.1094E-09	0.0000E+00	0.1158E-02
15	0	0.0000E+00	0.0000E+00	0.1162E-02

0	1	0.0000E+00	0.0000E+00	0.2660E-03
1	1	-0.8762E-10	0.3630E-09	0.3244E-03
2	1	-0.1631E-09	0.5723E-09	0.4265E-03
3	1	-0.2552E-09	0.7122E-09	0.5386E-03
4	1	-0.3473E-09	0.8223E-09	0.6466E-03
5	1	-0.4279E-09	0.9106E-09	0.7455E-03
6	1	-0.4897E-09	0.9787E-09	0.8339E-03
7	1	-0.5280E-09	0.1029E-08	0.9112E-03
8	1	-0.5401E-09	0.1064E-08	0.9776E-03
9	1	-0.5251E-09	0.1087E-08	0.1034E-02
10	1	-0.4839E-09	0.1100E-08	0.1079E-02
11	1	-0.4188E-09	0.1108E-08	0.1116E-02
12	1	-0.3331E-09	0.1111E-08	0.1144E-02
13	1	-0.2313E-09	0.1113E-08	0.1163E-02
14	1	-0.1185E-09	0.1113E-08	0.1175E-02
15	1	0.0000E+00	0.1113E-08	0.1179E-02

0	2	0.0000E+00	0.0000E+00	0.5321E-03
1	2	-0.1602E-09	0.3166E-09	0.5506E-03
2	2	-0.3090E-09	0.6327E-09	0.6039E-03
3	2	-0.4419E-09	0.9161E-09	0.6782E-03
4	2	-0.5506E-09	0.1156E-08	0.7600E-03
5	2	-0.6309E-09	0.1350E-08	0.8410E-03
6	2	-0.6814E-09	0.1501E-08	0.9166E-03
7	2	-0.7019E-09	0.1614E-08	0.9847E-03
8	2	-0.6927E-09	0.1696E-08	0.1044E-02
9	2	-0.6549E-09	0.1753E-08	0.1095E-02
10	2	-0.5905E-09	0.1790E-08	0.1137E-02
11	2	-0.5027E-09	0.1813E-08	0.1171E-02
12	2	-0.3950E-09	0.1827E-08	0.1196E-02
13	2	-0.2721E-09	0.1835E-08	0.1214E-02
14	2	-0.1387E-09	0.1838E-08	0.1225E-02
15	2	0.0000E+00	0.1839E-08	0.1228E-02

0	3	0.0000E+00	0.0000E+00	0.7981E-03
1	3	-0.2348E-09	0.3018E-09	0.8018E-03
2	3	-0.4479E-09	0.6470E-09	0.8267E-03
3	3	-0.6255E-09	0.9896E-09	0.8709E-03
4	3	-0.7592E-09	0.1300E-08	0.9268E-03